Biological and Medical Physics, Biomedical Engineering

Mohammad Ashrafuzzaman
Jack Tuszynski

Membrane Biophysics

Springer

Biological and Medical Physics, Biomedical Engineering

For further volumes:
http://www.springer.com/series/3740

The fields of biological and medical physics and biomedical engineering are broad, multidisciplinary and dynamic. They lie at the crossroads of frontier research in physics, biology, chemistry, and medicine. The Biological and Medical Physics, Biomedical Engineering Series is intended to be comprehensive, covering a broad range of topics important to the study of the physical, chemical and biological sciences. Its goal is to provide scientists and engineers with textbooks, monographs, and reference works to address the growing need for information.

Books in the series emphasize established and emergent areas of science including molecular, membrane, and mathematical biophysics; photosynthetic energy harvesting and conversion; information processing; physical principles of genetics; sensory communications; automata networks, neural networks, and cellular automata. Equally important will be coverage of applied aspects of biological and medical physics and biomedical engineering such as molecular electronic components and devices, biosensors, medicine, imaging, physical principles of renewable energy production, advanced prostheses, and environmental control and engineering.

Mohammad Ashrafuzzaman · Jack Tuszynski

Membrane Biophysics

Springer

Dr. Mohammad Ashrafuzzaman
Department of Biochemistry, College of Science
King Saud University
Riyadh
Saudi Arabia

Prof. Dr. Jack Tuszynski
Department of Physics, Cross Cancer Institute
University of Alberta
Edmonton
AB
Canada

ISSN 1618-7210
ISBN 978-3-642-16104-9 ISBN 978-3-642-16105-6 (eBook)
DOI 10.1007/978-3-642-16105-6
Springer Heidelberg New York Dordrecht London

Library of Congress Control Number: 2012942928

Printed on acid-free paper

Springer is part of Springer Science+Business Media (www.springer.com)

Preface

Over the past two decades, there has been a growing dialog between biologists and an ever-increasing number of physicists, mathematicians, and engineers. The reason for this mutual interest attraction is obviously the modern biology's pre-eminent role on the front lines of scientific research.

The connection between the physical and biomedical sciences has been developing rapidly over the past few decades, especially since the groundbreaking discoveries in molecular genetics. There is clearly a need for a continuing dialog and a cross-fertilization between life sciences and physical sciences. As a result of the naturally interdisciplinary nature of the life sciences numerous new border areas are being created and developed. Therefore, disciplines such as: mathematical biology, biophysics, computational biology, bio-statistics, biological physics, theoretical biology, biological chemistry (and of course bio-chemistry), and biomedical engineering have been undergoing exponential growth.

Diversity present in biological systems is a simple result of the multitude of possible combinations of the finite number of structural elements. The functioning of biological systems should also follow from this complexity with specific organization of complex molecular systems providing specific functions while they continue to be governed by fundamental physical laws. The principle of complexity begetting function is familiar to physicists and has often been referred to as an emergent phenomenon. It is a characteristic feature of atomic systems to display new emergent properties as they become more complex. This property is at the core of the instability of living organisms which acquire new functional features as their structural complexity grows with size from single-cell organisms to multi-cellular organisms.

This hierarchical, interconnected, but a coherently operating system of systems that sustains life poses a great scientific challenge not only to understand how its pieces work but also how the whole is organized internally to achieve specific functional advantages. Our quest to understand biology using physical laws and engineering principles is greatly aided by the rapid development of sophisticated experimental techniques that physics and technology has supplied for the use by biologists. Some of the most prominent examples are listed below:

- Light microscope (resolution: 400–600 nm) with various modern upgrades such as confocal, phase contrast, or cryomicroscopy.
- Electron microscope (10–100 nm)
- Neutron scattering (1–10 Å)
- X-ray crystallography (1 Å)
- Patch clamp electrophysiology
- STM, AFM, TEM
- NMR, MRI, fMRI
- Fluorescence spectroscopy
- Microwave absorption
- Laser light scattering
- Synchrotron radiation scattering
- Laser tweezers, etc.

Many other techniques that originated in physical laboratories have made their way to become standard equipment used by molecular biologists and chemists. From their original inventions as probes of physical phenomena these experimental techniques are then frequently adapted to molecular biology and eventually some of them are further transformed into diagnostic and therapeutic tools in modern medicine. X-ray machines are used for the detection of abnormalities, NMR, now called magnetic resonance imaging (MRI) by medical practitioners helps in the detection of tumor growth, which in turn can be treated by radiation from radioactive sources. Electrical manifestations of the activity of the heart are monitored by the cardiologist, who uses electrocardiography (ECG) and, likewise, brain activity is studied through the use of electroencephalography (EEG). Ultrasound has found applications in both diagnostics (e.g., fetal development) and therapeutics (gall and kidney stone shattering).

These techniques have allowed biologists to gain spectacular insights into the inner workings of cells, tissues and organisms. In addition, new physical concepts developed principally by nonlinear physicists are being used as an appropriate theoretical framework within which living systems can be better understood. These concepts involve hallmarks of biological structures such as: nonlinearity, self-organization, self-similarity, cooperativity, and collective behavior (synergy) as well as emergence and complexity mentioned above.

Attempts at applying physical laws to living systems can be traced to the early creators of modern science. Galileo analyzed the structure of animal bones using physical principles, Newton applied his optics to color perception, Volta and Cavendish studied animal electricity, and Lavoisier demonstrated that the process of respiration is a physiological example of an oxidative chemical reaction. Robert Mayer was inspired by physiological studies to formulate the first law of thermodynamics. A particularly fruitful area of application of physics to physiology is hydrodynamics where, for example, blood flow was analyzed by Poiseuille using fluid dynamics principles and air flow in the lungs has been described consistently with the laws of aerodynamics. An important figure in the history of biophysics is that of the German physicist and physiologist Hermann von Helmholtz who laid

the foundations for the fundamental theories of vision and hearing. The list of physicists who made a large impact on biology and physiology is very long, so we only name a few of the most well-known figures who have crossed this now rapidly thinning boundary between physics and biology. Delbrück, Kendrew, von Bekesy, Crick, Meselson, Hartline, Gamow, Schrödinger, Hodgkin, Huxley, Fröhlich, Davydov, Cooper and Szent-György (1972) have undoubtedly pushed the frontier of the life sciences in the direction of exact quantitative analysis. Of particular importance to membrane biophysics is the patch-clamp technique which is a refinement of the voltage clamp. E. Neher and B. Sakmann developed the patch clamp in the late 1970s and early 1980s and received the Nobel Prize in Physiology or Medicine in 1991 for this work. This discovery made it possible to record the currents of single ion channels for the first time, proving their involvement in fundamental cell processes such as action potential conduction in nerve cell's axons.

While increasingly present in many areas of physiology, biology, and medical research physics is helpful in providing deeper insight into the phenomena studied by these sciences, in some fields of investigation physics has actually provided the primary stimulus for development. One such area is electrophysiology where membranes of nerve cells are characterized by a voltage gradient called the action potential. The propagation of action potentials along the axons of nerve cells is the key observation made in the investigation of brain physiology. A physical theory of action potential propagation was developed by Huxley and Hodgkin, who earned a Nobel Prize for their discovery. Likewise, the structure of DNA, discovered by Crick and Watson, that ushered in a new area of molecular biology, would not have been possible without both experimental and theoretical tools developed by physicists. In this case, it was X-ray crystallography that revealed the double helix structure of DNA. More recently, investigations of DNA sequences have been pursued in the hope of revealing a molecular basis of genetically inherited diseases. Gel electrophoresis and fluorescent labeling techniques are the crucial methods perfected by physicists and biochemists for the studies of DNA sequences.

This book is intended to provide a broad overview of membrane biophysics. Membrane biophysics uses the methods of biophysics, biochemistry, and cell biology to study how membranes of living organisms function. The objects of study described here belong to the realm of biology, the language of description will be that of physics with a sprinkling of mathematics and chemistry where needed. Since life itself is a nonlinear far-from-equilibrium process, some aspects of the book will involve nonlinear physics.

Biophysics is the study of the physics of certain complex macromolecular systems—cells and organisms—whose functioning takes place under conditions of insignificant temperature and pressure changes. Biophysicists seek to understand biophysical processes by accounting for intra-molecular and intermolecular interactions, and their resulting electronic and structural conformational changes; and by studying the transfer of electrons, protons, metallic ions and various biomolecules and the associated energetical transformations within biological

systems. In order for these solutes to enter into a cell, their transfer across biological membranes must take place. In solid-state physics, such problems are solved by the methods of quantum mechanics, statistical physics and both equilibrium and non-equilibrium thermodynamics. However, since isolated biophysical systems are not found in nature, the description is complicated by the openness of livings systems and their far-from-equilibrium nature. It is clear that studies of biological systems have been advanced and largely dominated in the past by biochemistry, molecular and structural biology, as well as genetics. This has accrued tremendous benefits, the most obvious appears to be the precise information regarding the chemical composition of cells, in terms of macromolecules, and other structural components, followed by finding the reaction pathways in the production of the synthesized components and culminating in the discovery of the genetic code mechanism. We are now witnessing a paradigm shift where physical methods of both measurement and theoretical interpretation of biological mechanisms are starting to make a profound effect on the field of cell biology. Membrane biophysics is one of the best examples of this paradigm shift.

This book is focused on a detailed description of the diverse mechanisms and phenomena associated with cellular membranes. General membrane phenomena, mechanisms, and other properties will be discussed in Chap. 1. This will be followed by a discussion regarding transmembrane electrical potentials, ionic gradients, ion transport, specificities and directionalities in ion movements, membrane's capacitive effects and related aspects, etc. in Chap. 2. Chapter 3 will focus on the issue of lipid organization in membranes, lipid phase properties, and the thermodynamics of membranes, etc. Chapter 4 will provide a description of transport phenomena in membranes including the question how crucial electrical properties of membranes get compromised due to agents residing inside membranes or external agents interacting with membranes. Various classes of specific ion channels or non-specific pores used by ion flows temporarily appearing inside membranes will be explained here. Natural membrane proteins, antimicrobial peptides, chemotherapy drugs, certain types of lipids, other biomolecules, etc., will be analyzed in order to explain how those agents coexist with lipids and other membrane constituents to generate various membrane events, mainly those which are responsible for changing the membrane transport properties. Chapter 5 will bring additional aspects regarding the mechanisms underlying the generation of membrane transport events and provide a general picture of energetics responsible for statics and dynamics of lipids and membrane residing agents. This chapter will summarize all aspects of the regulation of membrane protein functions based on the electrical and mechanical properties of membranes and membrane proteins. Chapter 6 will attempt to explain how membrane-based nanotechnology can be used in drug delivery into cellular interiors. Electrical and mechanical properties of membranes determine the interactions between nanoparticles and membranes and lead to possible delivery methods beyond the membrane subject to the presence of other agents that induce membrane transport events. Novel membrane-based nanotechnology will be discussed in this chapter as a new dimension in developing drug delivery strategies. A number of serious diseases involving cell membrane

structures and functions will be discussed in Chap. 7. Information regarding the physical, chemical, and biological processes that are involved in disease initiation and progression will be provided in this chapter. Finally, certain diseases such as cancer, Alzheimer's disease, bacterial infections, and some other membrane based disorders and their potential treatments will be discussed in the context of membrane biophysics in this chapter.

The authors hope that this monograph will be of use as a source of valuable information and conceptual inspiration to both students of biophysics and expert researchers.

Acknowledgments

Md Ashrafuzzaman is thankful to Professor Olaf Sparre Andersen of Weill Cornell Medical College, New York and Professor Ronald McElhaney of the University of Alberta for many insightful discussions on various aspects that helped to develop some of the ideas incorporated in this book. Writing of this book would be impossible without using a bulk of experimental data from publications of Md Ashrafuzzaman with Drs. Andersen and McElhaney on his research during his tenures in those departments. Md Ashrafuzzaman is also thankful to Imtihan Ahmed for his assistance in drawing various model diagrams.

Jack Tuszynski would like to express his gratitude to his research collaborators Drs. Marek Duszyk, John Mercer and Horacio Cantiello for their many informative conversations and practical help. He also acknowledges continued help received from his group members, especially Dr. R. Tseng and Mr. Philip Winter.

Both authors appreciate the care and attention given to the technical aspects of manuscript preparation by Ms. Michelle Hanlon. Editorial assistance and encouragement provided by the staff members at Springer, especially Dr. Angela Lahee, is thankfully acknowledged. Last but not least, the authors thank their families for tolerating the long hours spent on preparing the monograph being often physically and mentally absent from family activities. We especially value the emotional support given to us by our wives.

Riyadh, Saudi Arabia, May 2012 — Mohammad Ashrafuzzaman
Edmonton, Canada, May 2012 — Jack Tuszynski

Contents

Chapter 1
Introduction

The origin of life clearly lies in a living cell first observed by Sir Robert Hooke, but exactly where in a cell the essence of life can be localized is still unclear. Over several centuries careful investigators have been trying to find a single source to claim it as the point of origin of life. Is it in the cellular inner core where metabolic processes take place, is it around the cellular boundary where the cell's transport properties couple with processes controlling many dynamical aspects of proteins, or is it in some other yet unknown region, or finally, is it nowhere specific but rather, due to a fundamental mechanism which causes animate matter to qualitatively differ from inanimate matter? Structural and molecular biology have considerably developed our understanding of cellular compartments and molecular building blocks of cells, but the ongoing developments in these fields have raised multifaceted questions regarding cells and cellular processes. Both the cellular inner core and the cellular wall, known as a membrane, have been understood as not just composites of different compartments working independently or collectively and performing many critical functions for a living body. Detailed analyses of the known functions of various cellular components suggest that the real discovery of the origin of their functions is yet to be made.

Living cells are the ultimate examples of complex dynamical systems. For the past several decades, biologists have greatly advanced the understanding of how living systems work by focusing on the structure and function of constituent molecules such as DNA, proteins, and enzymes. Understanding what the constituent parts of a complex machine are made of, however, does not explain how the entire system works. Scientific analysis of living systems has posed an enormous challenge and presented an enormous task. Conceptual advances in physics, vast improvements in the experimental techniques of molecular and cell biology (electron microscopy, STM, AFM, etc.), and exponential progress in computational techniques and related works have brought us to a unique point in the history of science when the expertise of many areas of science can be brought to bear on the main unsolved puzzle of life, namely how cells live, divide, and eventually, die.

M. Ashrafuzzaman and J. Tuszynski, *Membrane Biophysics*,
Biological and Medical Physics, Biomedical Engineering,
DOI: 10.1007/978-3-642-16105-6_1,

Cells are the key building blocks of living systems. Some of them are self-sufficient while others co-operate in multicellular organisms. The human body is composed of cells of 200 different types. A typical size of a cell is of the order of 10 μm and its dry weight amounts to about 7×10^{-16} kg. In its natural state, 70 % of the content constitutes water molecules. The fluid content of a cell is known as the cytoplasm. The cytoplasm is the liquid medium bound within a cell, while the cytoskeleton is the lattice of filaments with a network of attracting proteins formed throughout the cytoplasm.

Two major types of cells are:

(a) prokaryotic: simple cells with no nucleus and no compartments. Bacteria (e.g. *E. coli*) and blue-green algae belong to this group.
(b) eukaryotic: cells with a nucleus and a differentiated structure including compartmentalized organelles as well as a filamentous cytoskeleton. Examples here include higher developed animal and plant cells, green algae, and fungi. Eukaryotic cells emerged about 2 billion years ago, and comprise all the life kingdoms except monera. The Greek meaning of the word *eukaryotic* is "true nucleus".

Bacteria have linear dimensions in the 1–10 μm range while the sizes of eukaryotic cells range between 10 and 100 μm. The interior of a bacterium experiences considerable pressure reaching up to several atmospheres due to the presence of a membrane which, except for *Archaebacteria*, is composed of layers of peptidoglycan sandwiched between two lipid bilayers the inner of which is a plasma membrane.

Plant cells have linear dimensions that vary between 10 and 100 μm. They are bounded by a cell wall whose thickness ranges between 0.1 and 10 μm and is composed of cellulose. Among its organelles, plant cells have a nucleus, endoplasmic reticulum, Golgi apparatus, and mitochondria. Unique to plant cells is the presence of chloroplasts and vacuoles. Unlike bacteria, plant cells possess a cytoskeletal network adding to their mechanical strength. Animal cells tend to be smaller than plant cells since they do not have liquid-filled vacuoles. The organizing center for their cytoskeleton is a cylindrical organelle called a *centriole* that is approximately 0.4 μm long. Instead of chloroplasts that are sites of photosynthesis, animal cells have *mitochondria* that produce the required energy supply in the form of ATP molecules obtained from reactions involving oxygen and food molecules (e.g. glucose, sucrose, etc).

Eukaryotic cells possess membrane-bound internal structures called organelles briefly discussed below. *Mitochondria* produce energy, a *Golgi* apparatus (where various macromolecules are modified, sorted, and packaged for secretion from the cell for distribution to other organelles) is shaped like a stack of disks. The *endoplasmic reticulum* surrounds the nucleus and is the principal site of protein synthesis. Its volume is small compared to the surface area. A *nucleus* is the location of chromosomes and the site of DNA replication and transcription. All of the material within the cell excluding the nucleus is defined as the cytoplasm whose liquid components are referred to as the cytosol while the solid protein-based structures that float in it are called the cytoskeleton. The main component of the cytosol is water. Most of the organelles are bound within their own membranes. Most of the cell's DNA is stored

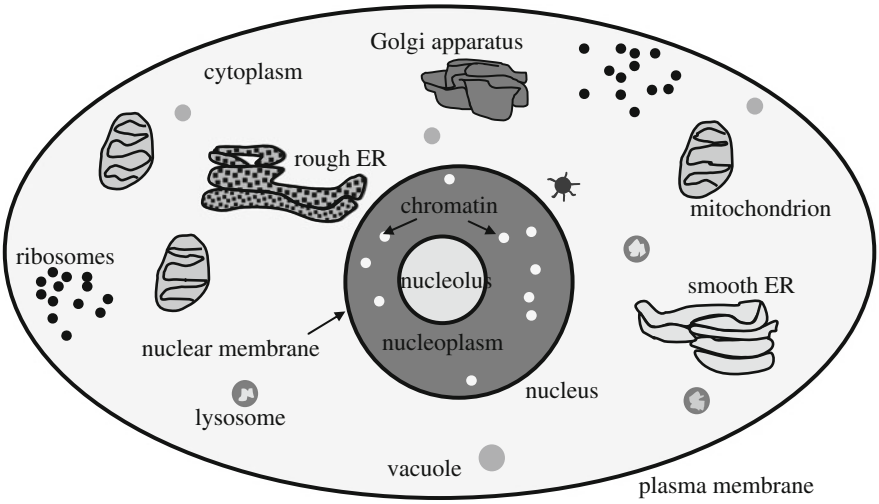

Fig. 1.1 Schematic diagram of a cell, showing different constituent parts. (Components illustrated here do not represent the true structure observed in a biological cell.) The constituents shown here are found in an animal cell. In a plant cell, in addition to all these structures, chloroplasts involved in photosynthesis also exist. A plant cell (not an animal cell) also consists of a cell wall surrounding the plasma membrane which provides tensile strength and protection against mechanical and osmotic stress

within the nucleus that is protected by the nuclear envelope. The rest is contained in mitochondria. Within the nucleus is the nucleolus which functions as the site of ribosomal-RNA synthesis. The diameter of a nucleus ranges between 3 and 10 μm. Despite many differences, both animal and plant cells have striking similarities in their organization and functions.

Although the origins of most of the cellular processes are not yet discovered, organisms that are made up of cells have been classified depending on the structure and organization of cellular building blocks. Organisms that exist as single cells are called unicellular—*Archaea* and *Bacteria*. Organisms that are made up of groups of cells working together are called multicellular—animals, fungi and plants. There is another kingdom which contains a mixture of both unicellular and multicellular organisms. This is called the *Protista*. Humans have about 10^{14} cells in their bodies; a typical cell size in the human body is of the order of 10 μm, with a mass of 1 ng. A schematic diagram showing different parts in a cell is presented in Fig. 1.1.

All cells are enclosed by cell envelopes which consist of cell walls covering plasma membranes. This book is dedicated to a better understanding of various aspects of cellular membranes. A more detailed explanation of the structure and functions of the cell's various components can be found in many text books on cell biology. In this book, we mainly focus on those cell components whose structure and functions are connected with the processes taking place inside membranes.

Both prokaryotic and eukaryotic cells have membranes which primarily separate the interior of a cell from its exterior, selectively regulate the movement of molecules across them, and most importantly, maintain an electric potential difference between the interior of a cell and its exterior. Membrane properties seem to be robust and simple but they reflect the states of a membrane which are, in turn, results of many very complicated processes taking place inside, across, and outside membranes. Understanding of those processes requires thorough analysis of the membrane constituents, electrical environment inside and outside the cell, mechanical membrane properties, dynamical processes taking place in the cell, and many specific as well as non-specific effects due to sources inside and outside the cell.

The fluid contents of a cell are known as the cytoplasm. The cytoplasm is hugely important because it provides the medium in which fundamental biophysical processes such as cellular respiration take place. Its properties are somewhat different than those of dilute aqueous solutions. The contents must be accurately known for in vitro studies of enzymatic reactions, protein synthesis, and other cellular activities. Typical constituents of the cytoplasm are ionic and bio-molecular. Most of the trace ions are positively charged; however, the cytoplasm does not have an overall electric charge, thus the difference is made up of the other constituents such as proteins, bicarbonate (HCO_3^-), phosphate (PO_4^{3-}), and other ions which are for the most part negatively charged, a few of which are significantly electronegative.

Most cells maintain a neutral pH and their dry matter is composed of at least 50 % protein. The remaining dry material consists of nucleic acids, trace ions, lipids, and carbohydrates. A few metallic ions are found which are required for incorporation into metallo-proteins but these ions such as iron(II) (Fe^{2+}) are typically found in nano-molar concentrations.

There is experimental evidence for the existence of two phases of the cytoplasm. These are the so-called liquid and solid phases, *sol* and *gel*, respectively. In the solid phase, the major constituents of the cell are rendered immobile while in the liquid phase, the cytoplasm's viscosity does not differ significantly from water. Diffusion in the cytoplasm is affected mainly by macromolecular crowding. In the solid phase, diffusion is slowed by a factor of three relative to diffusive movement in water. Such properties of the cytoplasm seem to be regulated in some sense by the cytoskeleton, but the manner in which this regulation is accomplished is largely unclear. It is believed that it involves the tangling and detangling of a mesh of various protein filaments. However, once the cell has acted to organize itself, the transition to a solid phase can allow it to expend relatively minimal energy to maintain its organization. Contrary to early perceptions, the cytoplasm is not a viscous soup-like amorphous substance but a highly organized, multicomponent, dynamic network of interconnected protein polymers suspended in a dielectrically polar liquid medium.

A variety of solute molecules are contained within cells. The cellular fluid (cytosol) has a chemical composition of 140 mM K^+, 12 mM Na^+, 4 mM Cl^-, and 148 mM A^- where 1 mM stands for a concentration of 10^{-3} mol/L. The symbol A stands for protein. Cell walls are semipermeable membranes which permit the transport of water easily but not solute molecules. We can apply the osmotic pressure

concept to cells, but this requires finding the osmotic pressure of a mixture of solute molecules. We use Dalton's Law to determine the osmotic pressure inside a cell.

A mixture of chemicals, with concentrations $c_1, c_2, c_3 \ldots$, dissolved in water has the total osmotic pressure equal to the sum of the partial osmotic pressures, Π, of each chemical. Thus,

$$\Pi = \Pi_1 + \Pi_2 + \Pi_3 + \cdots = RT(c_1 + c_2 + c_3 + \cdots) \tag{1.1}$$

The total osmotic pressure inside a cell, Π_{in} is therefore

$$\Pi_{\text{in}} = RT \frac{(140 + 12 + 4 + 148) \times 10^{-3}\,\text{mol}}{1\text{L}} \times \frac{1\text{L}}{10^{-3}\,\text{m}^3} = 7.8 \times 10^4\,\text{Pa} \tag{1.2}$$

where we used the concentrations given above and a physiological temperature of $T = 310\,\text{K}$ and the gas constant is $R = 8.31\,\text{J/mol K}$. Cell walls would be expected to burst under such large pressures. However, they do not, because the exterior fluid also exerts an osmotic pressure in the opposite direction. The cell exterior is composed of $4\,\text{mM}\ \text{K}^+$, $150\,\text{mM}\ \text{Na}^+$, $120\,\text{mM}\ \text{Cl}^-$ and $34\,\text{mM}\ \text{A}^-$. As a consequence, the total osmotic pressure of the cell exterior, Π_{out}, is given by

$$\Pi_{\text{out}} = RT \frac{(4 + 150 + 120 + 34) \times 10^{-3}\,\text{mol}}{1\text{L}} \times \frac{1\text{L}}{10^{-3}\,\text{m}^3} = 7.9 \times 10^4\,\text{Pa} \tag{1.3}$$

Here, Π_{out} is a large osmotic pressure but because Π_{in} and Π_{out} are very similar, the osmotic pressure difference between the exterior and interior part of the cell is very small, as it is the net pressure exerted on the cell wall that matters most. For fragile animal cells, it therefore becomes vitally important to keep their interior and exterior osmotic pressures closely matched. The cell has a sophisticated control mechanism to do this.

If two solutions have the same osmotic pressure, we call them iso-osmotic. However, if the pressures are different, the one at higher pressure is called hypertonic and the one at lower pressure is called hypotonic. When cells are placed in a solution and neither swell nor shrink we call the solution isotonic. In the tissues of most marine invertebrates the total osmotic concentration is close to that of the sea water. The salt concentration of sea water is about 500 mM. As long as the salt concentration remains near this value the blood of many crabs is isotonic with that of sea water. When it is outside this range, the system maintains the osmotic pressure difference across its membrane through the activity of ion pumps and the process is known as osmoregulation.

The cell composition begins to drift away from its optimal mixture if the ion pumps (which will be discussed in detail later in the book) are chemically destroyed. Across the cell wall the osmotic pressure difference then rises, causing the cell to swell, become turgid, and eventually explode. The cells of bacteria and plants are not osmotically regulated since their cell walls are able to withstand pressures in the range of 1–10 atm. The minimum work performed when n moles of solute are

transferred from one solution with a concentration c_1 to a solution with concentration c_2 is easily calculated as

$$W = nRT \ln \frac{c_1}{c_2} \tag{1.4}$$

where c_1 is the salt concentration in the cell and c_2 is the salt concentration in the extracellular space.

Osmotic pressure is also used by the cells of plants and, in particular, trees. Tree roots have a high osmotic pressure inside them which leads to absorption of water from the soil. A key role is also played, it is believed, by osmotic pressure in the growth of plants. The openings on the surfaces of cell leaves, called stomata, are bordered by guard cells that can regulate their internal pressure by controlling the potassium concentration. Water absorption causes these cells to swell under osmotic pressure and the stomata are closed.

Contained within the cytoplasm are the components of the cytoskeleton and certain smaller compartments known as organelles which are specialized to perform their respective functions. We refer the reader to cell biology and cell biophysics text books for information on these important subcellular structures.

A typical cell membrane maintains a transmembrane potential which is of the order of 100 mV. The value of this potential varies between different cells. The transmembrane potential across cancer cell membranes may vary dramatically from the normal cell membranes due to different electrical and metabolic conditions. Significant depolarization of the membrane potential has been found in cancerous breast biopsy tissues and in transformed breast epithelial cells when compared to normal cells [10]. In the case of mitochondria, a proton gradient exists across the mitochondrial inner membrane which determines the membrane potential there. An early stage study [8] suggests that mitochondria-specific interactions of cationic fluorescent probes (molecules) are dependent on the high transmembrane potential (negative inside the membrane) maintained by functional mitochondria. Marked elevations in mitochondria-associated probe fluorescence have been observed in cells engaged in active movement. These results obtained through various investigations suggest that membrane potentials vary considerably between various types of membranes, e.g., normal cell membranes, cancerous cell membranes, mitochondrial membranes, etc.

Like membrane potentials, the thicknesses of various membranes in normal cells, cancerous cells, mitochondria, etc., also vary on a nanometer (nm) scale. The membrane thickness is of the order of 3–6 nm. Taken together, the membrane potential being of the order of 100 mV and the membrane thickness of the order of several nm, results in the electric field across the cell membrane being in the range of $\sim 10^7$ V/m.

It is worth relating the above number to our everyday experience where the electric potential we use is 120 V in the Americas and 220−240 V in the rest of the world for lighting homes and offices. A comparison between the above potentials suggests that a cell membrane appears to act like a cellular power plant. Nature has given us this energy-generating nanoscale component which is present in each of our body's cells. The electric energy created in this power plant is enough to regulate the functions of many biological processes such as ion movements across

membranes, membrane protein dynamics, exclusion of large molecules and pathogens, etc. All membrane constituents such as lipids, membrane proteins, hydrocarbons, etc., reside in the presence of the electric field created by the membrane's electric power plant. Naturally, the electrostatic properties of all the membrane constituents are sensitive to its electric field. The presence of strong polarizing effects on the charges of individual atoms within any molecule and the overall charges of these molecules leads to directed molecular process. Therefore, general electrostatic properties of the various membrane constituents are critical to our understanding of their roles and functions. To gain a complete picture of any biological membrane process, a combined biochemical/biophysical approach is needed with the individual scientific methodologies of these disciplines. This book aims to explore this in detail. For existing general information regarding cell and specifically membrane there are many articles and books available but the readers can consider reading from references [1–13].

General membrane phenomena, mechanisms, and other properties will be addressed in Chap. 2. General transmembrane electrical potentials, ionic gradients, ion transport, specificities, and directionalities in ion movements, membrane's capacitive effects, and related aspects, will also be described in detail in Chap. 2.

Lipids, cholesterol, membrane proteins, hydrocarbons, etc., taken together constitute cell membranes. The proportion between different constituents is very much membrane-specific. Lipids are of various kinds, e.g., charge bearing, charge neutral, curvature bearing, curvature neutral, with different lipid head group geometry, with shorter or longer hydrocarbon tails, etc. Membrane proteins exhibit different morphologies and properties. The presence of cholesterol is organ specific. Membrane stabilizing hydrocarbons play crucial roles. All these aspects will be addressed in Chap. 3. Chapter 3 will rigorously address the issue of the lipid organizations in membranes, lipid phase properties, lipid's thermotrophic behavior, that is, the thermodynamics of membranes, etc. A complete understanding of these issues will create an important background for specific investigations of the various physical and biochemical processes that take place in membranes.

Chapter 4 is dedicated to the description of transport phenomena in membranes. The reader will be informed about how the crucial membrane electrical properties get compromised due to agents residing inside membranes or external agents interacting with membranes. Various classes of specific ion channels or non-specific pores used by ion flows temporarily appearing inside membranes will be explained here. Mainly, the geometric aspects of various membrane transport events will be discussed. Natural membrane proteins, antimicrobial peptides, chemotherapy drugs, certain types of lipids, other biomolecules, etc., will be analyzed in order to explain how those agents coexist with lipids and other membrane constituents to generate various membrane events, mainly those which are responsible for changing the membrane transport properties.

Chapter 5 will bring additional aspects regarding the mechanisms underlying the generation of membrane transport events as explained in Chap. 4, and a general picture of energetics responsible for statics and dynamics of lipids and membrane residing agents. Electrical and mechanical properties of the lipid bilayer, bilayer

constituents, and any agent responsible for creating an event inside the membrane will be explained in detail. Particular attention will be paid to the mechanisms that depend on the electrical properties of membranes relative to their mechanical properties. This chapter will summarize all aspects of the regulation of membrane protein functions based on the electrical and mechanical properties of membranes and membrane proteins.

Chapter 6 has been dedicated to explaining how membrane-based nanotechnology can be used in drug delivery into cellular interiors. Electrical and mechanical properties of membranes determine the interactions between nanoparticles and membranes and lead to possible delivery methods beyond the membrane subject to the presence of other agents that induce membrane transport events. Novel membrane-based nanotechnology is proposed in this chapter, which will hopefully open up a new dimension in developing drug delivery strategies.

A number of serious diseases involving cell membrane structures and functions have been discussed in Chap. 7. In addition to a brief description of the development of these diseases, drug discovery and treatment regimens are taken into consideration. The reader will find information about the physical, chemical, and biological processes that are involved in disease initiation and progression. Finally, certain diseases such as cancer, Alzheimer's disease, bacterial infections, and some other membrane-based disorders and their potential treatments will be outlined in this chapter.

References

1. Alberts, B., Bray, D., Lewis, J., Raff, M., Roberts, K., and Watson, J.D.: Molecular Biology of the Cell. Garland Publishing, London (1994)
2. Amos, L.A., and Amos, W.B.: Molecules of the Cytoskeleton. Macmillan Press, London (1991)
3. Benedek, G.B., Villars, F.M.H.: Physics with Illustrative Examples from Medicine and Biology. Springer, Berlin (2000)
4. Boal, D.: Mechanics of the Cell. Cambridge University Press, Cambridge (2001)
5. De Robertis, E.D.P., and De Robertis, E.M.F.: Cell and Molecular Biology. Saunders College, Philadelphia (1980)
6. Howard, J.: Mechanics of Motor Proteins and the Cytoskeleton. Sinauer Associates Inc., Sunderland (2001)
7. Ingber, D.E.: Tensegrity: The architectural basis of cellular mechanotransduction. Ann. Rev. Physiol. **59**, 575–599 (1997)
8. Johnson, L.V., Walsh, M.L., Bockus, B.J., and Chen, L.B.: Monitoring of relative mitochondrial membrane potential in living cells by fluorescence microscopy. J. Cell Biol. **68**, 526–535 (1981)
9. Luby-Phelps, K.: Physical properties of cytoplasm. Curr. Opin. Cell Biol. **6**, 3–9 (1994)
10. Marino, A.A., IIiev, I.G., Schwalke, M.A., Gonzalez, E., Marler, K.C., Flanagan, C.A.: Association between cell membrane potential and breast cancer. Tumour Biol. **15**, 82–89 (1994)
11. Pink, D.A.: Theoretical Models of Monolayers, Bilayers and Biological Membranes. In: Chapman, D. (ed.) Bio Membrane Structure and Function, pp. 319–354. McMillan Press, London (1984)
12. Singer, S.J., Nicolson, G.L.: The fluid mosaic model of the structure of cell membranes. Science **175**, 720, 1972
13. Volkenstein, M.V.: General Biophysics. Academic Press, San Diego (1983)

Chapter 2
Structure of Membranes

2.1 The Membrane as a Barrier and a Transporter

Amphipathic molecules adsorb themselves onto air–water or oil–water interfaces, such that their head groups are facing the water environment. They aggregate to form either spherical micelles or liquid crystalline structures. In general, amphipathic molecules can be anionic, cationic, non-ionic, or zwitterionic. The relative concentrations of these surfactants in an aqueous solution will affect the solution's physical and chemical properties. At a specific value, called the critical micelle concentration, micelles containing 20–100 molecules are formed spontaneously in the solution, with the hydrophilic head groups exposed and the hydrophobic tails hidden inside the micelle. The principal driving force for micelle formation is entropic, due to a negative free energy change accompanying the liberation of water molecules from clathrates. When phospholipids are mixed in water, they form double-layered structures, since their hydrophilic ends are in contact with water while the hydrophobic ends face inwards touching each other.

Membranes have unique amphipathic properties since they possess both hydrophobic and hydrophilic parts. As described in Chap. 1, the cell membrane is the thin, nearly invisible structure that surrounds the cytoplasm of the cell. It is a continuous boundary region that completely surrounds the cell, and which also connects the endoplasmic reticulum and the nuclear membrane. Membranes are composed of phospholipids, glycolipids, sterols, fatty acid salts, and proteins. The tails that come off of the sphere represent the hydrophobic (or water-fearing) end of the phospholipid. The two long chains coming off the bottom of this molecule are made up of carbon and hydrogen. Because both of these elements share their electrons evenly, these chains have no net electrostatic charge. Non-polar molecules are not attracted to water; as a result water molecules tend to push them out of the way as they are attracted to each other. This causes molecules with no electrostatic charge not to dissolve in water. At the other end of the phospholipid there is a phosphate group and several double-bonded oxygens. The atoms at this end of the molecule are not

M. Ashrafuzzaman and J. Tuszynski, *Membrane Biophysics*,
Biological and Medical Physics, Biomedical Engineering,
DOI: 10.1007/978-3-642-16105-6_2, © Springer-Verlag Berlin Heidelberg 2012

shared equally. This end of the molecule has a charge and is therefore attracted to water. Biomembranes also compartmentalize areas of different metabolic activity in the cell, and regulate the flow into and out of cells and cell compartments. Finally, membranes are sites of key biochemical reactions.

The key functions of cell membranes can be summarized as follows:

- They are a selectively permeable barrier between two predominantly aqueous compartments.
- They allow compartmentalization of the various structures in the cell.
- They enable the formation of a stable and fluid medium for reactions that are catalyzed.
- They provide a flexible boundary between the cell or an organelle and its surrounding medium.
- They maintain an electric potential difference, participate in signal transmission to the actin cycloskeleton (via integrins), and provide adhesion forces for the cells to their substrates (controlled by membrane elasticity).
- They enable mass transport (via ion channels).

The fluid mosaic model of Singer and Nicolson [23] views the membrane as a fluid bilayer of amphipathic complex lipids with proteins embedded in it and spanning it. The relative abundance of proteins in a membrane varies from species to species, and it correlates with metabolic activity. For example, the mitochondrial wall contains large amounts of protein (52–76 %) and smaller amounts of lipids (24–48 %), facilitating its high metabolic activity. Conversely, the inactive membrane of the myelin sheath in neurons contains only 18 % proteins and 79 % lipids.

A double layer of phospholipid molecules with a variety of embedded proteins makes up the plasma membrane of a cell (see Fig. 2.1). This plasma membrane does not resemble the surface of a fluid or even the interface between two fluids. The reason for this is that it has an essentially fixed surface area, i.e., there are only a fixed number of phospholipid molecules and proteins which, when packed together, make up the membrane. Each lipid molecule or protein has a preferred surface area so, unlike the surface of a fluid, the plasma membrane is, for practical purposes, inextensible.

The various components of membranes are subject to rapid movements. Rapid lateral movement of lipids is characterized by a diffusion constant of approximately $10^{-8}\,\mathrm{cm}^2/\mathrm{s}$, while those of proteins range between 10^{-10} and $10^{-12}\,\mathrm{cm}^2/\mathrm{s}$. On the other hand, flip-flop movements across the membrane are slow, of the order of $10^{-5}\,\mathrm{s}$. Indeed, the phospholipids of the membrane may undergo a phase transition from a gel phase to a liquid crystal phase. This may take place as a result of changing the ambient temperature, external pressure, or even membrane composition.

A cell membrane regulates transport of materials and signals across it, between internal and external regions with different physiological states. The barrier properties of membranes can be both specific and non-specific, that is, the mode of barrier action is not identical in all cases; membrane constituents play important roles.

Trans-membrane osmotic pressure, an electrostatic imbalance between the outer and inner regions, various membrane constituents—all of these factors play important independent and collective roles in characterizing the membrane's barrier properties. The barrier properties are due to a combination of different physical effects, (e.g., electrical, mechanical, geometrical etc.) and chemical effects (e.g., chemical species concentrations, the value of pH, etc). Due to the various dynamics continuously occurring inside and outside the membrane, its barrier properties also are subject to change. Furthermore, they are strongly time-dependent functions. Different physiological conditions cause perturbations in the membrane barrier properties, often temporarily—but there can also be permanent changes occurring mainly due to various chronic diseases, aging, and other physiological changes on a longer timescale. A single observation of the membrane using a specific technique cannot always find key clues, since effects originate from many sources. Traditional biological approaches, therefore, need to go beyond simple observations and descriptive characterization, and instead explore physical, chemical, as well as engineering technologies to be used in membrane science. All these techniques, when combined, have improved our understanding of the membrane seen as just a barrier. The applications of science and technology to date have made it possible to enable tracing the origins of many static and dynamic processes taking place inside and near membranes. Such approaches help us not only understand the membrane itself, but may also help find avenues for further development of scientific approaches to improved drug discovery using membrane-based technology. The reader will be exposed to this crucial issue via the chapters that follow.

2.2 Membrane Constituents

Lipids are the primary components of a biological membrane. Two layers of lipids make a bilayer, and the lipids align in such a way that the head groups point in outward directions in both lipid monolayers. Electrolytes and water molecules are expelled to the exterior of the membrane, while the inner membrane layer stays inside a cellular compartment.

The membrane structure looks deceptively simple, but complex static and dynamical phenomena take place in this crucial cellular component. We describe many of these phenomena in later chapters. Here we only wish to mention that the membrane constituents such as proteins and hydrocarbons, together with lipids continuously form, break, and translocate between different complex structures (e.g., ion channels, defects, etc.) inside and across membranes, which can be responsible for changing the membrane's insulating properties. As a result, materials such as ions, water molecules, other small molecules, etc. may pass through membranes.

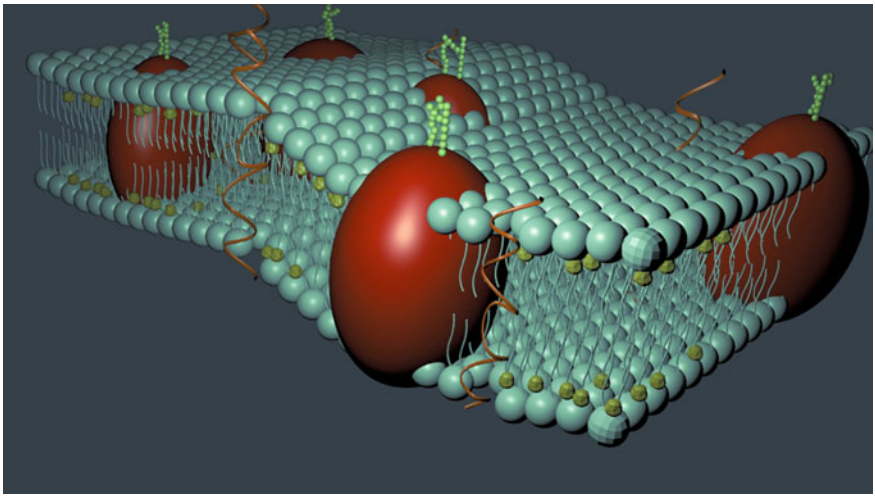

Fig. 2.1 A simplified membrane structure is presented here [2]. Two lipid monolayers are the primary components of a membrane. Near lipid head groups (*light blue color*) are seen the cholesterol molecules residing in the hydrophobic region. Globular proteins (*in red*) are shown to reside across the membrane. Alpha-helical proteins have both hydrophilic and hydrophobic parts. Membrane curvature and thickness change, which is also schematically diagrammed here. For simplicity, we did not include the presence of different ion channels, or other complicated membrane protein structures

2.3 Characteristics of Membranes

2.3.1 Physical Characteristics of Membranes

A membrane's primary role is to serve as a barrier as well as a transporter. It naturally serves as a compartment to ensure a controlled transport of material and information between the cell's inner and outer regions. A membrane maintains a constant osmotic pressure profile and a fairly constant (average) geometric thickness, which excludes other material such as electrolytes, water molecules, etc. from its vicinity. A specific back-to-back arrangement of lipids of different types, a possible presence of cholesterol, various types of membrane proteins and hydrocarbons, etc., taken together form the structure of a layer membrane with a certain approximately constant thickness. Membranes with a well-organized structure are characterized by observable geometric and physical properties, e.g., liquid crystalline structure [15], mechanical stiffness [1], capacitive effects [1], etc.

A membrane's mechanical rigidity is one of the most fundamental physical properties that have been investigated (Fig. 2.1). Suppose we increase the osmotic pressure of a cell. The cell will try to swell but this is prevented because the surface area of the plasma membrane is nearly fixed, i.e., an elastic stress will be built up inside the membrane and if this is too great the cell will burst—a condition called lysis.

To find the stress at which the membrane will burst suppose we cut the membrane along some line of length ℓ. To prevent the two sides of the cut from separating, a force, F, must be present which is proportional to ℓ. Writing $F = \gamma\ell$, then, the proportionality constant γ is called the elastic tension in the wall. This tension is not the surface tension, T, of a fluid, but it does play a similar role. The excess pressure inside a bubble of radius R, over and above atmospheric pressure, is $2T/R$. It turns out that a similar relation to this may be used to compute the excess pressure ΔP inside a spherical pressure vessel, such as a membrane, if we replace the surface tension T with the elastic tension γ. Thus we have:

$$\Delta P = \frac{2\gamma}{R} \tag{2.1}$$

The elastic stress, σ, inside the membrane is related to the elastic tension by

$$\gamma = D\sigma \tag{2.2}$$

where D is the wall thickness. The reason for this is that the surface area of the cut is ℓD and hence, the force per unit area on the surface of the cut is $F/\ell D = \gamma/D$, which is the stress of the membrane wall. From the two equations above, the elastic stress, σ, is given by

$$\sigma = \frac{R\Delta P}{2D} \tag{2.3}$$

so that the cell will burst when this stress exceeds the fracture stress of the material from which the cell membrane is made.

A large amount of diffusion in biological organisms takes place through membranes. These membranes are very thin, typically ranging from 65×10^{-10} to 100×10^{-10} m across. Most membranes are selectively permeable; that is, they allow only certain substances to cross them because there are pores through which substances diffuse. These pores are so small (from 7×10^{-10} to 10×10^{-10} m) that only small molecules can get through. Other factors contributing to the semi-permeable nature of membranes have to do with the chemistry of the membrane, cohesive and adhesive forces, charges on the ions involved, and the existence of carrier molecules. Diffusion through membranes is a relatively slow process.

In order to provide a simple mathematical description of passive diffusion across a membrane, we can apply Fick's Law to the transport of molecules across a membrane of thickness Δx. Assume also that the concentration of the solute on the left side is c_{L} and that on the right side is c_{R}. The solute diffusion current, I, across the membrane, according to Fick's Law, is given by [13]

$$I = k\frac{D}{\Delta x}A\Delta c \tag{2.4}$$

where $\Delta c = c_{\mathrm{R}} - c_{\mathrm{L}}$, k is the diffusion constant and A is the cross-sectional area of the membrane.

Under normal conditions, the physical characteristics stay constant, but in the case of abnormality (due to disease or disordered conditions) perturbations in the physical characteristics are inevitable. Different order parameters in lipid membranes are also sensitive to temperature and chemical compositions. Temperature-dependent alteration of physical properties like lipid phase properties, different dynamical properties etc. vary. The chemical composition-dependent capacitive effects of membranes also vary. Here, we should mention that plasma membranes are considered to be excellent insulators and dielectrics with a capacitance of the order of 1 μF. Membrane capacitance is a measure of the quantity of charge moving across unit area of the membrane to produce unit change of the membrane potential (which will be discussed later in detail).

2.3.2 Biochemical Characteristics of Membranes

A membrane maintains a chemical or biochemical environment inside it which differs from its interior and exterior environments. Since Robert Hooke's discovery of a cell in 1665, many further developments have been made in the understanding of the various properties of the interior and exterior environments of a cell. In the subcellular compartments exist the membrane, cytoskeleton, genetic material, organelles, etc. while structures outside the cell wall consist of capsules, flagella, fimbriae, etc. These two structural arrangements exist in different physical and chemical environments. The membrane's interior region is very different and unique. In the absence of water molecules and at low dielectric condition [20] it always maintains a gradient in most of the biochemical characteristics, compared to the exterior. For example, the membrane around peroxisomes shields the cell from peroxides. A membrane's most important selective permeability characteristics couple with the geometric size, charge, and chemical properties of the atoms and molecules attempting to cross it, and determine whether the biochemical properties [4] of both together allow the diffusion/permeabilization of the particles across the membranes. A membrane's transport proteins also play a very important role to allow particles to cross through the membranes. We discuss this issue in detail in Chap. 4.

2.3.3 Electrical Characteristics of Membranes

Membrane Potential

First measurements of the electrical properties of cell membranes were made on red blood cells by H. Fricke, and on sea urchin cells by K.S. Cole in 1937, and it was found that membranes act as capacitors maintaining a potential difference between oppositely charged surfaces composed mainly of phospholipids with proteins embedded in them. A typical value of the capacitance per unit area C/A is about 1 μF/cm^2

for cell membranes. This relates to the membrane's dielectric constant κ via the following equation:

$$\frac{C}{A} = \frac{\kappa \varepsilon_0}{d} \tag{2.5}$$

where $\varepsilon_0 = 8.85 \times 10^{-12}\,\mathrm{C}^2/\mathrm{Nm}^2$, giving a value of $\kappa \cong 10$, which is greater than $\kappa \cong 3$ for phospholipids above, resulting from the active presence of proteins. The cellular membrane is much more permeable to potassium ions than sodium ions (the intercellular fluid contains primarily sodium chloride) in the normal resting state, which results in an outward flow of potassium ions, and the voltage inside the cell is $-85\,\mathrm{mV}$. This voltage is called the resting potential of the cell. If the cell is stimulated by mechanical, chemical, or electrical means, sodium ions diffuse more readily into the cell since the stimulus changes the permeability of the cellular membrane. The inward diffusion of a small amount of sodium ions increases the interior voltage to $+60\,\mathrm{mV}$, which is known as the action potential of the cell. The membrane again changes its permeability once the cell has achieved its action potential, and potassium ions then readily diffuse outward so the cell returns to its resting potential. Depending on the state of the cell, the interior voltage can therefore vary from its resting potential of $-85\,\mathrm{mV}$ to its action potential of $+60\,\mathrm{mV}$. This results in a net voltage change of $145\,\mathrm{mV}$ in the cell interior. The voltage difference between the two sides of the membrane is fixed by the concentration difference. Having a salt concentration difference across a membrane, and allowing only one kind of ion to pass the membrane produces a voltage difference given by

$$V_\mathrm{L} - V_\mathrm{R} = \frac{k_B T}{e} \ln\left(\frac{c_\mathrm{R}}{c_\mathrm{L}}\right) \tag{2.6}$$

which is called the Nernst potential. This is the basic mechanism whereby electrical potential differences are generated inside organisms. Note that the Nernst potential difference only depends on the concentration ratio.

The membrane potential, also known as the transmembrane potential, quantifies the electrical potential difference between the interior and exterior of a cell. If the potential of the region just outside the membrane is V_o, and the potential of the region just inside the cell near the membrane is V_i, the membrane potential of the cell is $V_i - V_o$. Using the traditional definition of electrical potential, we can also define the membrane potential to be the energy required to transfer a unit charge from the exterior to the interior of a cell, crossing through the membrane. For example, if the transfer of a Q-coulomb charge from the exterior to the interior of a cell requires an energy of W joules, the potential difference (and hence the membrane potential of the cell) will be W/Q volts.

Both cellular interior and exterior regions exist with electrical conditions represented by electrical potentials. The electrical potentials of both regions depend mainly on the constituents comprising the regions. The fluids on both sides of the mainly lipid membrane contain high concentrations of various ions—both cations and anions. Among the cations, sodium (Na^+), potassium (K^+) and calcium (Ca^{2+})

are worth mentioning, while chloride (Cl^-) is the most important anion. Although both cations and anions exist in both the interior and exterior regions of a cell the concentrations of sodium and chloride ions in the exterior is higher than that in the interior. Similarly, potassium ions exist with a higher concentration in the interior region than the exterior region of a cell. The interior region is importantly characterized by a dominant presence of protein anions.

Due to the differences in charge types and concentrations between intracellular and extracellular regions, they exist with different potential conditions and, as a result, the membrane creates an electric field determining the membrane potential. The membrane therefore plays the role of the cell's electrical battery, by providing a continuous source of electrical energy originating from the potential imbalance between the intracellular and extracellular regions. This source of electrical energy also plays important roles in regulating many cellular processes, like transmitting signals between different parts of a cell, exciting ion channels across the membrane, etc. As the concentrations of each of the ions present in the intracellular and extracellular regions are different, there always exists a concentration gradient for each ion species across the cellular membrane. This gradient creates osmotic pressure for the ions to cross through the membrane. Potassium ions try to move from the intracellular to the extracellular region, while sodium and chloride ions try to flow in the opposite direction. The natural tendency of the movement of charges across the membrane causes changes in the membrane resting potential. Similarly, the changes in the membrane resting potential, due to natural or artificial stimuli, drive charges across the membrane. These rather slow dynamical processes are crucial to the normal functioning of the cell.

Resting Potential

Resting potential is simply the potential of a membrane's interior in the absence of any excitation. That is to say, this is the membrane potential of non-excitable cells, or the membrane potential of an excitable cell in the absence of any excitations. In addition to the uneven distribution of other charges as explained earlier, Na^+ concentrations of about 10 times higher on the outside and K^+ concentrations of 20 times higher on the inside of a membrane can cause huge charge density gradients. As a result, under conditions of rest, or in the absence of any excitation, the cell membrane is polarized, maintaining an effective electrostatically negative charge in the interior, which accounts for a negative interior resting potential on the order of -70 mV (Fig. 2.2).

As described above, the chemical gradient across the membrane for cells at rest causes a resting potential to be built. ATP-powered ion pumps or ion transporters play crucial roles in this process. In an animal cell, plasma membrane sodium-potassium pumps (Na^+ or K^+-ATPase) help to build sodium and potassium gradients across the membrane. The resting potential may also be altered due to the change of acidic environment across the cells. For example, in cancer cell membranes, due to elevated acidic conditions, the resting potential may be considerably altered.

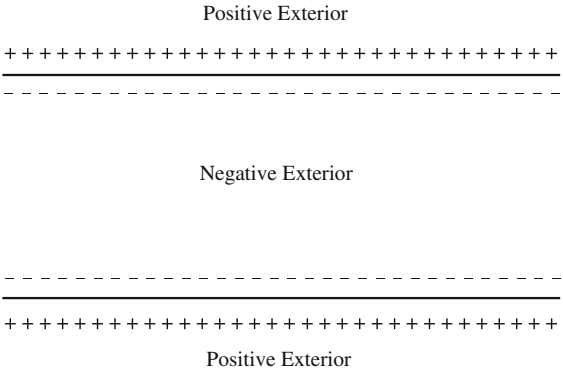

Fig. 2.2 An approximately −70 mV potential in the membrane interior region, relative to the membrane exterior region, is a general electrical condition found in normal cells. This is due to a resultant negatively charged interior and a positively charged exterior of the cell membrane

Resting Potential and the Neuron Membrane

The brain communicates with other parts of the body through neuron cells. The resting potentials in neuron membranes help transfer the messages in the form of electrical pulses. The membrane of a neuron is about 8 nm thick, containing two thick layers of fat molecules embedding larger protein molecules. In the polarized state, the membrane effectively maintains a −70 mV resting potential, due to uneven concentrations of anions and cations on both sides of the membrane. In the polarized state, the membrane is permeable to K^+ ions but does not allow larger Na^+ ions to cross through it. A nerve impulse is associated with information transfer along the axon towards the axon terminal. In this way, the transmission of information from one neuron to other neurons or different types of cells occurs. The nerve impulse or action potential is created by a depolarizing current. The passage of electrical current happens due to the movement of sodium and potassium ions across the membrane.

Action Potential

An action potential is an electrical event which lasts for a short of period of time and involves the cell membrane's electrical potential, which rapidly rises and then falls following a special type of time-dependent trajectory and spatial propagation. A typical action potential is shown in Fig. 2.3.

In several types of excitable cells such as neurons, muscle cells, endocrine cells, etc., action potentials are found to be generated [17]. An action potential occurs during the time when a neuron sends a signal down an axon which travels away from the cell body. These potentials are caused by an exchange of ions across the membrane of a neuron. Any stimulus first causes sodium channels to open; with it sodium ions move into the neuron leading the neuron to experience depolarization. Potassium channels usually take longer to open, but when they do, potassium starts moving out of the cell, which reverses the depolarization process. Consequently,

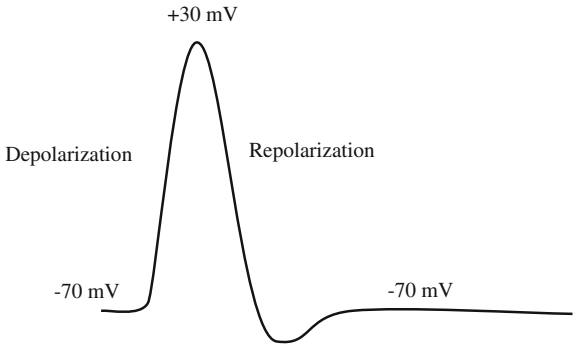

Fig. 2.3 A schematic diagram showing an action potential, illustrating electric depolarization and repolarization of the cell membrane. The membrane potential rises from $-70\,\text{mV}$ to $+30\,\text{mV}$ within about 1 ms before repolarization forces the trend to reverse, and finally the resting potential goes back to $-70\,\text{mV}$ after briefly experiencing a hyperpolarized state

sodium channels start to close. At this repolarization phase, the action potential goes past the $-70\,\text{mV}$ level, a state referred to as hyperpolarization. The ion concentration across the cell gradually returns to the resting level, and the cell returns to the usual resting potential of $-70\,\text{mV}$.

As discussed earlier, depolarization across a plasma membrane generates an action potential. Certain external stimuli reduce the charge across the plasma membrane. A stimulus may originate from various sources. Mechanical stimuli like stretching, sound waves, etc. activate mechanically gated sodium channels across the membrane. Certain neurotransmitters like acetylcholine open ligand-gated sodium channels. Various electrical impulses may also stimulate and cause depolarization. The favorable diffusion of sodium ions into the cell locally reduces the membrane's resting potential. If the reduction is considerable, e.g., if the potential is reduced to the threshold voltage level (in mammalian neurons, about $-50\,\text{mV}$), an action potential is generated in the cell. This kind of action potential usually lasts for less than 1 ms. Action potentials generated by voltage-gated calcium channels may last much longer, which is of the order of 100 ms or more. The action potential is very much organ-specific and is accompanied by various complexities because, in different parts of the body, the stimuli appear from different types of sources. For instance, in some types of neurons, a long burst of rapidly emitted sodium spikes appears due to the slow calcium spike-induced driving force, whereas, in cardiac muscle cells, muscle contraction takes place due to the rapid onset of a calcium spike provoked by an initial fast sodium spike.

The Nernst Potential and Membrane Potential

In physiology, the Nernst equation (mentioned above) finds its application in determining the potential of an ion across a membrane. The general form of the potential can be written as

$$V_{\text{Nernst}} = \left(\frac{RT}{zF}\right) \ln\left(\frac{[N]_{\text{out}}}{[N]_{\text{in}}}\right) \tag{2.7}$$

The Nernst equation determines the equilibrium potential, often called 'the Nernst potential' for an ion across the membrane. From the equation, it is clear that this potential depends on the ion concentrations outside ($[N]_{\text{out}}$) and inside ($[N]_{\text{in}}$) of the membrane, the valence of the ionic species, z, and the absolute temperature in Kelvin T. The constant R is the universal gas constant ($R = 8.314\,\text{J}\,\text{K}^{-1}\,\text{mol}^{-1}$) and F is the Faraday constant ($F = 96{,}485\,\text{C}\,\text{mol}^{-1}$). The development of a Nernst potential depends on the following two criteria: (i) the concentration gradient of an ion across the membrane, and (ii) selective ion channels creating a pathway for a specific type of ion flow across the membrane. It is, therefore, natural to associate the Nernst potential with an ion type. Nernst or equilibrium potentials V_{Na}, V_{K}, V_{Cl}, V_{Ca}, etc. can be found for Na^+, K^+, Cl^-, Ca^{2+}, etc. ionic species respectively. In the case when there exists only one ionic species in the system, and/or channels due to ion specificity of the channels, the corresponding Nernst or equilibrium potential is also the membrane potential (V_m). However, in cases where there exists the flow of different ions across the membrane, the membrane potential is the sum of all Nernst potentials referring to ions, normalized with the corresponding conductance. If there are a number of ions flowing across the membrane, the following relation exists:

$$V_m = \sum_i \left(\frac{g_i}{G}\right) V_{\text{Nernst},i} \tag{2.8}$$

where $V_{\text{Nernst},i}$ and g_i are respectively the Nernst potential and conductance (inverse Ohmic resistance) through the membrane, corresponding to the ion indexed i. Here, $G = \sum_i g_i$.

In physiology, the most common potentials due to ion flows through a membrane are V_{Na}, V_{K}, V_{Cl}, etc. If Na^+, K^+, Cl^- flow across a membrane with the corresponding Nernst potentials V_{Na}, V_{K}, V_{Cl}, we find the membrane potential to be represented by the following equation:

$$V_m = \left(\frac{g_{\text{Na}}}{G}\right) V_{\text{Na}} + \left(\frac{g_{\text{K}}}{G}\right) V_{\text{K}} + \left(\frac{g_{\text{Cl}}}{G}\right) V_{\text{Cl}} \tag{2.9}$$

Here, G is the sum of conductances g_{Na}, g_{K}, g_{Cl}, g_{Ca} corresponding to the Na^+, K^+, Cl^-, Ca^{2+} ions across the membrane, respectively.

In the presence of several ions flowing across the real cell membrane, the equilibrium of the cell depends on the relative membrane permeability for these ions. To determine the membrane resting potential, the following Goldman–Hodgkin–Katz (GHK) equation is used:

$$V_m = \left(\frac{RT}{F}\right) \ln\left(\frac{\sum_i P_i(N_i^+)[N_i^+]_{\text{out}} + \sum_j P_j(N_j^-)[N_j^-]_{\text{in}}}{\sum_i P_i(N_i^+)[N_i^+]_{\text{in}} + \sum_j P_j(N_j^-)[N_j^-]_{\text{out}}}\right) \tag{2.10}$$

Here, the symbols P stand for the respective relative permeabilities of the ions, the Ns in the square brackets stand for the ion concentrations, $+/-$ stand for

positive/negative species, and *out*/*in* stands for extracellular /intracellular regions, respectively. For example, in a real cell, in which Na^+, K^+ and Cl^- ions are the major contributors to the membrane potential, the GHK equation can be written as

$$V_m = \left(\frac{RT}{F}\right) \ln\left(\frac{\left(p_K[K^+]_{out} + p_{Na}[Na^+]_{out} + p_{Cl}[Cl^-]_{in}\right)}{\left(p_K[K^+]_{in} + p_{Na}[Na^+]_{in} + p_{Cl}[Cl^-]_{out}\right)}\right) \tag{2.11}$$

Here, $[K^+]$, $[Na^+]$ and $[Cl^-]$ represent ion concentrations with subscripts out and in standing for the region (outside and inside) of the cell. Further, p_K, p_{Na} and p_{Cl} are the relative membrane permeabilities of the ions K^+, Na^+ and Cl^-, respectively. Normally, permeability values for ions are reported as relative permeabilities (unitless) with p_K having the reference value of one.

The Membrane as a Capacitor

A cell membrane separates charges on both sides of it. The inner core of a membrane experiences a low dielectric state, while the outside experiences a high dielectric state [20]. The membrane therefore generally acts as an insulator, with conducting media on both sides.

Based on a simple electrostatic analysis, we know that the capacitance of an object is defined as the amount of charge separated across it and creating a potential difference between the two terminals. That is, if a potential V can hold a charge Q across a capacitor, the capacitance C can be defined as

$$C = \frac{Q}{V} \tag{2.12}$$

A cell membrane structure suggests a model where a relatively low dielectric medium is surrounded by two conducting media on both sides (intracellular and extracellular regions). This makes a membrane equivalent to a leaky capacitor, since ions are still allowed to flow through it.

To calculate the membrane capacitance, we need to use standard electrostatics with Coulomb's law applied to an equivalent model structure for the membrane, which produces a separation of two parallel conducting plates by an insulating medium. Here, the membrane is comparable to an insulating medium. The capacitance of a cell membrane can thus be defined as

$$C_m = \frac{\kappa\varepsilon_0}{d} \tag{2.13}$$

Here, κ is the dielectric constant for the membrane's inner core, ε_0 is the permittivity of free space, and d is the membrane thickness. A low dielectric medium (inner layer) exists in between two conducting media (outside membrane). Depending on the variations in the values of $\frac{\kappa\varepsilon_0}{d}$ in various types of cells, the values of

capacitance of the corresponding membranes may vary. However, a typical value is often found to be of the order of $1.0\,\mu\text{F/cm}^2$. Most importantly, it is worth mentioning that the cholesterol level, phospholipids and glycolipids, membrane proteins, hydrocarbons, etc. all together are responsible for yielding a certain value of membrane capacitance. Unlike animal cytoplasmic membranes, bacteria (prokaryotes) do not generate cholesterol, which may account for a considerable effect on their membranes' electrical properties, including their capacitance.

Understanding the capacitive effect of the membrane helps in analyzing the membrane's electrical properties, through a model often referred to as the *Electrical Circuit Model of the Cell Membrane* .

Here, the membrane is considered as a capacitor in parallel with a resistor. The (not necessarily Ohmic) resistance acts against the flow of ions across the membrane, which is represented by ion current I_{ion}. The capacitive current is given by $C_m \frac{\mathrm{d}V}{\mathrm{d}t}$. The capacitive current and the ion current together conserve the current flow between the inside and outside of the membrane. Therefore,

$$C_m \frac{\mathrm{d}V}{\mathrm{d}t} + I_{\text{ion}} = 0 \tag{2.14}$$

The analytical calculation of I_{ion} is a long-standing challenge. The following GHK current equation is one such expression for I_{ion} across the membrane:

$$I_{\text{ion}} = \frac{D}{L} \frac{z^2 F^2}{RT} V \frac{[N]_{\text{in}} - [N]_{\text{out}} e^{\frac{-zFV}{RT}}}{1 - e^{\frac{-zFV}{RT}}} \tag{2.15}$$

Here, D denotes Einstein's diffusion constant, L is the membrane thickness, and $[N]_{\text{in}}$ and $[N]_{\text{out}}$ are the ion concentrations inside and outside the cell across the membrane, respectively (see Fig. 2.4).

2.3.4 Excitability and the State of the Membrane Potential

Neurons, muscle cells, etc., are collectively called excitable cells, since they use their membrane potentials as signals. The operation of the nervous system, muscle contraction, etc., depends on the generation and propagation of electrical signals, and membrane potentials in these cases mainly serve this purpose. We have earlier described in detail how the membrane potential can be regulated by controlling certain cellular processes, such as the control of the ionic current carrying ion channels across membranes.

Electrical signaling in cells depends largely on the type of cell involved (see e.g., [17]). To understand it better, the cells are grouped into two categories, namely, non-excitable cells and excitable cells. Non-excitable cells maintain stable equilibrium potentials. If an externally applied current perturbs the membrane potential of a non-excitable cell, the withdrawal of the current ensures that the potential returns to

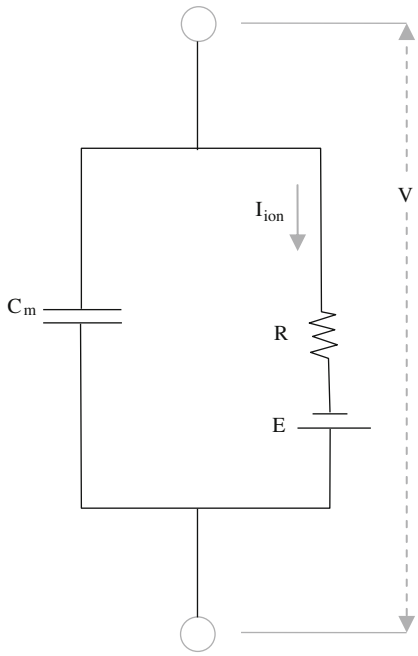

Fig. 2.4 Cell membrane representation in terms of an equivalent electric circuit showing capacitive effects. A parallel capacitor and resistor combination in schematic form represents the equivalent electrical circuit

its equilibrium state. Epithelial cells, photoreceptors, etc. fall into the non-excitable cell category.

Different research findings report that non-excitable cells are found not to generate all-or-none action potentials in response to depolarizing stimuli, due to a lack of voltage-gated Na^+ or Ca^{2+} channels [3, 5, 7, 22]. Consequently, membrane potential changes are proposed to influence the localized (intracellular) concentration of Ca^{2+} ions ($[Ca^{2+}]_i$) responses, mainly by altering the driving force for Ca^{2+} entry through ligand-gated or second messenger-operated channels. However, it was reported [16] that during stimulation of a non-excitable cell (e.g. metabotropic purinoceptors), membrane depolarization evokes an increase in Ca^{2+} concentration in the interior cellular regions, primarily due to the release of Ca^{2+} from intracellular stores. Although depolarization in non-excitable cells was found to result in a decrease in $[Ca^{2+}]_i$, hyperpolarization causes an increase of $[Ca^{2+}]_i$ during activation of mast cells, lymphocytes, and related cell lines [6, 14, 21]. The results of this research suggest that the electrogenic influences in non-excitable cells may also originate from various organ-specific mechanisms.

On the other hand, in excitable cells, a strong externally applied current causes the membrane potentials to undergo a large excursion, called an ‘action potential’, before eventually returning to rest. Most neurons, cardiac cells, smooth and skeletal muscle cells, secretory cells, etc., fall into the excitable cell category. In this section of the chapter, we mainly address the aspects of electrical signal propagation and its mathematical modeling in excitable cells. This is a century-old problem, which

has achieved a very high level of understanding following a few ground-breaking discoveries, such as the seminal work of Alan Hodgkin and Andrew Huxley, who in 1952 developed the first quantitative model of the propagation of an electrical signal along a squid giant axon. The Hodgkin–Huxley theory is applicable, not only to electrophysiology, but also to applied mathematics through appropriate modifications. The creation of a new field of mathematics called 'the study of excitable systems' has been made possible, thanks to the remarkable simplification and extensions of the Hodgkin–Huxley theory. We provide more details below.

The Hodgkin–Huxley Model of the Action Potential: A Quantitative Model

The cell membrane has well-defined biochemical and biophysical characteristics. We have briefly described these two aspects earlier in this chapter. The biophysical characteristics of a cell membrane are represented by the generally accepted Hodgkin–Huxley model. The lipid bilayer is represented as a capacitor—the low-dielectric ($\varepsilon \sim 2$) region inside the membrane relative to the outside region with high dielectric values ($\varepsilon \sim 80$) [20] makes the cell membrane an almost perfect capacitor. Voltage-gated and leak ion channels are represented by nonlinear (g_{n}) and linear (g_{L}) conductances, respectively. The electrochemical gradients driving ion flow are represented by batteries (E_{n} and E_{L}), and ion pumps and exchangers are represented by current sources (I_{p}). The voltage values for the batteries are determined from the Nernst potentials of specific ionic species.

In an idealized cell, with a small portion of the membrane represented as equivalent electrical circuit, we can apply the Hodgkin–Huxley model for calculating the membrane current (I_m) by the following current equation:

$$I_m = C_m \frac{\mathrm{d}V}{\mathrm{d}t} + I_{\mathrm{K}} + I_{\mathrm{Na}} + I_{\mathrm{L}} \tag{2.16}$$

Here, V is the membrane voltage, I_{K} and I_{Na} are the potassium and sodium currents, respectively, and I_{L} is the sum of all leakage currents due to the flow of other ions moving passively through the membrane.

The charge stored in the capacitive membrane is $q_m = C_m V$ where V is the voltage across the capacitor, which is comparable to the transmembrane potential. Earlier in this chapter, we have explained how currents across the membrane are conserved quantities, which is possible due to the fact that the cell membrane is modeled as a capacitor in parallel with ionic currents. Now, if ionic currents are considered to depend on both transmembrane voltage V and time t, the membrane capacitive current follows the formula

$$C_m \frac{\mathrm{d}V}{\mathrm{d}t} + I_{\mathrm{ion}}(V, t) = 0 \tag{2.17}$$

In the Hodgkin–Huxley theory, besides the main currents, sodium and potassium ion currents across the membrane, all other small currents are combined to form a leakage current I_L.

In the squid giant axon the I–V curves of open Na^+ and K^+ channels are approximated by linear equations. Therefore, the membrane capacitive current equation becomes:

$$C_m \frac{dV}{dt} = -g_{Na}(V - V_{Na}) - g_K(V - V_K) - g_L(V - V_L) + I_{ext} \tag{2.18}$$

Here, I_{ext} is the externally applied current, and g_{Na}, g_K and g_L represent conductances (reciprocal of Ohmic resistance) for Na^+ and K^+ ions and other ions responsible for leakage currents, respectively. Voltages V_{Na}, V_K, and V_L are membrane resting potentials, corresponding to Na^+, K^+ ions and other leakage ions across the membrane. The previous first-order ordinary differential equation can be rewritten as a more general form of equation, representing a capacitive current of the membrane according to:

$$C_m \frac{dV}{dt} = -g_{eff}(V - V_{eq}) + I_{ext} \tag{2.19}$$

Here, $g_{eff} = g_{Na} + g_K + g_L$ is the effective conductance across the membrane, and $V_{eq} = (g_{Na}V_{Na} + g_K V_K + g_L V_L)/g_{eff}$ is the membrane resting potential.

Specifically, in voltage-gated ion channels, the channel conductance g_i is a function of both time and voltage ($g_n(t, V)$), while in leak channels, g_L is a constant (g_L).

The above description can be summarized in a way similar to that in the original paper of Hodgkin–Huxley [12]. The electrical behavior of a membrane may be represented by a network, as shown in Fig. 2.5. Here, current can be carried through the membrane either by charging the membrane capacitor or by the movement of ions Na^+, K^+, etc. through the corresponding equivalent resistors in parallel. The ionic current corresponding to a specific ion is proportional to the difference between the membrane potential and the equilibrium potential for a specific ion. Here, the proportionality constant is the Ohmic conductance for the corresponding ion.

Voltage- and Time-Dependent Conductance in the Hodgkin–Huxley Model

As explained earlier, the total membrane current I_m can be subdivided into two main categories, which are capacitive currents and ionic currents. Thus, under normal conditions the following equation is valid:

$$I_m = C_m \frac{dV}{dt} + g_{Na}(V - V_{Na}) + g_K(V - V_K) + g_L(V - V_L) \tag{2.20}$$

This equation gives the values of the membrane capacitance that are independent of the magnitude and sign of V, and are little affected by the time course of V (see Table 1

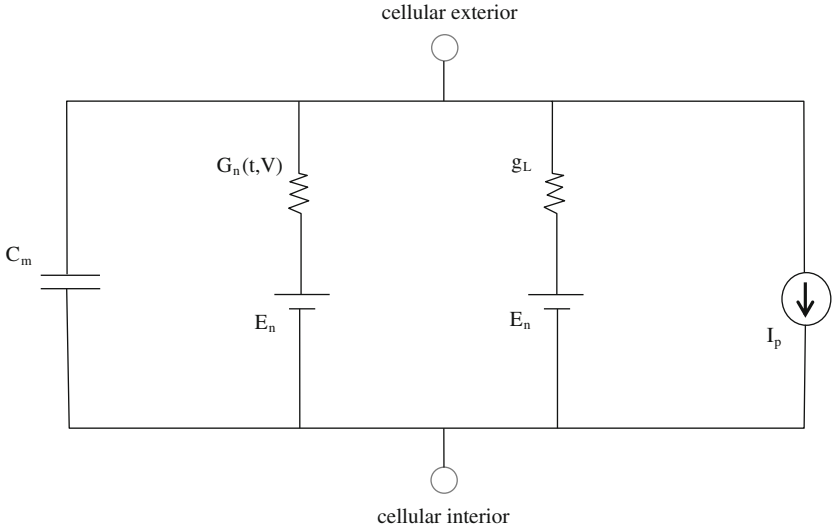

Fig. 2.5 A capacitor–resistor circuit representation of the cell membrane. This is a more detailed form of the equivalent circuit representation presented earlier in this chapter

of [8]). The evidence for the capacitive currents and ionic currents to be parallel was well-established in the study by Hodgkin et al. [8]. A major reservation, however, is that the earlier equation takes no account of dielectric loss in the membrane. Since the capacitive surge was found to be reasonably close to that calculated for a perfect capacitor [8], it was then predicted that the mentioned dielectric condition inside the membrane would not change the structure of the equation dramatically. So far this has been found consistent with the data obtained using modern approaches that include other constituents inside membranes.

The Potassium Conductance

Hodgkin and Huxley investigated the time dependence of ionic conductance both theoretically and experimentally. In their experimental investigations they studied in detail, for example, the case of potassium ion conduction. Based on their famous 1952 paper [12], it is clear that the rise of potassium conductance associated with depolarization of a potential is followed by the fall of conductance associated with repolarization of the resting potential. Here, the nonlinear rise (depolarizing effect) of conductance g_K is found to be mathematically very well-fitted by the function $(1 - e^{-t})^4$ while the fall is approximately by the function e^{-4t}. These two different 4th-order mathematical forms explain nicely the marked inflection for the rise, with a simple exponential for the fall for g_K. A similar mathematical fit to experimental data using other functional forms could also be possible, but might require other

terms, e.g., a term representing inactivation would be necessary in the case of a third power in the exponential power series expansion, making it much less elegant and not convincing.

Following a detailed analysis [12], the generalized form of g_K can be constructed as

$$g_K = \left(g_{K-}^{1/4} - \left[g_{K-}^{1/4} - g_{K0}^{1/4}\right]e^{-t/\tau_n}\right)^4 \tag{2.21}$$

where g_{K-} is the asymptotic value of the conductance, and g_{K0} is the conductance at $t = 0$. Also, τ_n is the inverse of the sum of the rate constants describing the timescale of the resultant net inward flow of ions. The proposed equation is a best fit to the experimental results, as presented in the original work [12].

The Sodium Conductance

The transient change in sodium conductance g_{Na} was described by considering two variables, both of which obey first-order equations. Following a few formal assumptions [12], g_{Na} was found to fit very well to experimental observations by taking the following form:

$$g_{Na} = g'_{Na}[1 - e^{-t/\tau_m}]^3 e^{-t/\tau_h} \tag{2.22}$$

Here, g'_{Na} is the value which the sodium conductance would attain in the case when the proportions of the inactivating molecules on the outside boundary of the membrane τ_m and τ_h are the inverse values of the net transfer rate constants for inside and outside directions, respectively.

A detailed analysis of the rate constants and other related aspects of membrane conductance described in the Hodgkin–Huxley models is not only interesting but also very important. However, due to space limitations and the scope of this book, we invite the reader to study the original material presented in the ground-breaking papers published by this pair independently and with others in the early 1950s [8–12, 19]. Below, we discuss a few more models which were subsequently built on the basis of the Hodgkin–Huxley model in order to perform a better qualitative analysis, and to better understand the various aspects of the Hodgkin–Huxley model.

2.3.5 The FitzHugh–Nagumo Model

Before discussing the FitzHugh–Nagumo model, we first further reduce the Hodgkin–Huxley model to a more generalized form. Based on the experiments performed by Hodgkin and Huxley on the squid giant axon between 1948 and 1952, they constructed a model for patch clamp experiments. This provided a mathematical description of the axon's excitable nature. Here, a key model assumption was that the membrane contains channels for potassium and sodium ion flows. Following the

assumption made by Hodgkin and Huxley, which replaces g_{Na} and g_{K} with $g^0_{\mathrm{Na}} m^3 h$ and $g^0_{\mathrm{K}} n^4$, the equation for the membrane's capacitive current becomes

$$C_m \frac{\mathrm{d}V}{\mathrm{d}t} = -g^0_{\mathrm{Na}}\, m^3\, h(V - V_{\mathrm{Na}}) - g^0_{\mathrm{K}} n^4 (V - V_{\mathrm{K}}) - g_{\mathrm{L}}(V - V_{\mathrm{L}}) + I_{\mathrm{ext}} \quad (2.23)$$

Here, the conductances for both sodium and potassium ions are expressed in terms of some baseline values g^0_{Na} and g^0_{K}, respectively, and secondary variables m, h, and n. The variables are hypothesized as potential-dependent gating variables, whose dynamics are assumed to follow first-order kinetics, and the equation takes the following form:

$$\tau_s(V) \frac{\mathrm{d}s}{\mathrm{d}t} = s_-(V) - s; \quad s = m, h, n, \quad (2.24)$$

where $\tau_s(V)$ and $s_-(V)$ are respectively the time constant and the rate constant determined from experimental data. The above two equations, taken together, represent a four-dimensional dynamical system known as the simplified Hodgkin–Huxley model, which provides a basis for qualitative explanation of the formation of action potentials in the squid giant axon.

FitzHugh later sought to reduce the Hodgkin–Huxley model to a two-variable model, for which phase plane analysis can be carried out reasonably easily. In the Hodgkin–Huxley model, the gating variables n and h were found to have slow kinetics relative to m, and that $n + h$ assumes an approximately constant value ($\sim$0.8). As a result of these two observations, a new two-variable model, referred to as the fast-slow phase model, was proposed by FitzHugh for calculating the capacitive current of the membrane, which is as follows:

$$C_m \frac{\mathrm{d}V}{\mathrm{d}t} = -g^0_{\mathrm{Na}} m^3_-(V)(0.8 - n)(V - V_{\mathrm{Na}}) - g^0_{\mathrm{K}} n^4 (V - V_{\mathrm{K}}) - g_{\mathrm{L}}(V - V_{\mathrm{L}}) + I_{\mathrm{ext}} \quad (2.25)$$

and

$$n_s(V) \frac{\mathrm{d}n}{\mathrm{d}t} = n_-(V) - n \quad (2.26)$$

Here, a phase-space description of the action potential's formation and decay has been provided. In these equations, V and n are the fast and slow variables, respectively. The V nullcline can be defined by $C_m \frac{\mathrm{d}V}{\mathrm{d}t} = 0$ and has a cubic shape, while the n nullcline is $n_-(V)$, and it increases monotonically. Since it can be approximated by a straight line, this suggests a polynomial model reduction of the form

$$\frac{\mathrm{d}v}{\mathrm{d}t} = v(v - \beta)(1 - v) - u + I \quad (2.27)$$

and

$$\frac{\mathrm{d}u}{\mathrm{d}t} = \delta(v - \gamma u) \quad (2.28)$$

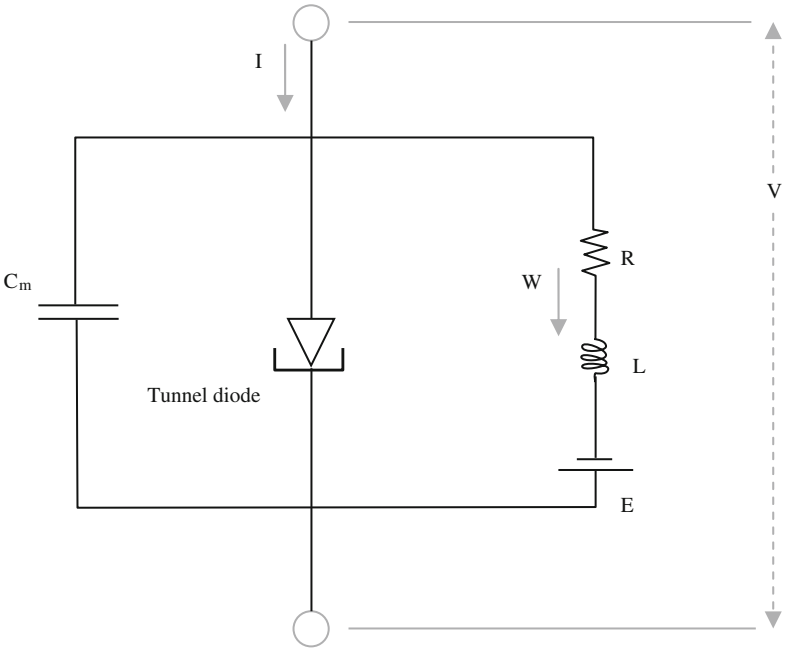

Fig. 2.6 An equivalent electric circuit diagram for the FiztHugh–Nagumo equations

The model equations have been transformed into dimensionless form, where v represents the fast variable which is the electrostatic potential, u represents the slow variable, the sodium gating variables, and β, δ and γ are constants which satisfy the conditions $0 < \beta < 1$ and $\delta \ll 1$, accounting for the slow kinetics of sodium channel. Later, Nagumo constructed a circuit using tunnel diodes for the nonlinear channel element, whose model equations are those of FitzHugh. Hence, the previous dimensionless equations are now generally accepted as the so-called FiztHugh–Nagumo model. The previous equations representing the FiztHugh–Nagumo model are often expressed in more generalized forms as:

$$\epsilon \frac{\mathrm{d}v}{\mathrm{d}t} = f(v, u) + I \tag{2.29}$$

and

$$\frac{\mathrm{d}u}{\mathrm{d}t} = g(v, u) \tag{2.30}$$

where, as described previously, the nullcline $f(v, u) = 0$ represents a cubic shape. That means that for a finite range of values of u, there are three solutions $v = v(u)$ of the equation $f(v, u) = 0$. The nullcline $g(v, u) = 0$ is assumed to have one intersection with the curve $f(v, u) = 0$.

Finally, the FiztHugh–Nagumo model represents a simplified model of the cell membrane as presented in Fig. 2.6. In this simplified model, the membrane patch consists of three components, a (membrane) capacitor, a nonlinear current–voltage device for the fast current W, and a resistor, an inductor and a battery in series for the recovery current. This circuit was built and tested in 1962 by Nagumo, a Japanese electrical engineer [18].

References

1. Ashrafuzzaman, Md., Lampson, M.A., Greathouse, D.V., Koeppe II, R.E., Andersen, O.S.: Manipulating lipid bilayer material properties by biologically active amphipathic molecules. J. Phys.: Condens. Mat. **18**, S1235–S1255 (2006)
2. Ashrafuzzaman, Md., Tuszynski, J.A.: Ion pore formation in lipid bilayers and related energetic considerations. Curr. Med. Chem. **19**, 1619–1634 (2012)
3. Berridge, M.J.: Elementary and global aspects of calcium signalling. J. Physiol. **499**, 290–306 (1997)
4. Mannella, C.A., Bonner, W.D., Jr.: Bio chemical characteristics of the outer membranes of plant mitochondria. Biochim. Biophys. Acta **413**, 213–225 (1975)
5. Clapham, D.E.: Calcium signaling. Cell **80**, 259–268 (1995)
6. Demaurex, N., Schlegel, W., Varnai, P., Mayr, G., Lew, D.P., Krause, K.H.: Regulation of Ca^{2+} influx in myeloid cells. Role of plasma membrane potential, inositol phosphates, cytosolic free [Ca^{2+}], and filling state of intracellular Ca^{2+} stores. J. Clin. Invest. **90**, 830–839 (1992)
7. Fewtrell, C.: Ca^{2+} oscillations in non-excitable cells. Annu. Rev. Physiol. **55**, 427–454 (1993)
8. Hodgkin, A.L., Huxley, A.F., Katz, B.: Measurements of current-voltage relations in the membrane of the giant axon of Loligo. J. Physiol. **116** (**4**), 424–448 (1952). PMID: 14946713
9. Hodgkin, A.L., Huxley, A.F.: Currents carried by sodium and potassium ions through the membrane of the giant axon of Loligo. J. Physiol. **116** (**4**), 449–472 (1952). PMID: 14946713
10. Hodgkin, A.L., Huxley, A.F.: The components of membrane conductance in the giant axon of Loligo. J. Physiol. **116** (**4**), 473–496 (1952). PMID: 14946714
11. Hodgkin, A.L., Huxley, A.F.: The dual effect of membrane potential on sodium conductance in the giant axon of Loligo. J. Physiol. **116** (**4**), 497–506 (1952). PMID: 14946715
12. Hodgkin, A.L., Huxley, A.F.: A quantitative description of membrane current and its application to conduction and excitation in nerve. J. Physiol. **117** (**4**), 500–544 (1952). PMID: 12991237
13. Keener, J., Sneyd, J.: Mathematical Physiology, p. 133. Springer, Berlin (1998)
14. Lewis, R.S., Cahalan, M.D.: Mitogen-induced oscillations of cytosolic Ca^{2+} and transmembrane Ca^{2+} current in human leukemic T cells. Cell Regul. **1**, 99–112 (1989)
15. Luzzatti, V., Husson, F.: The structure of the liquid-crystalline phases of lipid-water systems. J. Cell Biol. **12**, 207–219 (1962)
16. Mahaut-Smith, M.P., Hussain, J.F., Mason, M.J.: De-polarization-evoked Ca^{2+} release in a non-excitable cell, the rat megakaryocyte. J. Physiol. **515**, 385–390 (1999)
17. Morris, C., Lecar, H.: Voltage oscillations in the barnacle giant muscle fiber. Biophys. J. **35**, 193–213 (1981). doi:10.1016/S0006-3495(81)84782-0
18. Nagumo, J., Arimoto, S., Yoshizawa, S.: An active pulse transmission line simulating nerve axon. Proc. IRE **50**, 20612070 (1964)
19. Nelson, M.E., Rinzel, J.: The Hodgkin–Huxley Model. In: Bower, J., Beeman, D. (eds.) The Book of GENESIS: Exploring Realistic Neural Models with the GEneral NEural simulation System, pp. 29–49. Springer, New York (1994)
20. Parsegian, A.: Energy of an Ion crossing a Low dielectric Membrane: solutions to four relevant electrostatic problems. Nature **221**, 844–846 (1969)

21. Penner, R., Matthews, G., Neher, E.: Regulation of calcium influx by second messengers in rat mast cells. Nature **334**, 499–504 (1988)
22. Rink, T.J., Jacob, R.: Calcium oscillations in non-excitable cells. Trends Neurosci. **12**, 43–46 (1989). PMID: 2469208, doi:10.1016/0166-2236(89)90133-1
23. Singer, S.J., Nicolson, G.L.: The fluid mosaic model of the structure of cell membranes. Science **175**, 720 (1972)

Chapter 3
Lipids in Membranes

3.1 Geometry and Nature of Lipids

The most important components that make up cell membranes are various types of lipids. By cataloging lipid structures (referred to as lipidomics), eukaryotic cells have been found to invest substantial resources in generating various types of lipids [28]. Cells use about 5 % of their genes to encode for the synthesis of these lipids. Lipids perform a few general functions [32]. First of all, lipids are used for energy storage, principally as triacylglycerol and steryl esters, in lipid droplets. The matrix of cellular membranes is formed by polar lipids, which consist of a hydrophobic and a hydrophilic portion. Furthermore, lipids act as first and second messengers in signal transduction and molecular recognition processes.

A very comprehensive review of the lipid composition has been presented in a recent paper [32]. In eukaryotic membranes, the major structural lipid components are glycerophospholipids; that is, phosphatidylcholine (PC), phosphatidylethanolamine (PE), phosphatidylserine (PS), phosphatidylinositol (PI), and phosphatidic acid (PA). Their hydrophobic portion is a diacylglycerol (DAG), which contains saturated or *cis*-unsaturated fatty acyl chains of varying lengths. Figure 3.1 shows simplified model structures of these lipids [32].

PC appears to be the main lipid component (comprising more than 50 % of the cellular phospholipids) in most eukaryotic membranes. Most importantly, it is considered to be the neutral-type lipid, which is responsible for creating planar bilayers. Inclusion of PE, which has a conical molecular geometry in a PC bilayer, raises curvature stress in the membrane. The presence of lipids PE, PS, etc., and cardiolipin (CL) in a planar bilayer formed by PC causes regulatory effects on membrane proteins (MPs), antimicrobial peptides (AMPs), and ion channels/pores, etc. [4]. The membrane regulation of integral MPs/AMPs functions will be addressed in later chapters of this book. Organization of lipids in different bilayer phases is also different [10, 32]. Environmental parameters such as temperature, pH, ionic strengths, hydration, etc., of biological membrane regions determine how lipids assemble inside membranes. Many publications have addressed these issues from various view points

M. Ashrafuzzaman and J. Tuszynski, *Membrane Biophysics*,
Biological and Medical Physics, Biomedical Engineering,
DOI: 10.1007/978-3-642-16105-6_3, © Springer-Verlag Berlin Heidelberg 2012

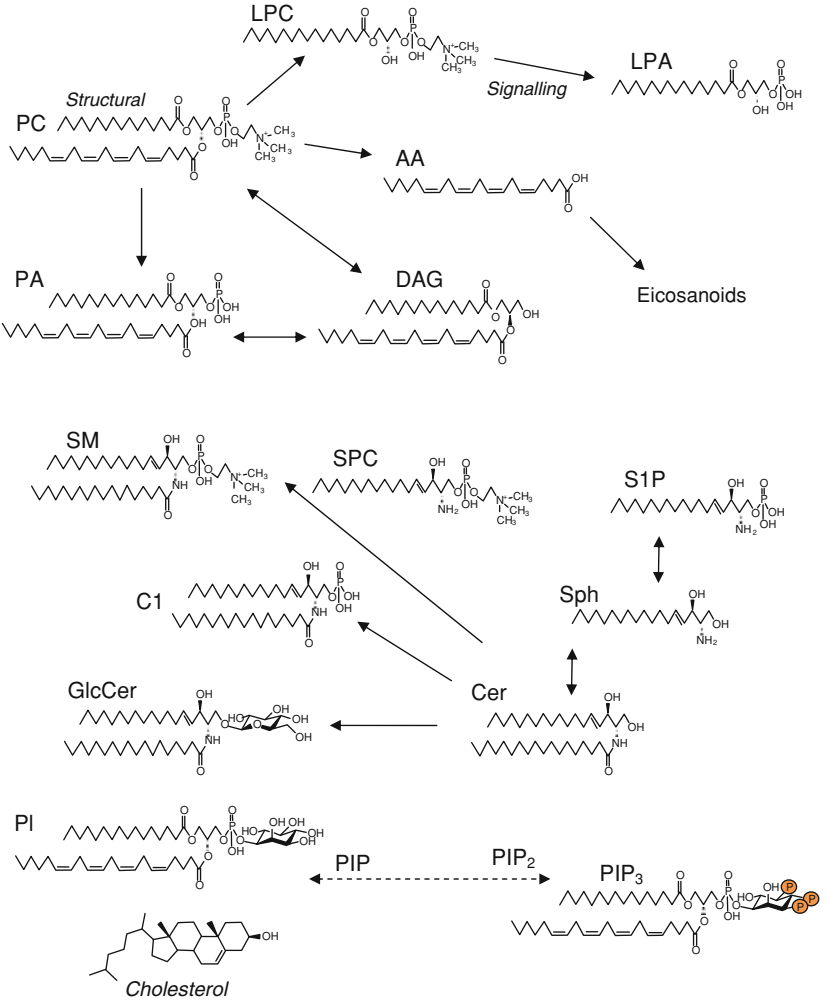

Fig. 3.1 The main eukaryotic membrane lipids are PCs. Their diacylglycerol (DAG) backbone carries a PA esterified to either a choline, ethanolamine, serine, or inositol. The prototypical phospholipid, dipalmitoyl-PtdCho, exhibits nearly cylindrical molecular geometry with a cross-sectional surface area of 64 $Å^2$ and a head-to-tail length of 19 Å [17]. The phosphosphingolipid sphingomyelin (SM) and the glycosphingolipid glucosylceramide (GlcCer) have a ceramide (Cer) backbone, consisting of a sphingoid base (such as sphingosine; Sph), which is amide-linked to a fatty acid. Yeast sphingolipids carry a C26 fatty acid and have phosphoinositol-X substituents that contain additional mannoses and phosphates. Breakdown products of membrane lipids serve as lipid second messengers. The glycerolipid-derived signaling molecules include lysoPtdCho (LPC), lysoPA (LPA), PA and DAG. The sphingolipid-derived signaling molecules include sphingosylphosphorylcholine (SPC), Sph, sphingosine-1-phosphate (S1P), Cer-1-phosphate (C1P), and Cer. Arachidonic acid (AA) yields the signaling eicosanoids and endocannabinoids (not shown). The various phosphorylated PtdIns molecules (PIPs; also known as the phosphoinositides) mark cellular membranes and recruit cytosolic proteins. They are interconverted by the actions of kinases and phosphatases. This figure is drawn based on a figure from [32] which was a modified version of an earlier figure from [31] ©Macmillan Publishers Ltd

and to gain detailed understanding the reader is encouraged to consult earlier works (for example [19, 25]). Considering the organizational diversity, it is now well accepted to classify lipid organization mainly into two generalized categories, namely, lamellar and non-lamellar phases. These will be discussed in Sect. 3.2, and further detailed in regard to other related aspects in subsequent sections of this chapter.

3.2 Various Lipid Phases in Membranes: Lamellar and Non-Lamellar Phase Propensities

Lamellar phases that exist in excess water are subclassified into different states: fluid (L_α), ripple (P_β), gel (L_β), and pseudo-crystalline or subgel (L_c), depending on the lipid head group and tail orientations and assemblies. Model diagrams of these structures have been presented in Fig. 3.2. It is generally accepted that the lamellar phases are probably compatible with the barrier functions of biological membranes. The famous fluid mosaic model used to describe bilayer barrier functions [27] is based on the liquid-crystalline phase of the biological membranes.

Although lamellar phases appear to be the primary states of the lipid assembly in biological membranes, there also exists a significant amount of lipids that do not spontaneously form any of the states illustrated in Fig. 3.2. These non-lamellar structure-forming lipids can further be classified into two major subcategories, namely inverted cubic (Q_{II}) and hexagonal (H_{II}) phases, considering the lipid compositions and their crystal structures. Figure 3.3 shows a model diagram representing the crystalline structure of a hexagonal (as an example) form of a non-lamellar lipid phase. Both non-lamellar structures of inverted cubic and hexagonal phases are observed in membranes under physiologically relevant conditions. The formation of structures following non-lamellar phases was originally assigned to the molecular geometries of lipids [9]. Naturally occurring phospholipids such as phosphatidyl ethanolamine, phosphatidyl ethylamine, *N*-methyl PE, phosphatidylserine, phosphatidylglycerol, phosphatidic acid, cardiolipin, etc., are often responsible for inducing non-lamellar phases. These non-lamellar phase-forming lipids are present in both phospho- and glycolipid-based cell membranes. Of course, the non-lamellar phase-forming propensity in certain lipids highly depends on the local ionic conditions. Temperature-dependent phase preference is an important established fact (see for example [26]). The inverted cubic and hexagonal phases are independent non-lamellar phases that appear to be favored over lamellar phases when the temperature of the lipid composition is raised. It has also been observed that the presence of cubic phases may be a general feature of H_{II}-forming lipids, which is supported by the consideration of the spontaneous radius of curvature of lipid monolayers, referred to as the intrinsic curvature hypothesis for bio-membrane lipid composition [7]. In this study, Gruner has presented a pictorial representation for non-lamellar H_{II} lipid phases, which has been redrawn in Fig. 3.3. The intrinsic curvature hypothesis [7]

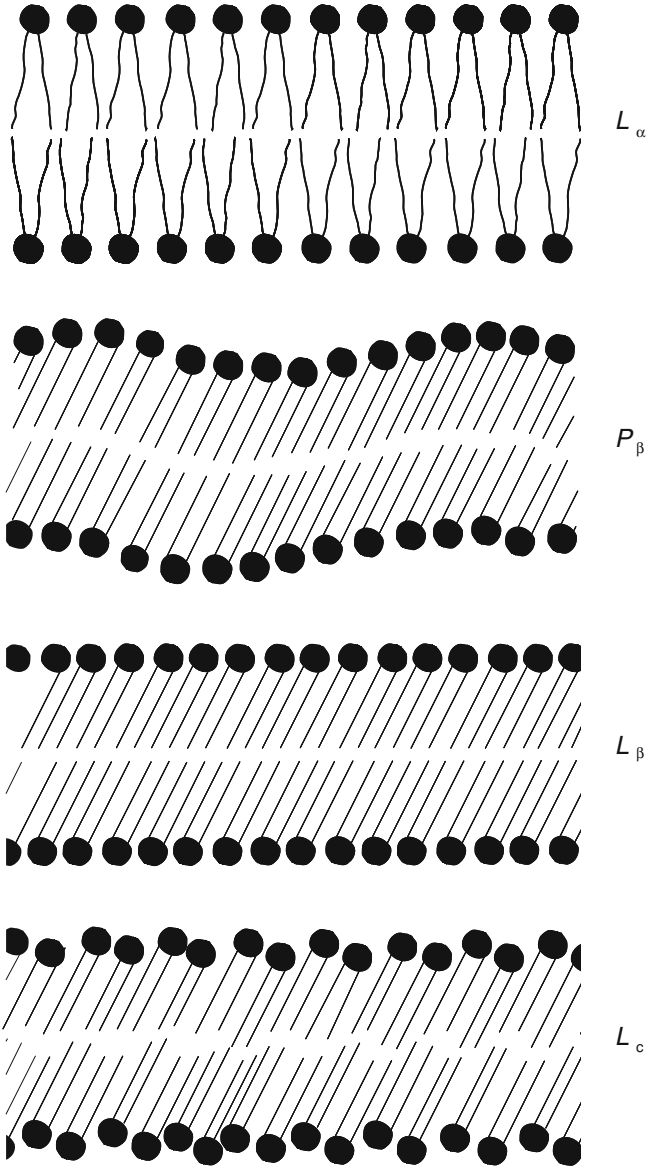

Fig. 3.2 *Top* to *bottom* structures schematically represent: fluid (L_α), ripple (P_β), gel (L_β), and pseudocrystalline or subgel (L_c) states, respectively, in the organization of lamellar bilayer phases of PC [10, 32]. Each lipid is schematically represented with a head group (*black sphere*) and two tails. Various lamellar phases correspond to different organizations and orientations of the lipids

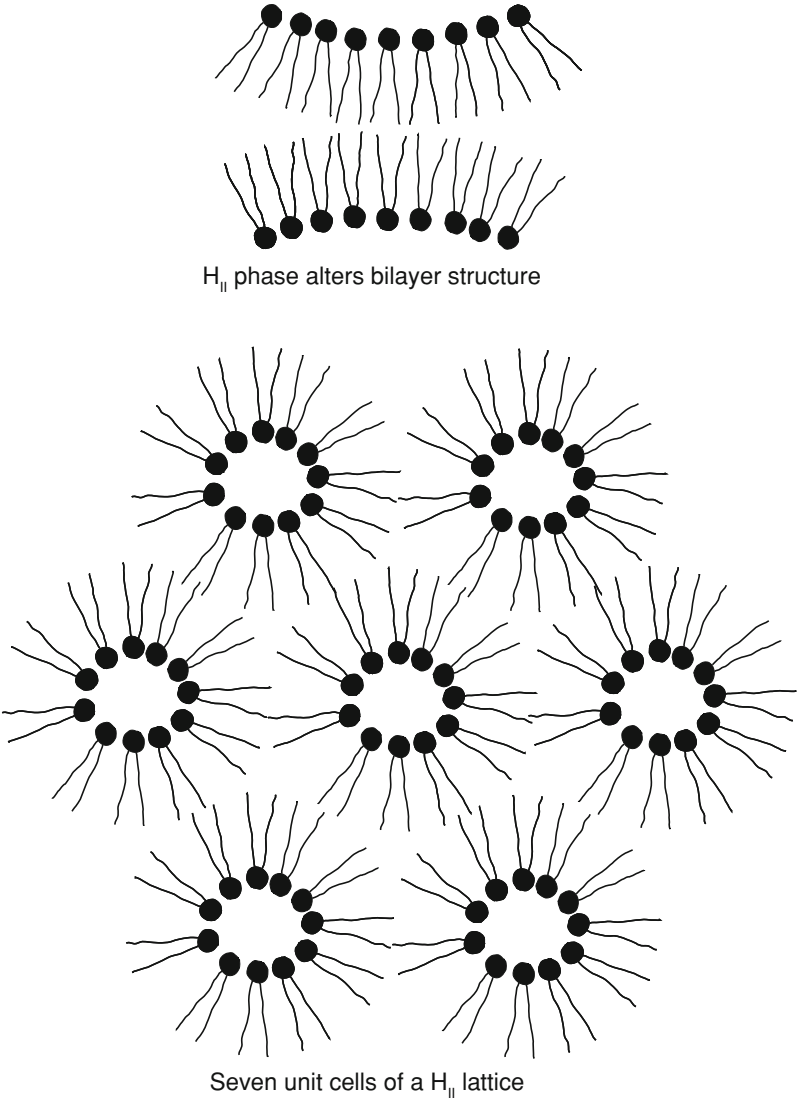

Fig. 3.3 In the non-lamellar phases the non-bilayer propensity is shown in the *top panel*. The *bottom panel* shows the seven unit cells of a hexagonal lattice. The huge intrinsic monolayer curvature makes a major structural difference between the non-lamellar structures and lamellar structures (shown in Fig. 3.2). The model structures are drawn in light of the previously published results [7, 14]. In Gruner's model [7] it is suggested that the annulus regions in inverse hexagonal structure, which exist at the farthest distance from the nearby polar cores, are filled with hydrocarbons at nearly relaxed lengths. This hypothesis is not well established based on experimental data and requires serious re-investigation

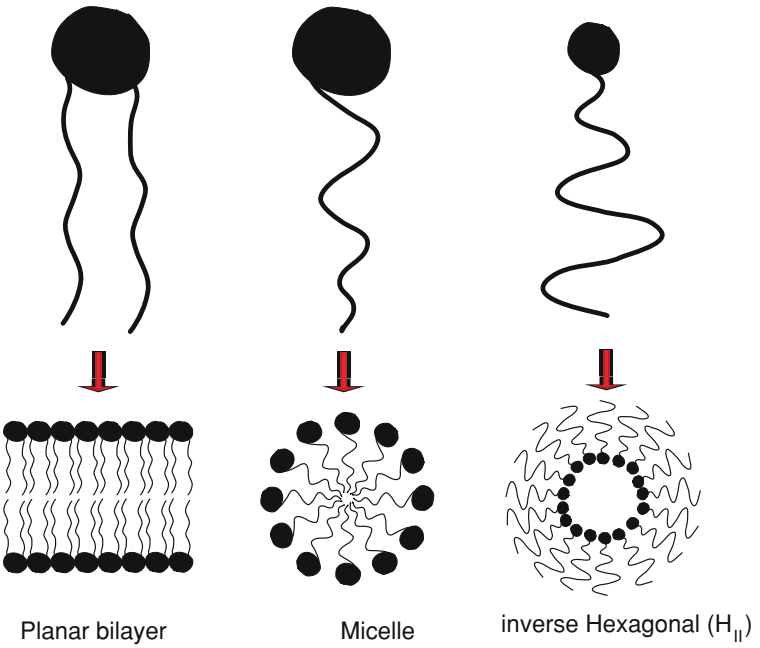

Fig. 3.4 Schematic model for altering bilayer physical properties by lipids or small amphiphiles [4]. In the *upper panel*, three basic shapes of molecules considering the relative head group-tail geometry are shown to determine cylindrical, conical, and inverted conical type structures, respectively. In the *bottom panel*, the resulting induced structures, which are planar bilayer, micelle, and inverse hexagonal phases are presented. The above-mentioned cylindrical, conical, and inverse conical molecule structures account for neutral, positive, and negative curvatures, respectively, which favor different lipid organizations as shown here

assumes that the lipid phase behavior is largely the result of a competition between the tendency for certain lipid monolayers to curl, and the hydrocarbon packing strains. In lipid molecules, the relative head group versus tail geometry is in fact responsible for favoring different lipid orientations which determine the curvature stress. As a result, bilayer formation, micelle structure, or inverse hexagonal structure, etc., emerge. This is schematically shown in Fig. 3.4.

The quantitative measure of the tendency of a monolayer to curl comes from the consideration of the lipid's intrinsic radius of curvature. The lipid's intrinsic curvature determines the monolayer bending energy, which clearly depends on the flexibility of the lipid layer, also referred to as the elasticity of a lipid monolayer. The geometrical structure, chemical composition, etc., which are specific inherited lipid properties, determine the elastic constants associated with the corresponding lipid layer. That is why the lipid organization in a biological environment is also lipid-specific. For instance, the lipid palmitoyl oleyl phosphatidyl choline (POPC) tends to form lamellar vesicles in solution, whereas smaller lipids with shorter acyl

chains, up to 8 carbons in length, such as detergents, form micelles when a critical micelle concentration is reached.

A theoretical analysis and relevant experimental investigations [7] indicate that the monolayer's intrinsic curvature fundamentally distinguishes the bilayer from the non-bilayer lipids due to lipid phase properties. A quantitative shape concept involves a determination of the free energy per lipid molecule when it occupies a given molecular volume of a given shape [15]. Here, it is assumed that the free energy per molecule may be partioned into components arising from the elastic bending of the lipid monolayers and hydrocarbon packing energies, besides other necessary lattice-specific energy components which come from hydration and electrostatic potentials. Lipid monolayers are practically flat in the lamellar L_α phase (see Fig. 3.2) but rolled into tight cylinders in the non-lamellar H_{II} phase (see Fig. 3.3). The theory suggests the following form for the elastic free energy:

$$\mu_{\mathrm{E}} = k\left(\frac{1}{R} - \frac{1}{R_0}\right)^2 \tag{3.1}$$

Here, k is the elastic constant and R is the radius of curvature of the lipid/water interface. For a cross-section of the membrane surface at a point under consideration, using two planes that are perpendicular to the surface and oriented in two special directions called the principal directions, the principal curvatures are the curvatures of the two lines of intercepts between the planes and the surface which have almost circular shapes in close proximity to the point under consideration. The radii of these two circular fragments are called the principal radii of curvature. For simplicity we have considered both to be R. R_0 is the equilibrium value or the intrinsic radius of curvature, which is defined self-consistently as the radius of curvature that minimizes μ_{E}. In an elastically relaxed lipid monolayer $R = R_0$. R_0 is a sole property of the lipid. Widening the splay of the lipid tails accounts for a decrease in R_0 while increasing the effective head group area accounts for an increase of R_0 (see Fig. 3.4). In this model [7] hydrocarbon-packing constraints are thought to prevent the expression of large radii of curvature. Depending on the lipid phase, not all hydrocarbon lipid tails may have the same relaxed lengths. As an example, Fig. 3.3 illustrates this in H_{II} phases. In this case, the hydrocarbon-packing free energy may be very large. That is why in curved structures a competition between the packing free energy and the elastic free energy (Eq. 3.1) is unavoidable, and this competition appears as a general phenomenon associated with local expression of the intrinsic curvature. It is, therefore, clear that the lipid phase properties are lipid structure-specific, because the energy contributions depend highly on the specific lipid head group and tail geometry, as well as the organization of the biological environment. The existence of lipids in lamellar or non-lamellar phases therefore follows from the participating lipid's physical properties. These phase preferences can be experimentally investigated by measuring the thermodynamic transition temperatures for the lipid mixture between lamellar/non-lamellar phases, or between different substates within both lamellar and non-lamellar phases. A calorimetric study is the best experimental tool in this

regard, while X-ray crystallography determines the crystal structures corresponding to the various phases.

Energetics of the lipid molecule assembly into various lipid phases is case specific, and it was shown [7] that the energetic contributions to the total free energy determining the lipid membrane conformation come from the properties of lipid monolayers and the participating lipids. The lipid monolayer's elastic property and the lipid's head group and carbon chain geometry are primarily considered to be the main factors in the so-called intrinsic curvature hypothesis for bio-membrane lipid composition [7]. A very important lipid property, the lipid's charge profile, is totally ignored in this model. We have made substantial contributions to the field in this regard. In later chapters the reader will be given detailed information about the lipid charge effects. We just wish to mention here that the lipid membrane's elastic properties fail to explain most of the regulatory membrane effects. However, the lipid's charge profiles do so. In the next sections of this chapter, we will discuss the lamellar/non-lamellar phase properties in view of mostly experimental studies of specific lipid systems. It has been found that the non-lamellar lipid assembly brings not only special membrane structures, but also often induces regulatory effects on other agents residing in the membrane environment. Perhaps the best example of an enzyme activated by the H_{II} phase-forming lipids is protein kinase C. Numerous publications on non-lamellar phase-forming lipids and the mechanisms are useful in this regard (e.g. [18] and references therein; also [14]). Our main interest here lies in the lipid phases and the regulation of these phase properties. A group of AMPs has been observed to be regulating the lipid's lamellar/non-lamellar preferential phase propensities. Interactions of AMPs with lipid membranes, using different techniques such as differential scanning calorimetry (DSC), ^{31}P-nuclear magnetic resonance (NMR) spectroscopy, X-ray diffraction, etc., elucidate how the lipid phase properties are regulated due to the effects of membrane-residing ingredients, such as various naturally occurring MPs, and artificial ones often used during treatment.

In the next few sections of this chapter, we provide more details regarding the physical interactions involving various classes of AMPs having varied structures and molecular mechanisms of actions, etc., with phospholipid bilayers with different membrane-forming components.

3.3 Lipid-Specific Phase Diagram: A Thermotropic Perspective

In the previous section, we have addressed the various lipid phases and the consequent mechanical energy components arising from the corresponding physical structure of organized lipid monolayers and lipids themselves. Here, we describe a lipid phase diagram, addressing the various lipid phases as a function of both temperature, representing the thermodynamic environment, and the hydrocarbon chain lengths of certain lipid types, determining the membrane's physical properties, in particular its

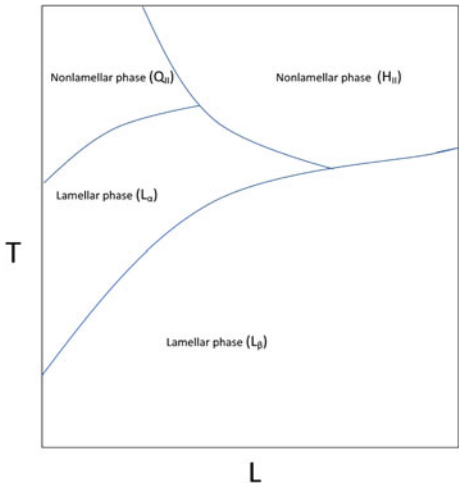

Fig. 3.5 Phase diagram showing different lipid phases and the change of the phase transition temperature (T, °C) as a function of the change of hydrocarbon chain length (L, Å) of lipid 1,2-dialkyl-3-O-(β-D-glucopyranosyl)-*rac*-glycerols. This figure is redrawn in light of the results published in Ref. [18]. The slope of each curve determining the boundary between two different phases and the intersection points between different curves are expected to vary substantially for different lipids

thickness. The phase diagram in Fig. 3.5 [18] shows how the various lipid phases depend on the structural component.

The transition temperatures between lamellar and non-lamellar, and between different substrates within both phases vary with the lipid hydrocarbon chain lengths. The whole picture needs to be replaced with a totally different phase diagram for a different type of lipid in the phospholipid composition. It is possible to maintain the same intrinsic lipid curvature as we extend the hydrocarbon acyl chain length. This means that the length of the hydrocarbon chain also plays a crucial role in determining the lipid phase or the phase transition temperature as the lipid organization undergoes a phase transition. The hydrocarbon-packing free energy, as mentioned earlier, may vary with the change of hydrocarbon chain length and as a result may also contribute differently into the overall free energy profile. The latter quantity includes the monolayer elastic energy and other contributions which arise from the consideration of lipid charges, etc. A thorough theoretical understanding of the experimentally determined phase diagram presented here may be possible, but only after we understand all the energy contributions due to the above-mentioned lipid phases. For more experimental observations on how the phase diagram varies for various lipids, we refer the reader to the relevant literature [e.g., 8, 20–22] dealing with the homologous series of *n*-saturated diacyl and dialkyl glycosyl glycerolipids. These studies suggest that the effects of hydrocarbon chain lengths on their non-lamellar phase behavior are similar to those observed with the PEs.

The lamellar-inverse hexagonal-lamellar phase transition may also dramatically depend on the concentration of water molecules associated with the membrane forming lipids. The L_α-to-$H_{\rm II}$ phase transition is observed to take place with the removal of water. A possible explanation is that the removal of water causes a reduction in the area per lipid polar head group which accounts for an increase of the probability of a high-curvature structure. For details see [25]. Somewhat surprisingly, a study [6] demonstrated that the removal of water can also induce an $H_{\rm II}$-to-L_α transition in dioleoylphosphatidylethanolamine. Careful mapping of the above-mentioned lipid phase diagrams by X-ray diffraction and nuclear magnetic resonance spectroscopy has revealed that this lipid in fact undergoes $H_{\rm II}$-to-L_α-$H_{\rm II}$ transitions with progressive hydration, which has been called a 'reentrant' transition [16, 24]. An attempt has been made [16] to explain the reentrant transition by using a model that takes into account a balance between elastic and hydration energies in the L_α and $H_{\rm II}$ phases of dioleoylphosphatidylethanolamine. Here, the chemical potentials of lipid and water molecules in both phases have been calculated to find the condition of phase equilibrium and the phase diagram of the system has been reconstructed.

Let us consider the chemical potentials are respectively $\mu_l(L)$ and $\mu_l(H)$ for lipid in lamellar and inverse hexagonal phases, while $\mu_w(L)$ and $\mu_w(H)$ are chemical potentials for water in lamellar and inverse hexagonal phases. In the case of non-equal or imbalanced chemical potentials for lipid and water, an independent phase (lamellar or hexagonal) exists. However, both lamellar and inverse hexagonal phases may coexist if the following condition is satisfied:

$$\mu_l(L) = \mu_l(H) \quad \text{and} \quad \mu_w(L) = \mu_w(H) \tag{3.2}$$

Considering the osmotic pressure that determines the chemical potential of the lipid [16] and the hydration, we can now draw the phase diagrams for a reentrant transition such as those in Figs. 3.6 and 3.7. There is no external reservoir of water in this case, and the chemical potential of water cannot be externally controlled. The system itself sets the chemical potentials of water and lipid to minimize the free energy.

Following Eq. 3.2, the coexisting lamellar and inverse hexagonal phases may occur near the curved boundary separating the independent lamellar and inverse hexagonal lipid phases (see Fig. 3.6). Identical coexisting lamellar and inverse hexagonal phases may occur near the independent lamellar and inverse hexagonal phase boundaries (see Fig. 3.7). In Fig. 3.7, the presence and absence of hydration in both lamellar and inverse hexagonal lipid phases is especially worth pointing out.

The phase diagrams plotted in Figs. 3.5, 3.6 and 3.7 exhibit various membrane and lipid geometries, hydration, osmotic pressure profiles, etc. However, as mentioned earlier, all of them ignored a very important lipid property, namely the charge profile of the participating lipids. Once the charge profile is considered, the whole picture of energetics in lipid membranes in different phases will require a major revision and perhaps a new phase diagram may also be necessary. In later chapters, the reader will learn about the importance of including charge profiles of lipids in view of our discovery of electrostatic lipid–lipid and lipid–membrane protein interactions. If we

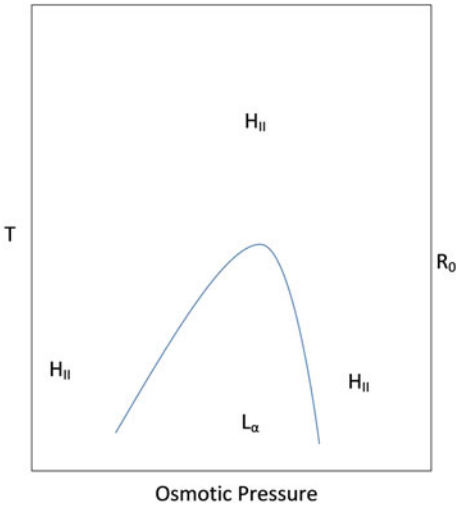

Fig. 3.6 This temperature (T, °C) versus osmotic pressure phase diagram for a reentrant phase transition (H_{II}-to-L_α-to-H_{II}) is schematically drawn in light of Ref. [16]. The right-hand axis plot represents the intrinsic lipid curvature (R_0 in Å; presented in Eq. 3.1 and explained there). The slope and shape of the curve separating lamellar and inverse hexagonal phases may dramatically change between different lipids, despite the fact that they may undergo the same type of phase transition

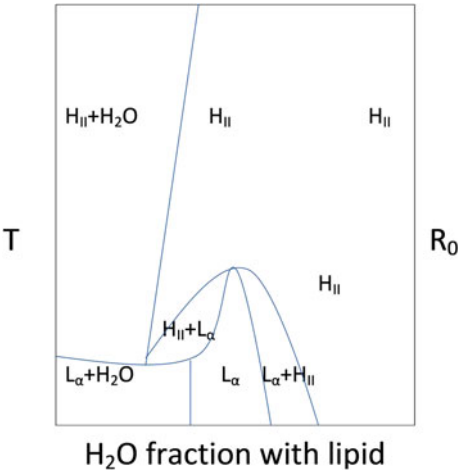

Fig. 3.7 This temperature (T, °C) versus hydration plot in a reentrant phase transition (H_{II}-to-L_α-to-H_{II}) is schematically drawn in light of Ref. [16]. The *horizontal axis* represents the increasing values of 'wt. fraction lipid'. The *right-hand axis plot* represents the intrinsic lipid curvature (R_0 in Å; presented in Eq. 3.1 and explained there). In this type of a phase transition, coexistence of different phases, as shown here, is evident. The slope and shape of the curve separating lamellar and inverse hexagonal phases may dramatically change between different lipids despite the fact that they may undergo the same type of a phase transition. In some samples the cubic phase is also observed [6]

consider $E(H)$ and $E(L)$ to be the free energies per lipid molecule in the inverse hexagonal and lamellar phases respectively, all phase boundaries representing the lamellar-inverse hexagonal phase transition are determined by the free energy change ($\Delta E = E(H) - E(L)$). The free energy change ΔE between two subsequent phases contains the following important energy contributions:

$$\Delta E = \Delta E_{\text{elastic}} + \Delta E_{\text{hydration}} + \Delta E_{\text{van der Waals}} + \Delta E_{\text{electrostatic}} \tag{3.3}$$

Although the elastic energy (which follows from Eq. 3.1), hydration and van der Waals energy contributions have been well described (see Ref. [16] and many other references therein), the electrostatic component is still missing. Another energy term ($\Delta E_{\text{interstitial}}$), the 'energy of voids in inverse hexagonal interstices' in a reentrant transition, is also needed to augment the four energy terms in Eq. 3.3. This rather passive energy contribution plays an important role in setting up the energy scale, and determines the temperature of the inverse hexagonal-to-lamellar transition and the temperature range of the reentrant transition. Although the van der Waals energy component is understood to be producing negligible effects [16], a careful examination of relevant modeling efforts suggests that both the van der Waals and electrostatic interactions appear to be dominant contributions to the membrane energetics, which is responsible for certain lipid phase properties, especially in the case when the membrane hosts different kinds of membrane proteins or antimicrobial peptides [2]. This will be elaborated on in later chapters.

3.4 Modulation of the Phase Properties of Lipids by Antimicrobial Peptides

We have so far addressed the various aspects of lipid phases in independent membrane environments. The lamellar and non-lamellar lipid phases are found to be modulated by the disproportionate presence of the natural constituents that are primarily responsible for constructing membranes. However, cell membranes also host various other components such as natural or artificial (used mainly during treatment) membrane proteins, antimicrobial peptides, etc. Those proteins or peptides are not often found to perform independent activities, but rather are found to be engaged in complex mechanisms involving lipids and other membrane constituents, which altogether have modulating effects on lipid phase properties. As a result, the phase diagrams may experience substantial modifications due to an alteration of the lipid phase distributions. In this section, we discuss the effects of a few antimicrobial peptides on the lamellar and inverse hexagonal phase properties. We also specifically address the effects of the antimicrobial peptides on the transition temperatures between different lipid phases and different subphases or states within major well-defined phases.

Gramicidin S, a cyclic peptide, has been found to disrupt the structural integrity of specific lipid bilayer membranes by promoting the formation of cubic or other

three-dimensional non-lamellar lipid phases [23]. Other structurally different peptide antibiotics are known to be involved in similar activities. For example, the linear peptides, such as gramicidins A, B, and C [12, 13, 30] and alamethicin [11], also induce non-lamellar phase formation when incorporated into appropriate lipid dispersions. It is, therefore, suggestive that membrane disruption mediated by localized increases in the membrane monolayer curvature stress could be a general mode of action of many antimicrobial peptides. Other studies (see [33] and references therein) suggest that lipid-peptide interactions are sensitive to relatively small alterations in the chemical structure and physical properties of both the peptide and the host lipid bilayer. In many cases, the subtlety and complexity of these interactions are not readily predicted or rationalized by current theoretical models. However, it is also true that if we can find the mechanisms by which the peptides alter membrane properties, then we would be able in most cases to draw the picture of energetics (see Eq. 3.3) and, as a result, perhaps also identify the near-correct phospholipid organizations or phases in the membrane environment. This will be attempted in the next few chapters.

We now discuss some experimentally observed phenomena [1] which offer an insight into the antimicrobial peptide-induced modulation of the lipid phase properties. Peptides alamethicin (Alm), gramicidin S (GS) and Ac-K_2-$(LA)_{12}$-K_2-amide ($(LA)_{12}$) are used to study the thermotropic phases in dielaidoylphosphatidylethanolamine (DEPE) dispersions. In addition to understanding the effects of independent peptides, measuring the effects of their binary mixtures reveals some important lipid phase properties. These projects were designed by Md Ashrafuzzaman in collaboration with Dr. Ronald McElhaney.

Figure 3.8 shows DSC heating scans of DEPE dispersions containing alamethicin. Only raw scans showing alamethicin effects are presented here; alamethicin-free scans are identical to previous reports [23]. We observe pronounced gel/liquid-crystalline (L_β/L_α) and lamellar/reverse hexagonal ($L_\alpha/H_{\rm II}$) phase transitions at temperatures T_m (∼37.6 °C) and T_H (∼63.6 °C), respectively. On cooling, $L_\alpha/H_{\rm II}$ shows hysteresis (lower T_H) but T_m shows negligible reduction [23]. The enthalpies (ΔH) at the L_β/L_α and $L_\alpha/H_{\rm II}$ transitions are 8.9 ± 0.3 and 0.64 ± 0.05 kcal/mol, respectively [29].

AMPs generally change the co-operativity and energetic strength of both the L_β/L_α and $L_\alpha/H_{\rm II}$ transition phases (see, for example, Fig. 3.8). Enthalpy (ΔH) values for the L_β/L_α and $L_\alpha/H_{\rm II}$ transitions decrease with increasing AMP levels; about a 50 % reduction was observed for 1 mole % Alm, and a 30 % reduction was observed for 2.72 mole % GS (scans are not shown here). T_m decreases only modestly, although the AMPs affects T_H dramatically. The effects of an AMP are greatly altered if said AMP co-exists along with another AMP. For example, the effects of Alm change significantly if there is a binary presence of GS in the lipid dispersion. As an example, Fig. 3.9 illustrates the DSC scans showing the effects of a binary Alm/GS presence in DEPE dispersions. The most important effects are observed in the transition temperature T_H.

Figure 3.10 shows that at low AMP/lipid mole ratios (between 0 and 0.2 %) and a GS–lipid ratio between 0 and 0.136 %, T_H decreases considerably. When GS is at a lower concentration (∼50 %), there is a relatively greater decrease in T_H compared

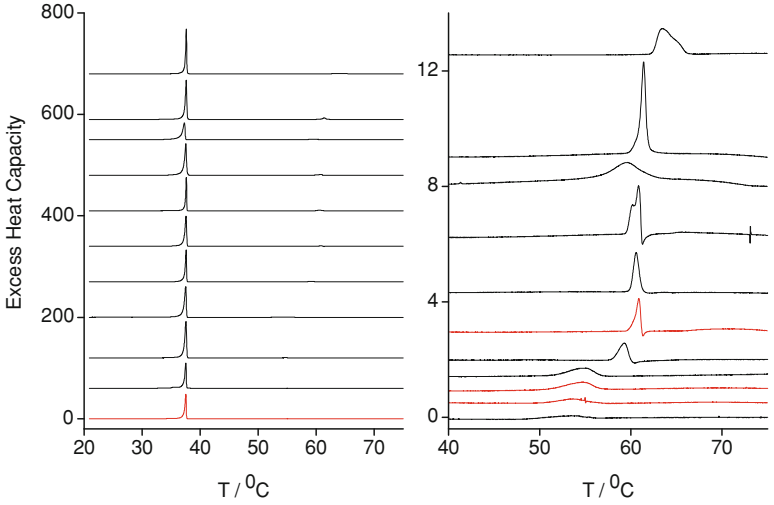

Fig. 3.8 DSC heating thermograms of DEPE dispersions without or with Alm (*top* to *bottom* 0, 0.15, 0.2, 0.22, 0.25, 0.3, 0.5, 0.55, 0.6, 0.75, 1.0, respectively mole % Alm in DEPE) [1]. The *left panel* covers the whole temperature range (20–75 °C) while the *right panel* covers only the range showing a L_α/H_{II} phase transition

to Alm. With a further increase of the AMP level (Alm–lipid ratio between 0.2 and 0.3 %) with GS–lipid ratio between 0.136 and 0.34 %, T_H modestly increases. It slightly decreases again with increasing the Alm level (Alm–lipid ratio between 0.3 and 0.5 %) but slightly increases with an increasing GS level (GS–lipid ratio over 0.34). At a still higher Alm level (AMP–lipid ratio over 0.5 %), T_H first decreases sharply (between 0.5 and 0.6 %) and then continues to decrease modestly; whereas at still higher GS levels, T_H continues to increase modestly. An inverse relation between Alm/GS-induced changes of T_H and co-operativity of the L_α/H_{II} transition is also noticed. $(\mathrm{LA})_{12}$, at a ratio of under 0.5 % with respect to lipid concentration, negligibly decreases T_H, although at ultra-low concentrations, $(\mathrm{LA})_{12}$ causes T_H to also decrease further; however, the drop is clearly less, and much less than that for Alm and GS. Interestingly, at a low level, we observe a trend showing a higher drop in T_H due to the effects of an even lower level of AMP, with its being more non-transmembrane. A modest reduction in T_m, ΔH, co-operativity etc., is detected at the investigated range of the $(\mathrm{LA})_{12}$ concentration.

In a binary mixture of Alm (fixed 0.5 %) and different GS/$(\mathrm{LA})_{12}$ concentrations in DEPE dispersions, the changes in T_m, ΔH and co-operativity almost follow (albeit with slightly higher effects) that of independent GS/$(\mathrm{LA})_{12}$ effects on the L_β/L_α transition. In the L_α/H_{II} transition, 0.5 % Alm alone reduces T_H and ΔH, but changes the co-operativity only modestly. With an increasing GS/$(\mathrm{LA})_{12}$ ratio, the L_α/H_{II} transition initially broadens, with a decreasing co-operativity at low GS or $(\mathrm{LA})_{12}$/lipid ratios. However, with increasing ratios, the L_α/H_{II} transition gradually regains co-operativity, and at a very high GS/$(\mathrm{LA})_{12}$ level, the transition becomes weaker

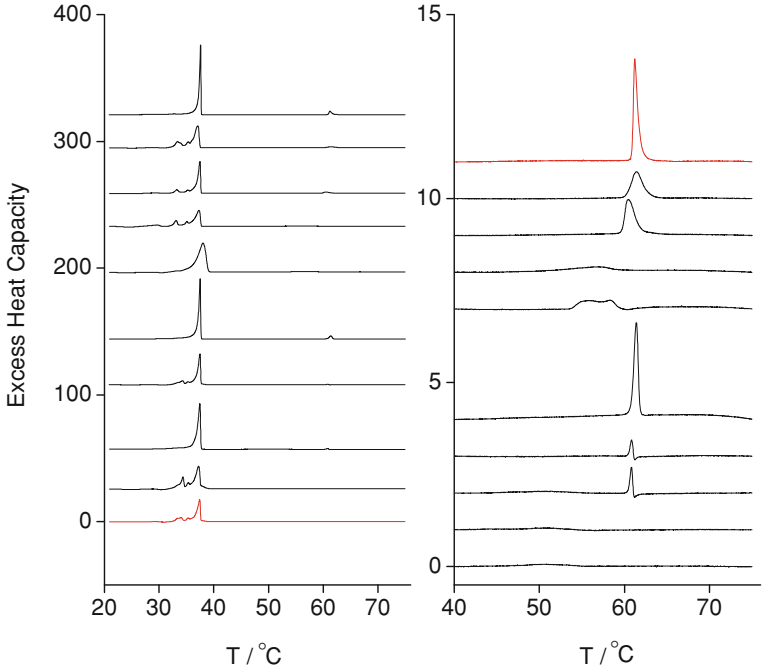

Fig. 3.9 DSC heating thermograms of DEPE bilayers with both 1.36 mole % GS and different mole % Alm in the aqueous phase (*top* to *bottom* 1.36 mole % GS + 0, 0.1, 0.15, 0.2, 0.25, 0.3, 0.5, 0.6, 0.75 or 1, respectively mole % Alm in DEPE) [1]. The *left panel* shows the heating thermograms for a 20–75 °C temperature range while the *right panel* shows a shorter temperature range mainly showing the L_α/H_{II} phase transition

but experiences no further broadening. Importantly, at a higher GS/$(LA)_{12}$ level, the L_α/H_{II} transition reveals the trend of independent GS/$(LA)_{12}$-induced effects with only a modest visibility of 0.5 % Alm's effects. In a reverse investigation, different Alm concentrations in the presence of fixed GS (1.36 %) or $(LA)_{12}$ (0.2 %) produce no qualitatively different changes in T_m, ΔH and co-operativity, compared to those due to Alm alone.

The effect of binary AMPs on T_H shows remarkable features. At a low GS level (GS–Alm ratio between 0 and 0.136) with 0.5 % Alm, T_H drops sharply to a much lower value than the value for low GS alone, and slightly lower than the dropped values of T_H for high Alm (∼0.6 mole %) alone. The sharp drop also occurs at a half-GS level (GS–lipid ratio at 0.068 %) compared to that (GS–lipid ratio at 0.136 %) without Alm. With an increasing GS (GS–Alm ratio between 0.136 and 0.68), T_H increases quickly to as high as the T_H induced by GS alone, and continues to modestly increase when further increasing GS (GS–Alm ratio over 0.68) keeping T_H always a little lower than what it would be without 0.5 % Alm. At a low $(LA)_{12}$ level [$(LA)_{12}$–Alm ratio over 0.1] with 0.5 % Alm, T_H sharply drops to much lower values than

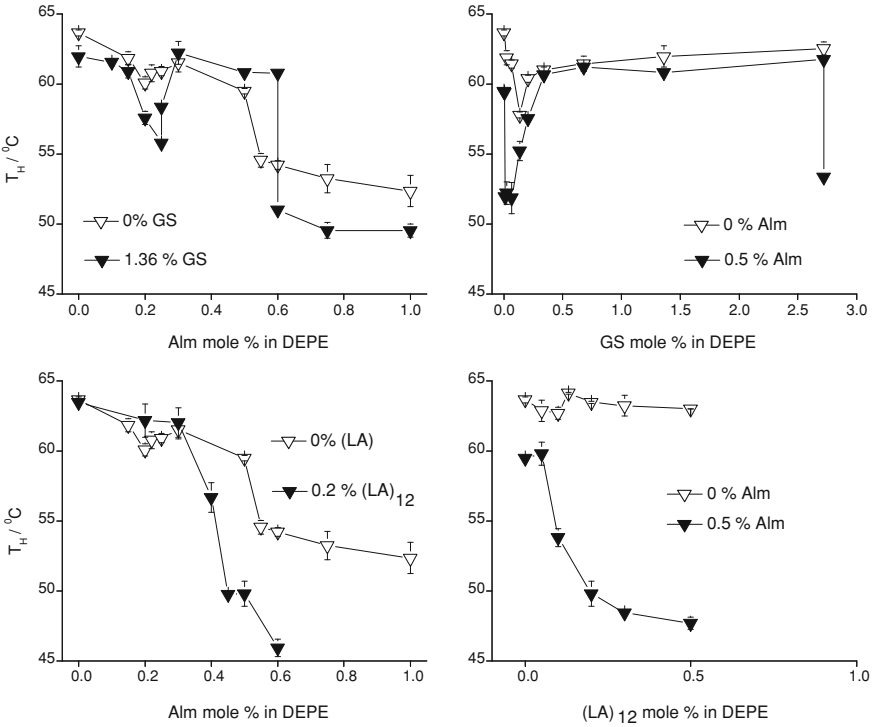

Fig. 3.10 Effect of the binary presence of AMPs on T_H in DEPE dispersions [1]

that induced by 0.6 mole % Alm alone, and continues experiencing quick drops with increasing $(LA)_{12}$, before experiencing saturation.

In a reverse investigation, at low Alm (Alm–GS ratio between 0 and 0.184) with 1.36 % GS, T_H decreases considerably, experiencing higher drops than without GS, but requiring a relatively higher Alm level (Alm–lipid ratio of 0.25 %). With increasing Alm (Alm–GS ratio between 0.184 and 0.22) T_H increases substantially, overshooting the Alm-alone value, and again slightly decreasing with a further increased Alm level (Alm–GS ratio between 0.22 and 0.44). However, at a still higher Alm level (Alm–GS ratio over 0.44), T_H decreases sharply and drops to values which are considerably lower than the Alm-alone values, and continues to modestly decrease with increasing Alm/GS ratios. Due to the effects of low Alm [Alm–$(LA)_{12}$ ratio between 0 and 1.5] with 0.2 mole % $(LA)_{12}$, we observe T_H to modestly decrease, but then [Alm–$(LA)_{12}$ ratio over 1.5] T_H continues to experience quick and continuous drops. Interestingly, non-transmembrane GS enhances, but transmembrane $(LA)_{12}$ reduces the ultra-low level Alm-induced drop in T_H, which is identical to a transmembrane property-dependent trend observed in their independent (low level) effects [$(LA)_{12}$, Alm and GS cause negligible, moderate and substantial drops in T_H], although at a cost of a little higher Alm in the former but a little lower Alm in the latter cases. Sim-

ilarly, at a high Alm level, the sharp drop in T_H occurs at relatively higher Alm/lipid ratios (over 0.6 %) with 1.36 % GS but lower Alm–lipid ratios (over 0.3 %) with 0.2 % $(LA)_{12}$ than that (Alm–lipid ratio over 0.5 %) without GS/$(LA)_{12}$. Here also, similarly to the low level, non-transmembrane and transmembrane peptides ensure a higher and a lower, respectively, amount of Alm needed to create sharp drops in T_H. This comparable study suggests that in binary mixtures between a high level semi-transmembrane peptide Alm and other AMPs, the transmembrane-like $(LA)_{12}$ exerts higher effects on Alm than the non-transmembrane-like GS in destabilizing a lamellar phase in cell membranes. An important message is that the effects of any AMP in the presence of multi-component AMPs in lipid dispersions on different thermodynamic bilayer parameters heavily fluctuate under the influences of varied levels of other AMPs.

Our investigation suggests that Alm clearly shows different concentration-dependent qualitative effects on the thermodynamic properties of DEPE dispersions. It also hints at support for the replacement of the H_{II} phase with the cubic phase at its higher level (over 0.5 %) by showing a huge drop in T_H, which is comparable to the effects of the level (1 % or higher) of Alm at which previous structural studies showed the Alm-induced appearance of the cubic phase in the lipid's liquid crystalline state [11]. Importantly, we find that non-transmembrane GS and transmembrane $(LA)_{12}$ both generally modulate the Alm-induced possible formation of the cubic phase. $(LA)_{12}$ favors Alm for inducing the possible cubic phase at relatively lower concentration, but GS requires higher Alm levels—both, however, heavily reduce the phase transition temperature. The transmembrane property of a peptide may also appear as an important factor, either for its direct effects or for its ability to modulate the effects of another peptide on the thermotropic lipid phase behavior. Although Alm up to 0.5 % mole shows no dramatic effects on the lipid's thermodynamic properties, an almost negligible amount of both GS and $(LA)_{12}$ (which also show no considerable effects on their own) in combination with 0.5 % Alm causes a drastic drop in T_H (perhaps due to the promotion of the cubic phase at a much lower temperature than the H_{II} phase). This suggests that any AMP, no matter how large or small the amount, may heavily perturb the effect(s) of another AMP in a lipid bilayer system. Generally, we find that in binary mixtures of AMPs, [e.g. Alm and either GS or $(LA)_{12}$], their combined effects show neither plain additiveness of their independent effects, nor do they antagonize each other's effects. The resultant effect rather mimics the effect(s) of one component AMP (primary effects), while the other appears as a modulator (secondary effects) of the effects of the first component AMP, and vice versa depending on their relative concentrations.

Although Alm at high concentrations independently or in a binary presence with any other AMP (ultra low–high concentration) promotes a cubic phase instead of (or in addition to) the H_{II} phase in the liquid crystalline phases of DEPE dispersions, Alm at an ultra-low ion channel-forming concentration (10^{-8} M) alone certainly cannot disintegrate the lipid structure. However, another electrophysiology study [3] suggests that GS at ultra-low concentrations can also perturb the Alm channel properties, probably by changing physical bilayer properties such as its elasticity,

monolayer curvature, and lipid intrinsic curvature profiles. These changes certainly affect membrane energetics [2, 5], with considerable effects on lipid phase properties.

Based on the above research, it is clear that the presence of peptides in membranes alters lipid phase properties, and it is also clear that the presence of multicomponent peptides may help multiple lipid phases (e.g., inverse hexagonal, cubic, etc.) to co-exist. This study again confirms the possibility of co-existence of various phases, not only due to the membrane-forming primary biophysical parameters such as osmotic pressure, hydration, etc., but also due to other natural or artificial external agents, such as various peptides. Also, we have found that specific lipid phases may be due to the effects of certain peptides. In biological membranes, the lipid phase diagrams are therefore more complicated than the ones presented earlier in this chapter or proposed elsewhere so far. Considering the biophysical contributions from all participating agents that are directly responsible for constructing membranes, and agents that reside inside membranes, the construction of exact lipid phase diagrams is yet to be achieved.

References

1. Ashrafuzzaman, Md.: Department of Biochemistry, University of Alberta, unpublished (2007)
2. Ashrafuzzaman, Md., Tuszynski, J.A.: Ion Pore Formation in Membranes due to Complex Interactions Between Lipids and Antimicrobial Peptides or Biomolecules. In: Goddard, W., Brenner, D., Lyshevki, S., Iafrate, G. (eds.) Handbook on Nanoscience, Engineering and Nanotechnology. Taylor & Francis Group (in CRC press), Boca Raton (2011)
3. Ashrafuzzaman, Md., McElhaney, R.N., Andersen, O.S.: One antimicrobial peptide (gramicidin S) can affect the function of another (gramicidin A or alamethicin) via effects on the phospholipid bilayer. Biophys. J. **94**, 21a (2008)
4. Ashrafuzzaman, Md., Koeppe, R.E., II, Andersen, O.S.: Lipid bilayer elasticity and intrinsic curvature as regulators of channel function: a comparative single molecule study. New J. Phys. (2011) (Accepted)
5. Ashrafuzzaman, Md., Tseng, C.-Y., Tuszynski, J.A.: Chemotherapy drugs form ion pores in membranes due to phyical interactions with lipids (2011) (Submitted)
6. Gawrisch, K., Parsegian, V.A., Hajduk, D.A., Tate, M.W., Gruner, S.M., Fuller, N.L., Rand, R.P.: Energetics of a hexagonal-lamellarhexagonal transition sequence in dioleoylphosphatidylethanolaminemembranes. Biochemistry **31**, 2856–2864 (1992)
7. Gruner, S.M.: Intrinsic curvature hypothesis for biomembrane lipid composition: a role for nonbilayer lipids. Proc. Natl. Acad. Sci. USA **82**, 3665–3669 (1983)
8. Hinz, H.-J., Kuttenreich, H., Meyer, R., Renner, M., Frund, R., Koynova, R., Boyanov, A.I., Tenchov, B.G.: Stereochemistry and size of supar headgroups determine structure and phase behavior of glycolipid membranes: densitometric, calorimetric and X-ray studies. Biochemistry **30**, 5125–5138 (1991)
9. Israelachvili, J.N., Marcelja, S., Horn, R.G.: Physical principles of membrane organization. Q. Rev. Biophys. **13**, 121–200 (1980)
10. Jain, M.: Introduction to Biological Membranes, 2nd ed. Wiley, New York (1988)
11. Keller, S.L., Gruner, S.M., Gawrisch, K.: Small concentrations of alamethicin induce a cubic phase in bulk phosphatidylethanolamine mixtures. Biochim. Biophys. Acta **1127**, 241–246 (1996)
12. Killian, J.A., de Kruijff, B.: The influence of proteins and peptides on the phase properties of lipids. Chem. Phys. Lipids **40**, 259–284 (1986)

13. Killian, J.A., Burger, K.N., de Kruijff, B.: Phase separation and hexagonal H_{II} phase formation by gramicidins A, B and C in dioleoylphosphatidylcholine model membranes. A study on the role of the tryptophan residues. Biochim. Biophys. Acta **897**, 269–284 (1987)
14. Kinnunen, P.K.J.: On the molecular-level mechanisms of peripheral protein-membrane interactions induced by lipids forming inverted non-lamellar phases. Chem. Phys. Lipids **81**, 151–166 (1996)
15. Kirk, G.L., Gruner, S.M., Stein, D.L.: A thermodynamic model of the lamellar to inverse hexagonal phase transition of lipid membrane-water system. Biochemistry **23**, 1093–1102 (1984)
16. Kozlov, M.M., Leikin, S., Rand, R.P.: Bending, hydration and interstitial energies quantitatively account for the hexagonal-lamellar-hexagonal reentrant phase transition in dioleoylphosphatidylethanolamine. Biophys. J. **67**, 1603–1611 (1994)
17. Kucerka, N., Tristram-Nagle, S., Nagle, J.F.: Closer look at structure of fully hydrated fluid phase DPPC bilayers. Biophys. J. **90**, L83–L85 (2006)
18. Lewis, R.N.A.H., Mannock, D.A., McElhaney, R.N.: Membrane lipid molecular structure and polymorphism. Curr. Top. Membr. (Academic Press) **44**, 25–102 (1997)
19. Luzzati, V.: X-ray Diffraction Studies of Lipid Water Systems. In: Chapman, D. (ed.) Biological Membranes: Physical Fact and Function, Vol. 1, pp. 71–123. Academic Press, London (1968)
20. Mannock, D.A., McElhaney, R.N.: Differential scanning calorimetric and X-ray diffraction studies of a series of synthetic β-D-galactosyl diacylglycerols. Biochem. Cell Biol. **69**, 863–867 (1991)
21. Mannock, D.A., Lewis, R.N.A.H., Sen, A., McElhaney, R.N.: The physical properties of glycosyl diacylglycerols: calorimetric studies of a homologous series of 1,2-di-O-acyl-3-O-(β-D-glucopyranosyl)-sn-glycerols. Biochemistry **27**, 6852–6859 (1988)
22. Mannock, D.A., Lewis, R.N.A.H., Sen, A., McElhaney, R.N.: Physical properties of glycosyl diacylglycerols. 1. Calorimetric studies of a homologous series of 1,2-di-O-acyl-3-O-(β-D-glucopyranosyl)-sn-glycerols. Biochemistry **29**, 7790–7799 (1990)
23. Prenner, E.J., Lewis, R.N.A.H., Neuman, K.C., Gruner, S.M., Kondejewski, L.H., Hodges, R.S., McElhaney, R.N.: Nonlamellar phase induced by the interaction of gramicidin S with lipid bilayers. A possible relationship to membrane-disrupting activity. Biochemistry **36**, 7906–7916 (1997)
24. Rand, R.P., Fuller, N.L.: Structural dimensions and their changes in a reentrant hexagonal-lamellar transition of phospholipids. Biophys. J. **66**, 2127–2138 (1994)
25. Seddon, J.M.: structure of the inverted hexagonal (H_{II}) phase and nonlamellar phase transitions of lipids. Biochim. Biophys. Acta **1031**, 1–69 (1990)
26. Shyamsunder, E., Gruner, S.M., Tate, M.W., Turner, D.C., So, P.T.C., Tilcock, C.P.S.: Observation of inverted cubic phase in hydrated dioleoylphosphatidylethanolaminemembranes. Biochemistry **27**, 2332–2336 (1988)
27. Singer, S.J., Nicholson, G.L.: The fluid mosaic model of the structure of cell membranes. Cell membranes are viewed as two dimensional solutions of oriented globular proteins and lipids. Science **175**, 720–731 (1972)
28. Sud, M. et al.: LMSD: Lipid MAPS structure database. Nucleic Acids Res. **35**, D527–D532 (2007)
29. Takahashi, H., Sinoda, K., Hatta, I.: Effects of cholesterol on the lamellar and the inverted hexagonal phases of dielaidoylphosphatidylethanolamine. Biochim. Biophys. Acta **1289**, 209–216 (1996)
30. Tournois, H., Fabrie, C.H., Burger, K.N., Mandersloot, J., Hilgers, P., Van Dalen, H., De Geir, J., De Kruijff, B.: Biochemistry **29**, 8297–8307 (1990)
31. van Meer, G.: Cellular lipidomics. EMBO J. **24**, 3159–3165 (2005)
32. van Meer, G., Voelker, D.R., Feigenson, G.W.: Membrane lipids: where they are and how they behave. Nature Rev. Mol. Cell Biol. **9**, 112–124 (2008)
33. Zhang, Y.-P., Lewis, R.N.A.H., Hodges, R.S., McElhaney, R.N.: Peptide models of the helical hydrophobic transmembrane segments of membrane proteins: interactions of acetyl-K_2-$(LA)_{12}$-K_2-amide with phosphatidylethanolamine bilayer membranes. Biochemistry **40**(**2**), 474482 (2001)

Chapter 4
The Membrane as a Transporter, Ion Channels and Membrane Pumps

A cell membrane's primary role is to create a barrier against materials transferring between cellular exterior and interior regions. However, the presence of certain natural or artificial agents (especially during treatment) such as membrane proteins (MPs), antimicrobial peptides (AMPs), etc., occasionally induces transient or stable transport events into cell membranes. These properties are often found to be highly dynamic, time dependent, and specific to the agents inducing them. The events also fall into different classes due to the diversity of their structures and mechanisms. In this chapter, we discuss in detail a few classes of such events with a special focus on their membrane effects.

The cell membrane's function, in general, depends on the constituent membrane proteins. Floating around in the cell membrane are various types of proteins, generally globular proteins. They are not held in any fixed pattern, but instead exhibit a high degree of mobility in the phospholipid layer. In general, these proteins can be structurally classified into three categories:

- carrier proteins that regulate transport and diffusion,
- marker proteins that identify the cell to other cells,
- receptor proteins that allow the cell to receive instructions, communicate, transport proteins to regulate what enters or leaves the cell.

Membrane proteins are either (a) peripheral or (b) integral. Peripheral proteins are bound electrostatically to the exterior parts of head groups and hence can be easily extracted. Integral proteins are tightly bound to lipid tails and are insoluble in water. Steroids are sometimes a component of cell membranes in the form of cholesterol; when present, it reduces the fluidity of the membrane. However, not all membranes contain cholesterol.

Transport proteins come in two forms. Carrier proteins are peripheral proteins that do not extend all the way through the membrane. They bond and drag specific molecules through the lipid bilayer one at a time and release them on the opposite side. Channel proteins extend through the lipid bilayer. They form a pore through the membrane that can move molecules in several ways. In some cases the channel

M. Ashrafuzzaman and J. Tuszynski, *Membrane Biophysics*,
Biological and Medical Physics, Biomedical Engineering,
DOI: 10.1007/978-3-642-16105-6_4, © Springer-Verlag Berlin Heidelberg 2012

proteins simply act as a passive pore, where molecules randomly move through the opening via diffusion. This requires no energy, and molecules move from an area of high concentration to an area of low concentration. Symports also use the process of diffusion. In this case, a molecule that is moving naturally into the cell through diffusion is used to drag another molecule into the cell. For example, glucose hitches a ride with sodium.

Marker proteins extend across the cell membrane and serve to identify the cell. The immune system uses these proteins to tell own cells from foreign invaders.

The cell membrane can also engulf structures that are much too large to fit through the pores in the membrane proteins. This process is known as endocytosis, and in it the membrane wraps itself around the particle and pinches off a vesicle inside the cell. The opposite of endocytosis is exocytosis. Large molecules that are manufactured in the cell are released through the cell membrane. A prominent example of this process is the exocytosis of neurotransmitter molecules into the synapse region of a nerve cell.

The primary function of bilayer-spanning proteins is to catalyze the selective transfer of materials and information across biological membranes. In this process, MPs undergo conformational changes, e.g., the opening/closing transitions in ion channels [38, 39, 54], the shift in substrate binding site accessibility in conformational carriers and ATP-driven pumps [53], etc. To the extent that these protein conformational changes involve the protein/bilayer interface, where the protein is coupled to the bilayer through hydrophobic interactions, they will perturb the bilayer immediately adjacent to the protein [1, 16, 25, 28, 42]. That is, protein conformational changes involve not only rearrangements within the protein, but more importantly, also interactions with the environment, particularly with the host bilayer. Some of these phenomena have been schematically illustrated in Fig. 4.1, in light of the investigations on the gating mechanisms observed in mechanosensitive channels in model membranes [39]. Here, the mechanosensitive channels are predicted to act as membrane-embedded mechano-electrical switches. The switches induce opening of large water-filled pores that hydrophobically couple with lipid bilayers. This pore bilayer coupling (or binding) forces the bilayer to deform near the pore opening to adjust the mismatch between pore length and the bilayer's resting thickness. The elastic properties of a bilayer [27] ensure that due to a possible continuous bending in the lipid monolayers near both longitudinal edges of the pore, the bilayer does not disintegrate. A structural change in the channel-forming agents is also a prediction made in the qualitative model (see Fig. 4.1). We have made this prediction mainly as a result of the observed structural rearrangements in the mechanosensitive channels during the back-and-forth transitions between the channel's closed and open states [39]. These structural changes may be due to rotation, bending, translation, etc. Behind the structural changes within both pore and lipid monolayers, near the pore, there exists a driving force. This driving force causes the coupling between pores/channels and a bilayer by creating structural changes in both lipid layers and the channels. We have recently discovered the origin of this driving force to be the coupling energy, originating from the interactions primarily due to the localized electrical properties of channel-forming agents (MPs, AMPs, etc.) and lipids within the

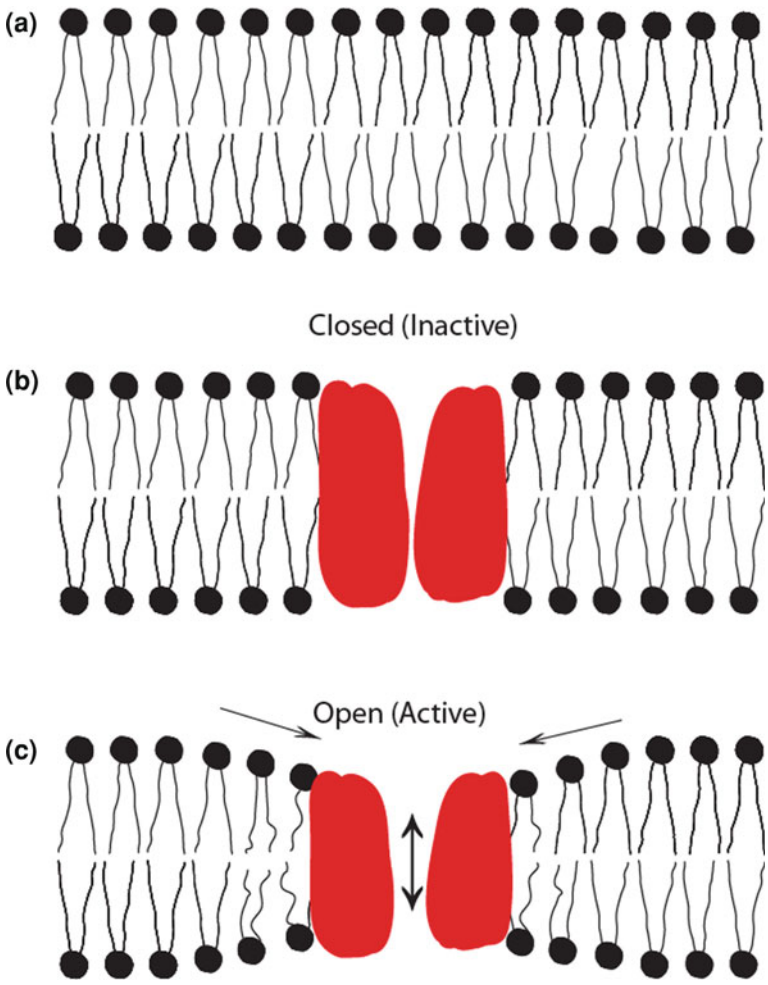

Fig. 4.1 A lipid bilayer membrane exists with an average constant thickness unless a random membrane protein or an ordered channel induces bilayer deformations. In **a**, a plain lipid bilayer membrane has been schematized. A lipid bilayer behaves like a barrier against ion flow across the membrane. In **b**, a lipid bilayer membrane with a possible inactive ion channel (in *red color*) within it has been schematized. In this case, despite the presence of an ion channel, the lipid bilayer still behaves as a barrier against ion flow across the membrane. The channel in this case is apparently considered to be an inactive or non-transporting agent. In **c**, a lipid bilayer membrane with a possible active ion channel has been schematized. In this case, unlike in the cases represented by (**a**) and (**b**), the bilayer conducts ions across the membrane. A decrease or increase in bilayer thickness near the channel interface as the channel undergoes a conformational transition from closed to open states or vice versa is an important hypothesis in this pictorial representation. A structural change (especially size) in the channel forming agents is also a theoretical prediction. These schematic diagrams have been drawn in light of the gating mechanisms observed in mechanosensitive channels in model membranes [39]

bilayer [6]. Chapter 5 is dedicated to discussing a comprehensive model of energetics related to the channel formation and the general functions of MPs.

The transport properties of lipid bilayer membranes depend on the type and number of membrane constituents. However, the hydrophobic MP-lipid coupling which generates certain lipid-protein, protein-lipid-protein, or lipid-protein-lipid complexes truly controls most of the processes occurring across membranes. AMPs are active in changing the biophysical properties of cell membranes. They often interact with lipids [11] and create AMP-lipid complexes which lead to the creation of protein-lined or lipid-lined well-structured ion channels/pores, less-structured ion flowing pores, and localized disorders or defects, etc. In the formation of such special structures in a membrane involving AMPs and lipids, various mechanisms are observed, which are mostly specific to AMPs. The complexes often appear with various distinguishable structures: a few of them are, for example, a linear β-helix created by gramicidin A, a barrel-stave pore created by alamethicin, a toroidal pore created by magainin, melittin, etc., lipidic channels created by ceramides (which is an example of a non AMP-induced channel), and defects created by gramicidin S, etc. In this chapter, we discuss the structures of these membrane-disrupting events, and the primary mechanisms which dictate their formation and functions. Based on the results of various model studies, we create a complete platform to address the antimicrobial effects of a group of AMPs. As mentioned earlier, this chapter will be organized around the structural aspects of the events that change membrane transport properties, mainly induced by AMPs, but sometimes even by certain classes of lipids. All these membrane events not only follow certain structural complexities due to the biophysical coexistence between channel-forming agents and the lipid membrane, as (for example) mentioned in Fig. 4.1, but these phenomena often satisfy complex energetics as well. We discuss the structural aspects of these processes in detail in this chapter, and the energetic aspects will be explained in Chap. 5.

4.1 Protein-Lined Ion Channels in Lipid Membranes

The membrane possesses pores or channels that allow a selective passage of metabolites and ions into and out of the cell. They can even drag molecules from an area of low concentration to an area of high concentration, working directly against diffusion. An example of this is the sodium/potassium pump. Most of the work done on the transport across membranes is done via ion pumps such as sodium-potassium pumps. The energy required for the functioning of the pump comes from the hydrolysis of ATP, in which a phosphorylated protein is identified as an intermediate in the process. The hydrolysis of a phospho-protein usually causes a conformational change that opens a pore that drives the sodium and potassium transport. Some membrane proteins actively use energy from the ATP in the cell to perform mechanical work. Here, the energy of a phosphate is used to exchange sodium atoms for potassium atoms. It can be demonstrated that the free energy change in the hydrolysis of a phospho-protein with a value of 9.3 kJ/mol will drive a concentration gradient of

50:1 uphill. For each ATP molecule hydrolyzed, three sodium ions are pumped out and two potassium ions are pumped in. Ion channels come in three general classes: (a) voltage-gated, (b) ligand-gated, and (c) so-called gap junctions. They differ not only in their design geometry, but also in the use of physical and chemical mechanisms for the selection of ions for passage.

In protein-lined channels it is generally accepted that channel-forming peptides align themselves along the channels. Ions flow through the longitudinal axis of the channel's interior between cellular exterior and interior regions. Hence, they most likely experience interactions with channel-forming peptides. Only at the entry and exit levels of the channels ions are expected to experience interactions with lipids (similar to the illustration in Fig. 4.1). Usually linear, cylindrical, or more complex types of structures are found in the class of protein-lined channels. This class refers to highly ordered peptide structures in association with lipids in membranes. Lipids play an important role in the regulatory phase of the channels, but the creation of such channels primarily depends on the properties (chemical, electrical, mechanical including geometry and material, etc.) of both the channel-forming peptides and lipids in the membrane. The number and type of the amino acid sequences and other constituents in the peptides, geometrical sizes (length, cross-section, etc.) of the peptides, and charge properties of the participating atoms and the effective total charge of the peptides in the hydrophobic membrane environment, etc., all play crucial roles in the construction of the protein-lined channels. The best examples of these effects can be found in two special ion channels, namely the gramicidin A and alamethicin channels. Therefore, this section will be dedicated to discussing key issues related to protein-lined channels using gramicidin A and alamethicin channels as important examples.

4.1.1 Gramicidin A Channels

A gramicidin A channel is a simple dimer of two right-handed, $\beta^{6.3}$-helical subunits or gramicidin A monomers [5, 29, 52]. This channel is formed by reversible, transbilayer association of the subunits [37]:

$$M_{\text{left}} + M_{\text{right}} \underset{k_1}{\overset{k_{-1}}{\rightleftharpoons}} D$$

Here, M and D denote a gramicidin A monomer and dimer, respectively. The subscripts (left and right) denote monomers residing in each bilayer leaflet, and k_1 and k_{-1} are two rate constants determining the channel appearance rate ($f_g = k_1 \cdot [M]^2$; $[M]$ being the monomer concentration) and channel lifetime ($\tau = 1/k_{-1}$). A schematic representation of the model is shown in Fig. 4.2. Peptides residing inside a membrane occasionally approach each other and, depending on the bilayer environment, associate with each other making a dimer with a very short lifetime, of the order of milliseconds (ms). The range of channel lifetimes depends on the strength of the

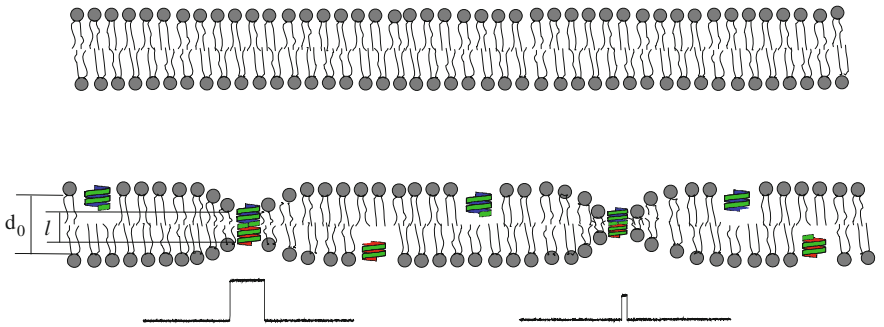

Fig. 4.2 A bilayer deforms at the bilayer gramicidin A channel coupling area, which incurs an energetic cost (see Chap. 5). This schematic diagram showing gramicidin A channels in lipid bilayers follows identical morphology as that presented in Fig. 4.1. The *upper panel* shows a lipid bilayer without any integral membrane proteins. The *lower panel* shows a bilayer with integral gramicidin A monomers and dimers of different lengths. When gramicidin A channels are formed inside a lipid bilayer under a trans-membrane potential difference between two sides, the bilayer conducts a current pulse with a specific average pulse width (proportional to the gramicidin A channel lifetime) and height (proportional to the gramicidin A channel conductance) depending on the gramicidin A channel type (the number of amino acids in the structures of gramicidin A monomers). Two types of gramicidin A monomers are schematically illustrated here to produce two gramicidin A channels of different lengths (l). d_0 is the unperturbed thickness of the bilayer [6, 10]

hydrophobic coupling between the channel and the bilayer. A more detailed description of the various properties of the ordered channel versus non-channel phases of the membrane will be provided in Chap. 5. It is important to mention that in these kinds of channels, only a dimer state is a stable structure for a channel. No other channel states are physically stable.

4.1.2 Alamethicin Channels

Alamethicin channels form barrel-stave pores [15, 26]. In this type of pore, the peptides align in such a way as to make a cylinder where the peptides stay on the surface of the cylinder. Many conductance states are possible, depending on the number of monomers involved in forming the cylindrical channel. A model diagram is shown in Figs. 4.3 and 4.4, and will be revisited in more detail in Chap. 5. Here, the channel is assumed to be formed due to inter-monomer binding. The channel also experiences hydrophobic coupling with lipid monolayers in both its longitudinal terminals. Unlike gramicidin A channels, where we observe only one ordered gramicidin A dimer state, there is no experimentally observed unique cylindrical alamethicin channel state. Alamethicin channels with various cylindrical states are possible. It appears physically plausible that a transition between different cylindrical channel states can take place. These states are modeled in various diagrams [6, 15, 26]. A phenomenological explanation of how the conformational transitions

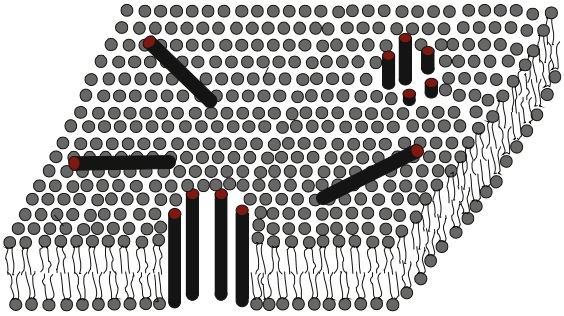

Fig. 4.3 Barrel-stave model for alamethicin channel formation inside lipid bilayers [8, 15, 26]. *Cylindrical rods* are schematic diagrams for alamethicin monomers in 3D view

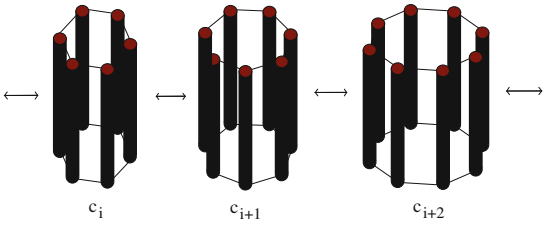

Fig. 4.4 The transition between different conduction pores of alamethicin channels

between different energy states in a barrel-stave pore occur (Figs. 4.3 and 4.4) has recently been offered [6]. A more detailed discussion of the stability, energetics, and regulation of the channel conformational states is given in Chap. 5.

4.2 Lipid-Lined Ion Channels in Membranes

In lipid-lined channels, it is generally assumed that channel-forming peptides interact with the lipid membrane, which creates the alignment of lipids along the channels. Ions flow through the opening between cellular exterior and interior regions, and possibly through the lipid regions, avoiding the peptides involved in creating channels. The lipid alignment causes an opening which may look like a long cylindrical lipid-aligned channel, where the membrane thickness may not change dramatically. The other possibility is that the membrane thickness slowly vanishes at the channel opening, which can equivalently be considered as a broken membrane condition. In many investigations this broken membrane structure has been predicted as a model for the lipid lined channels. Figure 4.5 shows a schematic diagram of this situation. This kinds of structures are found to be induced by both AMPs, e.g., magainin [31, 34], melittin [57], colicin [50], etc., or by other non-antimicrobial agents, such as the recently discovered pores by chemotherapy drugs thiocolchicocide and taxol molecules [7]. The magainin-, melittin- and colicin-induced toroidal pores can also be considered to be protein-lined channels, because here the peptides are always associated with the lipid head groups, with the result that the lipid monolayers bend

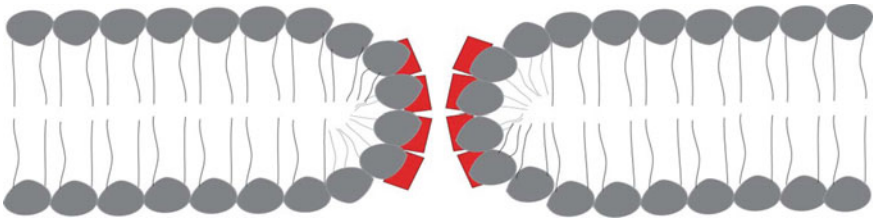

Fig. 4.5 Chemotherapy drugs TCC and TXL induced toroidal-type ion pores in a lipid bilayer membrane, which is possibly associated with a spontaneous change of the pore cross-section. This new model is explained in recent publications [6, 7]

continuously inward, so that the pore is lined by both peptides and lipid head groups. We have recently observed lipid-lined ion channels being induced by chemotherapy drugs in model membrane studies [6, 7].

4.3 Lipidic Channels in Membranes

In Sects. 4.1 and 4.2, we have described the structures of a few AMP-induced ion channels with different structures, which are responsible for an occasional compromise of the membrane's insulating properties. Here, we discuss how an ion channel can be formed by lipids. Although lipids primarily exist across the lipid layers, in a membrane, ceramides behave differently. Ceramides form channels, called ceramide channels, due to special organization of ceramides in phospholipid membranes. A ceramide channel is also an example of a lipidic channel. A ceramide is a lipid molecule, composed of the amino acid sphingosine and a fatty acid. Ceramides exist in great concentrations in the plasma membrane of a cell, and act as signaling molecules for a number of cellular functions. Ceramides may also play a role in certain pathological states, including cancer, obesity, diabetes, inflammation, etc. Understanding ceramide organization in membranes is therefore of great medical interest. A model structure of ceramide channel is presented in Fig. 4.6. From the model diagram, it is clear that the ceramide channels look more like alamethicin's barrel-stave pore, but have no resemblance to the structures of other channels, like the toroidal or β-helical types described earlier in this chapter. That means the lipid membrane adjusts with the complex of ceramide molecules at the channel membrane interface, and without affecting the membrane thickness, in contrast to what is proposed in the case of toroidal pores. Detailed understanding of the mechanism of the lipidic channels is still lacking but some insights have been made in the research papers published by several groups [3, 43, 48].

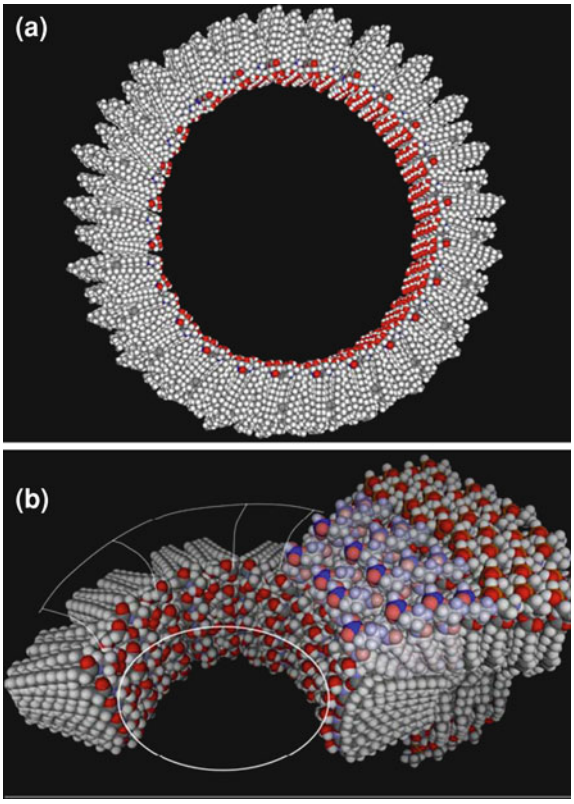

Fig. 4.6 These model diagrams of the C16-ceramides in membranes (ceramide channel) were provided by Professor Marco Colombini, and were previously published in [43]. In addition to this paper, earlier papers of the group, (e.g. [48]) also provide details of the ceramide channel phenomena in lipid membranes. **a** The channel is slightly tilted to illustrate the columns that span the membrane, each consisting of six ceramide monomers. The pore is lined by hydroxyl groups. The hydrocarbon tails are oriented parallel to the plane of the membrane. The columns are arranged in an antiparallel fashion, so that the carbonyl oxygen of the amide linkage (*red*) is only visible in every other column. The pore diameter of this 48-column channel is 10 nm. **b** A model of a segment of a smaller ceramide channel, showing how it might interface with the phospholipid membrane. Note the slightly hourglass shape of the pore, and the distorted phospholipids (*lighter colors*) that cover the hydrocarbon chains of the ceramides at the end of the channel. The structure of this interface is an illustration of the results reported from molecular dynamic simulations by the same group [3]. This figure and its caption has been taken with the publisher's permission from [43]

4.4 Defects in Membranes

In Sects. 4.1–4.3 we have discussed how membranes can be forced to compromise with the lipid-created bilayer's electrical insulating properties, by inducing some complexes of the participating antimicrobial peptides, lipids, specific biomolecules, etc. In all of these cases, the structure of the complexes, together with the lipids in

the membranes takes some specific forms which are understandable and can be modeled. However, there exist some other ways a few agents can create disorders inside membranes, in contrast to these ordered structures. These structural disorders, often referred to as 'defects', may occasionally be compared to events that are responsible for creating conductive properties in a non-channel fashion inside membranes. Since they are random disorders, it is hard to schematize them, due to their diverse appearances. Nonetheless, many attempts have been made by researchers to model them using scientific analogy. The in-plane diffusion model of Bechinger or similar models (as in [12, 13]) are relevant examples. In the Bechinger model, the insertion of antimicrobial peptides into phospholipid bilayers is assumed to disorganize the hydrocarbon chains of adjacent phospholipid molecules, creating a local thinning of the bilayer and increasing the cross-sectional area per phospholipid molecule. This process finally leads to local disturbances in bilayer packing, and leads to an increased bilayer permeability. Such a bilayer perturbation requires minimal peptide aggregation, which would be both entropically and electrically unfavorable. Yet, these regions of instability may eventually overlap due to lateral diffusion within the membrane, thereby producing transient "openings" of a variety of sizes. Evidence of such defects has recently been found by us while investigating the membrane effects of a small AMP gramicidin S [9]. This gramicidin S-induced destabilization of the phospholipid bilayer is expected to be enhanced with the insertion of additional peptide molecules, and with an increasing trans-membrane potential, as was indeed observed. Also, the bilayer properties, participating lipids, andhydrocarbons were all found to play a concomitant role in the induction of the AMP-induced defects or non-channel conductance events in our study that found a novel mechanism of action [9].

4.5 Comparative Analysis of the Electrical Conductance States that Determine the Membrane's Transport Properties Induced by Ion Channels or Other Conductance Events

In Fig. 4.7 we have presented our electrophysiology results in terms of current traces recorded across phospholipid/n-decane membranes doped with channel-forming antimicrobial peptides or chemotherapy drug molecules as examples of current traces through ion channels. The AMP-induced channels are found to be transporting currents with distinguishable amplitudes considering their different conformational states and rectangular current events in current-versus-time plots which are found in these cases (see for example both linear β-helical gramicidin A and barrel-stave alamethicin channel currents). The transitions between different current states are transient, meaning the transition takes no measurable time. The current traces through the proposed thiocolchicoside (TCC)- and taxol (TXL)-induced toroidal channels show no clear constant current amplitudes that might represent any specific conductance state. We believe that the triangular current events in these cases represent a

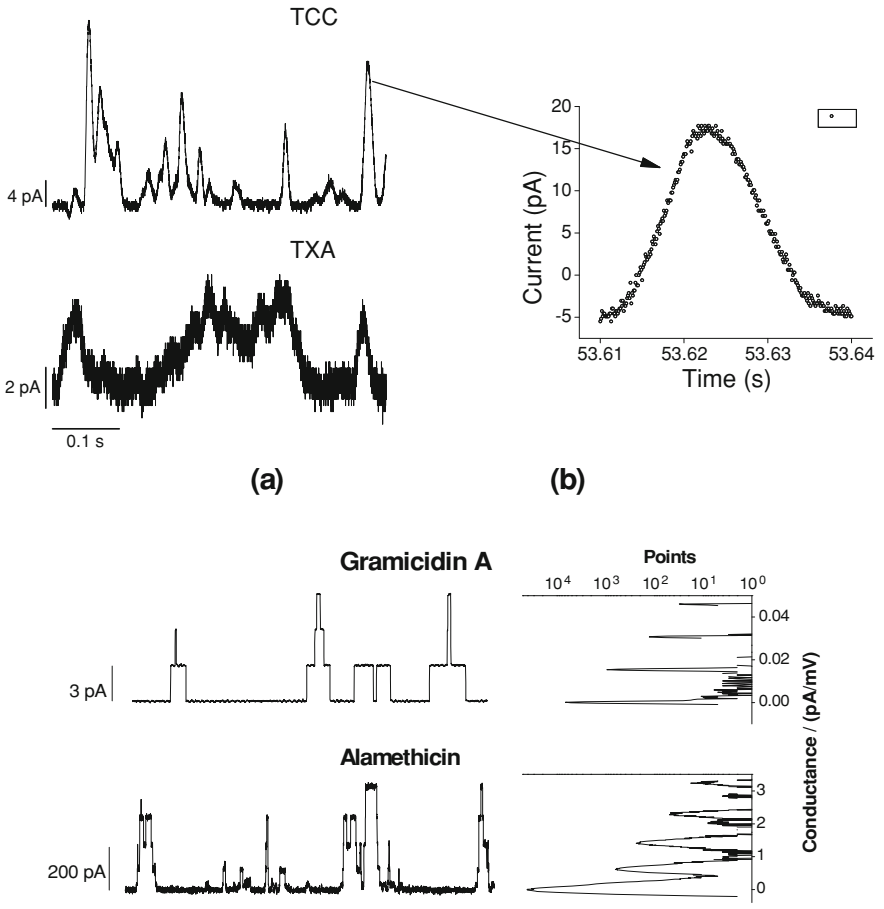

Fig. 4.7 Electrical conductance states that determine the membrane's transport properties induced by ion channels. The *upper panel* shows triangular-shape conductance events induced by thiocolchicoside (TCC) and taxol (TXL), both at 90 μM. (pH = 5.7, V = 100 mV.) Both traces were filtered at 20 kHz, but the *lower* one shows higher noise due to its presentation (current axis) at an amplified scale. In a high-resolution plot (shown in the *right side* of the *arrow*) of a single event showing individual points (in Origin 8.5 plot) we observe all points (*open circle*) with values of conductance increasing and decreasing, respectively, at both *left*- and *right*-lateral sides of the chemotherapy drug-induced triangular conductance events. The *lower panel* (**a**) illustrates rectangular-shape conductance events in gramicidin A (gA) and alamethicin (Alm) channels [9]. gA channel activity was recorded at 200 mV and Alm at 150 mV. Traces representing gA and Alm channel activities in phospholipid bilayers were recorded at filter frequencies 2 and 20 kHz, respectively. A lower filter frequency for traces representing gA channel activity is acceptable because of the channel's relatively higher stability. In panel (**b**) the point count plots of the current traces through gA and Alm channels peak at discrete values of conductance

channel pore whose cross-sectional area changes back-and-forth freely over time. Unlike transient current transitions in AMP channels, the transition of current in chemotherapy drug channels is a time-dependent phenomenon. This clearly suggests that AMP channels undergo structural transitions between distinguishable structures, e.g., gramicidin's monomer and dimer states (see Fig. 4.2) and alamethicin's different states depending on the participating alamethicin monomers in its barrel-stave pore, which determine the cylindrical channels' distinguishable cross-sections (see Figs. 4.3 and 4.4). Each distinguishable structure represents a discrete current level in a single AMP channel conductance state. Since all distinguishable structures are relatively stable, we observe stable amplitudes in all corresponding current levels. An entirely different current structure is observed in the case of chemotherapy drug channels. The spontaneous change of current amplitude clearly suggests no specific structure of the channel with a constant geometrical dimension. Only the broken membrane model (see the two-dimensional view in Fig. 4.5) can support the idea of a time-dependent continuous change of a pore's cross-sectional area. This is a new effect [6, 7]. The lipidic channels created, for example, by ceramides show no difference compared to barrel-stave pore type current transitions (for details see [3, 43, 48]). However, the current traces which represent defects inside membranes (see Fig. 4.8) show another novel behavior. Sudden spikes with apparently no specific 'amplitude and stability' represent conductance events inside membranes. These spikes certainly do not provide evidence of an instability of any distinguishable structure or any specific complex created by the antimicrobial peptide gramicidin S with lipids. Unlike the certain presence of discrete peaks at specific values of conductance (representing stable structures of channels) in the point-count-versus-conductance plots in gramicidin A and alamethicin channels, we observed no discreteness in the point count plots of the current traces due to both chemotherapy drug channels and gramicidin S-induced defects.

Based on the analysis of the current traces, we conclude that membrane transport is characterized by various distinguishable properties of current flows, seen through the conductance events. Furthermore, the structures of the conductance events show diverse behavior, depending on the properties of the participating agents and the membranes.

4.6 General Models for Peptide Pathways and the Creation of Channels in Membranes

Peptides interacting with lipids in the hydrophobic lipid bilayer environment create membrane effects through the creation of various morphological disorders in membranes. We have so far addressed a few specific cases using a set of AMPs: gramicidin A, alamethicin, magainin, melittin, colicin, gramicidin S, etc. A specific peptide is found to create a specific peptide-lipid complex, which means that active events in membranes are highly specific to the membrane active agents. The

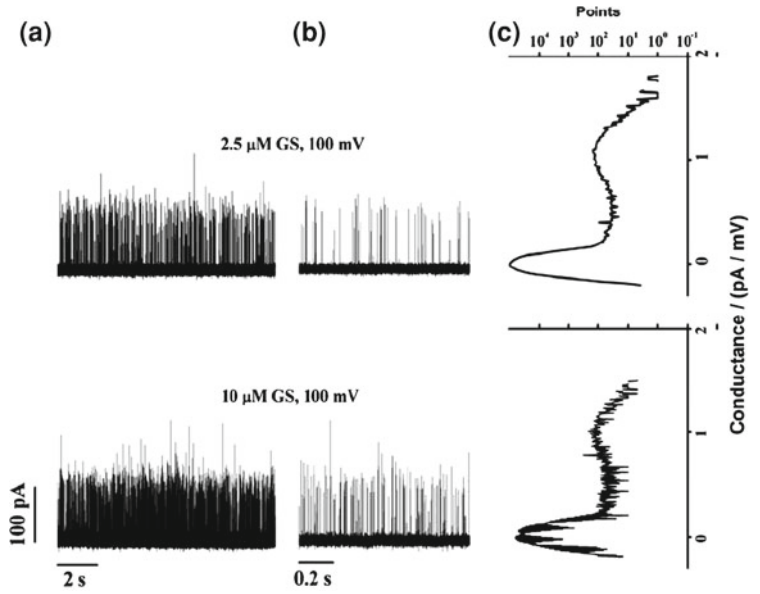

Fig. 4.8 Electrical conductance states that determine the membrane's transport properties induced by defects. Gramicidin S (GS) induced ion conductance events in zwitterionic phosphatidylcholine/n-decane bilayers with 1.0 M NaCl, pH 7.0 on both sides. In (**a**) and (**b**) show long-time (11 s) and short time (1 s) current traces of GS-induced ion conductance events, respectively. In (**c**) shows all point conductance level histograms constructed from the long time traces (**a**). Two peaks in (**c**) at 0 pA/mV and around 1 pA/mV, respectively, represent the baseline conductance of the "unperturbed" bilayer and the conductance levels of the GS-induced ion conductance events. Additional details of the GS effects can be found in [9]

membrane effects of peptides are also highly dependent on the environment in the peptide pathway (see Fig. 4.9). The properties of peptides such as water solubility, the diffusion coefficient across the hydrophilic/hydrophobic boundaries, and, above all, the energetics in the membrane interface are all important factors that determine the membrane effects of peptides.

In order to generate cytolytic activity, peptides need to survive their exposure to serum and other media, and pass through different barriers in the extracellular matrix, the bacterial lipopolysaccharides, outer membrane regions, and/or peptidoglycan layers [2]. After reaching the cell membrane environment, the structures and topologies of peptides are in dynamic interchange [30, 44]. Solid-state nuclear magnetic resonance (NMR) spectroscopy and other biophysical techniques indicate that peptide antibiotics strongly interact with lipid membranes. Bechinger's work [12, 13] and other studies suggest that in a bilayer environment, many peptides with a higher number of amino acids in their sequences, such as cecropins, magainins, etc., exhibit amphipathic α-helical conformations and their helix axes become parallely aligned to the membrane surface. On the other hand, other peptides such as alamethicin, gramicidin A, etc., are found to experience trans-membrane

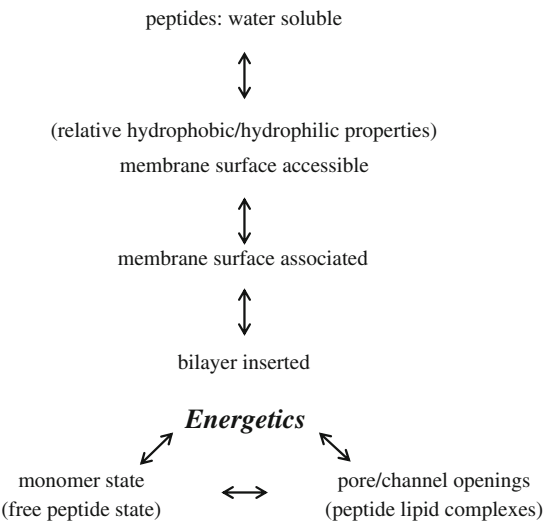

Fig. 4.9 Peptide pathway flowchart addresses how peptide insertion into membrane (peptide pathway) ends up creating membrane effects. The membrane action of any peptide mainly depends on the following two factors: (i) the relative hydrophobic/hydrophilic properties of any peptide determining the relative probability of insertion into the membrane, (ii) energetics between peptides and a lipid bilayer in the hydrophobic membrane environment that determines the stability of any peptide-lipid complex. An in-depth analysis of the energetics of these processes can be found in Chap. 5

orientations. Figure 4.10 shows how the orientations of the peptide helix axis emerge using NMR spectra studies on peptides interacting with membranes. During the membrane insertion, the structures of peptides may change dramatically. This can be a complete transition of structures from a random coil to a highly helical (e.g. α-helix) arrangement, or an orientation, rotation, and any other specific type of structural distortion, etc. A detailed analysis, based on a number of studies, is summarized in [12].

As the peptides approach or enter the lipid membrane region, the electrostatic and hydrophobic interactions of the peptides with the lipid bilayer appear to strongly regulate the peptides' membrane association properties, and a subsequent potentially lethal effect on the cell. The surface charge density of lipid bilayers, the localized charges in lipids (especially in the head group regions), etc., have a huge effect on the membrane association of cationic peptides. The peptides' own identical charges also repel each other, which might also affect their membrane association coefficients. The distribution of charges associated with the lipids in membranes is also membrane specific. Moreover, as the peptides approach lipid head group regions, the presence of charges, brought onto the peptides, causes polarization in the localized charge conformations in lipid head groups. This is a very simple electrostatic effect. About three decades ago, Seelig et al. [46] reported their experimental investigations, which indicated that the phospholipid head groups are sensitive to electric charges and dipole

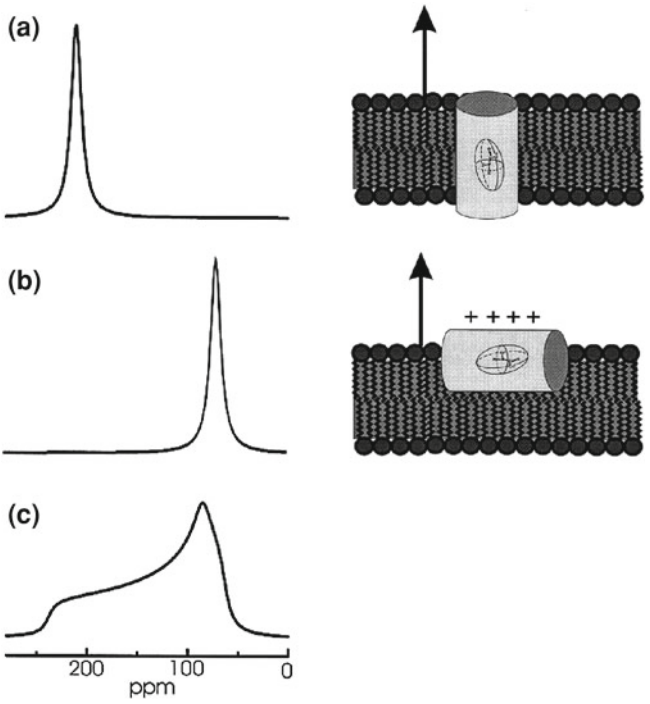

Fig. 4.10 Calculated proton-decoupled 15N solid-state NMR spectra of helical peptides 15N-labeled at a single site and reconstituted into oriented membranes (illustrated to the *right* of the spectra). The membrane normal is aligned parallel to the magnetic field direction (*arrows*). **a** Trans-membrane orientation of the helix axis. **b** Orientation of the peptide approximately perpendicular to the magnetic field direction. **c** Powder pattern line shape where a random distribution of molecular orientations has been assumed. This figure has been adapted from [13] with due permission from the publisher

fields. This group also suggested, through convincing analysis, that the lipid polar groups act as 'molecular electrometers' that respond to both molecules partitioning into the lipid bilayers, and any process that modifies the electrical properties of the membrane surface. Earlier, the dipole moment of the phosphocholine group was calculated, which, in its 200 declination with the membrane surface, was found to induce a very high 90 mV dipole potential in the membrane environment [46, 47]. Depending on the direction of the dipole moment, the potential can enhance or reduce the existing electric potential, and is sufficiently large to trigger conformational and/or functional changes in membrane proteins, or to facilitate peptide or protein insertion into the membrane's hydrophobic core. The membrane absorption of peptides bearing electrostatic charges therefore substantially influences the functions of these molecular electrometers, with the lipids having reverse effects on the peptide aggregation or any general function. From the discussion presented above, it is clear that all kinds of lipids may cause localized charge effects, and these effects become complex with the

presence of charge-bearing peptides in the vicinity. For example, the outer monolayers of bacterial plasma membranes are rich in negative phospholipids (which usually increase the local concentrations of cationic peptides), whereas the membranes of healthy vertebrate cells appear neutral. Most of the tumor cells lose part of their lipid asymmetry, and thus exhibit anionic character in their exterior. In addition to these asymmetries in membrane charge properties, there exists a trans-membrane electric potential. Large inner-negative trans-membrane potentials are observed in respiring prokaryotic cells, but not in erythrocytes [35]. Despite all these electrical properties due to the composition of the outer leaflet of red cell membranes and the negligible trans-membrane electric potential, electrostatic contributions are claimed to be small in the membrane association of peptides [14, 35]. Membrane association and the lytic activities of cationic amphiphiles are claimed to be governed by hydrophobic interactions with membranes instead. These hydrophobic interactions are functions of the hydrophobic angle, the hydrophobic moment, and the overall hydrophobicity of the peptides [21, 54, 56]. To better understand the effects related to membrane association of peptides, the reader is referred to a very important review [13] and an earlier publication [12] by Bechinger. The lipid membrane's hydrophobic properties along with local charge properties of both lipids and peptides together determine the membrane association of peptides. However, once the peptides are already on or inside the lipid bilayer membrane, the peptide membrane's energetic coupling determines how the functions of the various peptide-induced membrane transport events and their biophysical properties are regulated. The energetics of these interactions also determine transitions between different peptide states, such as a monomer (or free) state and states of various complexes associated with lipids. The flowchart in Fig. 4.9 shows the region where the energetics discussed above play a role. In the previous sections, we have discussed the structural complexities of a few of these different peptide states in membranes, and the consequent antimicrobial activities due to specific AMPs. Despite this specificity the models of channel formation or general membrane effects of peptides can be separated into several general classes. These are briefly explained below.

4.6.1 The Trans-Membrane Helical Bundle Model

A step-wise conductance change (increase or decrease) is often explained using this model. Figure 4.11a [13] is a general representation of this type of model. Alamethicin channels (as described in Sect. 4.1.2) best represent this trans-membrane helical bundle model. The addition or subtraction of peptides into or from a cylindrical channel accounts for the increase or decrease, respectively, of the channel's cross-sectional area. As a result, the channel conductance experiences a sharp transition between different current levels. Based on this hypothesis, we have also provided a model diagram for alamethicin channel structure as presented earlier in Sect. 4.1.2 [6].

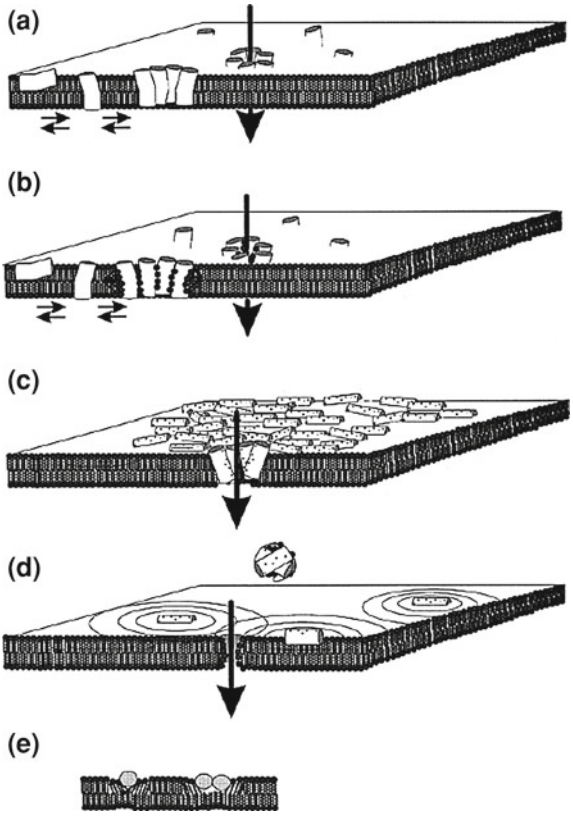

Fig. 4.11 These model diagrams represent various events that might change the transport properties of phospholipid membranes through the creation of ion-conducting pores or other membrane-disrupting events. **a** Hydrophobic polypeptides form trans-membrane helical bundles. **b** The wormhole model. **c** The carpet model. **d** The in-plane diffusion model: peptide monomers are surrounded by areas of bilayer with irregular lipid packing characteristics. These diffuse along the surface of the bilayer causing transient openings when zones of metastability overlap. Alternatively, the detergent-like action of amphipathic peptides leads to the formation of peptide-lipid micelles, bilayer openings, and the transient formation of pores. **e** The disruption of the lipid bilayer packing due to in-plane inserted peptides is schematically illustrated for monomers and side-to-side dimers. In all these schematic diagrams one thing can be found in common, which is the mechanism behind the creation of these membrane-disrupting events. The possible lipid peptide interactions play an important role behind the creation of any lipid peptide complexes. For details beyond the description presented the reader is referred to Chap. 5. This figure has been adapted from [12, 13] with due permission from the publisher

4.6.2 The Wormhole Model

This is a modified form of a trans-membrane helical bundle model, in which lipids, together with peptides, are assumed to be lining across the cylindrical pore's surface.

In the model diagram presented in Fig. 4.11b [13], two monolayers meet each other through a lipid line where the lipid head groups touch the cylindrical channel. This model, therefore, represents a type of toroidal structure where both lipids and peptides align across the toroidal openings [31, 33]. Magainin was, for example, found to form a pore of this type [18].

4.6.3 The Carpet Model

Figure 4.11c represents a schematic diagram [13] of the Carpet model. The model suggests that as peptides accumulate on the membrane and in the pore, they experience an approximately 90° rotation (which is considered to be trans-membrane orientation) to penetrate into the bilayer. The peptides then participate in creating a trans-bilayer pore. In this case, the bilayer thickness near the pore is assumed not to vanish, as is partially shown in the toroidal pore in Fig. 4.10b. Some peptides with 11–15 leucines or lysines, for example, were found to have high levels of antibiotic activities [14], but the peptides with maximal antibiotic activity are too short to cross the membrane. Therefore, these peptides and other similar ones are observed to be oriented parallel to the membrane surface [17]. However, a 34-residue peptide called dermaseptin, which is rich in lysine and can be configured into an amphipathic α-helix through residues 1–27, is found to apparently not follow the previously claimed length-dependent membrane model. Despite having a greater length, it is found to localize at the membrane surface and then associate in a carpet-like structure, specifically in the presence of negatively charged lipids in the membrane and at high peptide concentrations [41]. This suggests that the model structure followed by any peptide depends not only on the properties of that specific peptide, but also to some extent on the membrane constituents.

4.6.4 Detergent-Like Effects

Cationic amphiphiles are most likely to induce considerable cytotoxic activity by disrupting the bilayer, if not always in a gross manner, perhaps often locally. Any bilayer disruption causes the loss of bilayer barrier properties, leading to substantial diffusion of materials across the membrane between inner and outer cellular regions. This also interferes with the membrane-associated energy metabolism. Detergents are often found to create this kind of bilayer disruption, which is schematized in Fig. 4.11d [13]. In this detergent-like membrane disruption, it is possible that at the boundary of the disrupted region the lipids align like a toroidal pore in which the lipid head groups align across the pore region and the tails point toward the hydrophobic membrane interior core. To create the detergent-like effects that cause the membrane disruption (Fig. 4.10d), a relatively high concentration of detergent (e.g. triton X-100) or in some cases peptides (e.g. magainin) is needed [24, 45].

4.6.5 The In-Plane Diffusion Model

In this model, the peptides are assumed to enter into phospholipid bilayers and disorder the hydrocarbon chains of adjacent phospholipid molecules. This creates bilayer thinning or local disruption in bilayer packing. Figure 4.11e is a schematic diagram representing this model [13]. This bilayer perturbation requires minimal peptide aggregation and the peptides are assumed to be aggregated partially. Usually, small size peptides are the best candidates for this kind of bilayer disruption. Gramicidin S is such a candidate [9]. As there is no trans-bilayer association of the peptides, any stable bilayer pore formation (like those in Fig. 4.10a–d) can be ruled out using this model. Peptides either independently or by being aggregated partially reduce the local bilayer thickness and lead to increased conductance. Therefore, any instantaneous conductance events (not stable channel-like) across a bilayer can be created. Such an event was first reported due to gramicidin S [9] which has been described in an earlier section. As the change in lipid packing is an important aspect, the membrane's constituents, thickness, charge properties, etc., have a huge role in creating any peptide-induced event that follows the in-plane diffusion model.

4.6.6 The Linear β-Helix

The gramicidin A channels, described earlier, do not fit into any of the models described by Bechinger [13]. This unique structure which creates a linear dimer called a 'linear β-helix' where the dimer's longitudinal edges hydrophobically couple with the lipid bilayer certainly defines an important and unique class. Figure 4.12 explains the model, drawn in light of the structure presented in Fig. 4.2 for the gramicidin A channel. Here, the dimer length can be smaller, of the order of the bilayer thickness, or can even be larger than the bilayer thickness. In the case when the channel length is smaller than the bilayer thickness, the lipid bilayer thickness is reduced near the channel. That means, the monolayers bend inward towards the membrane's hydrophobic inner core. However, when the channel length is smaller than the bilayer, the bilayer becomes locally thicker, that is, the monolayers bend outwards toward hydrophilic regions. The bilayer's elastic properties enable it to change its thickness, but the real cause of this thickness change lies behind complicated energetics, which will be explained in the next chapter.

4.7 Sodium–Potassium Pumps in Membranes

Electrochemical gradients for sodium and potassium ions, generated by the Na^+, K^+-ATPase, are vital to animal cells, exchanging three sodium ions for two potassium ions across the plasma membrane during each cycle of ATP hydrolysis. The Na^+,

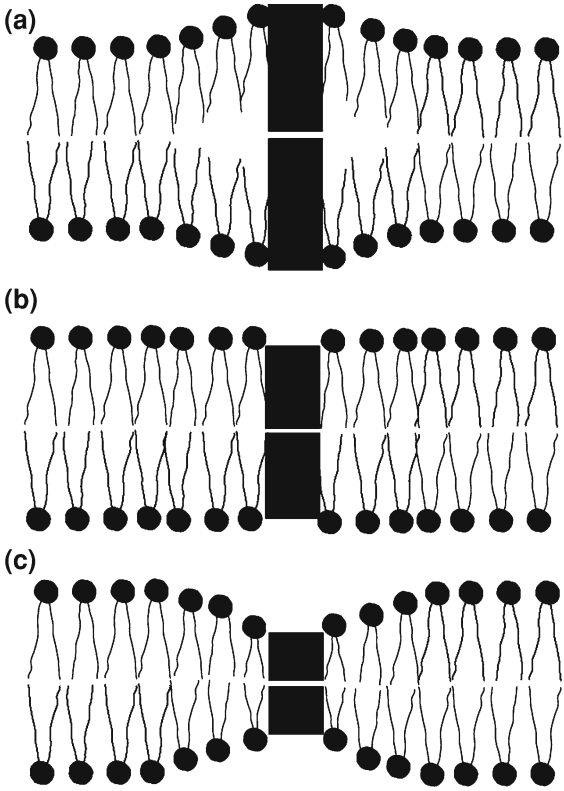

Fig. 4.12 A model diagram for a linear β-helix located in the membrane. **a** Channel length is larger than the bilayer thickness. **b** Channel length matches the bilayer thickness. **c** Channel length is smaller than the bilayer thickness. To hydrophobically match a bilayer and a channel at the two channel edges, the bilayer deformation, channel orientation, stretching, etc., can be possible. Due to the higher stiffness of the protein (channel) structure, it is hypothesized that the bilayer (due to its elastic properties) is more likely to undergo necessary deformations. The previously discussed gramicidin A channel (Sect. 4.1.1) falls in this category

K^+-ATPase, originally described more than a half century ago [49], is a membrane-bound ion pump belonging to the family of P-type ATPases. By using energy derived from ATP hydrolysis, the Na^+, K^+-ATPase generates electrochemical gradients for Na^+ and K^+ across the plasma membranes of animal cells, as required for electrical excitability, cellular uptake of ions, nutrients, and neurotransmitters, and the regulation of cell volume and intracellular pH. The transport function is accomplished by enzyme conformational changes between two states, E1 and E2, that selectively bind three Na^+ and two K^+ ions, respectively (see Fig. 4.13); the ions become transiently 'occluded', that is, inaccessible to the medium on either side of the membrane [23, 40]. The pump is sensitive to the membrane potential—the major voltage-dependent steps being associated with the binding and release of one of the three Na^+ ions [4, 19].

The Na^+, K^+-ATPase consists of α- and β-subunits. The α-subunit has binding sites for Na^+, K^+, and ATP, and is homologous to single-subunit P-type ATPases such as the Ca^{2+}-ATPase. The β-subunit is unique to the K^+-counter-transporting P-type ATPases, Na^+, K^+-ATPase and H^+,K^+-ATPase. The β-subunit is required for routing the α-subunit to the plasma membrane and for occlusion of the K^+ ions

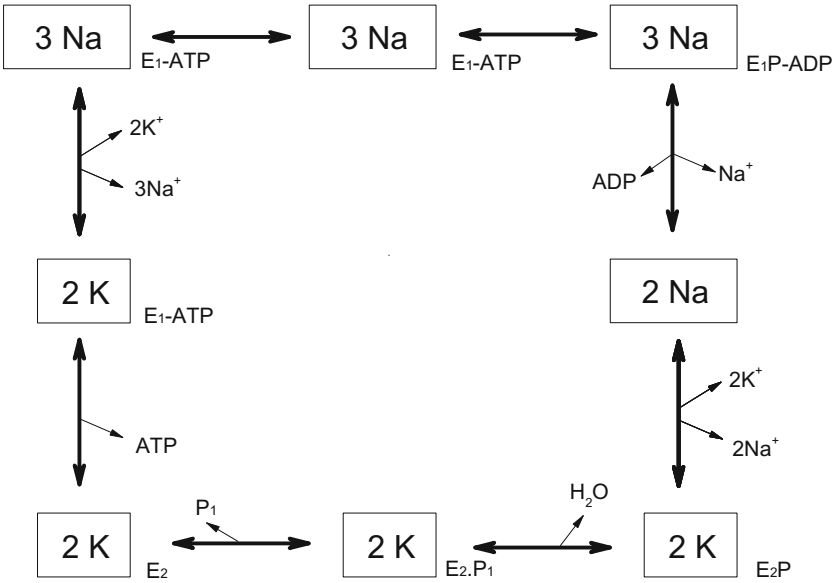

Fig. 4.13 The reaction cycle of the Na^+, K^+-ATPase [23, 40]

[22, 32]. A FXYD family member protein often associates itself with the $\alpha\beta$-complex as a third subunit, and regulates the pumping activity in a tissue- and isoform-specific way [20, 51].

A recent study of the crystal structure on the sodium–potassium pump [36] has described clearly how the membrane component is relevant to the activity of the pump. In light of the sensitivity of the Na^+, K^+-pump activity to the membrane potential, it is notable that arginines make the area around the C-terminus in the membrane edge region highly electropositive. In various types of voltage-dependent ion channels, arginine clusters act as voltage sensors that move in response to membrane depolarization, and in the Na^+, K^+-ATPase the arginine cluster associated with the C-terminus could function similarly as a control point for a voltage-sensitive switch that alters the relations of the C-terminus in its binding pocket during depolarization/repolarization, with consequences for the Na^+ affinity. The hypothesis involving a direct structural and functional relation between the C-terminus and the third Na^+ site is in accordance with the high voltage-sensitivity of the binding and release of one of the three Na^+ ions [4, 19].

References

1. Andersen, O.S., Sawyer, D.B., and Koeppe II, R.E.: Bio membrane structure and Function. edited by K. R. K. Easwaran and B. Gaber (Schenectady, New York: Adenine), 227–244 (1992)

2. Andreu, D., Rivas, L.: Animal antibacterial peptides: an overview. *Biopolymers* **47**, 415–433 (1999)
3. Anishkin, A., Sukharev, S., Colombini, M.: Searching for the molecular arrangement of transmembrane ceramide channels. Biophys. J. **90**, 2414–2426 (2006)
4. Apell, H.J. & Karlish, S.J.: Functional properties of Na, K-ATPase, and their structural implications, as detected with biophysical techniques. *J. Membr. Biol.* **180**, 1–9 (2001)
5. Arseniev, A.S., Barsukov, I.L., Bystrov, V.F., and Ovchinnikov, Y.A.: *Biol. Membr.* **3**, 437–62 (1986)
6. Ashrafuzzaman, Md. and Tuszynski, J.A.: Ion pore formation in membranes due to complex interactions between lipids and antimicrobial peptides or biomolecules. *Handbook on Nanoscience, Engineering and nanotechnology*. Edited by Goddard, Brenner, Lyshevki and Iafrate; Taylor & Francis Group (CRC press) (2011)
7. Ashrafuzzaman, Md., Tseng, C.-Y., Tuszynski, J.A. Chemotherapy drugs form ion pores in membranes due to physical interactions with lipids. (submitted) (2011)
8. Ashrafuzzaman, Md., Duszyk, M. and Tuszynski, J. A.: Chemotherapy drugs Thiocolchicoside and Taxol Permeabilize Lipid Bilayer Membranes by Forming Ion Pores. J. of Physics: Conf. Series **329**(012029), 1–16 (2011)
9. Ashrafuzzaman, Md., Andersen, O.S., and McElhaney, R.N. The antimicrobial peptide gramicidin S permeabilizes phospholipid bilayer membranes without forming discrete ion channels. Biochim. Biophys. Acta **1778**, 2814–2822 (2008)
10. Ashrafuzzaman, Md., Lampson, M.A., Greathouse, D.V., Koeppe II, R.E., Andersen, O.S.: Manipulating lipid bilayer material properties by biologically active amphipathic molecules. *J. Phys.: Condens. Mat.* **18**, S1235–1255 (2006)
11. Ashrafuzzaman, M. and Tuszynski, J. Regulation of channel functions due to coupling with a lipid bilayer. Biophys. J. **98**, 51a (2010) and J. Comp. Nanosci. 9, 564–570 (2012)
12. Bechinger, B. structure and functions of channel-forming peptides: Magainins, Secropins, Melittin and Alamethicin. *J. Membr. Bio.* **156**: 197–211, (1997)
13. Bechinger, B. (1999) The structure, dynamics and orientation of antimicrobial peptides in membranes by multidimensional solid-state NMR spectroscopy, Biochim. Biophys. Acta 1462, 157–183.
14. S.E. Blondelle, R.A. Houghten, Biochemistry 31 (1992) 12688–12694.
15. Boheim, G. (1974) Statistical analysis of alamethicin channels in black lipid membranes. J. Mem. Biol. 19:277–303.
16. Brown, M.F.: Modulation of rhodopsin function by properties of the membrane bilayer. Chem. Phys. Lipids 73: 159–180 (1994)
17. Castano, S., Desbat, B., Laguerre, M., Dufourq, J.: Structure, orientation and affinity for interfaces and lipids of ideally amphipathic lytic $L_i K_j$(i=2j) peptides. Biochim. Biophys. Acta **1416**, 176–194 (1999)
18. Cruciani, R.A., Barker, J.L., Durell, S.R., Raghunathan, G., Guy, H.R., Zasloff, M., Stanley, E.F.: Magainin 2, a natural antibiotic from frog skin, forms ion channels in lipid bilayer membranes. Eur J Pharmacol.**226(4)**, 287–296 (1992)
19. Gadsby, D.C., Rakowski, R.F. & De Weer, P.: Extracellular access to the Na, K Pump: Pathway similar to ion channel. Science **260**, 100–103 (1993)
20. Garty, H., Karlish, S.J.: Role of FXYD proteins in ion transport. Annu. Rev. Physiol. **68**, 431–459 (2006)
21. Gazit, E., Lee, W.J., Brey, P.T., Shai, Y.: Biochemistry **33**, 10681–10692 (1994)
22. Geering, K.: The functional role of β subunits in oligomeric P-type ATPases. J. Bioenerg. Biomembr. **33**, 425–438 (2001)
23. Glynn, I. M.: Annual review prize lecture. 'All hands to the sodium pump'. J. Physiol. (Lond.) **462**, 1–30 (1993)
24. Grant, E., Beeler, T.J., Taylor, K.M.P., Gable, K., Roseman, M.A.: Biochemistry **31**, 9912–9918, (1992)
25. Gruner, S.M.: Lipid membrane curvature elasticity and protein function in Biologically Inspired Physics, edited by L. Peliti (New York: Plenum): 127–135 (1991)

26. He, K., Ludtke, S.J., Huang, H.W., and Worcester, D.L.: Antimicrobial peptide pores in membranes detected by neutron in-plane scattering. Biochemistry **34**, 15614–15618 (1995)
27. Helfrich, W.: Elastic properties of lipid bilayers: theory and possible experiments. Z. Naturforsch. **28C**, 693–703 (1973)
28. Israelachvili, J.N.: Refinement of the fluid-mosaic model of membrane structure. Biochim. Biophys. Acta **469**, 221–225 (1977)
29. Ketchem, R.R., Roux, B., and Cross, T.A. 1997. High-resolution polypeptide structure in a lamellar phase lipid environment from solid state NMR derived orientational constraints. structure 5: 1655–69.
30. S. Lambotte, P. Jasperse, B. Bechinger, Biochemistry 37 (1998) 16–22.
31. Ludtke, S.J., He, K., Heller, W.T., Harroun, T.A., Yang, L., and Huang, H.W. 1996. Membrane pores induced by magainin. Biochemistry 35:13723–13728.
32. Lutsenko, S. & Kaplan, J. H. An essential role for the extracellular domain of the Na, K-ATPase β-subunit in cation occlusion. Biochemistry 32, 6737–6743 (1993).
33. K. Matsuzaki, Biochim. Biophys. Acta 1376 (1998) 391–400.
34. Matsuzaki, K., Murase, O., Tokuda, H., Fujii, N., and Miyajima, K. 1996. An antimicrobial peptide, magainin 2, induced rapid flip-flop of phospholipids coupled with pore formation and peptide translocation. Biochemistry 35: 11361–11368.
35. K. Matsuzaki, K. Sugishita, N. Fujii, K. Miyajima, Biochemistry 34 (1995) 3423–3429.
36. J. P. Morth, B. P. Pedersen, M. S. Toustrup-Jensen, T. L.-M. Sørensen, J. Petersen, J. P. Andersen, B. Vilsen, P. Nissen. Crystal structure of the sodium-potassium pump. NATURE 450: 1043–50 (2007)
37. O'Connell, A.M., Koeppe II, R.E., and Andersen, O.S. 1990. Kinetics of gramicidin channel formation in lipidbilayers: trans-membrane monomer association. Science 250: 1256–1259.
38. Perozo, E., Cortes, D.M., and Cuello, L.G. 1999. Structural Rearrangements Underlying K^+- Channel Activation Gating. Science 285: 73–78.
39. Perozo, E., Cortes, D.M., Sompornpisut, P., Kloda, A., and Martinac, B. 2002. Open channel structure of MscL and the gating mechanism of mechanosensitive channels. Nature 418: 942–948.
40. Post, R. L., Hegyvary, C. & Kume, S. Activation by adenosine triphosphate in the phosphorylation kinetics of sodium and potassium ion transport adenosine triphosphatase. J. Biol. Chem. 247, 6530–6540 (1972).
41. Y. Pouny, D. Rapaport, A. Mor, P. Nicolas, Y. Shai, Biochemistry 31 (1992) 12416–12423.
42. Sackmann, E. 1984. In Biological Membranes, edited by D. Chapman (London: Academic): 105.
43. S. Samanta, J. Stiban, T.K. Maugel, M. Colombini. Visualization of ceramide channels by transmission electron microscopy. Biochim. Biophys. Acta 1808: 1196–201 (2011)
44. M.S.P. Sansom: Curr. Opin. Colloid Interface Sci. 3 518–524 (1998)
45. P. Schlieper, E. De Robertis: Arch. Biochem. Biophys. 184 204–208 (1977)
46. J. Seelig, P. M. Macdonald and P. G. Scherer. phospholipid head groups as sensors of electric charge in membranes. Biochemistry 26; 7535–7541 (1987)
47. Shepherd, J. C. W., & Buldt, G.: Biochim. Biophys. Acta 514, 83–94 (1978)
48. L. J. Siskind, A. Davoody, N. Lewin, S. Marshall, and M. Colombini.: Enlargement and Contracture of C2-Ceramide Channels. Biophysical Journal 85: 1560–1575 (2003)
49. Skou, J. C.: The influence of some cations on an adenosine triphosphatase from peripheral nerves. Biochim. Biophys. Acta 1000, 439–446 (1957)
50. Sobko, A.A., Kotova, E.A., Antonenko, Y.N., Zakharov, S.D., and Cramer, W.A.: Lipid dependence of the channel properties of a colicin E1-lipidtoroidal pore. The J. of Biol. Chem. 281: 14408–16 (2006)
51. Therien, A. G. & Blostein, R.: Mechanisms of sodium pump regulation. Am. J. Physiol. Cell Physiol. 279, C541–C566 (2000)
52. Townsley, L.E., Tucker, W.A., Sham, S., and Hinton, J.F.: structures of gramicidins A, B, and C incorporated into sodium dodecyl sulfate micelles. Biochemistry 40: 11676–11686 (2001)

53. Toyoshima, C., and Mizutani, T.: Crystal structure of the calcium pump with a bound ATP analogue. Nature 430: 529–535 (2004)
54. E.M. Tytler, J.P. Segrest, R.M. Epand, S.Q. Nie, R.F. Epand, V.K. Mishna, Y.V. Venkatachalapathi, G.M. Anantharamaiah, J. Biol. Chem. 268 22121 (1993)
55. Unwin, P.N.T., and Ennis, P.D.: Two configurations of a channel-forming membrane protein. Nature 307: 609–613 (1984)
56. Wieprecht, T., Dathe, M., Krause, E., Beyermann, M., Maloy, W.L., MacDonald, D.L., Bienert, M. *FEBS Lett.* **417**: 135–140, (1997)
57. Yang, L., Harroun, T., Weiss, T.M., Ding, L., and Huang, H.W. Barrel-stave model or toroidal model? A case study on melittin pores. Biophys. J. **81**: 1475–1485, (2001)

Chapter 5
Lipid Bilayer-Membrane Protein Coupling

Lipid organization in membranes forms liquid crystalline structures. Membrane proteins, like all other proteins, exist with solid structure, if not generally, then at least relate to the structure of lipid membranes. The coupling between these two different structural components is rather complicated. Biological membranes are dynamical macromolecular assemblies, composed of lipid bilayers with embedded bilayer-spanning proteins that move within the plane of the membrane. This seminal membrane concept was originally proposed as the fluid mosaic membrane model [82]. A lipid bilayer's primary function is to serve as a semipermeable barrier for solute movement between different, membrane-separated fluid compartments. This barrier function depends on the bilayer's hydrophobic core being a poor "solvent" for polar solutes. The bilayer permeability coefficient for solute X (P_X) can be approximated as:

$$P_X = \frac{\alpha_X D_X}{\zeta}, \tag{5.1}$$

where α_X is the solute partition coefficient between the bilayer core and the aqueous phase, D_X is the solute diffusion coefficient in the bilayer core (which varies little among small solutes [29]), and ζ denotes the bilayer hydrophobic thickness ($\sim$30 Å for hydrocarbon-free bilayers [54, 81], or 40–60 Å for hydrocarbon-containing bilayers [16]). Experimental results obtained for a wide variety of solutes show that P_X is proportional to X, as approximated by the solutes' oil/water partition coefficient [29, 70, 90], and that the solute diffusion coefficient in the bilayer core is similar to the diffusion coefficient in bulk hydrocarbons (10^{-6} to 10^{-5} cm^2/s [79]).

The elucidation of the role of membrane proteins requires a specific mechanism of lipid regulation of the membrane protein function which is extremely important, but poorly understood so far. The free kinetic characteristics of membrane proteins inside a lipid bilayer are imaginary. In reality, the dynamical properties of membrane proteins are a result of various contributions from their interactions with host phospholipid layers and other integral constituents such as other membrane proteins, hydrocarbons, cholesterols, etc. The background dielectric properties also play important roles. In this chapter, we focus on different components that

M. Ashrafuzzaman and J. Tuszynski, *Membrane Biophysics*,
Biological and Medical Physics, Biomedical Engineering,
DOI: 10.1007/978-3-642-16105-6_5, © Springer-Verlag Berlin Heidelberg 2012

contribute to the strength of the hydrophobic coupling of the membrane proteins with the host phospholipid bilayer. Several novel analytical and numerical techniques will be introduced to correctly address this important problem. Although we have developed a theoretical model published earlier, which aims to explain the related experimental phenomena, we have also presented the results here to describe the problem in a comprehensive fashion.

The experimental study focused on a few ion channel phenomena which will be used as tools to address the problem. We also discuss some of the lipid- membrane protein interactions using molecular dynamics (MD) simulations. The powerful MD methodology mimics the cell membrane with most of the constituents within the membrane simulated by computer modeling. This helps understand the dynamics and energetics of various compartments, especially considering them to be independent of other compartments in membranes in real time which is experimentally almost impossible to investigate due to the complex organization of biological systems. It is also necessary to emphasize that MD can never provide absolute values of the physical parameters which should fit the biological environment but it can often provide enough information to help understand the phenomena involved.

5.1 Lipid Membrane–Membrane Protein Coupling Due to Membrane Elasticity

5.1.1 Definition of Elasticity

According to the fluid mosaic model [82], lipids freely move on the membrane surface like a fluid. This is well-known, as a liquid crystalline structure. Liquid crystalline membranes exist in different thermotropic phases. This was discussed in Chap. 3. Within any specific phase, the structure requires specific organization of the lipid molecules, and such organization raises the possibility of the membrane having certain distinguishable biophysical properties. Elasticity is claimed to be one of the few most important ones. However, the question arises whether this type of elasticity resembles the elasticity of a solid state material, which follows Hooke's law. If any object quickly regains its original shape and dimensions following the withdrawal of the force creating the deformation in the first place, with the molecules or atoms of the object returning to their initial state of stable equilibrium, the object is considered to be elastic and it obeys Hooke's law. Specifically, in mechanics, Hooke's law of elasticity is an approximation that states that the amount of deformation (represented by strain) is linearly related to the force causing the deformation (represented by stress). This hypothesis best fits with the extension of a spring due to the suspension of a load at the bottom (see Fig. 5.1). If the load is removed, the extended spring returns to its original structure and length.

The mathematical form of the spring's distortion follows the equation

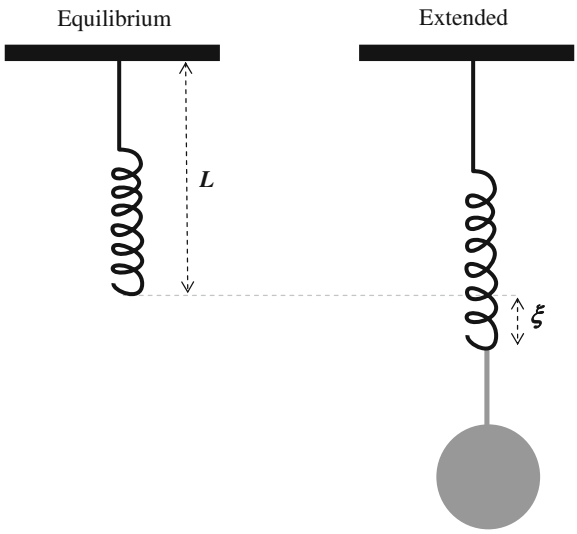

Fig. 5.1 A vertically suspended spring with an equilibrium length L extends to its new length L+ξ due to a load W [kg] suspended at the bottom of the spring

$$F = -k\xi, \tag{5.2}$$

where F is the restoring force exerted by the material, and k is the force constant (spring constant in the case of a spring). If $\xi \ll L$, the spring behaves as a harmonic oscillator. Here, F and ξ are measured using the conventional units of force (newtons) and linear dimension (meters), respectively.

The associated energy stored in the spring following the Eq. 5.2 is given by

$$U = \frac{1}{2}k\xi^2. \tag{5.3}$$

One of the important conditions of Hooke's law is that the body returns to its equilibrium state instantaneously as soon as the suspended weight is removed, which means that in the case of the above-mentioned spring, it will regain its original length L soon after the weight W is taken away from its attachment point.

Does the lipid membrane behave like a spring which can be extended or deformed without breaking its molecular organization or specific structure? Does the membrane return to its original length and shape once the membrane extending or deforming force is withdrawn? Does the membrane follow Hooke's law; represented either by the restoring force F (see Eq. 5.2) or elastic energy U (see Eq. 5.3)? These are some intriguing questions, which membrane biophysicists have been trying to answer during over almost a half-century since the publication of the famous paper by Helfrich on the elastic behavior of the lipid membrane [37]. Various groups of researchers have attempted to address the bilayer's elastic problems using different techniques which will be discussed later in this chapter. However, first we wish to mention a generally accepted fact about lipid membranes which states that they form liquid

crystalline structures (see for example [64]). It is still not clear whether some or all of the elastic properties are satisfied by a liquid crystalline membrane. Despite the lack of any cross-examination between the membrane's elasticity and its liquid crystalline nature, a group of scientists have already asserted the absolutely elastic nature of liquid crystalline lipid bilayers. Furthermore, membrane regulation of most of the membrane protein dynamics and general functions have also been concluded to be governed mainly by the bilayer elastic properties and geometries like lipid curvature profiles, etc. However, in addition to the elasticity of membranes, the electric properties of lipids, membrane proteins, and other participating constituents are very important but much less studied and understood. In this chapter, we provide an in-depth analysis of these aspects as well. First, we describe the membrane's elastic properties and related aspects using some experimental studies considering a few ion channel phenomena.

5.1.2 The Membrane's Elasticity Helps It to be Flexible: A Study Using the Gramicidin A Channel as a Tool

We first focus on an ion channel, that is, a channel formed by a small peptide gramicidin A; these channels are used as probes which hydrophobically couple with host lipid membranes. The advantage of using gramicidin A peptides to investigate membrane elastic properties is that they usually make channels which are smaller in length than the normal thickness of phospholipid bilayers (see Fig. 5.2). The length of gramicidin A channels can be varied by changing the lengths of gramicidin A peptides. It is worth mentioning that gramicidin A channels can also be artificially synthesized, such that their length may exceed the bilayer thickness.

Based on generally accepted schematic diagrams depicting gramicidin A channels inside lipid membranes (see Fig. 5.2), it is clear that the main condition for the formation of stable channels is a hydrophobic mismatch between bilayer thickness and gramicidin A channel lengths, which needs to be geometrically adjusted. Before we explore this issue, we need to understand how a bilayer deformation may occur. Due to the bilayer's elastic nature, we can consider the presence of an unlimited number of virtual springs attached between two lipid monolayers. This has been schematically shown in Fig. 5.3. The springs oscillate and maintain harmonic motion, keeping the average thickness of the bilayer uniform unless any membrane proteins or other bilayer structure-deforming agents appear in the vicinity; both inside the bilayer's hydrophobic core and in the hydrophobic/hydrophilic boundaries on both sides. Any bilayer deformation due to an independent bilayer elastic property must be much smaller than the thickness of the bilayer. Additionally, any deformation is certainly instantaneous. The elasticity-originated instantaneous thickness fluctuations follow Hooke's law and a related equation of motion for a harmonic oscillator which was stated earlier. However, the physics of the problem changes when there happens to be a molecular force acting to induce a substantial permanent deformation which

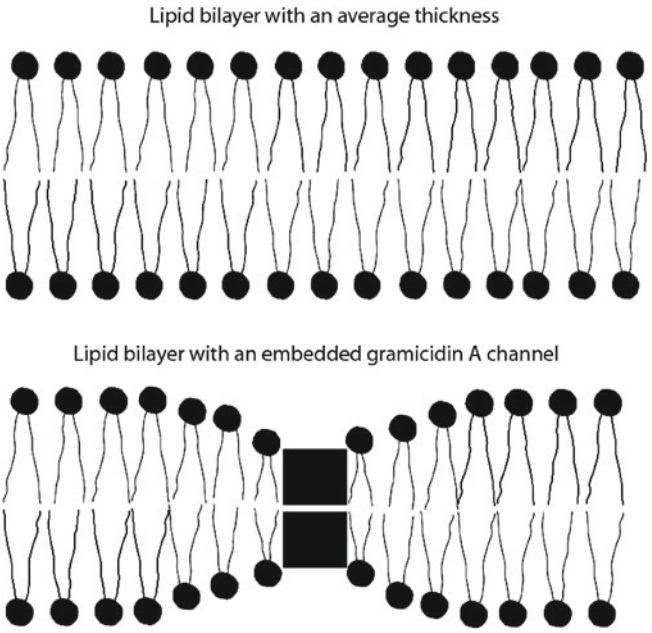

Fig. 5.2 The bilayer deforms near the gramicidin A channels where the channels are considered to be coupled with the host bilayer incurring an energetic cost [13]. The *upper panel* shows a lipid bilayer without any integral membrane protein, which is why the bilayer exists with an average bilayer thickness d_0 (see Fig. 4.2). The *lower panel* shows a bilayer with an integral gramicidin A channel. For simplicity, we use two blocks in the figure to represent a gramicidin A dimer. The channel's length l can differ, depending on the type of monomers participating in constructing the channel (see Fig. 4.2). d_0 is the unperturbed thickness of the bilayer, and is on the order of 4–5 nm in hydrocarbon-containing lipid bilayers. The value of d_0 depends highly on the type of hydrocarbons residing inside the bilayer. In the model lipid membrane construction, decane or squalene are usually used. Decane accounts for a relatively thicker bilayer than squalene. By varying the lipid acyl chain lengths, the bilayer thickness can be varied. The channel length l is on the order of 2 nm depending on the number of amino acid sequences involved in constructing the gramicidin A monomers. The channels form a rigid structure which means that the lengths are almost constant

might act as a molecular force transducer. The presence of ion channels inside a lipid membrane sometimes takes the form of a molecular force transducer, such as gramicidin A, in a lipid bilayer (see Fig. 5.2). The gravitational push (for example by a drug) on the membrane, or a pull exerted on the lipid layers by integral membrane proteins due to their hydrophobic coupling with lipid layers, may create considerable permanent or stable deformations. These deformations may sometimes cause drastic effects, such as a local breaking in the bilayer structure, or an induction of substantial flow of ions through pores or channels. Figure 5.4 schematically illustrates the equilibrium condition which can take the deformed form presented in Fig. 5.2 for gramicidin A channel. It is important to understand whether bilayer elasticity can

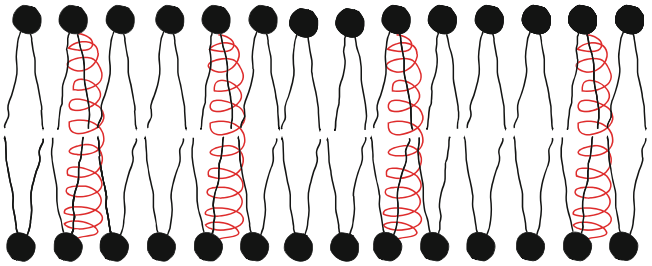

Fig. 5.3 Virtual springs (shown in *red*) are longitudinally attached to the two monolayers. For simplicity of presentation we have shown that those virtual springs are attached with lipid head group layers on each monolayer of the bilayer. The choice of the number and shape of the springs is arbitrary

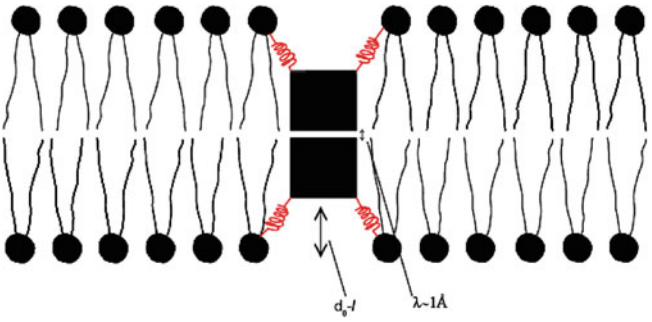

Fig. 5.4 A bilayer- integral gramicidin A channel coupling phenomenon is modeled here as a harmonic interaction. Any gramicidin A channel is attached to a lipid monolayer with many imaginary springs where any of these springs follows the motion of a harmonic oscillator following Eq. 5.2. Two gramicidin A monomers are attached to each other by hydrogen bonds and the monomer-monomer separation falls within $\lambda \approx 1$ Å or 0.1 nanometer (nm). To simplify the diagram we draw two blocks representing two gramicidin A monomers in this figure instead of showing them as spiral structures shown in Fig. 5.2

still be used as the main ingredient which causes the necessary energetic changes required for this type of mechanical deformation.

Since both channel formation and channel breaking are statistical processes, the geometrical adjustment of the free length $d_0 - l$ is a very temporary effect, but certainly not instantaneous. The bilayer's elastic nature can help it to deform to adjust with the channel's length so that a real physical binding between the lipid layers and the channel's longitudinal edges may happen. In the case of gramicidin A channels, we assume that if the channels try to extend linearly to compensate for the mismatch $d_0 - l$, the bonding at the center of the channel between two gramicidin A monomers will be broken, so that the gramicidin A channels will themselves be diluted into gramicidin A monomers. Instead, if the rather soft structured membrane exhibits a deformation near the channel, the problem can be solved and gramicidin A channels will show some stability. However, this requires a change of free energy due

to the membrane deformation, and many researchers proposed that the free energy change is contributed due to the elastic bilayer properties. We present here a detailed analysis of the bilayer's elastic energy, which arises from the consideration of the mechanical properties of the lipid bilayer. A spontaneous bending near the channel's edges (as diagrammed in Fig. 5.2) is a possible model. The crucial issue is to find the force which drives the lipid layers inward to bind with the channel's edges. Is it a harmonic energetic coupling as schematized in Fig. 5.4? If so, then we can model the bilayer-gramicidin A channel coupling through many virtual springs which will pull both of the lipid layers toward the channel's longitudinal edges. Each lipid layer then needs to spontaneously bend through a free length, which is proportional to $(d_0 - l)/2$ in each longitudinal edge of the channel, to satisfy the condition of the hydrophobic bilayer channel coupling as diagrammed in Fig. 5.2. The bilayer's elastic property certainly helps the monolayers to spontaneously bend (see Fig. 5.2), but since the bending is permanent, with a high level of stability proportional to the channel lifetime, the mechanism certainly falls outside simple harmonic coupling. In this case, the virtual springs presented in Fig. 5.4 need to compress by a length proportional to their equilibrium lengths. Therefore, the virtual springs do not just follow the motion of a harmonic oscillator (see Eq. 5.2), but rather, higher order anharmonic terms appear in the potential energy formula in addition to the harmonic oscillator terms (see Eq. 5.3).

The scientific arguments presented here clearly suggest that a brand-new formula is needed to describe bilayer channel coupling energetics, and one has to include both harmonic (originating from elastic properties) and anharmonic (originating from unknown properties) bilayer integral channel coupling terms. We discuss this in the next section, but first we address the existing bilayer channel coupling energetics based on the bilayer's mechanical properties, especially bilayer elasticity.

5.1.3 The Membrane's Elastic Property Contributes to the Membrane–Membrane Protein Coupling: A Study Using the Gramicidin A Channel as a Tool

The general or primary function of membrane proteins is to catalyze the selective transfer of material and information across biological membranes. In the case of catalyzing this transfer, membrane proteins undergo conformational changes, namely: (a) the opening/closing transitions in ion channels [72, 73, 88] and (b) the shift in substrate binding site accessibility in conformational carriers and ATP-driven pumps [87]. To the extent that these protein conformational changes involve the protein/bilayer interface, they will perturb the bilayer immediately adjacent to the protein [3, 20, 33, 42, 76], cf. Figs. 4.1 and 5.2. That is, protein conformational changes involve not only rearrangements within the protein, but also interactions with the environment, particularly with the host bilayer. This was discussed in an

earlier chapter and also earlier in this chapter. Here, we focus only on the energetic part.

The bilayer deformation, in general, incurs an energetic cost, ΔG^0_{def}, that contributes to the overall free energy difference ($\Delta G^{I->II}_{\text{tot}}$) between two different protein functional states (conformations), denoted here as I and II, respectively, such that

$$\Delta G^{I->II}_{\text{tot}} = \Delta G^{I->II}_{\text{prot}} + \Delta\Delta G^{I->II}_{\text{def}}, \tag{5.4}$$

where $\Delta G^{I->II}_{\text{prot}}$ denotes the energetic cost of the protein conformational change *per se* (including contributions from interactions with the environment, such as changes in the protein/solution interface, not considered in the protein-bilayer interactions) and $\Delta\Delta G^{I->II}_{\text{def}}$, the difference in bilayer deformation energy between protein conformations I and II ($\Delta\Delta G^{I->II}_{\text{def}} = \Delta G^{II}_{\text{def}} - \Delta G^{I}_{\text{def}}$). Consequently, the equilibrium distribution between the different protein conformations is given by:

$$K^I_{II} = \exp\left(-\frac{\Delta G^{I->II}_{\text{prot}} + \Delta\Delta G^{I->II}_{\text{def}}}{k_B T}\right), \tag{5.5}$$

where K^I_{II} denotes the equilibrium distribution coefficient between protein states I and II, T stands for the absolute temperature of the bilayer environment and k_B is Boltzmann's constant. If ΔG^0_{def} is significant, meaning $|\Delta G^0_{\text{def}}| > k_B T$, then $\Delta\Delta G^{I->II}_{\text{def}}$ may be sizable, such that the equilibrium distribution between different membrane protein conformations—and the kinetics of the conformational changes—could be modulated by the bilayer in which the proteins are embedded [3, 20, 33, 76].

The success of Eq. 5.1 in predicting small molecule permeability coefficients naturally leads to the notion of lipid bilayers being thin sheets of liquid hydrocarbons, stabilized by the lipid polar head groups, as implied in the original formulation of the fluid mosaic membrane model [82]. If that were the case, one would expect that $|\Delta G^0_{\text{def}}| \ll k_B T$, in which case membrane protein function would be little affected by changes in bilayer properties—except in cases where the interfacial surface charge densities vary [39, 59, 65]. However, lipid bilayers are not just thin sheets of liquid hydrocarbon; they are liquid crystals that exhibit both short- and long-range order [64]. By virtue of being liquid crystals, lipid bilayers also have elastic properties [27, 37], with material properties (average thickness, intrinsic monolayer curvature and elastic moduli) that can be manipulated by the adsorption of amphipathic compounds [13, 28, 58, 77, 80, 84, 93] and other ones. The permeability of small molecules across lipid bilayers given by Eq. 5.5 can, on a broader scale, become highly regulated by the hydrophobic coupling between the lipid bilayer and the bilayer-spanning membrane proteins. To address this hydrophobic coupling between the lipid bilayer and the membrane proteins-induced regulation, we have investigated here both experimentally and theoretically the energetics of gramicidin A channels in lipid bilayers with different thickness. To generalize the problem, later in this

chapter, we also investigate the functions of another structurally different channel produced by alamethicin peptides.

We have learned earlier that the gramicidin A channel is a linear dimer. The atomic resolution structure of this channel is well-established, with the channels being dimers of two right-handed, $\beta^{6.3}$-helical subunits [8, 46, 86]. The bilayer-spanning channels are formed by the reversible, trans-bilayer association of these $\beta^{6.3}$-helical monomers [68]:

$$M_{\text{left}} + M_{\text{right}} \underset{k_{-1}}{\overset{k_1}{\rightleftharpoons}} D, \tag{5.6}$$

where M and D denote gramicidin A monomers and dimers, respectively, and the subscripts denote monomers residing in each bilayer leaflet. Here, k_1 and k_{-1} are two rate constants determining the channel appearance rate ($f_{\text{gA}} = k_1 \cdot [M]^2$; with $[M]$ being the gramicidin A monomer concentration) and gramicidin A channel lifetime ($\tau = 1/k_{-1}$). Within limits, the channel structure is invariant when the lipid bilayer thickness is varied [45, 89], meaning that the gramicidin A channels are more rigid than the host bilayer. Consequently, when the bilayer's hydrophobic thickness is larger than the channel's hydrophobic length, as is the present case, the bilayer will adjust locally to match the channel length, which incurs an energetic cost corresponding to the bilayer deformation energy ΔG^0_{def}. When a channel disappears, a transition state is reached when two of the six H-bonds that stabilize the bilayer-spanning dimer are broken [26, 61], in which case the two subunits have moved a distance $\lambda+$, which may be slightly greater than the average length λ ($\approx$1.0 Å) of the bonds attaching two gramicidin A monomers in a gramicidin A dimer. The movement of the two subunits relative to each other is very complex, involving both a rotation and a lateral axial displacement [61]. For simplicity, here we focus on just the linear gramicidin A association/dissociation mechanism only.

Changes in ΔG^0_{def} will shift the equilibrium distribution between non-conducting gramicidin A monomers and conducting channels. Using Eq. 5.5, the dimerization constant for gramicidin A channel formation, K_D, is found as

$$K_D = \frac{[D]}{[M]^2} = \frac{k_1}{k_{-1}} = \exp\left(-\frac{\Delta G^0_{\text{prot}} + \Delta G^0_{\text{def}}}{k_B T}\right), \tag{5.7}$$

where ΔG^0_{prot} denotes the energetic contributions due to the channel subunit-subunit interactions. Here, $[D]$ is the concentration of dimeric gramicidin A channels. Because bilayer deformation energy ΔG^0_{def} varies as a function of the mismatch between the bilayer thickness and the gramicidin A channel length ($d_0 - l$), the bilayer responds to the deformation by imposing a disjoining force on the bilayer-spanning channels:

$$F_{\text{dis}} = -\left(-\frac{\partial}{\partial r}\Delta G^0_{\text{def}}\right). \tag{5.8}$$

This force can, in principle, be determined theoretically, although this requires a complicated numerical calculation. If we assume that ΔG^0_{prot} does not considerably respond to bilayer deformation, changes in F_{dis} will mainly be observable as changes in channel lifetime τ, which means that gramicidin A channels become molecular force transducers embedded in the lipid bilayers [5]. This is so because $\tau = 1/k_{-1}$, where k_{-1} is the dimer dissociation rate constant. The disjoining force alters k_{-1} by altering the activation energy for channel dissociation:

$$k_{-1} = \frac{1}{\tau_0} \cdot \exp\left(\frac{\Delta G^{\ddagger}}{k_B T}\right) = \frac{1}{\tau_0} \exp\left(-\frac{\Delta G^{\ddagger}_{\text{prot}} + \Delta\Delta G^{\ddagger}_{\text{def}}}{k_B T}\right), \tag{5.9}$$

where τ_0^{-1} denotes the frequency factor for the reaction, $\Delta\Delta G^{\ddagger}_{\text{def}}$ and $\Delta G^{\ddagger}_{\text{prot}}$ denote the difference in bilayer deformation energy and the protein transition energy, respectively, as the two subunits move apart by a distance $(\lambda^+ - \lambda)(\ll (d_0 - l))$ to reach the transition state for dimer dissociation, and $\Delta G^{\ddagger}$ is their sum. With some approximation in the case $(\lambda^+ - \lambda) \approx 0$ (ignoring the change in protein conformational energy before the actual event of the real dissociation) the following equation is found:

$$\Delta\Delta G^{\ddagger}_{\text{def}} \approx F_{\text{dis}} \cdot (\lambda^+ - \lambda). \tag{5.10}$$

The transition between a gramicidin A dimer (D) and monomer (M) and vice versa, via the intermediate energy state where the dissociation/association between two gramicidin A monomers ($D \leftrightarrow M$) happens, is illustrated in Fig. 5.5.

Based on the molecular dynamics simulation of gramicidin A in lipid bilayers considering an all-atom force field [2], we have gained an important insight into how a gramicidin A channel exists inside lipid bilayers. We observe here that at the binding site of the channel bilayer interface, the lipid head group region is more effectively regulating the lipid bilayer gramicidin A channel hydrophobic coupling. That is, the lipid head groups, due to their physical presence, compensate for the hydrophobic free length $(d_0 - l)$ between the bilayer thickness and the channel length in the channel bilayer coupling interface (see the illustration of the model in Fig. 5.2). The bilayer, however, exerts a restoring force F_{dis} on the two longitudinal edges of the gramicidin A channel to return it to its original thickness and, as a result, the gramicidin A dimer experiences destabilization. It finally dissociates from the bilayer, and gramicidin A monomers also dissociate from each other.

Calculation of the F_{dis} acting against the bilayer gramicidin A channel coupling has been a long-standing challenge, and the form of F_{dis} mainly depends on how one treats a lipid bilayer membrane, such as whether it is treated as equivalent to a perfect elastic body or as a liquid crystalline structure. Based on the theory of elastic bilayer deformation [38, 40, 66, 67] the bilayer deformation energy has been found to show bi-quadratic form in terms of $(d_0 - l)$ and intrinsic monolayer curvature c_0 parameters [55, 66, 67]

$$\Delta G^0_{\text{def}} = H_B \cdot (d_0 - l)^2 + H_X \cdot (d_0 - l) \cdot c_0 + H_C \cdot c_0^2, \tag{5.11}$$

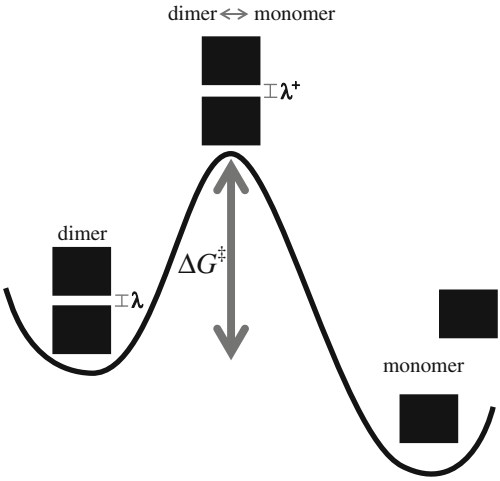

Fig. 5.5 Chemical kinetics illustration of the back-and-forth transitions between gramicidin A dimer (D) and monomer (M) states. The monomers in the far left energy well are bound to each other, but the monomers in the far right energy well are free from each other. The back-and-forth transition between dimer and monomer states happens near the central energy state. The gramicidin A monomer has been schematically shown as a block. As to the role of the energy state representing the left-most energy well, the contribution of the central energetic barrier with barrier height $\Delta G^{\ddagger}$ (*vertical double arrow*) relative to the energy well representing the dimer state is very important for the stability of the gramicidin A dimer (channel) state. The dissociation between the monomers may happen due to linear displacement, rotational bending, etc. To easily understand the problem, we analyze the dissociation mechanism here using only the linear displacement of the monomers along the channel length

where H_B, H_X and H_C are phenomenological elastic constants, depending mainly on the bilayer elastic properties, namely compression and bending moduli (for details see [13]). In this elastic model, the bilayer deformation free energy has been calculated based on the original proposal that for small deformations, the free energy consists of a layer-compression term, a splay-distortion term, and a surface-tension term, equivalent to the elastic free energy of a two-layer smectic liquid crystal with surface tension [40]. Consequently, F_{dis} follows a linear relationship with respect to $(d_0 - l)$ and c_0 [6, 13] such that

$$F_{\text{dis}} = -\left(-\frac{\partial}{\partial(d_0 - l)}\Delta G^0_{\text{def}}\right) = 2H_B \cdot (d_0 - l) + H_X \cdot c_0. \tag{5.12}$$

Increasing $(d_0 - l)$ and/or c_0 leads to an increase in F_{dis} which causes destabilization of gramicidin A channels following this general relation between F_{dis} and gramicidin A channel lifetime via the bilayer deformation energy contributions:

$$\tau \sim \exp\left(-\frac{\Delta\Delta G^{\ddagger}_{\text{def}}}{k_B T}\right) = \exp\left(-\frac{(\lambda^{+} - \lambda) F_{\text{dis}}}{k_B T}\right) \tag{5.13}$$

F_{dis} here follows from Eq. 5.12 in the elastic bilayer consideration.

In this elastic bilayer deformation energy calculation, the decomposed local bilayer compression and monolayer bending energy densities are often calculated considering the bilayer as an almost perfect elastic body. Equation 5.11 provides only the quadratic energy form of the mismatch $d_0 - l$, which is the harmonic energy coupling term (Eq. 5.3). This energy term does not consist of any anharmonic terms, which are highly needed especially in the case of having a considerable value of $d_0 - l$. Consequently, the lack of presence of nonlinear terms other than the linear term (proportional to $d_0 - l$) in the value of F_{dis} makes the form of F_{dis} in Eq. 5.12 incomplete and scientifically incorrect. This has been explained in detail in an earlier section, as well as in ([11] in Chap. 4). Therefore, a general form for F_{dis} must be formulated, using a totally different scientifically acceptable model, considering all general properties of the lipid bilayer and integral membrane proteins. We have done so using a screened Coulomb interaction model for calculating the hydrophobic bilayer-membrane protein coupling energy by including electrical properties of the lipids and membrane proteins ([11] in Chap. 4). We explain briefly below.

5.2 Lipid Membrane–Membrane Protein Coupling Due to Electrical Properties of Lipids and Proteins

In Sect. 5.1 we have discussed how the membrane's elastic properties raise the possibility of conditional mechanical energetic coupling between lipid layers and integral membrane proteins. We have also found that although the mechanical property of lipid layers (or generally, the bilayer elasticity) provides important contributions to the membrane functions, there are even more important biophysical properties, namely the electrical properties of the membrane constituents and the integral membrane proteins that generate primary effects on most of the membrane transport properties ([11] in Chap. 4). Based on this latter publication, it is clear that a traditional mechanical energetic coupling between the bilayer and membrane proteins does not contribute the primary regulatory effects on membrane proteins. Instead, the electrical energetic coupling does so.

5.2.1 Screened Coulomb Potentials and Lennard–Jones Interactions Between Peptides on Ion Channels and Lipids in the Membrane: A Study Using Gramicidin A Channel as a Tool

Using specific 'elastic parameters' in a fluid-like membrane is a good first-order approximation that works well within the limitations of a linear theory. However,

in order to extend the applicability of the theory to a non-linear regime, we propose to use the screened Coulomb interaction approximation instead of using the form of energy (Eq. 5.11) found from elastic considerations of the bilayer model. This screened Coulomb interaction approach has often been used in condensed matter physics as the so-called Thomas–Fermi approximation [9] as well as in biophysics for interacting systems of charged biomolecules in solution employing traditional Debye screening to account for the presence of water and ions, first introduced in the Debye-Hückel model [22]. Also, zwitterionic lipids having a dipole moment provide support for calculating localized (in the intermediate range) interaction energies between channel-forming peptides and nearby lipid head group regions in a manner equivalent to a free energy profile of interacting charged-zwitterionic lipid layers using the Debye-Hückel theory [60]. Here, we wish to mention that the presence of aqueous ions in the outer leaflet of the bilayer still leaves room for head group dipoles to show considerable localized charge effects in the inner region where channel lipid interactions take place. Moreover, the bilayer's spontaneous bending near channels (see Fig. 5.2) is obtained by finding the energy required to bend a straight charged chain where the screened Coulomb interactions lead to high values of induced stiffness [69], which is an example where the elastic model [38, 40] requires an extension to a nonlinear regime. The interaction energy between a gramicidin A channel and a host bilayer has been calculated based on experimentally observable parameters, such as bilayer thickness d_0 [16], lipid head group cross-sectional area [35], channel length l [41], lipid charge q_L [1, 75], and dielectric parameters of the lipid bilayer core [71], etc. Bilayer elastic parameters appear in the screened Coulomb interaction as secondary ingredients. In this screened interaction we assume that the gramicidin A channel couples with the lipid bilayer through a deformation of the bilayer at the channel bilayer interaction interface (see Fig. 5.2). Considering that the gramicidin A channel length is smaller than the thickness of the bilayer, the channel extends its Coulomb interaction toward lipids sitting on the bilayer's resting thickness. The gramicidin A channel directly interacts with the nearest-neighbor lipid (lp1) by the Coulomb interaction and this lipid interacts directly with its next-nearest-neighbor lipid (lp2) but this second lipid experiences an interaction with the channel which is screened due to the presence of the channel's nearest-neighbor lipid; a first-order term in the extension of V_{sc} (see Eq. 5.14). The interaction between the third-nearest-neighbor lipid (lp3) and the channel is screened by both the nearest- and next-nearest-neighbor lipids (the second-order term in the extension of V_{sc}). Figure 5.6 illustrates this in a diagrammatic view. The chain peptide-lipid interaction can be better explained by the curvilinear model diagram in Fig. 5.7, but the real condition is that the peptides interact with lipids in all directions on each monolayer leaflet. The general form of the screened Coulomb interaction is as follows:

$$V_{\mathrm{sc}}(\boldsymbol{r}) = \int d^3k e^{(i\boldsymbol{k}\cdot\boldsymbol{r})} V_{\mathrm{sc}}(\boldsymbol{k}), \tag{5.14}$$

where the screened Coulomb interaction in Fourier space is given by [9].

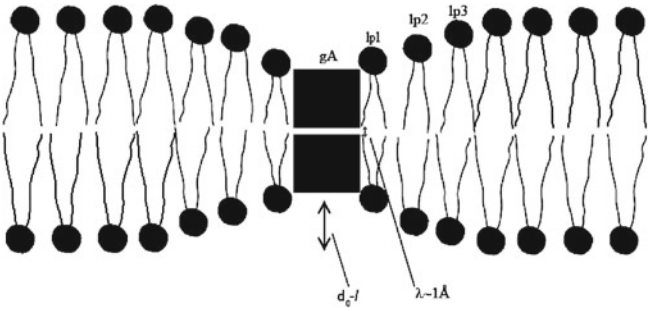

Fig. 5.6 Gramicidin A monomer (gA) and lipids on each monolayer make a chain (with chain reaction) with continuous bending until the equilibrium membrane thickness is reached. A gA monomer interacts with lp1 (direct Coulomb interaction which is the zeroth-order term in the expansion of the screened Coulomb interaction, Eq. 5.14), with lp2 (first-order screened Coulomb interaction), with lp3 (second- order screened Coulomb interaction), etc. The interactions extend to all directions on each lipid monolayer surface

$$V_{\rm sc}(\boldsymbol{k}) = \frac{V(\boldsymbol{k})}{1 + \frac{V(\boldsymbol{k})}{2\pi k_B T} n}, \tag{5.15}$$

where $V(k) \approx (1/\epsilon_0\epsilon_r) q_{\rm gA} q_L / k^2$ (in two-dimensional Fourier space) is the direct Coulomb interaction between particle 1 (gramicidin A monomer with effective charge $q_{\rm gA}$) and particle 2 (the gramicidin A monomer's nearest-neighbor lipid, with an effective charge on its head group region, q_L). Here, ϵ_0 is the dielectric constant in vacuum and ϵ_r is the relative dielectric constant (~2) [17] inside the membrane. The wave number is $k \approx 2\pi/a$, and a is the lattice constant or the closest distance over which a lipid head group can approach the gramicidin A channel's center of mass. The condition is better presented in the schematic 2D diagrams in Figs. 5.6 and 5.7. For simplicity, we assume $a = r_{\rm LL}$, the average lipid-lipid distance, which is about 7.7 Å [35]. n denotes the density e.g., lipid density $\sim 1/60\,\text{Å}^2$. $k_B T \approx 1.38 \times 10^{-23}$ J/K (at 300 K). $n/(2\pi k_B T) \approx 6.4 \times 10^{17}/\text{J Å}^2$, or $n \approx 3.84 \times 10^{19}/$ J (in general). Let us consider $q_{\rm gA} q_L \approx f q_{\rm gA}^2$, f ($\approx q_L/q_{\rm gA}$, assumed to be $\ll 1$) is the ratio of effective charges in lipid and in protein (gramicidin A monomer).

The screened Coulomb interaction (see Eqs. 5.14 and 5.15) underscores that the bilayer-gramicidin A channel mismatch may control the stability of the gramicidin A channel which is already dealt with in the order of the expansion of the interaction potential (through the number of lipids involved in the screening phenomenon). When there is no hydrophobic mismatch, the zeroth-order term (direct Coulomb interaction) in the expansion of Eq. 5.14 is to be the only one considered.

The binding energy between two gramicidin A monomers can be expressed as:

$$U_{gA,gA}(r) = U_{\rm LJ} + U_{\rm coulomb}(r), \tag{5.16}$$

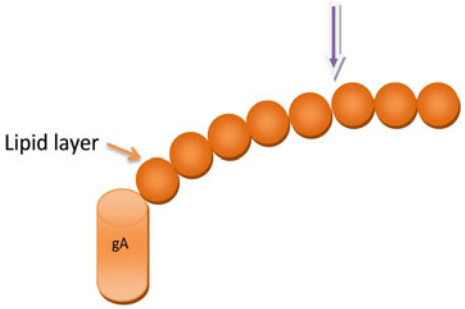

Fig. 5.7 Gramicidin A monomer (gA) in a channel is assumed to find a lipid (just the head group is schematically shown) on the perturbed region of the bilayer next to it with a bare Coulomb interaction, but the next-neighboring lipid with the first-order screened Coulomb interaction, and so on. The gA monomer can no longer extend its interaction beyond the lipid on the right side of the downward pointing arrow where the bilayer regains the form of its unperturbed thickness. Here, we have shown only they are mainly because most probably they are mainly responsible for the effective localized charges in lipids

where the Lennard–Jones potential between the two gramicidin A monomers is given by

$$U_{\mathrm{LJ}}(r) \cong U_{\mathrm{LJ}}(r^*) + \frac{1}{2}\left(\frac{\partial^2 U}{\partial r^2}\right)_{r=r^*}(r-r^*)^2 \frac{1}{6}\left(\frac{\partial^3 U}{\partial r^3}\right)_{r=r^*}(r-r^*)^3$$

$$+ \frac{1}{24}\left(\frac{\partial^4 U}{\partial r^4}\right)_{r=r^*}(r-r^*)^4 + \ldots \tag{5.17}$$

$$U_{\mathrm{LJ}}(r^*) + A'(r-r^*)^2 + B'(r-r^*)^3 + C'(r-r^*)^4 + \ldots,$$

where $r^* \approx$ average length of a hydrogen bond.

The Coulomb interaction between the two gramicidin A monomers is given by

$$U_{\mathrm{coulomb}}(r) = \frac{q_{\mathrm{gA}}^2}{4\pi\epsilon_0\epsilon_r r}. \tag{5.18}$$

The formation of a gramicidin A channel due to dimerization of two monomers inside lipid membranes is a well-studied issue. The way in which the presence of the ordered matrix of a lipid bilayer ensures the membrane-associated gramicidin A structure was already thoroughly addressed in an investigation some three decades ago [89]. The strong binding involving two gramicidin A monomers with identical charges is supported by an earlier work on the derivation of an effective attractive interaction potential between charges of the same type in solution [32]. In this chapter, the primary goal is to investigate the effect of hydrophobic bilayer thickness channel length mismatch on the stability of the already formed gramicidin A

channels. The binding energy between monomers in a channel mentioned above (Eq. 5.16) is always a standard condition, no matter how we derive this energy, and the monomer-monomer binding is kept constant throughout this study by not disturbing the membrane's inner region where the binding occurs. In the presence of a hydrophobic bilayer thickness gramicidin A channel length mismatch, τ observed in other studies was mainly seen not to follow the modest change in $U_{\mathrm{gA,gA}}$ due to a slight change of the gramicidin A monomer's charge profile in the case of binding of amphiphiles, anti-fusion, or antimicrobial peptides with channels in a varied membrane environment. All these observations, taken together, suggest that a change of (the already formed) gramicidin A channel stability is mainly due to the change of the gramicidin A channel bilayer coupling energy ($U_{\mathrm{gA,bilayer}}$), though the total potential energy between two gramicidin A monomers in a membrane-associated gramicidin A channel is given by

$$U(r) = U_{\mathrm{gA,gA}}(r) + 2U_{\mathrm{gA,bilayer}}(r). \tag{5.19}$$

Here, $U_{\mathrm{gA,bilayer}}(r)$ is the first-, second-, etc. order term in the expansion of $V_{\mathrm{sc}}(r)$ (Eqs. 5.14 and 5.15) for the hydrophobic mismatch to be filled by single, double etc. lipids representing the first-, second-, etc. order screening in the screened Coulomb interaction. The protein-protein interaction energy $\Delta G^0_{\mathrm{prot}}$, and the bilayer deformation energy $\Delta G^0_{\mathrm{def}}$ (mentioned in an earlier section) are proportional to $U_{\mathrm{gA,gA}}$ and $U_{\mathrm{gA,bilayer}}$ (in Eq. 5.19), respectively. The zeroth-order term in the expansion of $V_{\mathrm{sc}}(r)$ (Eqs. 5.14 and 5.15) represents the direct Coulomb interaction when the gramicidin A channel length exactly matches the bilayer thickness. In practice, gramicidin A channels appear with some level of hydrophobic mismatch between the bilayer thickness and the gramicidin A channel length, so there is some amount of screened Coulomb interaction to be expected. The coefficients in the interaction terms can be calculated using an energy minimum criterion $\partial U(r)/\partial r = 0$ resulting in the condition

$$A' = 2r^{*2}C'\frac{3 - r^*}{r^* - r_0}, \quad B' = 4r^*C', \tag{5.20}$$

where $r_0 (\approx (d_0 - l)/2)$ represents one-half of the hydrophobic mismatch of the bilayer thickness and the channel length.

According to Eqs. 5.14–5.19 and the description here, changes in F_{dis} (recall the definition from Eq. 5.8) could arise largely from changes in bilayer thickness (determined mainly by lipid acyl chain lengths), from changes in lipid geometry (mainly lipid curvature), changes in relative charges between lipids and gramicidin A monomers, bilayer dielectric condition, and the bilayer elastic moduli. In an experimental protocol we can vary $d_0 - l$ by choosing bilayers with different thickness or gramicidin A monomers with different lengths, or both, which consequently changes $\Delta G^0_{\mathrm{def}}$ and F_{dis} and, as a result, the stability of the gramicidin A channels becomes regulated. We discuss the experimental techniques used and a few test cases investigated in the next section. In the case when $d_0 - l \approx 0$, the channel experiences negligible destabilization due to bilayer deformation at the channel bilayer

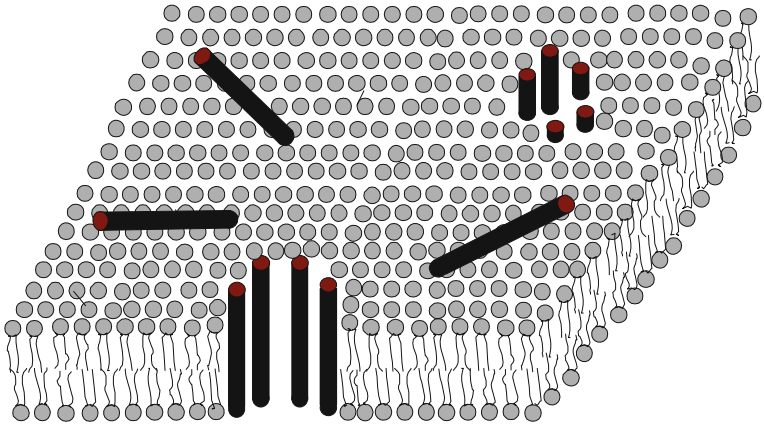

Fig. 5.8 Barrel-stave model for alamethicin channel formation inside lipid bilayers [14, 19, 36]. Cylindrical rods are schematic diagrams for alamethicin monomers in 3D view

interaction sites, but the channel may still experience slight destabilization due to any possible fluctuation in ΔG^0_{prot}.

5.2.2 Screened Coulomb Interactions and Lennard–Jones Potentials Between Peptides on Ion Channels and Lipids on the Membrane: A Study Using an Alamethicin Channel as a Tool

In the previous section, we have learned that the bilayer-spanning gramicidin A channels are formed by the reversible, trans-bilayer association of $\beta^{6.3}$-helical gramicidin A monomers [68]. Alamethicin channels form 'barrel-stave' type pores [14, 19, 36] where the alamethicin monomers align across the cylindrical surface of the channel with many possible conductance states, depending on the number of alamethicin monomers involved in the formation of a cylindrical channel (see the proposed alamethicin channel model in Figs. 5.8, 5.9 and 5.10).

Extrapolation of Gramicidin A Channel Energetics to the Alamethicin Channel

The form of V_{sc} (Eq. 5.14) in the case of alamethicin channels is still the same, but instead of considering only two screened Coulomb interactions between the channel and the bilayer at the two longitudinal ends of the channel as is considered in the gramicidin A channel's interaction sites with the bilayer, each alamethicin monomer

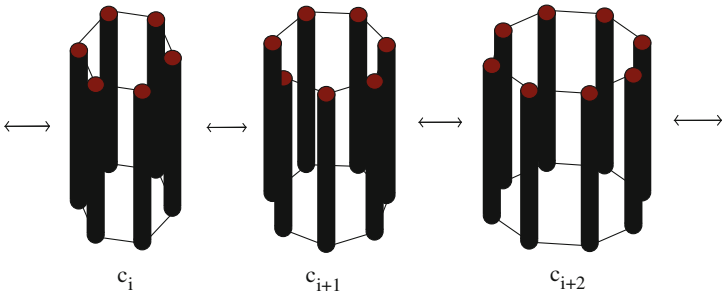

Fig. 5.9 The transition between different conduction pores of alamethicin channels

accounts for two such screened Coulomb interactions (see Eq. 5.14). The interaction between alamethicin monomers takes the form of the standard Coulomb energy formula given below:

$$U_{\text{coulomb}}(r) = \frac{1}{2}\sum_{i\neq j}^{n} \frac{q_i q_j}{4\pi\epsilon_0\epsilon_r|\boldsymbol{r_i} - \boldsymbol{r_j}|}. \tag{5.21}$$

If, for example, three monomers make the lowest conductance state in an alamethicin channel, we can assume that $|\boldsymbol{r_i} - \boldsymbol{r_j}| \approx r$. In the case of isotropic alamethicin peptides, we can also assume that $q_i q_j \approx q_{\text{Alm}}^2$ where q_{Alm} is the charge on an alamethicin monomer. However, for other higher conductance states, where the number of monomers involved is more than three, the distances between non-adjacent monomers on each cylindrical alamethicin channel should be greater than those between adjacent monomers. The term $U_{\text{LJ}}(r)$ in alamethicin channels follows an identical form to that in Eq. 5.17.

5.3 Channel Energetics and Related Probabilities in the Context of Channel Stability in Lipid Bilayers

We have discussed how we can generally apply the screened Coulomb interaction model calculation for both gramicidin A and alamethicin channels. This qualifies the model for general applications, which could involve the bilayer regulation of the functions of membrane proteins with varied structures. Despite all indications of the existence of identical bilayer membrane protein coupling energetics, the probabilities emerging from different channel conformations require an independent treatment. The gramicidin A channel's stability appears through its lifetime, which follows Eq. 5.13. That means the gramicidin A channel lifetime directly corresponds to the strength of the bilayer channel energetic coupling. This concept is also partially valid in the case of alamethicin channels and similar ones. As explained earlier,

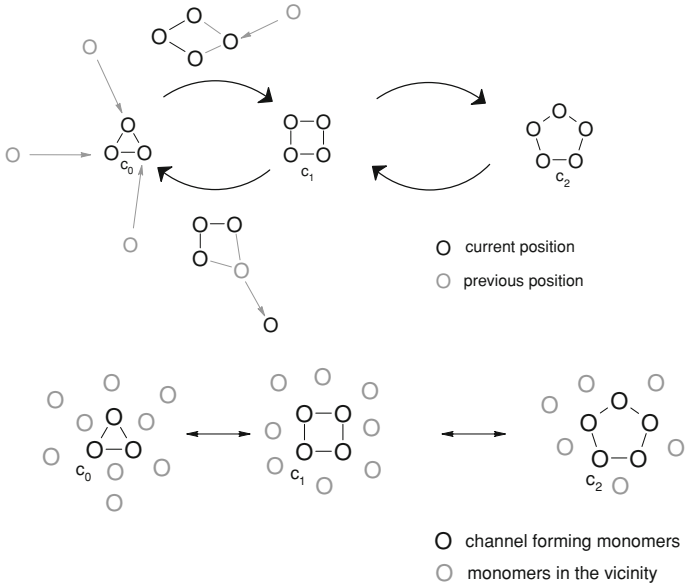

Fig. 5.10 2D view of the channels only, from the membrane surface (where alamethicin monomers are seen only along their longitudinal direction so they appear as circles) represent the two possible mechanisms of inter-channel conduction level transformations. In the bottom panel, we assume that the monomers already exist in a structured form of the alamethicin channel where the pore radius changes by reorganization of the channel forming monomers. The other 2D view illustrates a possible model of alamethicin channel formation, and a transformation between different conduction levels where the pore radius increases by addition of monomers from the surrounding space where monomers randomly move into the channel. The reduction in the pore radius occurs by releasing the monomers from the cylindrical surface of the channels. Both of the models in 2D views are valid explanations of the upper 3D structures of alamethicin channels (Figures 5.8 and 5.9). Taking three monomers in the zeroth conductance level is an arbitrary choice but the reverse calculation using experimental values of cylindrical alamethicin pore conductances and the theoretical values of the cross-sectional areas of different alamethicin pores hint that three monomers may form the zeroth conductance level. *Faded circles* and bonds in 2D views are shown to distinguish their inactivity in the channel's conduction mechanism

gramicidin A channels experience only monomer state ↔ dimer state transitions, so the channel functions do not require overly complicated analyses, but mainly the understanding of the channel stability. We have addressed this sufficiently so far for the two distinguishable gramicidin A energy states corresponding to the dimer and monomer states. However, if gramicidin A states present a continuum distribution of local energy traps, the gramicidin A channel's phenomena require a unique theoretical treatment. We briefly address this here. Due to structural complexity, alamethicin channels, and some other complex channels require complicated phenomenological models to completely explain the channel energetics. Specifically, the transitions between different channel conformations and associated independent and transition probabilities need to be clearly understood. Alamethicin channels'

independent probability corresponding to a specific energy state and transition probability between different energy states follow a straight-forward statistical mechanical formalism but a feasible physical analysis of the problem has just been published ([11] in Chap. 4). We wish to address that here first.

5.3.1 Analysis of the Alamethicin Channel Experiments

It is generally known that alamethicin channels may exist with different current levels, due to the varied number of participating alamethicin monomers. The current flowing through an alamethicin channel is directly proportional to the cross-sectional area of the cylindrical structure representing the channel. The model diagrams presented in Figs. 5.8, 5.9, 5.10 clearly address this possibility. It is also possible that any channel undergoes transitions between different structures and consequently the current through that channel undergoes transitions between different current levels. The current trace across a membrane doped with alamethicin channels shows all these features. Fig. 5.11 shows such a membrane current due to the presence of alamethicin channels inside the membrane. Detailed experimental techniques will be discussed in the next section and can be found in the literature [12].

We need to develop a unique phenomenological treatment to understand the various current transitions through alamethicin channels, as shown in Fig. 5.11 [12]. This is done below.

The probability (W_i) of an alamethicin channel having a current level i is estimated as:

$$W_i = \frac{A_i}{\sum_{i=0}^{n} A_i + A_{\mathrm{nc}}}, \tag{5.22}$$

where A_i denotes the area under the peak in the current level histogram (see Fig. 5.11c) representing a current level i ($i = 0, 1, 2, 3, \ldots, n$, where $n + 1$ is the maximal number of current levels in the experiment) and A_{nc} is the area under the peak representing the baseline (no channels). The probability of the channel having a current level i, relative to the baseline, is given by

$$r_i = \frac{A_i}{A_{\mathrm{nc}}} = \frac{W_i}{W_{\mathrm{nc}}} = \exp\left(-\frac{\Delta G^{\mathrm{nc}\to i}}{k_B T}\right), \tag{5.23}$$

where $\Delta G^{\mathrm{nc}\to i}$ (which still needs to be normalized by the alamethicin monomer concentration in the bilayer) is the free energy of the channel in current level i relative to the baseline, T is the temperature in kelvin, and k_B is Boltzmann's constant. $\Delta G^{\mathrm{nc}\to i}$ is, in fact, a measure of the change in the bilayer deformation energy required to form an alamethicin channel in a bilayer membrane.

It turns out to be helpful to consider the probability of having a current level, relative to the baseline

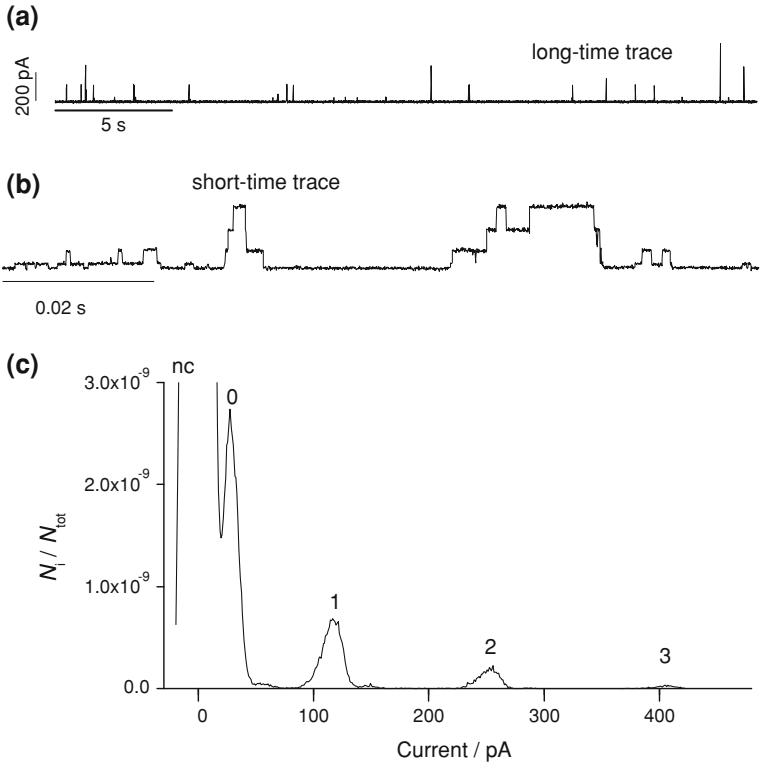

Fig. 5.11 Alamethicin channel activity in a 1,2-Dioleoyl-sn-Glycero-3-Phosphocholine ($DC_{18:1}PC$)/n-decane bilayer. **a** and **b**, long- (30 s) and short- (0.1 s) time records, respectively, of current traces through alamethicin channels. **c** current level histograms obtained from 30 s traces. N_i is the point count at any value of current ($\geq$ 0pA) and $\sum_i N_i = N_{\text{tot}} (= 2 \times 10^6)$ is the total point count during the whole record time. Sum of the probabilities ($W_{\text{nc}} + W_0 + W_1 + W_2 + W_3 + \ldots$) is 1.0 ($W_i = N_i/N_{\text{tot}}$) in the point count plots. W_{nc}, W_0, W_1, W_2, W_3, etc. are 9809.19×10^{-4}, 134.43×10^{-4}, 42.305×10^{-4}, 12.39×10^{-4}, 1.68×10^{-4}, etc. respectively. Current levels 0, 1, 2, and 3 are at 29 ± 2, 113 ± 5, 243 ± 9, and 386 ± 10pA, respectively. Mean $\pm$ S.D., $n \geq 6$ are the numbers of current traces collected at independent experimental conditions. Trans-membrane applied potential V = 150 mV. Alamethicin was added to the trans side of the lipid bilayer at $\sim 10^{-8}$ molar (M) in the aqueous phase bathing the lipid bilayer. The cis side was the electrical ground. The aqueous phase contained 1.0 M NaCl, pH 7.0

$$r_{\text{tot}} = \sum_{i=0}^{n} r_i \tag{5.24}$$

such that the changes of the properties of an alamethicin channel hosting a lipid bilayer, such as thickness, lipid curvature, bilayer elasticity, etc. alter the value of r_{tot}, but the value can be kept constant or at least comparable by changing the alamethicin channel molar concentration in the aqueous phase. However, the

relative probabilities of observing different current levels (channel conformations) e.g., W_{j+k}/W_j between levels $j+k$ and j, may show different control values as the bilayer properties change. The corresponding free energy distribution between different current levels can be determined by

$$\frac{W_{j+k}}{W_j} = \exp\left(-\frac{\Delta G^{j\to j+k}}{k_B T}\right), \tag{5.25}$$

where $\Delta G^{j\to j+k}$ is the free energy of the channel in current level $j+k$ relative to level j.

5.3.2 Derivation of Gramicidin A Channel Lifetime (τ) in a Continuum Distribution of Local Energy Traps

As discussed earlier, the relationship between the lifetime and the deformation energy change is proposed to be: $\tau = \exp(-\frac{\Delta\Delta G^{\ddagger}_{\text{def}}}{k_B T})$ (Eq. 5.13) which assumes that the difference in protein transition energy $\Delta\Delta G^{\ddagger}_{\text{prot}}$ does not change considerably as the gramicidin A subunits move apart by a distance $(\lambda^+ - \lambda)$ to dissociate from each other [30]. For a particular bilayer deformation, the negative exponential energy dependence of the channel lifetime is a valid approximation. However, in the case where a continuum distribution of local energy traps is involved, an integration over all trap levels is needed to find the average value of the channel lifetime τ_{av}. Here, the appropriate formula to be used is

$$\tau_{\text{av}} = \int \tau \exp\left(-\frac{\Delta E}{k_B T}\right)\rho(E)\mathrm{d}E, \tag{5.26}$$

where ΔE stands for $\Delta\Delta G^{\ddagger}_{\text{def}}$ (for simplicity) and $\rho(E)$ denotes the probability distribution of having a trap with a particular energy level. Following the detailed calculations provided in reference [85] we find that the dependence of the average lifetime τ_{av} on deformation energy change $\Delta\Delta G^{\ddagger}_{\text{def}}$ transforms from exponential to a power law relation:

$$\tau_{\text{av}} \approx (\Delta\Delta G^{\ddagger}_{\text{def}})^{-a} \approx ((\lambda^+ - \lambda)F_{\text{dis}})^{-a}. \tag{5.27}$$

Here, a is a parameter which is dependent on chemical and thermodynamic conditions.

5.4 Experimental Studies of the Functions of Gramicidin A and Alamethicin Channels in Lipid Membranes

So far we have discussed theoretical aspects of both gramicidin A and alamethicin channel functions in lipid membranes. We have successfully addressed how membrane protein functions become regulated due to energetic lipid bilayer membrane protein coupling, using a very traditional theoretical approach which involves screened Coulomb interactions [9]. Although both of these channels have been extensively experimentally investigated, we reiterate some of the aspects of the experimental studies using our own investigations (see [11] in Chap. 4). The rather novel parameters emerging from the studies help to validate the theoretical approaches explained in earlier sections. These experimental studies were done by Md Ashrafuzzaman in collaboration with Dr. Olaf Sparre Andersen during his tenure in Cornell University Weill Medical College.

5.4.1 Materials and Methods

Materials

1,2-Dioleoyl-sn-Glycero-3-Phosphocholine ($DC_{18:1}PC$), 1,2-Diecosenoyl-sn-Glycero-3-Phosphocholine ($DC_{20:1}PC$), 1,2-Dierucoyl-sn-Glycero-3-Phosphocholine ($DC_{22:1}PC$), 1,2-dioleoyl-sn-glycero-3-phosphoethanol-amine ($DOPE$), and 1,2-dioleoyl-sn-glycero-3-[phospho-L-serine] ($DOPS$) were from Avanti Polar Lipid (Alabaster, AL, USA) and used without further purification. *n*-Decane was 99.9 % pure from ChemSampCo (Trenton, NJ, USA) and squalene (squalene was filtered through chromatographic alumina (acid type) from Sigma to make it radical-free) was from Sigma (St. Louis, MO, USA). Alamethicin (Alm), an antibiotic from Tricoderma viride that is a mixture of alamethicin homologs, was from Sigma. Gramicidin A (gA) analogue [Ala^1]gA (with 15 amino acids in the sequence) (AgA(15)) and the sequence-shortened analogue, des-(D − Val^1 − Gly^2)-gA (with 13 amino acids in the sequence) ($gA^-(13)$) were generous gifts from Drs. R.E. Koeppe II and D.V. Greathouse (see [11] in Chap. 4). They were synthesized and purified as described in [31]. The amino acid sequences, channel lengths, phospholipids, bilayer thicknesses and abbreviations used in this article are shown in Tables 5.1 and 5.2. The electrolyte solution (NaCl) was buffered with N-2-Hydroxyethylpiperazine-N'-2-ethanesulfonic Acid (HEPES) (pH 7.0) and was from Sigma.

Methods

Planar lipid bilayers were formed from $DC_{18:1}PC$, $DC_{20:1}PC$, $DC_{22:1}PC$, $DOPE$ or $DOPS$/*n*-decane or squalene (2.5 % w/v) solutions across a 1.5 mm hole in

Table 5.1 Gramicidin sequences and their channel lengths

Gramicidin analogue	Abbreviation	Sequence	Hydrophobic Channel Length [41] Å
[Ala^1]gA	AgA(15)	f-A-G-A-L-A-V-V-V-W-L-W-L-W-L-W-ea	22
Des-(D-Val^1-Gly^2)gA	$gA^-(13)$	f-A-L-A-V-V-V-W-L-W-L-W-L-W-ea	19

Table 5.2 Phospholipids and their thicknesses

Phospholipid	Abbreviation	Bilayer Thickness (with *n*-decane) Å
1,2-dioleoyl-*sn*-glycero-3-phosphocholine	$DC_{18:1}PC$	47.7 ± 2.3 [16]
1,2-diecosenoyl-*sn*-glycero-3-phosphocholine	$DC_{20:1}PC$	53.9 ± 2.5 [16]
1,2-dierucoyl-*sn*-glycero-3-phosphocholine	$DC_{22:1}PC$	58.4 ± 2.5 [16]
1,2-dioleoyl-*sn*-glycero-3-phosphoethanolamine	$DOPE$	Unknown
1,2-dioleoyl-*sn*-glycero-3-phospho-L-serine	$DOPS$	Unknown

Teflon® separating the two electrolyte solutions of 2.5 mL each, using the pipette method of Szabo et al. [83]. All experiments were performed at 25 ± 0.5 C. The aqueous electrolyte solutions were 1.0 M NaCl, buffered to pH 7.0 using 10 mM HEPES added to the solution. Care was taken to minimize the total amount of lipid (and *n*-decane or squalene) that was added; the total volume of the lipid/decane or squalene solution was typically 1,000-times smaller than the volume of the aqueous solution.

For the experiments with Alm, we added an appropriate amount of Alm from its 10^{-5} M stock solution in dimethyl sulfoxide to the *trans* side of the lipid bilayer; the *cis* side was the electrical ground. In the experiments across DOPE and across thicker bilayers of $DC_{20:1}PC$ and $DC_{22:1}PC$, we needed a 10-fold and more than 10–100-fold denser solution of Alm compared to that for $DC_{18:1}PC$. Experiments with gA were done in $DC_{18:1}PC$/*n*-decane or squalene, $DC_{20:1}PC$/squalene and $DOPE$/*n*-decane bilayers with a 15-residue and a 13-residue gA analog of opposite chirality, e.g. AgA(15) and $gA^-(13)$ (added to both sides of the bilayer), an experimental design that allows for a direct test of how changes in the hydrophobic mismatch due to changes in the channel length may affect the channel stability. The reason for using gA analogs of opposite chirality is to ensure against the formation of heterodimers between the 13-amino acid and 15-amino acid analogs [25, 50] which would complicate the data analysis. Using lipids with different acyl chain lengths results in changing the bilayer thickness, and also in the hydrophobic mismatch between bilayer thickness and channel lengths (see Tables 5.1 and 5.2). In all experiments with Alm channels, the applied potential across the membrane was 150 mV, and with gA analogs the applied potential was 200 mV.

After peptide addition, the aqueous phases were stirred for about 5 min before the measurements resumed. The total amount of added dimethyl sulfoxide was less than 0.5 % of the volume of the electrolyte solution, a concentration that has no effect on Alm or gA channel function. The lipid bilayer membrane containing *n*-decane was 3–4 h stable whereas the membrane containing squalene was very unstable, especially when a potential was applied across the membrane.

Single-channel experiments were performed using the bilayer-punch method [4] and a Dagan 3900A patch-clamp amplifier (Dagan Corp., Minneapolis, MN) with a 3910 bilayer-expander module. The current signal in experiments with Alm channels was filtered at 20 kHz, and digitally filtered at 8 kHz while the current signal in experiments with gA channels was filtered at 2 kHz, digitized at 20 kHz, and digitally filtered at 500 Hz before the single-channel transitions were detected using the algorithm described by Andersen [4] and implemented in Visual Basic (Microsoft Corp., Redmond, WA). Relative total times spent by different open (conducting) states and the closed (non-conducting) state of Alm channels were determined by using frequency counts (in Origin 6.1 from OriginLab Corp., Northampton, MA) of the recorded current traces of about 1–3 min. The frequency counts were plotted as functions of the conductance of Alm channels for each recorded current trace, and peaks were found at the non-conducting and all conducting levels.

Single-channel lifetimes for gA channels were determined as described by Sawyer et al. [78] and Durkin et al. [25], a procedure that allows for separate determination of the lifetimes of different channel types.

5.4.2 Results

Gramicidin A Channel Results

Figure 5.12a shows representative current traces obtained in the $DC_{18:1}PC/n$-decane bilayer in the presence of gA^- (13) and AgA(15). Figure 5.12b shows how gA channels formed from different gA monomers appear with different current transition amplitudes, namely gA^- (13) channels at 1.95 ± 0.12 pA and AgA(15) channels at 3.05 ± 0.11 pA, respectively. The average gA channel lifetimes (τ) were estimated by fitting a single-exponential distribution (see Fig. 5.12c)

$$\frac{N(t)}{N(0)} = \exp\left(\frac{t}{\tau}\right), \tag{5.28}$$

where $N(t)$ is the number of channels lasting longer than time t (for details see [13]).

Figure 5.13 summarizes the average lifetimes $\tau_{\mathrm{AgA(15)}}$ and $\tau_{\mathrm{gA^-(13)}}$ of gA channels formed by dimerization of two gA monomers AgA(15) and gA^-(13), respectively, in lipid bilayers of different thickness (see Table 5.2). In a $DC_{18:1}PC$ bilayer we observe that by increasing the gA channel length by only about 3 Å

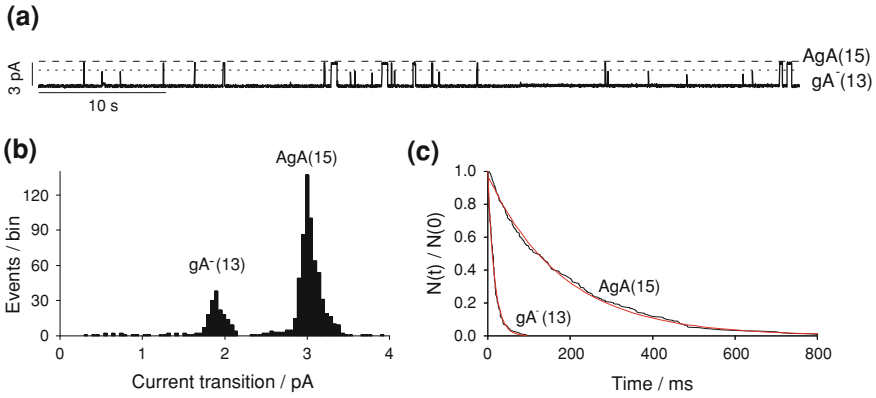

Fig. 5.12 **a** A 60 s current traces recorded from a $DC_{18:1}PC/n$-decane bilayer that was doped with gA^- (13) and AgA(15) on both sides. **b** The current transition amplitudes for gA^-(13) and AgA(15) channels are 1.95 ± 0.12 and 3.05 ± 0.11 pA. **c** Lifetime histograms (and their exponential fits) for gA^-(13) channels and AgA(15) channels (for details see [13])

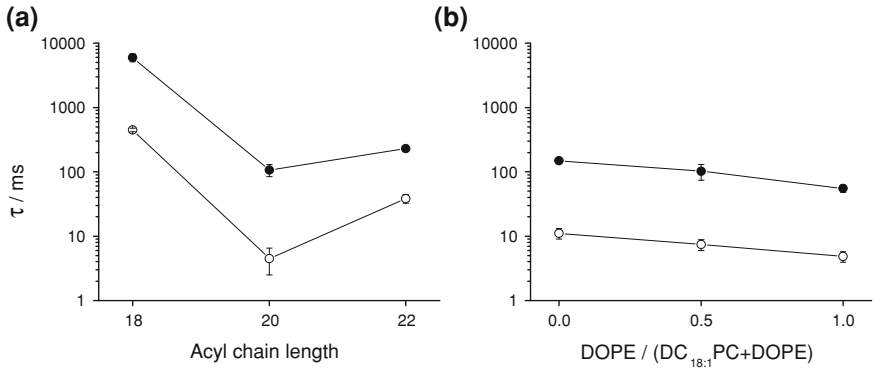

Fig. 5.13 Average τ (gA dimers of AgA(15) or gA-(13)) changes with d_0 (A. squalene in bilayer reduces d_0 over n-decane, τ increases 35-fold) and c_0 (B. introducing 1,2-dioleoyl-*sn*-Glycero-3-phosphoethanolamine (DEPE) into membranes/n-decane). For experimental protocols and methods see [13]. Acyl chain lengths 18, 20, and 22 represent bilayer-constructing lipids $DC_{18:1}PC$, $DC_{20:1}PC$, and $DC_{22:1}PC$, respectively. Trans-membrane potential 200 mV. Aqueous conditions 1.0 M NaCl, pH 7.0 (see [11] in Chap. 4)

the channel stability increases approximately 13-fold ($\tau_{\mathrm{AgA(15)}} = 149 \pm 11$ ms and $\tau_{\mathrm{gA^-(13)}} = 11.2 \pm 2.1$ ms, consequently the ratio $\tau_{\mathrm{AgA(15)}}/\tau_{\mathrm{gA^-(13)}} \approx 13$). Under identical conditions, if we replace the PC bilayer by a more negative curvature bearing DOPE bilayer [49] with comparable thickness [52], we observe that both short ($gA^-(13)$) and long ($AgA(15)$) gA channels experience almost equal (~2.5-fold) destabilization (see Fig. 5.13). Here, by using a shorter $gA^-(13)$ monomer over a longer $AgA(15)$ monomer we have introduced a higher (~3 Å) hydrophobic mismatch between the bilayer thickness and the channel length. As a consequence,

we have observed a 13-fold reduction in the gA channel lifetime. Whereas by replacing $DC_{18:1}PC$ bilayer with DOPE bilayer bearing a relatively more negative curvature with comparable thickness [52] we observe much less reduction in the gA channel lifetime for both short and long gA channels, and the stepwise introduction of DOPE (0, 50, and 100 %) over $DC_{18:1}PC$ we observe that the gA channel lifetime decreases almost linearly with an increasing negative curvature (see Fig. 5.13). This observation suggests that bilayer thickness and the gA channel length mismatch appears as a stronger gA channel regulator than the lipid curvature. On the other hand, we observe that the shorter gA channels are about 13- and 23-fold less stable than longer gA channels in $DC_{18:1}PC$/squalene (thinner bilayer) and $DC_{20:1}PC$/squalene (thicker bilayer) bilayers, respectively. We also observe that shorter $gA^-(13)$ and longer $AgA(15)$ channels become about 100- and 55-fold less stable, respectively, when equal amounts of increase in the hydrophobic mismatch between bilayer thickness and gA channel lengths for both $gA^-(13)$ and $AgA(15)$ channels occur by replacing $DC_{18:1}PC$ with $DC_{20:1}PC$ in squalene-containing lipid bilayers. With a further increase in bilayer thickness, by choosing $DC_{22:1}PC$ lipids to form lipid bilayers, we observe no formation of linear β-helical gA dimers, probably due to extremely high values of the hydrophobic bilayer thickness gA channel length mismatch $(d_0 - l)$. Nonetheless, even under this condition the gA channels are still formed, although a different conformational mechanism is at work, namely the gA monomers no longer form linear dimers as shown in the model diagram (see Fig. 5.2) but instead the monomers partially bind with each other through their whole lengths [62]. Thus, the channel length is on the order of just a single gA monomer and not on the order of the sum of two gA monomer lengths (see Fig. 5.2). These experimental results, taken together, suggest that the increase in hydrophobic mismatch between bilayer thickness and the gA channel length by either increasing the lipid acyl chain length or reducing the gA channel length appears as a very strong regulator of gA channel stability. Lipid curvature is also an important regulator of gA channel stability, but not as strong as $(d_0 - l)$. Another important parameter is the peptide concentration required to form readily observable gA channels in lipid bilayers. The appearance frequency of gA channels f_{gA} increases more rapidly (proportional to the second power or greater) than the gA monomer concentration ($[M_{gA}]$), although the average gA channel lifetime remains almost unchanged. The required peptide concentration is therefore an important parameter in determining the change of bilayer deformation energy. We observe that about a 100-fold higher $[M_{gA}]$ is required in the $DC_{20:1}PC$ bilayer over the $DC_{18:1}PC$ bilayer while about a 10-fold higher $[M_{gA}]$ is required in the DOPE bilayer over the $DC_{18:1}PC$ bilayer. Here, we also observe higher effects on the gA channel appearance frequency f_{gA} due to the change of $d_0 - l$ than those due to the lipid intrinsic curvature.

Alamethicin Channel Results

We have already presented a representative current trace obtained in the $DC_{18:1}PC$/*n*-decane bilayer in the presence of Alm peptide in Fig. 5.11. To initiate the formation

of considerable Alm channel activity under the experimental conditions, a minimum of 10^{-8} M Alm peptide concentration ($[M_{\mathrm{Alm}}]$) is required in $DC_{18:1}PC/n$-decane bilayers [12]. However, once the Alm channel starts showing, we observe that the Alm channel activity increases considerably (reported in earlier observations to be a power of 2.6 of the concentration at 25 °C [51]) as $[M_{\mathrm{Alm}}]$ increases. We also observed that the Alm channel activity shows significant dependence on bilayer thickness and on lipid curvature. Higher lipid charges also considerably destabilize the probability of observing any Alm channel current level, especially higher order current levels [18]. To observe comparable Alm channel activity (i.e., comparable value of $\sum_i r_i = \sum_i (A_i/A_{\mathrm{nc}})$ (see Sect. 5.3.1), where A_i and A_{nc} are the areas under the peaks representing a current level i and the baseline in Alm channel current traces as shown in Fig. 5.11), about 10^{-8} M of $[M_{\mathrm{Alm}}]$ in $DC_{18:1}PC/n$-decane bilayers was required while 10-fold higher ($\sim 10^{-7}$ M) of $[M_{\mathrm{Alm}}]$ was required in DOPE/n-decane (also previously observed (see [11] in Chap. 4)) or DOPS/n-decane bilayers (with a very low probability of observing higher order current levels in bilayers formed with DOPS lipids). On the other hand, a more than 10- or even 100-fold increase in the concentration $[M_{\mathrm{Alm}}]$ was required when $DC_{18:1}PC$ was replaced with $DC_{20:1}PC$ or $DC_{22:1}PC$ bilayers containing n-decane or squalene to observe comparable Alm channel activity. The additional free energy ($\Delta G^{\mathrm{nc}\to i} = -k_B T \ln r_i$) (see earlier section) involved in raising any current level in an Alm channel in thicker bilayers or bilayers with higher amounts of negative curvature is perhaps compensated by the requirement of a higher $[M_{\mathrm{Alm}}]$ [92]. Once comparable Alm channel activity is observed, the relative probability of observing different Alm conductance levels e.g., $j+k$ and jW_{j+k}/W_j (see Sect. 5.3.1) in different bilayer system is also found to be different, but does not vary within the same lipid system. The values of W_2/W_1 and W_3/W_1 are observed to be 0.25 ± 0.05 and 0.04 ± 0.01 for $DC_{18:1}PC$, 1.38 ± 0.21 and 0.88 ± 0.21 for $DC_{20:1}PC$, 1.52 ± 0.2 and 1.06 ± 0.25 for $DC_{22:1}PC$, and 2.05 ± 0.8 and 2.23 ± 1.0 for DOPE/n-decane bilayers. Consequently, the mean values of the changes in average free energies $\Delta G^{1\to 2}$ and $\Delta G^{1\to 3}$ are observed to be $-0.6 k_B T$ and $-1.39 k_B T$ for $DC_{18:1}PC$, $0.14 k_B T$ and $-0.55 k_B T$ for $DC_{20:1}PC$, $0.182 k_B T$ and $0.025 k_B T$ for $DC_{22:1}PC$, and $0.31 k_B T$ and $0.35 k_B T$ for DOPE/n-decane bilayers. The values of W_2/W_1 and W_3/W_1 are observed to be 0.21 ± 0.15 and 0.053 ± 0.04, respectively. Consequently, $\Delta G^{1\to 2}$ and $\Delta G^{1\to 3}$ are found to be $-0.68 k_B T$ and $-1.28 k_B T$, respectively, in DOPS/n-decane bilayers with negligible presence of current levels above the third current level.

5.5 Theoretical Results/Numerical Results Regarding the Functions of Gramicidin A and Alamethicin Channels Due to Their Coupling with Lipid Membranes

Based on the model of gA channels in lipid bilayers (see Fig. 5.2) we deduce that any gA channel exists in a lipid bilayer through bilayer deformations at the channel bilayer interfaces to compensate for the hydrophobic mismatch ($d_0 - l$) between

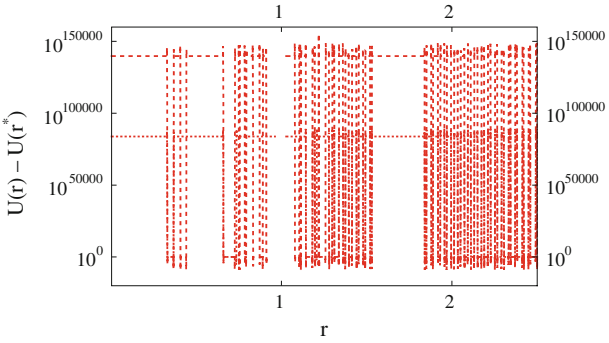

Fig. 5.14 Plot of the energy as a function of the reaction coordinate (using Eq. 5.19 here and hereafter) for gA channels in lipid bilayer energetics at different orders of screening (single- and double-dashed curves are for the first- and second-order screening, respectively). Only real parts of the energies have been considered and for simplicity $U(r*)$ has been used for $U_{\rm LJ}(r*)$ here and other energy plots in all next figures. $q_L/q_{\rm gA} = 0.005$, $(1/\epsilon_0)q_L q_{\rm gA} \approx 1$ has been chosen (here and in Figs. 5.15 and 5.16) for simplicity, $r_{\rm LL} = 7.74597$ Å. In the plot, the energy at $r = 0$ Å has been excluded to avoid the associated singularity. Numerical integration here (and hereafter) has been performed using Mathematica 7 within $(-k_{\rm max}2\pi/r_{\rm LL}, k_{\rm max}2\pi/r_{\rm LL})$, where $k_{\rm max} = 100$ and the step size for integration $d_r = 0.001$ have been taken as judicious choices

bilayer thickness and gA channel lengths. The 'barrel-stave' pore type Alm channels (see Fig. 5.8) [19, 36] exist with different sizes, depending on the number of Alm monomers participating in the pore formation and the pore continuously experiences structural transitions between different conformations representing different pore conductance levels (which experimentally manifest themselves as current levels) following the energetic profile as described in Sect. 5.3.1. Note that the higher the cross-sectional area of the pore, the higher the value of the conductance through the Alm channel.

Figures 5.14, 5.15, and 5.16 demonstrate the energetics (in arbitrary units) of a gA channel in lipid bilayers with different lipid screening orders and lipid dimensions using the model calculation. In Figs. 5.14 and 5.15 G_I and G_{II} ($G_I > G_{II}$) represent energy levels at conformational states I and II where two gA monomers exist in free form (no channel formation: M_I) and gA dimer form (channels formed: D_{II}), respectively. Formation of a channel with any level of stability requires an energetic transition (reduction) $\Delta G_{I,II}$ $(= G_I - G_{II})$. Although the energy minima appear at different values of reaction coordinates, we have chosen the transition $G_I \leftrightarrow G_{II}$ at a certain value of reaction coordinate (as shown in Fig. 5.15) to illustrate how the corresponding back-and-forth conformational changes between gA monomers and dimers ($M_I \Leftrightarrow D_{II}$) may become regulated due to $\Delta G_{I,II}$, which depends mainly on the bilayer physical properties for a certain channel type. The binding energy between two gA monomers alone in a gA channel is many orders of magnitude smaller than the binding energy of the gA channel with the bilayer at the channel bilayer interface. $\Delta G_{I,II}$ (see Figs. 5.14 and 5.15) represents the amount of energy gA monomers need

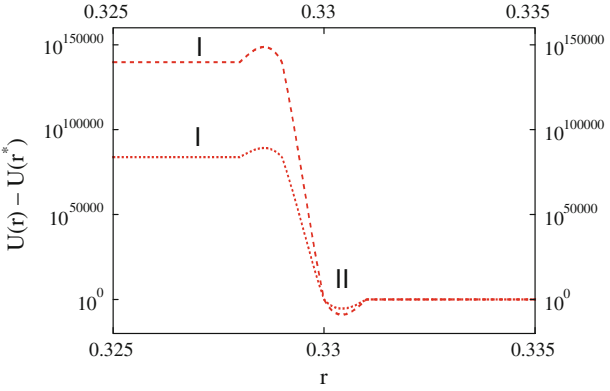

Fig. 5.15 A plot of the energy as a function of the reaction coordinate for gA channels in lipid bilayer energetics at different orders of screening (single- and double-dashed curves are for the first- and second-order screening, respectively). I and II represent levels with free energies G_I and G_{II} respectively, where gA monomers exist as free (no channel formed) and gA dimer (gA channel formed). $q_L/q_{\mathrm{gA}} = 0.005$, $r_{\mathrm{LL}} = 7.74597$ Å. *Ad hoc* assumptions ($q_{\mathrm{gA}} \sim$ electron charge and other relevant parameters [1, 16, 17, 35, 41, 71, 75]) give an estimate of G_I and G_{II} to be 10^{-1} and 10^{-8} in first-order and 10^5 and 10^{-4} in second-order lipid screening in units of kJ/mole which seriously depends on q_L as d_0 increases. The energy orders for G_I and G_{II} as mentioned here are also valid approximations for the corresponding free energy levels presented in the subsequent Figs. 5.16, 5.17, and 5.18

to compensate to form a stable gA channel which arises mainly from the hydrophobic binding between the gA channel and the bilayer at the two bilayer channel interfaces. The smaller the value of $\Delta G_{I,II}$, the higher the stability of gA channels. We observe that the value of $\Delta G_{I,II}$ for the second-order lipid-screening is orders of magnitude higher than that for the first-order lipid-screening (higher orders of lipid screening account for higher values of $d_0 - l$). Knowing the effective values of charges (in units of coulombs) on a gramicidin monomer, q_{gA}, and that of a lipid's head group region, q_L, one can readily calculate and show in real energy units (J), using the screened Coulomb interaction theory, that G_I has values which are drastically reduced and hence the value of $\Delta G_{I,II}$ collapses as the value of $d_0 - l$ approaches 0 Å. For example, making an *ad hoc* assumption that q_{gA} and q_L should be on the order of a few electron charges, we find $\Delta G_{I,II}$ to be on the order of kJ/mole for the first-order lipid screening, which closely corresponds to the phenomenological bilayer deformation energy calculated in another study [13]. The same *ad hoc* assumption ensures that $\Delta G_{I,II}$ increases to the order of 105 kJ/mole for the second-order lipid screening. This drastic increase in bilayer deformation energy requirements for stable channel formation with increasing the bilayer thickness channel length mismatch causes gA channel formation to be extremely difficult at a higher order of lipid screening. Beyond a certain level of hydrophobic bilayer channel mismatch, the deformation energy reaches values which are outside a biological binding energy scale, which suggests that at this high energy level the β-helical gA channels must experience

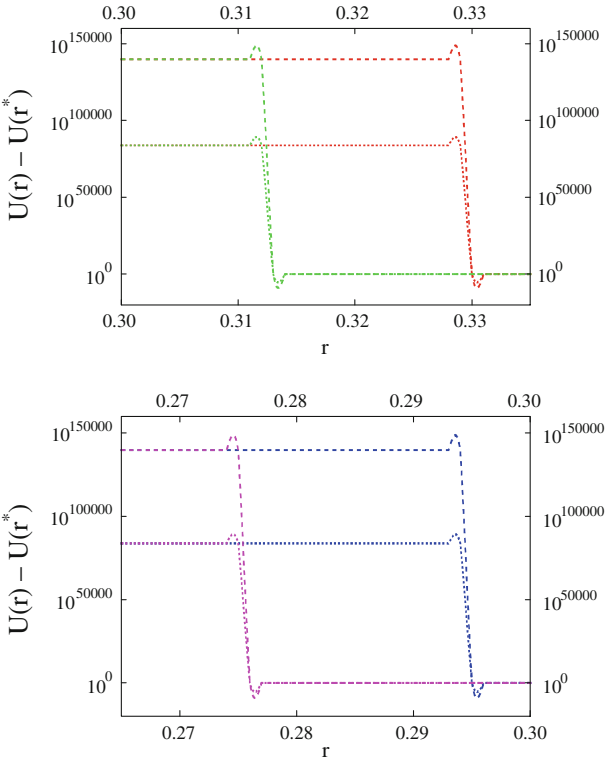

Fig. 5.16 A plot of the energy as a function of the reaction coordinate for a gA channel in lipid bilayer energetics at different values of r_{LL} (left $\rightarrow$ right: $r_{\mathrm{LL}} = 6.48074$, 6.9282 (*lower panel*), 7.34847, 7.74597 Å (*upper panel*)) for the first- (single-dashed curve) and second-(double-dashed curve) order lipid screening. $q_L/q_{\mathrm{gA}} = 0.0025$

exponential growth in their instability and finally may undergo a structural transition which has been experimentally observed (see Fig. 5.13). As $(d_0 - l)$ approaches 0 Å, the drastic drop in the values of G_I causes the value of $U(r)$ to quickly approach the level whose order of magnitude is comparable to that of the smaller interaction energy level ($U_{\mathrm{gA,gA}}(r)$—see Eq. 5.16) between two gA monomers with only direct Coulomb binding effects with the bilayer. Under this condition, the bilayer deformation energy is no longer an important regulator of channel function. Figure 5.16 demonstrates that the geometry of the lipids is an important regulator, and the transition $G_I \leftrightarrow G_{II}$ occurs at increasing reaction coordinates with increasing values of lipid dimension parameter r_{LL}. Identical trends with quantitatively slightly different energetics have been observed for Alm channels in lipid bilayers (see Figs. 5.17 and 5.18).

Figures 5.19 and 5.20 show how lipid charge relative to the charge of the channel-forming peptides changes the values of both G_I and G_{II} (see Fig. 5.19) and

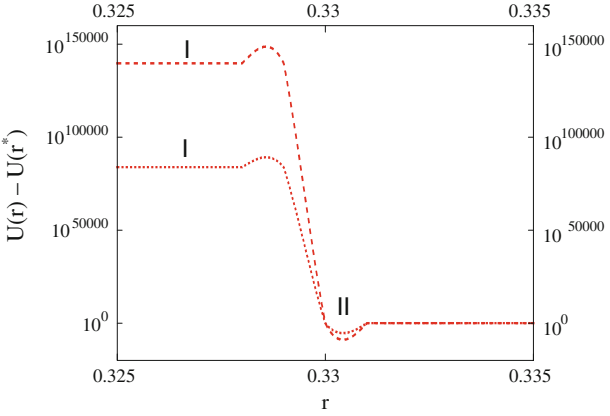

Fig. 5.17 A plot of the energy as a function of the reaction coordinate for Alm channels in lipid bilayer energetics at different order of screening (single- and double-dashed curves are for the first- and second-order screening, respectively). Here and in Fig. 5.18, $q_L/q_{\text{Alm}} = 0.005$, $(1/\epsilon_0)q_L q_{\text{Alm}} \approx 1$ has been chosen (for simplicity), and $r_{\text{LL}} = 7.74597$ Å

consequently $\Delta G_{I,II}$ (see Fig. 5.20). We observe about three times higher values of both G_I and G_{II} for both the first- and second-order of lipid screening for an Alm channel with three monomers in the 'barrel-stave' pore, compared to a gA channel as shown in Fig. 5.19. Quantitatively similar (3-fold increases) higher values of $\Delta G_{I,II}$ (see Fig. 5.20) are observed for both lipid screening orders for an Alm channel, compared to those for a gA channel. The three-times higher values of G_I, G_{II}, and $\Delta G_{I,II}$ in the Alm channel with three monomers are obvious, because in this specific Alm channel conformation there are six channel bilayer interaction sites, while a gA channel always has only two interaction sites with the bilayer (see Figs. 5.2 and 5.8). It seems that the interaction energy between monomers in both gA and Alm channels becomes irrelevant in comparison to the binding energy between the channel and the bilayer. We also observe that G_I, G_{II} and $\Delta G_{I,II}$ increase with the increase of lipid peptide charge ratio following:

$$G_I, G_I, \Delta G_{I,II} \propto \left(\frac{q_L}{q_M}\right)^3, \tag{5.29}$$

where $s = 1, 2$, etc. for the first-, second-, etc. order lipid screening, respectively, for both gA and Alm channels. Here, q_M stands for gA (q_{gA}) or Alm (q_{Alm}) monomer charges.

In Fig. 5.21 we observe a modest and linearly proportional effect of the lipid dimension r_{LL} on $\Delta G_{I,II}$, for both the first- and second-order lipid screening with three-times higher effects for Alm channels than for gA channels. Figure 5.22 shows that, for both gA and Alm channels, the reaction coordinate at which we have shown

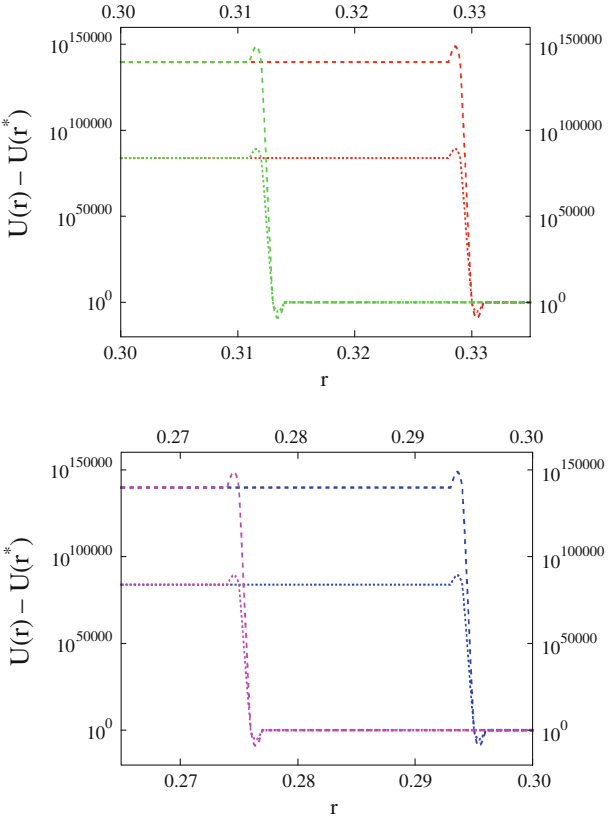

Fig. 5.18 A plot of the energy as a function of the reaction coordinate (r) for an Alm channel in lipid bilayer energetics at different values of r_{LL} (left $\rightarrow$ right: $r_{\mathrm{LL}} = 6.48074$, 6.9282 (*lower panel*), 7.34847, 7.74597 Å (*upper panel*)) for the first- (single-dashed curve) and second-(double-dashed curve) order lipid screening. $q_L/q_{\mathrm{Alm}} = 0.0025$

the calculation of $\Delta G_{I,II}$ increases (shifts toward higher values) in linear proportionality to r_{LL} for both the first- and second-order lipid screening.

The most dramatic theoretical result is illustrated in Fig. 5.23, where $\Delta G_{I,II}$ increases exponentially with the increase of $d_0 - l$ (here we have rephrased the order of screening by $d_0 - l$):

$$\Delta G_{I,II} \propto \exp(d_0 - l). \tag{5.30}$$

Consequently, as $\Delta G_{I,II}$ is proportional to $\Delta G^0_{\mathrm{def}}$, the dissociation force:

$$F_{\mathrm{dis}} = -\left(-\frac{\partial \Delta G_{I,II}(d_0 - l)}{\partial (d_0 - l)}\right) \tag{5.31}$$

also follows an exponential relation:

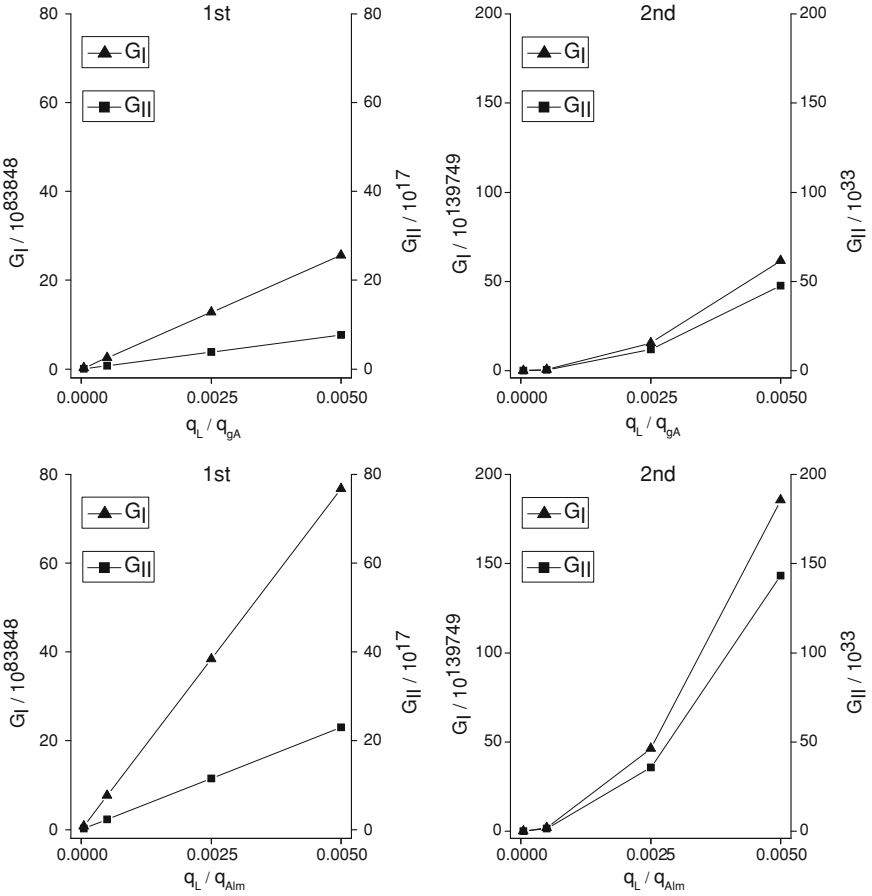

Fig. 5.19 Energy (G_I and G_{II}) as a function of q_L/q_{gA} for the gA channel (*upper panel*) or q_L/q_{Alm} for the Alm channel (*lower panel*) in lipid bilayer energetics in the first- and second-order of lipid screening, respectively. Here, $r_{\mathrm{LL}} = 7.74597\,\text{Å}$

$$F_{\mathrm{dis}} \propto \exp(d_0 - l) \tag{5.32}$$

which is very different from the dissociation force calculated based on the bilayer elastic model [38, 40, 66, 67] where F_{dis} on a gA channel has been reported to change linearly with the change of $d_0 - l$ (see Eq. 5.12 for comparison) [6, 13].

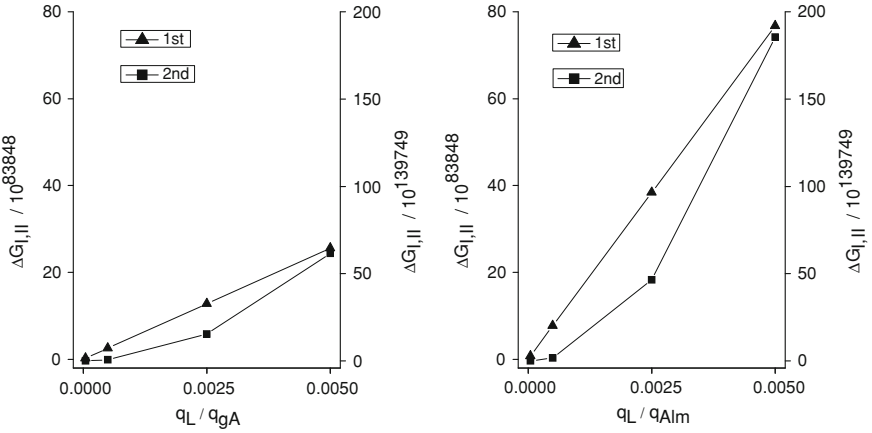

Fig. 5.20 Plot of $\Delta G_{I,II}$ as a function of q_L/q_{gA} (*left panel*) or q_L/q_{Alm} (*right panel*) in lipid bilayer energetic in the first- and second-order of lipid screening. Here, $r_{\mathrm{LL}} = 7.74597\,\text{Å}$

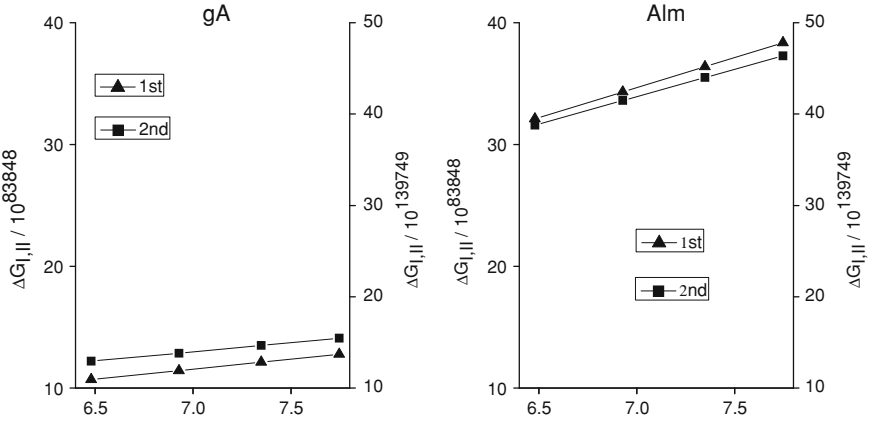

Fig. 5.21 Plot of $\Delta G_{I,II}$ as a function of r_{LL} for the gA channel (*left panel*) and the Alm channel (*right panel*) in lipid bilayer energetics in the first- and second-order of lipid screening, respectively. Here, $q_L/q_M = 0.0025$

5.6 Fitting Theoretical Predictions to Experimental Results

The experimental results presented in Sect. 5.4 show that the gA channel's lifetime τ decreases drastically as the bilayer thickness increases, and at a sufficiently high thickness, the gA channel structure experiences a conformational transition. The trend in the value of τ in a PC bilayer shows that it decreases almost exponentially with the increase of bilayer thickness. A recent study [6] has also supported this conclusion that τ decreases almost exponentially with the increase of the bilayer-channel hydrophobic mismatch. Within a reasonable approximation, since it can

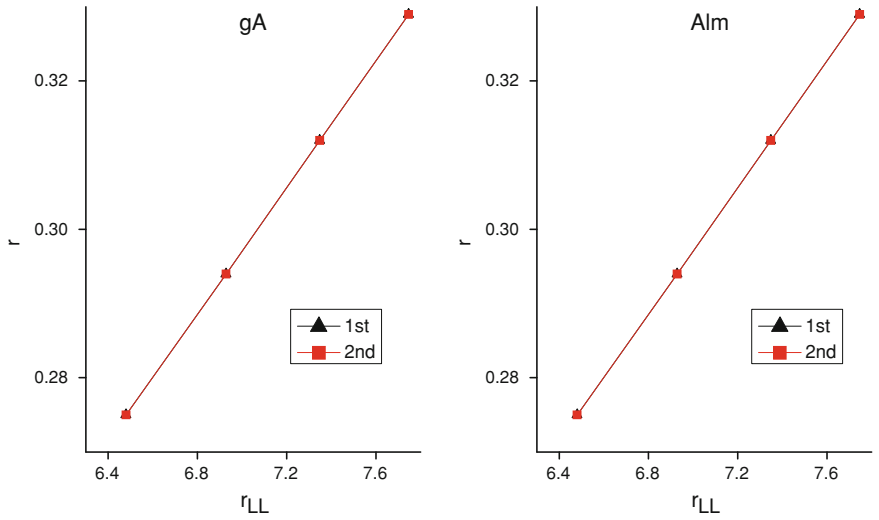

Fig. 5.22 The reaction coordinate which was used in the plot of $\Delta G_{I,II}$ as a function of r_{LL} for the gA channel (*left panel*) and Alm channel (*right panel*) in lipid bilayer energetics in the first- and second-order of lipid screening, respectively. Here, $q_L/q_M = 0.0025$

be assumed that the gA channel stability decreases with the increase of the bilayer induced dissociation force, we conclude that $\tau \propto \exp(-(d_0 - l))$. Considering the theoretical value of F_{dis} in Eq. 5.13, this experimental channel lifetime relation with the mismatch is supported by a previously presented derivation of gA channel lifetime (Eq. 5.27) in a continuum distribution of local energy traps [85] which is also borne out elsewhere [6, 56].

Another possibility is to use the traditional way of deriving lifetime, using the relation presented in Eq. 5.13. Slight differences in the bilayer thickness gA channel length mismatch dependence of the theoretical trend of gA channel lifetime appear to depend on whether we use the expression for F_{dis} from the screened Coulomb model ($\sim \exp(d_0 - l)$), or the elastic bilayer model ($\sim (d_0 - l)$) in the case when c_0 is assumed to be unchanged. In both of these cases the theoretical channel destabilization increases (lifetime τ_{th} decreases) exponentially at small values of $d_0 - l$ but as $d_0 - l$ increases, higher channel destabilization is observed in the former case compared to the latter case (see Fig. 5.24). For any constant thermodynamic condition, the average channel lifetime therefore changes as a negative exponential function (or more strongly) of the hydrophobic mismatch between the bilayer thickness and channel length.

The origin of this difference is readily found if we expand the exponential expression (screened Coulomb model) in a power series as:

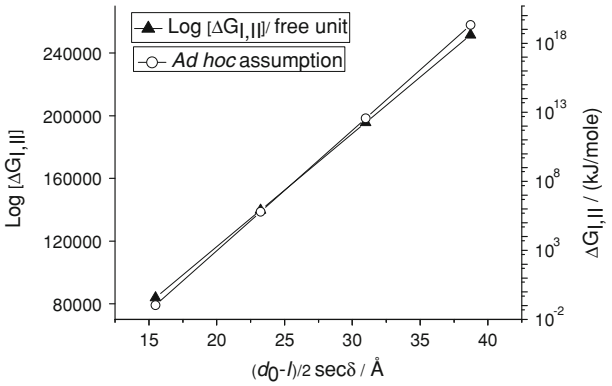

Fig. 5.23 Plot of Log$[\Delta G_{I,II}]$ as a function of $d_0 - l$. Here, $(d_0 - l)$ sec δ is the distance covered by the lipid head groups in the deformed regions of the bilayer at the bilayer gA channel interaction sites. δ(for simplicity, they can be assumed to appear with a constant value within $0-90^\circ$ in a particular lipid bilayer membrane for all participating lipids in all orders of screening at the gA channel bilayer interface), the angle at which lipids in the deformed portion of the bilayer couple with the extension of the gA channel length. $\Delta G_{I,II}$ increases exponentially with $d_0 - l$. $\Delta G_{I,II}$ at lower values of $d_0 - l$ (e.g., $d_0 - l \approx 0$) or at other higher values of $d_0 - l$ can be extrapolated from the plot. For a certain type of lipid with a fixed lipid charge, $\Delta G_{I,II} \propto \exp(d_0 - l)$. Consequently, the dissociation force imposed by the bilayer on the gA channel (F_{dis}) increases exponentially with $d_0 - l$, i.e., $F_{\text{dis}} = -\left(-\frac{\partial \Delta G_{I,II}(d_0-l)}{\partial(d_0-l)}\right) \propto \exp(d_0 - l)$. As a result, the gA channel lifetime decreases exponentially with the increase of $d_0 - l$. *Ad hoc* assumptions ($q_{\text{gA}} \sim$ electron charge and other relevant parameters [1, 16, 17, 35, 41, 71, 75] give an estimate of $\Delta G_{I,II}$ / (kJ/mole) which strongly depends on q_L as d_0 increases. Results in previous figure fall within the second-order screening ($d_0 - l < 40$ Å). Experimentally, this was observed in previously published data [6, 56] and here in the experimental results section

$$\begin{aligned}\Delta G_{I,II} = \mathrm{e}^{(d_0-l)} &= \frac{(d_0-l)^2}{2} + \left(1 + (d_0-1) + \frac{(d_0-1)^3}{6} + \frac{(d_0-1)^4}{24} + \ldots\right) \\ &= \Delta G_{I,II}(\text{Harm}) + \Delta G_{I,II}(\text{A.Harm}). \end{aligned} \tag{5.33}$$

The symbols Harm and A.Harm denote the harmonic and anharmonic contributions in $\Delta G_{I,II}$, respectively. The necessity to include $\Delta G_{I,II}$(A.Harm) is generally expected in the case with higher values of $d_0 - l$ (see Fig. 5.21) whereas the elastic bilayer theory predicts the presence of only a harmonic term $\sim (d_0 - l)^2$ in the bilayer deformation energy, which is adequate for sufficiently small deformation values. This is also readily found in the screened Coulomb energy. Consequently, $F_{\text{dis}} = \frac{\partial}{\partial(d_0-l)} \Delta G_{I,II}$ in the screened Coulomb model also contains additional terms (different orders) besides the term $(d_0 - l)$, which is the only geometric mismatch term found in the elastic bilayer theory to regulate the change of the gA channel lifetime (in the case of non-changing lipid curvature profiles). Although both the screened Coulomb model and the elastic bilayer model calculations generally suggest an exponential damping in gA channel lifetime with increasing $d_0 - l$ which is consistent with the experimental data presented in Sect. 5.4 (and in [6, 56]), the

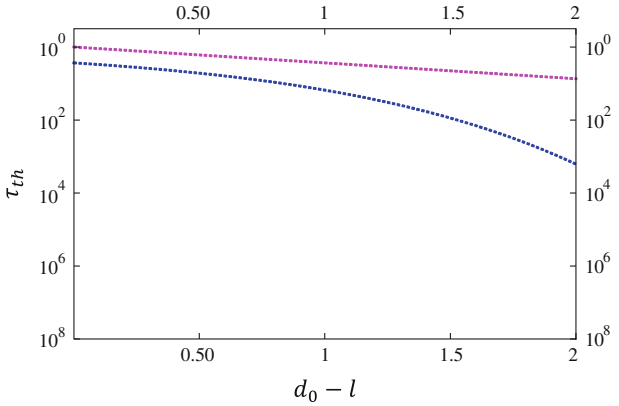

Fig. 5.24 Plot of theoretical values of gA channel lifetime τ_{th} (arbitrary units, using $\tau_{\text{th}} \sim e^{-\frac{(\lambda^+ - \lambda)F_{\text{dis}}}{k_B T}}$, Eq. 5.13) as a function of the bilayer thickness gA channel length mismatch $d_0 - l$ (arbitrary units). The *lower curve* represents τ_{th} using the screened Coulomb theory while the upper curve represents τ_{th} derived from the elastic bilayer theory, both explained earlier. In both plots $\lambda^+ - \lambda$ is considered constant. Both curves are straight lines (in log-lin plot) meaning τ_{th} drops exponentially with increasing $d_0 - l$ at the low mismatch level but τ_{th} (from the screened Coulomb formula) drops even faster (lower curve) as $d_0 - l$ increases due to the inclusion of anharmonic terms (explained earlier and in Fig. 5.25) in the energy at high values of mismatch

screened Coulomb model calculation hints at the presence of extra damping, due to higher order anharmonic terms in the energy expression. This better explains why at high mismatch values, the channel experiences not just destabilization but also structural transitions (see Sect. 5.4) due to the energetic cost of the super-heavy bilayer deformation energy (see Fig. 5.23). We therefore conclude that although the elastic bilayer model [38, 40] which yields the deformation energy dependence according to $\sim(d_0 - l)^2$ [6, 13] may be applicable in the small deformation limit, it requires a modification for values outside this limit. For the same reason, the theory based on a linear spring approximation for the coupling between the bilayer and gA channels [57], which explicitly shows an exponential damping of gA channel lifetime with an increasing $d_0 - l$, can be a very good approximation when $d_0 - l$ is relatively small. However, when $d_0 - l$ is large enough and the interaction between a gA channel and the bilayer extends to other next-neighbor lipids in the deformed regions of the bilayer near the channel, an extension of the elastic model is warranted.

Theoretical and experimental results also show identical trends in the regulation of the gA channel stability induced by the lipid curvature properties. The energy barriers modestly change due to the change of the lipid-lipid separation r_{LL} (determined from the square root of the average lipid cross-sectional area in a bilayer) which changes as the lipid curvature changes. For simplicity, in the theoretical analysis we have assumed the same value of r_{LL} for both the lipid-lipid separation and the lipid-peptide separation at the channel bilayer interface. The energy barrier also shows a modest change due to the change of lipid charge. To some extent, lipid charge also

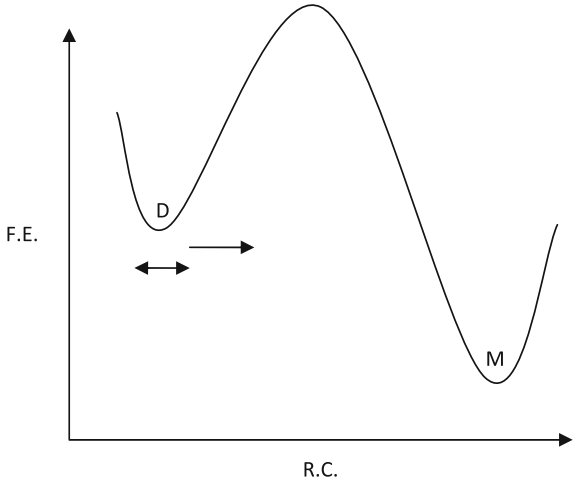

Fig. 5.25 Schematic illustration showing the free energy (F.E.) dependence on the reaction coordinate (R.C.) when protein conformational transitions between different energy states occur. The back-and-forth transitions between gA dimer (D) and monomers (M) have been demonstrated here. These states have different energy values and are separated by a potential barrier. $\Delta G_{I,II}$(Harm) and $\Delta G_{I,II}$(A.Harm) energy terms are effective in the small deformation (bi-directional arrow in the figure, within a very short range from the point of the energy minimum, thanks to harmonic behavior) and beyond the small deformation region (*right arrow*), respectively, to ensure transitions from D to M states and vice versa of gA. Only in the limit of extremely small bilayer deformation ($d_0 - l \sim 0$) the inclusion of only the harmonic term $\Delta G_{I,II}$(Harm) $\sim (d_0 - l)^2$ may be sufficient. When $d_0 - l$ increases beyond the immediate vicinity of the free energy minima, higher order anharmonic energy terms dominate in the transition between D and M states. All such energy states appear together in the screened Coulomb interaction model calculation but are missing in the elastic bilayer model calculation of the bilayer deformation energy as explained in the text

determines the lipid curvature properties. Hence, the change in the lipid charge also regulates the gA channel functions in lipid bilayers. The model calculation hints for a stronger lipid charge effect on gA channel stability in the case of higher values of $d_0 - l$ (see Eq. 5.29).

The experimental data for the Alm channel in a lipid bilayer also show considerable agreement with the results of the theoretical model (see Figs. 5.17 and 5.18). To initiate the formation of an Alm channel under the experimental conditions mentioned in Sect. 5.4, a minimum peptide concentration of $\sim 10^{-8}$ M is required [12]. However, once the Alm channel starts forming, we observe that the Alm channel activity increases considerably with the increase of $[M_{\text{Alm}}]$. These data are in good agreement with the theoretical prediction of channel activity depending mainly on $\Delta G_{I,II}$ in the initiation phase. Once the channels start forming, the bilayer's physical parameters which determine $\Delta G_{I,II}$ appear to be very critical in the regulation of the channel formation mechanism and the channel formation rate sharply increases with peptide concentration. We have also experimentally observed that the detailed Alm channel activity shows considerable dependence on bilayer thickness and on lipid

curvature. Higher lipid charges strongly destabilize the probability of observing any Alm channel current level, especially higher order current levels [18]. The higher concentration $[M_{\mathrm{Alm}}]$ required in thicker bilayers or bilayers containing lipids with negative curvature or charges are likely to change the free energy profile in bilayers [92] which compensates for the changed values of the theoretically calculated $\Delta G_{I,II}$. The experimentally observed changes in free energies $\Delta G^{1\to 2}$ and $\Delta G^{1\to 3}$ of any Alm channel within a lipid bilayer system are not drastically different, which is consistent with the calculated values of $\Delta G_{I,II}$ for any specific order of lipid screening where the values of $\Delta G_{I,II}$ do not considerably change due to the change of the number of monomers in Alm channels. In particular, $\Delta G_{I,II}$ values stay within the same order of magnitude but slightly increase with the increase of the number of Alm monomers participating in Alm channel formation mainly due to the increased channel-bilayer interaction sites. However, $\Delta G_{I,II}$ changes exponentially between different lipid orders which can be compared with the compensation of free energy changes [92] due to the requirement of higher geometric orders of $[M_{\mathrm{Alm}}]$ (or $[M_{\mathrm{gA}}]$ in the case of gA channels) when the bilayer thickness increases or neutral lipids are replaced by more negative curvature bearing lipids in the bilayers.

5.7 Evidence of Physical Interactions Between Lipids and Channel-Forming Peptides or Other Drugs: A Case Study Using Molecular Dynamics Simulations

We designed an *in silico* molecular dynamics (MD) simulation [15] in order to model the drug-lipid interactions and to gain deeper insights into the problem. This simulation illustrates how an empirical calculation of the force field finds partial charges on each atom in the drugs or peptides interacting with lipids on lipid membranes, irrespective of their net molecular charges [24, 43, 44, 53].

In charge-bearing peptide-induced ion channels, e.g., gA and Alm, or charge-neutral chemotherapy drug-induced ion pores [14], both ion channel/pore forming agents and lipids approach each other through hydrophobic coupling (e.g., see Figs. 5.2, 5.6, 5.7, 5.8, 4.5, etc.). So naturally, charges on charge-bearing lipids e.g., phophatidylserine (PS), phosphatidylglycerol (PG), etc. and charge-bearing peptides, e.g., gA, Alm, etc. experience electrical fields created by each other. But what happens if both lipids and channel-forming drugs have no net molecular charges? This question naturally appears as most of the lipids in cell membranes are zwitterionic phosphatidylcholines (PCs) with no net electric charges. Also, the finding of channel formation by charge neutral chemotherapy drugs [14] raises the question if there is any possibility to observe interactions between the channel-forming drugs and bilayer constituents, especially lipids, due to the electrical properties of drugs and lipids in a manner equivalent to the claimed peptide lipid screened Coulomb interactions in gA channels lipid bilayer binding ([11] in Chap. 4). To clearly understand this general issue we have performed MD simulations.

5.7.1 MD Techniques

We considered five different relative locations and orientations randomly generated in each drug-lipid complex as initial structures for MD simulations. For each location- and orientation-specific complex, a 6 ns (chemotherapy drugs) or 10 ns (gA or Alm) explicit water MD simulation at 300 K in a solution at pH 7 was performed. We applied the software package Amber 11 [84], specifically the Amber force field ff03 was used. The explicit water TIP3P model was used to simulate solvent effects. The force field parameters for drugs and lipids (PC and PS) were generated using an Amber module antechamber [28, 77]. Twenty complexes were energy-minimized using the steepest descent method for the first ten cycles, and then followed by a conjugate gradient for another one thousand cycles. We then applied Langevin dynamics during the process of heating up the system for 200 ps with the energy-minimized complex, in which drug and lipid molecules were being restrained using a harmonic potential with a force constant $k = 100$ N/m. Afterward, we introduced pressure regulation to equilibrate water molecules around the complex, and to reach an equilibrium density for another 200 ps in addition to temperature regulation. The MD production run then was continued for 6 ns. Note that the phospholipid was gently restrained with a harmonic potential with a force constant $k = 10$ N/m, applied only to the phosphate during the production runs.

5.7.2 MD Results and Discussion

The Drug/Peptide Lipid Physical Interactions as a Possible Cause of Their Induced Pore Formation

MD results presented in Figs. 5.26 and 5.27 suggest that the drug/ peptide lipid complex fluctuates within a separation over a period of time. These results suggest that both drugs and peptides likely bind with PC and PS given appropriate initial conditions [15]. In the in-depth analysis, we found evidence suggesting that the hydrophobic effect is unlikely to contribute into the distance dependent drug/peptide lipid binding. The analysis of energy contributions from two non-bonded interactions, E_{vdW} and E_{ES} versus $d_{\mathrm{drug-lipid}}$ revealed crucial insights into the cause of the observed stability of the drug/peptide lipid complexes. Both E_{vdW} and E_{ES} appear to be the main contributors to the energetic drug/peptide lipid binding and vdW interactions contribute slightly more than ES interactions as the drug and lipid approach closer. Binding stability generally is found to decrease quickly with increasing $d_{\mathrm{drug-lipid}}$. Both vdW and ES interactions contribute comparably with both energies decreasing with increasing $d_{\mathrm{drug-lipid}}$. Large standard deviations (Figs. 5.26 and 5.27) are suggestive of the conformational space of the drug/peptide lipid complexes not being completely explored in MD simulations. Nonetheless, this incompleteness does not preclude the proposed interpretation. Importantly, the drug/peptide

lipid interactions resemble the protein lipid vdW and ES interactions found in MD simulations of a gA channel in phospholipid membranes [91].

These results suggest that the observed vdW and ES binding energies, which presumably arise from the electrical properties of both of the participating agents, do not depend on the molecular net charges. We observe the presence of both vdW and ES, even in cases where either or both of the participating agents (e.g. PC, chemotherapy drugs, etc.) have no net molecular charges. Therefore, it is clear that the interactions appear due to the partial charges on each atom in the drugs or peptides interacting with lipids on lipid membranes, irrespective of their net molecular charges [24, 43, 44, 53]. This hypothesis has appeared in the screened Coulomb interaction model through the consideration of the localized charges on the participating agents, irrespective of the consideration of their net molecular charges.

5.8 Discussion and Conclusions

In this chapter, we have investigated the issue of how the hydrophobic coupling between a lipid bilayer and integral channels regulates the channel stability, using two structurally different gramicidin A and alamethicin channels as primary examples. Conformational changes of both trans-bilayer dimerized linear gramicidin A channels and 'barrel-stave' pore type alamethicin channels are regulated mainly by the bilayer channel coupling energetics. Experimental results show that an increased hydrophobic mismatch between bilayer thickness and channel length ($d_0 - l$) appears as a major channel destabilizing factor. Increased negative lipid curvature and lipid charge also induce considerable destabilization into channel formation. To theoretically address the observed lipid bilayer-induced regulation of channel stability, we have developed a simple physical model of the 'screened Coulomb interaction', which has been used to calculate the binding energy of a gramicidin A dimer with a lipid bilayer required for the stability of the channel structure. The model calculates the binding energy, considering mainly the electrical properties of both the lipids on the bilayer and the channel-forming agents. The same model can be extended to also calculate the binding energy of an alamethicin channel with a lipid bilayer. In this screened Coulomb interaction model, the calculation of the binding energy of a channel with a lipid bilayer considers most of the relevant properties such as the localized charges of both peptides and lipids, geometry of the environment (bilayer thickness, channel length, channel cross-sectional area, lipid head group cross-sectional area, lipid intrinsic curvature), the change in the dielectric constant (relative to the aqueous phase) of the hydrophobic region near the channel interface, and a specific mechanical property such as bilayer elasticity. Changes in any of these properties modulate the binding energy between the bilayer and the channel, which alters the channel's stability. We have compared the model results directly with the experimental results on stability and energetics of the gramicidin A and alamethicin channels in lipid bilayers, and have found them to be in very good agreement.

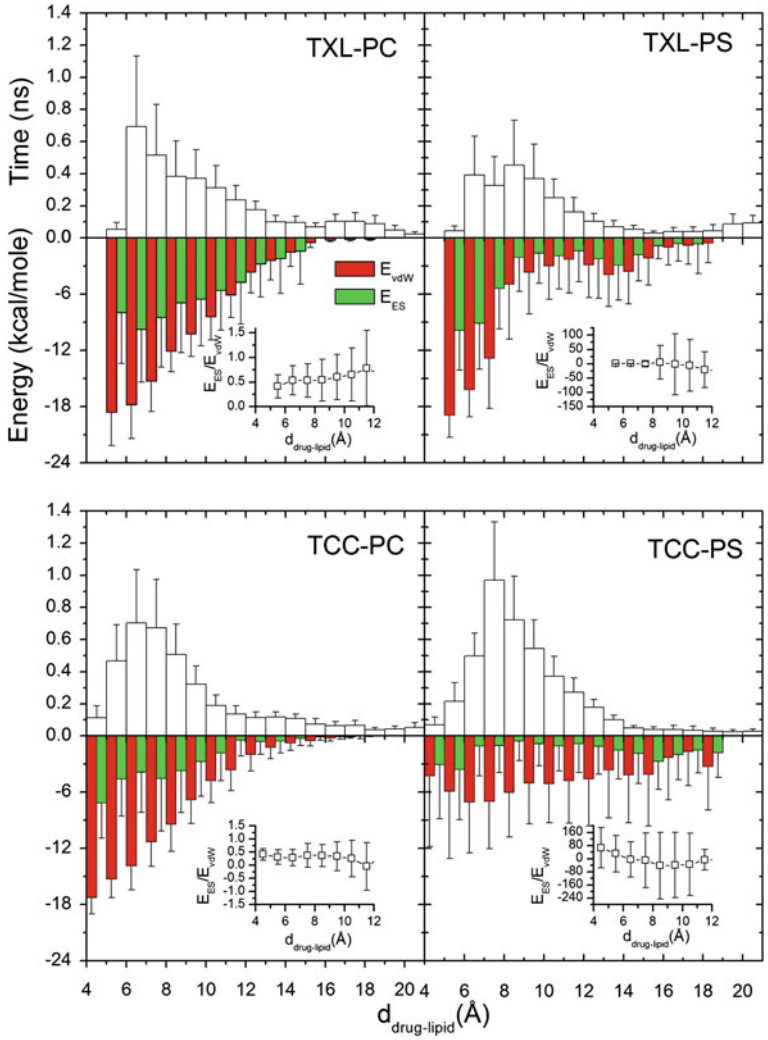

Fig. 5.26 In all the histograms (*upper panel*) of time versus $d_{\text{drug}-\text{lipid}}$, the duration of the drug/lipid complex staying together (height) within a distance (width) in 6 ns MD simulations is presented. *Lower panels* show the histograms of non-bonded van der Waals (vdW) energy (E_{vdW}) and electrostatic (ES) interaction energy (E_{ES}). To avoid color conflict, E_{vdW} and E_{ES} are shown to occupy half–half widths although each half represents the whole width of the corresponding histogram

The calculations using screened Coulomb interactions demonstrate that the bilayer deformation energy ($\Delta G_{I,II} \approx \Delta G^0_{\text{def}}$) increases by orders of magnitude with the increase of the order of the lipid screening. The increasing lipid screening order is a measure of the hydrophobic bilayer thickness channel length mismatch, due to either an increase in bilayer thickness or decrease in channel length, or both.

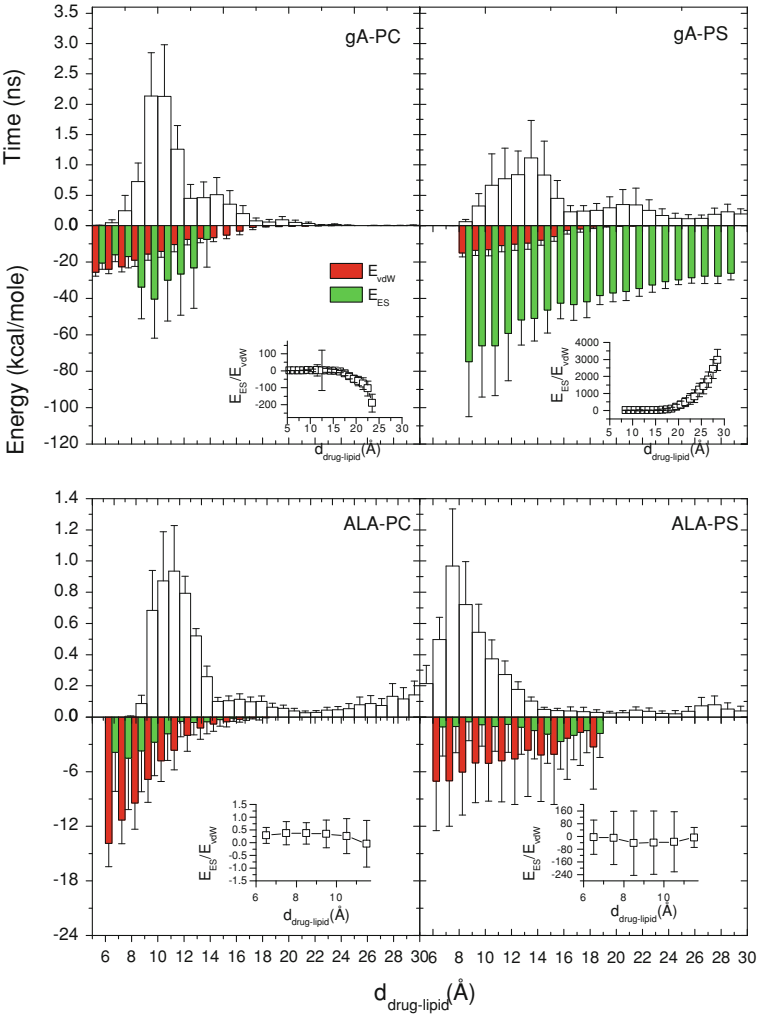

Fig. 5.27 In all the histograms (*upper panel*) of time versus $d_{\text{drug}-\text{lipid}}$, the duration of the drug/lipid complex staying together (height) within a distance (width) in 6 ns MD simulations is presented. *Lower panels* show the histograms of non-bonded van der Waals (vdW) energy (E_{vdW}) and electrostatic (ES) interaction energy (E_{ES}). To avoid color conflict, E_{vdW} and E_{ES} are shown to occupy half–half widths though each half represents the whole width of the corresponding histogram

Other studies using β-helical gramicidin A channels [7] and α-helical peptides like acetyl-GWW(LA)$_n$LWWA-amide (WALP) [47, 48], incorporated in lipid bilayers with different thicknesses, provide experimental evidence for the response between bilayer and protein structural alterations and the hydrophobic mismatch. An increase in the values of $\Delta G_{I,II}$ causes destabilization of the corresponding channels. Therefore, the stability or the average lifetime of a channel can decrease by decreasing

the channel length or increasing the bilayer thickness. The experimental results fit perfectly with the trends found in the theoretical model. A shorter gramicidin A channel (gA-(13)) is experimentally observed to be less stable than a longer gramicidin A channel (AgA(15)), or both of these channels are exponentially less stable in a thicker ($DC_{20:1}PC$) bilayer than in a thinner ($DC_{18:1}PC$) one. Other important parameters in the theoretical model are the intrinsic lipid curvature and the lipid charge. An increased effective lipid cross-sectional area is a result of either a higher negative curvature, e.g. PE's over PC's, or the lipid head group charges causing Coulomb repulsion between lipids. The model calculation shows that increased lipid cross-sectional areas ($\sim r_{\mathrm{LL}}^2$) result in a modest increase in $\Delta G_{I,II}$, which makes the channel formation harder so the lifetime of a channel decreases. The experimental results show that gramicidin A channel lifetimes in a negative curvature-bearing DOPE bilayer are shorter than those in a neutral $DC_{18:1}PC$ bilayer: the effect of negative curvature induces linear destabilization in gramicidin A channels. As the value of r_{LL}^2 increases with the increase in lipid intrinsic curvature, we conclude that a very good agreement exists between the theoretical predictions and experimental observations. Using the theoretical expression for the channel-bilayer binding energy, one can also derive the elastic force constants and consider higher order effects on elastic force constants with an increased value of s (representing a higher mismatch) exactly illustrating the effects of lipid charges, as shown in Eq. 5.29. Thus, an increased bilayer elasticity helps the bilayer to deform near the channels. Despite elasticity effects being secondary relative to the charge effects, the increased bilayer elasticity reduces the bilayer deformation energy which favors the stability of a channel in a bilayer membrane. Higher values of s, corresponding to a higher mismatch $d_0 - l$, also indirectly confirm that an equal increase in bilayer elasticity reduces $\Delta G_{I,II}$ for shorter gramicidin A channels (accounting for a larger mismatch) more than that for longer gramicidin A channels (accounting for a smaller mismatch). As a result, stability of shorter gramicidin A channels increases relatively more strongly than that of longer gramicidin A channels. The experimental studies [10, 11, 13] claimed to induce increased elasticity into bilayers by bilayer-active amphipathic molecules, such as several anti-fusion peptides, amphiphiles like triton X-100 and capsaicin, and even an antimicrobial peptide gramicidin S. They also demonstrated that channels generally show higher stability with an increase of the elasticity of the lipid bilayers. Furthermore, in [13] it was shown that by increasing bilayer elasticity, the bilayer deformation energy is reduced which in the model calculation appears as a decrease in $\Delta G_{I,II}$. Requirements of higher gramicidin A and alamethicin concentrations in both thicker bilayers and more negative-curvature bearing PE bilayers over PC bilayers also confirm that a higher mismatch between the bilayer's hydrophobic thickness and channel length and negative lipid curvature are two very important regulators of channel functions, which the theoretical model predicts and experimental results confirm.

In this chapter, we have developed a theoretical model for bilayer channel energetics based on experimentally measurable values of general physical properties, such as charge and size of the channel-forming peptides and the bilayer constituents e.g. mainly lipids. By considering a simple model of screened Coulomb

interactions, we have formulated a relatively simple and tractable method, and avoided the previously encountered complications in a method of calculating the elastic bilayer deformation energy [21, 38, 40, 66, 67, 74] based on the assumption of complicated individual contributions from the intrinsic monolayer curvature, local compression and bending moduli of two bilayer leaflets, and the associated energy densities [34, 63]. The molecular dynamics simulations of gramicidin A in lipid bilayers utilizing an all-atom force field [2] and computation of the potential of mean force in a lipid mediated protein-lipid hydrophobic coupling [23] helped us confirm that the lipid head group region effectively regulates the lipid bilayer gramicidin A channel hydrophobic coupling. The acyl chains may also produce some direct partial pressure profile on the gramicidin A channels at the channel bilayer interaction sites, but that should be averaged out by their contributions from all sides of a gramicidin A channel. One very important insight gained through the model is that the bilayer imposed dissociation force on gramicidin A channel increases (and as a result, the gramicidin A channel lifetime decreases) at least exponentially, which matches with the experimental observations (see Fig. 5.3 and [6, 56]). The experimental observation of increasing the negative lipid curvature-induced linear decrease in gramicidin A channel stability verified by the theoretical results also provides evidence in favor of the approach of regulating membrane protein functions due to the hydrophobic energetic membrane–membrane protein coupling. In the alamethicin channel, the requirement of higher orders of concentration $[M_{\mathrm{Alm}}]$ in thicker lipid bilayers may compensate for the huge variation in $\Delta G_{I,II}$, but the experimentally observed small changes in the free energies $\Delta G^{1\to 2}$ and $\Delta G^{1\to 3}$ of any alamethicin channel within a lipid bilayer system correspond to a little variation in the theoretical values of $\Delta G_{I,II}$ for alamethicin channels consisting of different numbers of monomers. It should also be stressed that the model calculation is valid for an arbitrary hydrophobic mismatch between bilayer thickness and channel length and is equally applicable to at least two types of protein-lined channels, i.e. linear β-helical gramicidin A type and 'barrel-stave' pore alamethicin type. We have found very good agreements between the results on channel stability/lifetime emerging from the binding energy calculation using screened Coulomb interactions and the experimental observations on gramicidin A and alamethicin channels. The molecular dynamics simulations also suggest the presence of distance-dependent electrostatic and van der Waal's interactions between lipids and membrane active agents (peptides or other biomolecules like chemotherapy drugs, nucleic acid oligomers, or aptamers, etc.). These simulation results also support the existence of interactions between the membrane and active agents, due primarily to their electrical properties. The use of the screened Coulomb interaction model in the membrane–membrane protein energetics is also supported by molecular dynamics simulations. This theoretical screened Coulomb interaction model calculation can therefore be generally applied to the energetics and dynamics of several kinds of membrane proteins with a variety of membrane effects, as long as they are hydrophobically coupled with lipid bilayers.

Finally, we conclude that the physical lipid-membrane protein interactions, due mainly to their electrical properties and the related energetics, appear as primary regulators of membrane protein functions. A membrane's elasticity helps it to bend, due

to the pull originating primarily from the electrostatic and van der Waal's interactions between localized charges on lipids and membrane proteins or any other membrane-active drug molecules. Both electrical energetic coupling (primary regulator) and mechanical energetic coupling (secondary regulator) between a lipid bilayer and integral membrane proteins regulate the membrane protein functions.

References

1. Aguilella, V. M. and Bezrukov, S. M.: Alamethicin channel conductance modified by lipid charge. Eur. Biophys. J. **30**, 233–241 (2001).
2. Allen, T. W., Andersen, O.S. and Roux, B.: Energetics of ion conduction through the gramicidin channel. Proc. Natl. Acad. Sci. **101**, 117–122 (2004).
3. Andersen, O.S., D. B. Sawyer and Koeppe, R.E. II. In: Biomembrane structure and Function, K. R. K. Easwaran and B. Gaber (eds.) p227. Schenectady, New York: Adenine (1992).
4. Andersen, O.S.: Ion movement through Gramicidin A Channels - Studies on the Diffusion-controlled Association Step. Biophys. J. **41**, 147–165 (1983).
5. Andersen, O.S., Nielsen, C., Maer, A. M., Lundbæk, J. A., Goulian, M. and Koeppe, R.E. II: Gramicidin channels: molecular force transducers in lipid bilayers. Biol. Skr. Dan. Vid. Selsk. **49**, 75–82 (1998).
6. Andersen, O.S. and Koeppe, R.E. II: Bilayer thickness and membrane protein function: an energetic perspective. Annu. Rev. Biophys. Biomol. Struct. **36**, 107–130 (2007).
7. Andersen, O.S., Koeppe, R.E. II and Roux, B.: Gramicidin Channels. IEEE Trans. Nanobiosci. **4**, 10–20 (2005).
8. Arseniev, A. S., Barsukov, I. L., Bystrov, V.F. and Ovchinnikov, Yu. A.: Biol. Membr. **3**, 437 (1986).
9. Ashrafuzzaman, M. and Beck, H.: In Vortex dynamics in two-dimensional Josephson junction arrays, University of Neuchatel, ch 5 p 85, (2004) http://doc.rero.ch/record/2894ln=fr
10. Ashrafuzzaman, M. and Andersen, O.S.: Lipid bilayer elasticity and intrinsic curvature as regulators of channel function: a single molecule study. Biophys. J. **421A** (2007).
11. Ashrafuzzaman, M., McElhaney, R. N. and Andersen, O.S.: One antimicrobial peptide (gramicidin S) can affect the function of another (gramicidin A or alamethicin) via effects on the phospholipid bilayer. Biophys. J. **94** 6–7, (2008).
12. Ashrafuzzaman, M., Andersen, O.S. and McElhaney, R. N.: The antimicrobial peptide gramicidin S permeabilizes phospholipid bilayer membranes without forming discrete ion channels. Biochim. Biophys. Acta **1778**, 2814–2822 (2008).
13. Ashrafuzzaman, Md., Lampson. M.A., Greathouse, D.V., Koeppe II, R.E., Andersen, O.S.: Manipulating lipid bilayer material properties by biologically active amphipathic molecules. J. Phys.: Condens. Mat. **18**, S1235–1255 (2006).
14. Ashrafuzzaman, Md., Duszyk, M. and Tuszynski, J. A.: Chemotherapy drugs Thiocolchicoside and Taxol Permeabilize Lipid Bilayer Membranes by Forming Ion Pores. J. of Physics: Conf. Series **329**(012029), 1–16 (2011).
15. Ashrafuzzaman, Md., Tseng, C.-Y., Duszyk, M. and Tuszynski, J. A.: Chemotherapy drugs form ion pores in membranes due to physical interactions with lipids. submitted (2011).
16. Benz, R., Fröhlich, O., Läuger, P., and Montal, M.: Electrical capacity of black lipid films and of lipid bilayers made from monolayers. Biochim. Biophys. Acta **394**, 323–334, (1975).
17. Berneche, S. and Roux, B.: Molecular Dynamics of the KcsA K^+ Channel in a Bilayer Membrane. Biophys. J. **78**, 2900–2917 (2000).
18. Bezrukov, S.M., Rand, R.P., Vodyanoy, I. and Parsegian, V. A.: Lipid packing stress and polypeptide aggregation : alamethicin channel probed by proton titration of lipid charge. Faraday Discuss. **111**, 173–183 (1998).

19. Boheim, G.: Statistical analysis of alamethicin channels in black lipid membranes. J. Mem. Biol. **19**, 277–303 (1974).
20. Brown, M.F.: Modulation of rhodopsin function by properties of the membrane bilayer. Chem. Phys. Lipids **73**, 159–180 (1994).
21. Dan, N. and Safran, S.A.: Effect of Lipid Characteristics on the structure of Trans-membrane proteins. Biophys. J. **75**, 1410–1414 (1998).
22. Daune, M.: Molecular Biophysics: structures in Motion, Oxford University Press, Oxford (1999).
23. de Meyer, F. and Smit, B. Comment on "cluster formation of trans-membrane proteins due to hydrophobic mismatching". Phys. Rev. Lett. **102**, 219801 (2009).
24. Duan, Y., Wu, C., Chowdhury, S., Lee, M.C., Xiong, G., Zhang, W., Yang, R., Cieplak, P., Luo, R., Lee, T.: A point-charge force field for molecular mechanics simulations of proteins based on condensed-phase quantum mechanical calculations. J. Comput. Chem. **24**, 1999–2012 (2003).
25. Durkin, J. T., Koeppe, R.E. II and Andersen, O.S.: Energetics of gramicidin hybrid channel formation as a test for structural equivalence *1: Side-chain substitutions in the native sequence. J. Mol. Biol. **211**, 221–234 (1990).
26. Durkin, J. T., Providence, L. L., Koeppe, R.E. II and Andersen, O.S.: Energetics of heterodimer formation among gramicidin Analogues with an NH_2-terminal addition or deletion consequences of missing a residue at the join in the channel. J. Mol. Biol. **231**, 1102–1121 (1993).
27. Evans, E. A. and Hochmuth, R.M.: Curr. Top. Membr. Transp. **10**, 1 (1978).
28. Evans, E., Rawicz, W. and Hofmann, A.F.: In Bile Acids in Gastroenterology Basic and Clinical Advances, edited by A.F. Hofmann, G. Paumgartner and A. Stiehl (Dordrecht: Kluwer-Academic), p 59 (1995).
29. Finkelstein, A.: Water and nonelectrolyte permeability of lipid bilayer membranes. J. Gen. Physiol. **68**, 127–135 (1976).
30. Goulian, M., Mesquita, O.N., Fygenson, D.K., Nielsen, C., and Andersen., O.S.: Gramicidin channel kinetics under tension. Biophys. J. **74**, 328–337 (1998).
31. Greathouse, D. V., Koeppe, R.E. II, Providence, L. L., Shobana, S. and Andersen, O.S.: Design and characterization of gramicidin channels. Meth. Enzymol. **294**, 525–550 (1999).
32. Grønbech-Jensen, N., Mashl, R. J., Bruinsma, R. F., and Gelbart, W. M.: Counterion-induced attraction between rigid polyelectrolytes. Phys. Rev. Lett. **78**, 2477–2480 (1997).
33. Gruner, S. M.: In Biologically Inspired Physics, edited by L. Peliti (New York: Plenum), p 127 (1991).
34. Gruner, S. M.: Intrinsic curvature hypothesis for biomembrane lipid composition: a role for nonbilayer lipids. Proc. Natl. Acad. Sci. **82**, 3665–69 (1985).
35. Harper, P.E., Mannock, D.A., Lewis, R.N.A.H., McElhaney, R.N. and Gruner, S.M.: X-Ray diffraction structures of some phosphatidylethanolamine lamellar and inverted hexagonal phases. Biophys. J. **81**, 2693–2706 (2001).
36. He, K., Ludtke, S. J., Huang, H. W. and Worcester, D. L.: Antimicrobial peptide pores in membranes detected by neutron in-plane scattering. Biochemistry **34**, 15614–15618 (1995).
37. Helfrich, W.: Elastic properties of lipid bilayers: theory and possible experiments. Z. Naturforsch. **28C**, 693–703 (1973).
38. Helfrich, P. and Jakobsson, E.: Calculation of deformation energies and conformations in lipid membranes containing gramicidin channels. Biophys. J. **57**, 1075–1084 (1990).
39. Heyer, R. J., Muller, R. U. and Finkelstein, A.: Inactivation of monazomycin-induced voltage-dependent conductance in thin lipid membranes. I. Inactivation produced by long chain quaternary ammonium ions. J. Gen. Physiol. **67**, 703–729 (1976).
40. Huang, H. W.: Deformation free energy of bilayer membrane and its effect on gramicidin channel lifetime. Biophys. J. **50**, 1061–1071 (1986).
41. Hwang, T. C., Koeppe, R.E. II and Andersen, O.S.: Genistein can modulate channel function by a phosphorylation-independent mechanism: importance of hydrophobic mismatch and bilayer mechanics. Biochemistry **42**, 13646–58 (2003).
42. Israelachvili, J.N.: Refinement of the fluid-mosaic model of membrane structure. Biochim. Biophys. Acta **469**, 221–225 (1977).

43. Jakalian, A., Bush, B.L., Jack, D.B., Bayly, C.I.: Fast, efficient generation of high-quality atomic charges. AM1-BCC model: I. Method. J. Comput. Chem. **21**, 132–146 (2000).
44. Jakalian, A., Jack, D.B., Bayly, C.I.: Fast, efficient generation of high-quality atomic charges. AM1-BCC model: II. Parameterization and Validation. J. Comput. Chem. **23**, 1623–1641 (2002).
45. Katsaras, J., Prosser, R. S., Stinson, R. H. and Davis, J. H.: Constant helical pitch of the gramicidin channel in phospholipid bilayers. Biophys. J. **61**, 827–830 (1992).
46. Ketchem, R. R., Roux, B. and Cross, T. A.: High-resolution polypeptide structure in a lamellar phase lipid environment from solid state NMR derived orientational constraints. Structure **5**, 1655–1669 (1997).
47. Killian, J. A. and Nyholm, T. K.: Peptides in lipid bilayers: the power of simple models. Curr. Opin. Struct. Biol. **16**, 473–479 (2006).
48. Killian, J. A., Salemink, I., de Planque, M. R., Lindblom, G., Koeppe, R.E. II, Greathouse, D. V.: Induction of nonbilayer structures in diacylphosphatidylcholine model membranes by trans-membrane alpha-helical peptides: importance of hydrophobic mismatch and proposed role of tryptophans. Biochemistry **35**, 1037–1045 (1996).
49. Kirk, G. L. and Gruner, S. M.: Lyotropic effects of alkanes and headgroup composition on the l_α -H_{II} lipid liquid crystal phase transition : hydrocarbon packing versus intrinsic curvature. J. Phys. **46**, 761–769 (1985).
50. Koeppe, R.E. II, Providence, L. L., Greathouse, D. V., Heitz, F., Trudelle, Y., Purdie, N. and Andersen, O.S.: On the helix sense of gramicidin A single channel. Proteins Struct., Funct., Genet. **12**, 49–62 (1992).
51. Latorre, M. and Alvarez, O.: Voltage-dependent channels in planar lipid bilayer membranes. Physiol. Rev. **61**, 77–150 (1981).
52. Lee, M. T., Hung, W. C., Chen, F. Y. and Huang, H. W.: Many-Body Effect of Antimicrobial Peptides: On the Correlation Between Lipid's Spontaneous Curvature and Pore Formation. Biophys. J. **89**, 4006–4016 (2005).
53. Lee, M.C., Duan, Y.: Distinguish protein decoys by using a scoring function based on a new Amber force field, short molecular dynamics simulations, and the generalized Born solvent model. Proteins **55**, 620–634 (2004).
54. Lewis, B.A. and Engelman, D.M.: Lipid bilayer thickness varies linearly with acyl chain length in fluid phosphatidylcholine vesicles. J. Mol. Biol. **166**, 211–217 (1983).
55. Lundbæk, J. A., Birn, P. H. A. J., Søgaard, R., Nielsen, C., Girshman, J., Bruno, M. J., Tape, S. E., Egebjerg, J., Greathouse, D. V., Mattice, G. L., Koeppe, R.E. II and Andersen, O.S.: Regulation of sodium channel function by bilayer elasticity. The importance of hydrophobic coupling. Effects of micelle-forming amphiphiles and cholesterol. J. Gen. Physiol. **123**, 599–621 (2004).
56. Lundbæk, J. A.: Lipid Bilayer - mediated Regulation of Ion Channel Function by Amphiphilic drugs. J. of Gen. Physiol. **131**, 421–429 (2008).
57. Lundbæk, J.A. and Andersen, O.S.: Spring constants for channel-induced lipid bilayer deformations. Estimates using gramicidin channels. Biophys. J. **76**, 889–895 (1999).
58. Ly, H. V. and Longo, M. L.: The Influence of Short-Chain Alcohols on Interfacial Tension, Mechanical Properties, Area/Molecule, and Permeability of fluid Lipid Bilayers. Biophys. J. **87**, 1013–1033 (2004).
59. McLaughlin, S.: Electrostatic Potentials at Membrane-Solution Interfaces. Curr. Top. Membr. Transp. **9**, 71–98 (1977).
60. Mengistu, D. H. and May, S.: Debye-Hückel theory of mixed charged-zwitterionic lipid layers. Eur. Phys. J. E **26**, 251–260 (2008).
61. Miloshevsky, G. V. and Jordan, P. C.: Gating gramicidin channels in lipid bilayers: reaction coordinates and the mechanism of dissociation. Biophys. J. **86**, 92–104 (2004).
62. Mobashery, N., Nielsen, C. and Andersen, O.S.: The conformational preference of gramicidin channels is a function of lipid bilayer thickness. FEBS Lett. 412, 15–20 (1997).
63. Mtheitsen, O. G. and Bloom, M.: Mattress model of lipid-protein interactions in membranes. Biophys. J. **46**, 141–153 (1984).

64. Mtheitsen, O. G. and Andersen, O.S.: In Biol. Skr. Dan. Vid. (Selsk Munksgaard, Copenhagen: B) (1998).
65. Muller, R. U. and Finkelstein, A.: The Effect of Surface Charge on the Voltage-Dependent Conductance Induced in Thin Lipid Membranes by Monazomycin. J. Gen. Physiol. **60**, 285–306 (1972).
66. Nielsen, C., Goulian, M. and Andersen, O.S.: Biophys, Energetics of inclusion-induced bilayer deformations, Biophys. J. **74**, 1966–1983 (1998).
67. Nielsen, C. and Andersen, O.S.: Inclusion-induced bilayer deformations: effects of monolayer equilibrium curvature. Biophys. J. **79**, 2583–2604 (2000).
68. O'Connell, A. M., Koeppe, R.E. II and Andersen, O.S.: Kinetics of gramicidin channel formation in lipid bilayers: trans-membrane monomer association. Science 250, 1256–1259 (1990).
69. Odijk, T.: Polyelectrolytes near the rod limit. J. Plym. Sci., Polym. Phys. Ed. 15, 477–483 (1977).
70. Orbach, E. and Finkelstein, A.: The nonelectrolyte permeability of planar lipid bilayer membranes. J. Gen. Physiol. **75**, 427–436 (1980).
71. Parsegian, A.: Energy of an Ion crossing a low dielectric membrane: solutions to fthe relevant electrostatic problems. Nature **221**, 844–846 (1969).
72. Perozo, E., Cortes, D.M. and Cuello, L.G.: Structural Rearrangements Underlying K^+- Channel Activation Gating. Science 285, 73–78 (1999).
73. Perozo, E., Cortes, D. M., Sompornpisut, P., Kloda, A. and Martinac, B.: Open channel structure of MscL and the gating mechanism of mechanosensitive channels. Nature **418**, 942–948 (2002).
74. Ring, A.: Gramicidin channel-induced lipid membrane deformation energy: influence of chain length and boundary conditions. Biochim. Biophys. Acta **1278**, 147–159 (1996).
75. Rostovtseva, T. K., Aguilella, V. M., Vodayanoy, I., Bezrukov, S. M. and Parsegian, A.: Membrane surface-charge titration probed by gramicidin A channel conductance. Biophys. J. **75**, 1783–1792 (1998).
76. Sackmann, E.: In Biological Membranes. Chapman, D. (ed.) (London: Academic), p 105 (1984).
77. Santore, M. M., Discher, D. E., Won, Y-Y., Bates, F. S. and Hammer, D. A.: Effect of Surfactant on Unilamellar Polymeric Vesicles: Altered Membrane Properties and Stability in the Limit of Weak Surfactant Partitioning. Langmuir **18**, 7299–7308 (2002).
78. Sawyer, D. B., Koeppe, R.E. II and Andersen, O.S.: Induction of conductance heterogeneity in gramicidin channels. Biochemistry **28**, 6571–6583 (1989).
79. Schatzberg, P. J.: Polymer Sci. Part C 10, 87–92 (1965).
80. Seddon, J. M.: Structure of the inverted hexagonal (H_{II}) phase, and non-lamellar phase transitions of lipids. Biochim. Biophys. Acta **1031**, 1–69 (1990).
81. Simon, S.A., McIntosh, T.J. and Latorre, R.: Influence of cholesterol on water permeation into bilayers. Science **216**, 65–67 (1982).
82. Singer, S.J. and Nicolson, G.L.: The fluid mosaic model of the structure of cell membranes. Science **175**, 720–731 (1972).
83. Szabo, G., Eisenman, G. and Ciani, S.: The effects of the macrotetralide actin antibiotics on the electrical properties of phospholipid bilayer membranes. J. Membr. Biol. 1, **346** (1969).
84. Tate, M. W., Eikenberry, E. F., Turner, D. C., Shyamsunder, E. and Gruner, S. M.: Nonbilayer phases of membrane lipids. Chem. Phys. Lipids **57**, 147–164 (1991).
85. Teh, C.K., Tuszynski, J. and Weisman, F.L.: The decay of carbon luminescence in liquid-encapsulated czochralski-grown semi-insulating GaAs. J. Mater. Res. **5**, 365–371 (1990).
86. Townsley, L. E., Tucker, W. A., Sham, S. and Hinton, J. F.: Structures of gramicidins A, B, and C incorporated into sodium dodecyl sulfate micelles. Biochemistry **40**, 11676–11686 (2001).
87. Toyoshima, C. and Mizutani, T.: Crystal structure of the calcium pump with a bound ATP analogue. Nature **430**, 529–535 (2004).
88. Unwin, P.N.T. and Ennis, P. D.: Two configurations of a channel-forming membrane protein. Nature **307**, 609–613 (1984).
89. Wallace, B. A., Veatch, W. R. and Blout, E. R.: Conformation of gramicidin A in phospholipid vesicles: circular dichroism studies of effects of ion binding, chemical modification, and lipid structure. Biochemistry **20**, 5754–5760 (1981).

90. Walter, A. and Gutknecht, J.: Monocarboxylic acid permeation through lipid bilayer membranes. J. Membrane Biol. **77**, 255–264 (1984).
91. Woolf, T.B. and Roux, B.: Molecular dynamics simulation of the gramicidin channel in a phospholipid bilayer. Proc. Natl. Acad. Sci. USA **91**, 11631–11635 (1994).
92. Wu, Y., He, K., Ludtke, S. J. and Huang, H. W.: X-ray diffraction study of lipid bilayer membranes interacting with amphiphilic helical peptides: diphytanoyl phosphatidylcholine with alamethicin at low concentrations. Biophys. J. **68**, 2361–2369 (1995).
93. Zhou, Y. and Raphael, R. M.: Effect of Salicylate on the Elasticity, Bending Stiffness, and Strength of SOPC Membranes. Biophys. J. **89**, 1789–1801 (2005).

Chapter 6
Membrane-Based Nanotechnology and Drug Delivery

6.1 Introduction

Can we track life's molecular processes within a living cell? Observing all its organelles, biomolecules, and even individual chemical species in the cellular environment is rapidly becoming possible in real time and with ever-increasing spatial resolution. This will help us to better understand the numerous mechanisms which allow life to emerge and to continue within the organism so that it behaves like a coherent whole. Moreover, environmental assaults, pathological changes, or any manifestations of biological disorder inside cells require sometimes prompt and at other times slow repair processes for life to endure and continue. Over the past several centuries, pharmacology has developed medicinal means to enable and assist patients to recover from both specific and non-specific diseases and health problems. Most of these medicines are destined to eventually find their way inside the cellular environment, where needed, to exert their action. A rather new area of technology in the service of pharmacology is called 'targeted drug delivery', and it is dedicated to improvement in the delivery of certain drugs to their target organs. Pharmaceutical companies and research laboratories in academia have been investing in this sector heavily, due to its early promise. Encouraging advances in specific areas, especially in regard to the outer cellular regions, have been made, but no considerable progress has so far been seen regarding the issue of drug delivery into specific sections or targets in a cellular interior environment. Most of the infectious and chronic diseases have origins inside cells, especially due to aberrations in nucleic acids, mitochondria, and other organelles. It is generally recognized that cancer, Alzheimer's disease, and a host of chronic diseases of the old age are largely incurable diseases causing a heavy burden on the health systems of individual countries. Unfortunately, enormous investment in medical research into these diseases has so far been producing surprisingly minimal tangible results. Paradoxically, while there are many therapeutic agents which can cure many specific diseases, this is only possible if those agents can be delivered to the correct organ, avoiding non-specific delivery to other organs in the vicinity or elsewhere in the body. Lack of proper targeting commonly results in the failure of such drugs in clinical trials, due to the adverse side effects they produce.

M. Ashrafuzzaman and J. Tuszynski, *Membrane Biophysics*,
Biological and Medical Physics, Biomedical Engineering,
DOI: 10.1007/978-3-642-16105-6_6,

Avoiding delivery of drugs, which are mainly natural or synthetic biomolecules, peptides, proteins, etc., to unwanted regions and ensuring their delivery to right target organs is expected to soon be made using nanoparticles, provided the technology required for this task becomes sufficiently developed under the right scientific conditions. In combination with other secondary therapeutic agents, nanoparticles can find the correct pathways and carry drugs and other agents attached to the nanoparticles to the targets of interest. Major progress has been recently made in the use of nanoparticles/nanomaterials in biology and medicine. The interested reader can acquire substantial knowledge on the use of nanoparticles in specific areas for distinct purposes by consulting the various published papers in the field, e.g.,

- Drug and gene delivery [13, 20]
- Fluorescent labels [3, 4, 25]
- Tissue engineering [5, 12]
- Hyperthermia of tumor [27]
- Radionuclide tumoral therapy [7]
- Biological molecules and cells separation and purification [18]
- MRI contrast enhancement [26]
- Phagokinetic studies [21]
- Biodetection of pathogens [6]
- Protein detection [19]
- DNA structure probes [14]

The above papers address the use of nanomaterials, not only for multiple purposes such as imaging, therapeutic, engineering and technological, etc., but also aimed at targeting multiple anatomical organs or their internal sections inside and outside cellular environments. The most important problem to date is to find an appropriate or near-perfect technique to deliver drugs into the cellular interior. Despite the development of advanced technology related to this subject, a very general non-toxic way is yet to be discovered. In this chapter, we provide some details about both scientific and technological aspects of nanoparticle drug delivery into the cellular interiors, using both existing ideas and some novel concepts. We address this problem using both analytical and technological analogies applied to a specific compartment, which is the cell membrane, to make the problem much simpler and understandable. We use some supporting experimental results on drug pathways depending on the properties of cell membranes, which determine the partition coefficients involved.

6.2 The Membrane's Selective Transport and General Barrier Properties

As discussed in earlier chapters of this book, a cell membrane's primary role is to serve as a barrier against the solutes trying to diffuse across it. With the physical presence of a membrane, the cytoplasm maintains a different composition from the materials surrounding the cell. The membrane is very impermeable to ions and

charged molecules. It is permeable to small molecules in the cell environment in inverse proportion to their size, but in direct proportion to their lipid solubility. The membrane also contains various pumps and ion channels made of specific membrane proteins that allow concentration gradients to be maintained between the inside and outside of the cell. For example, the cation pump actively extrudes sodium ions (Na^+) from the cytoplasm and builds up a concentration of potassium ions (K^+) within it. The major anions inside the cell are chlorine ions (Cl^-) and negatively charged protein molecules, the latter of which cannot penetrate the membrane. The presence of the charged protein molecules leads to a build-up of electro-osmotic potential across the membrane, which has an important regulatory role to play. Action potentials, resulting from the transient opening of sodium (Na^+) or calcium ion (Ca^{2+}) channels, depolarize the membrane, followed by an opening of K^+ channels leading to repolarization. All these chemical and physical properties control the natural transport through membranes. Although ions (Na^+, K^+, Cl^-, Ca^{2+}, etc.) are able to use cellular mechanisms to cross through the membrane, foreign objects like nanoparticles with unique physical properties find no direct way to cross through the membrane, which is about 3 nm thick. The lipid cross-sectional area in a monolayer of a membrane is of the order of $0.6\,nm^2$ [8]. Nanoparticles are supposed to be of the order of a few nm in spatial dimension. The membrane is a liquid crystalline structure, where the lipids experience continuous lateral movement in the plane of the membrane monolayer. However, the lipid–lipid separation is always maintained at about 0.8 nm [8] unless any membrane disorder occurs due to the effects of internal agents (for example, membrane proteins) or external agents (for example, drugs, antimicrobial peptides, etc.). Despite the possibility of very slow diffusion of the nanoparticles into the cellular interior due to the potentially high concentration of nanoparticles on the membrane surface, a satisfactory level of nanoparticle transport cannot always be ensured. For this to occur we need to discover a controlled transport mechanism or a unique 'nanotechnology process' which must involve the consideration of the physical and chemical properties of both the membrane, which needs to be crossed, and the nanoparticles that need to be delivered. Due to the cell membrane's natural barrier against most of the agents except a very few ions residing in the cellular environment, an entirely novel nanotechnology is required, which would involve a few membrane-active agents. These agents may instantaneously destroy the membrane's barrier properties in a controlled manner and allow the nanoparticles to cross through the membrane. By compromising the membrane's barrier properties, the membrane's transport properties may be modulated.

6.3 The Membrane as a Transporter of Nanoparticles: A Nanoparticle–Membrane Interaction Perspective

Transmembrane flow mainly depends on two external agents. First, the difference in hydrostatic pressure between the two fluid compartments on either side of the membrane is a key flow regulator. This pressure gradient is physiological, and it

exerts natural effects on all particle flow across the membrane. The second agent is the gradient of solute concentration between the two compartments separated by a membrane. The physiological pressure gradient is organ-specific, and the transport of particles naturally needs to deal with this second agent, playing the role of an input condition in the case of nanoparticle transport across the membrane. With an appropriate technique, we can control the number density of nanoparticles just outside the membrane (extracellular regions) and consider that, in the beginning, the number density of nanoparticles beyond the membrane (intracellular regions) is zero. Besides these two agents, there is a very important mechanism that should be considered. This mechanism determines the free energy of nanoparticles while crossing the membrane. This section is mainly dedicated to a better understanding of the physical phenomena involved in the membrane transport of nanoparticles. This involves the energetics of nanoparticles inside the membrane, and based on this understanding we wish to develop novel nanotechnology able to deliver nanoparticles beyond membranes.

Understanding the membrane transport of nanoparticles requires specific information about the geometry and constituents of the membrane, which determine the partition either against or in favor of transport of any particles across the membrane. The membrane's partition coefficient (K_m) and the particles' experimentally measurable free energy of interaction with the membrane (ΔG_m) are related through the following equation:

$$\Delta G_m = -RT \ln(K_m) \tag{6.1}$$

Here R is the universal gas constant (8.31 J/K) and T is the absolute temperature.

It is very important to note that the values of K_m play a key role in determining the membrane permeability (P_m) for any drug transport across membranes. A linear relation is generally assumed between P_m and K_m [23], which follows from:

$$P_m = \frac{D_m K_m}{L} \tag{6.2}$$

where D_m is the membrane diffusion coefficient of the particles involved, and L is the bilayer membrane thickness. The membrane permeability coefficient of particles (P) or drugs is equal to the linear velocity (nm/s) of the drugs through the membrane. This is, in fact, the rate of particle transport through the membrane. Derivation of P requires a very accurate consideration of all components of D_m and K_m. We can instead consider the fractional release of the particles by the membrane into the cellular interior, considering that the number density of particles ($\rho_{\mathrm{np,ext}}$) at the entry level into the membrane (just outside the membrane) is known. Let us assume that the number density of particles at the release level beyond the membrane (just inside the cell) is $\rho_{\mathrm{np,int}}$. We can then propose an analytical relation between these two number densities following the equation

$$\rho_{\mathrm{np,int}} = f(L, H, \epsilon_m, \rho_{\mathrm{np,ext}}) \tag{6.3}$$

where $f(L, H, \varepsilon_m, \rho_{\text{np,ext}})$ denotes a function of L, H, ϵ_m, and $\rho_{\text{np,ext}}$. Here, H is the average Hamiltonian of any nanoparticle inside the membrane and ϵ_m is the relative dielectric constant characteristic of the membrane. The most important component contributing to H can be expressed as follows:

$$H = U_{\text{np}-\text{lip}} + T_{\text{np}} \tag{6.4}$$

Here, $U_{\text{np}-\text{lip}}$ stands for the sum of all interaction potentials felt by a nanoparticle and T_{np} stands for the nanoparticle's kinetic energy while inside the membrane. For experimental purposes, synthetic lipids (for example from Avanti Polar, 700 Industrial Park Drive, Alabaster, Alabama 35007-9105) are used in model membrane systems. If we use no other membrane proteins but the lipids and membrane-stabilizing hydrocarbons to form a membrane (e.g., see [1, 2]), we can consider the expression of $U_{\text{np-lip}}$ to follow the relation

$$U_{\text{np-lip}} = U_{\text{ES}} + U_{\text{vdW}} + U_{\text{mechanical}} + U_{\text{hydration}} \tag{6.5}$$

where U_{ES} is the total electrostatic interaction (ES) energy and U_{vdW} is the sum of the van der Waals (vdW) interaction energies of the nanoparticle with lipids in the pathways of the nanoparticle. $U_{\text{mechanical}}$ is the energy arising from the mechanical properties, namely the membrane elasticity and membrane monolayer curvature. $U_{\text{hydration}}$ is the contribution due to the hydration energy. For the sake of simplicity, we have ignored the energy contributions due to the interactions with hydrocarbons and any other possible sources.

Previous chapters have discussed how the various energy contributions can be derived if the structural and charge properties of the participating components are known. Since this chapter is dedicated to a better understanding needed to develop new technology which will help to deliver nanoparticles into the cell's interior regions, here we focus more on developing engineering insights and less on the understanding of scientific analogies. To understand the general particle diffusion across membranes, the interested reader can consult many excellent articles or books (e.g. [24]). In this chapter, we aim to develop an understanding of how nanoparticles interact with membranes, which is a key to the engineering of nanotechnology tools needed to deal with controlled nanoparticle transport across the membrane.

6.3.1 Certain Nanoparticles Disrupt Membranes

Instantaneous disruption of membrane's barrier properties may raise the possibility for various agents to reach inside the cellular interior regions. Nanoparticles that are designed to deliver drugs beyond the membrane may interact with the membrane itself and create holes or defects there. The meaning of the term 'hole' or 'pore' with respect to a living cell membrane used here is consistent with that described in Chap. 4. The complete loss of a region of the plasma membrane where the lipids are

removed can be referred to using the word hole or pore. In Chap. 4 we have discussed the various antimicrobial peptide-induced membrane transport events, such as ion flowing channels, pores, defects, etc. For details of experimental observations of such events in supported lipid bilayers (SLBs) induced by nonpeptides the reader may consult various publications such as [15–17], etc. The above-mentioned complete loss of lipids is usually a transient phenomenon. Due to the liquid crystalline nature of the lipid membrane and the presence of strong statistical-mechanical effects on membrane dynamics, the nearby lipids fill in the gap quickly. In this section we address the issue of the possible nanoparticle disruption of the membrane, using a few reference studies.

6.3.2 Membrane Disruption Depends on Size and Structure of Nanoparticles

In a recent study [11] polycationic organic nanoparticles were found to disrupt model biological membranes and living cell membranes. Few nanoscale (∼3, 5 and 7 nm) polymeric scaffolds called polyamidoamine (PAMAM) dendrimers were studied for their effects on membranes. The degree of membrane disruption is shown to be related to nanoparticle size and charge, as well as to the lipid phase states (such as fluid, liquid crystalline, or gel) of the biological membrane (see Chap. 3).

Disruption events in model membranes have been directly imaged using scanning probe microscopy, whereas disruption events in living cells have been analyzed using cytosolic enzyme leakage assays, dye diffusion assays, and fluorescence microscopy as described in the above-mentioned study [11]. The results presented here (Fig. 6.1) suggest that a 20 nm diameter hole is created in the supported lipid bilayer (SLB) by the G7 dendrimer. The relatively smaller G5 dendrimer does not create a hole, but can still participate in the expansion of the existing nanosize holes and defects in the bilayer. Here, the main message is that larger size dendrimers can possibly create larger holes or cause greater membrane disruption. A set of polycationic organic polymers such as poly-L-lysine (PLL), polyethyleneimine (PEI), and dielthylaminoethyl-dextran (DEAE-dextran) and neutral polymers such as polyethylene glycol (PEG) and polyvinyl alcohol (PVA) were also investigated for their membrane disruption in the same studies [11]. As presented in Fig. 6.2 (panel I), we observe that the polycationic polymers exhibit substantial membrane disruption behavior, including nanoscale hole formation. However, the neutral polymers PEG and PVA are not found to induce membrane disruption. More studies, though, are needed to understand the role of size and charge density of these membrane-disrupting polymers in their induction of nanosize holes in the membranes. LDH leakage results from both figures (see Figs. 6.1 and 6.2) are consistent with the observed effects.

Identical results of polycationic polymer effects on bilayer disruption were also reported in an earlier publication [16]. Holes with 15–40 nm diameters were observed here to be induced due to polymers, and the hole size was found to be largely reduced

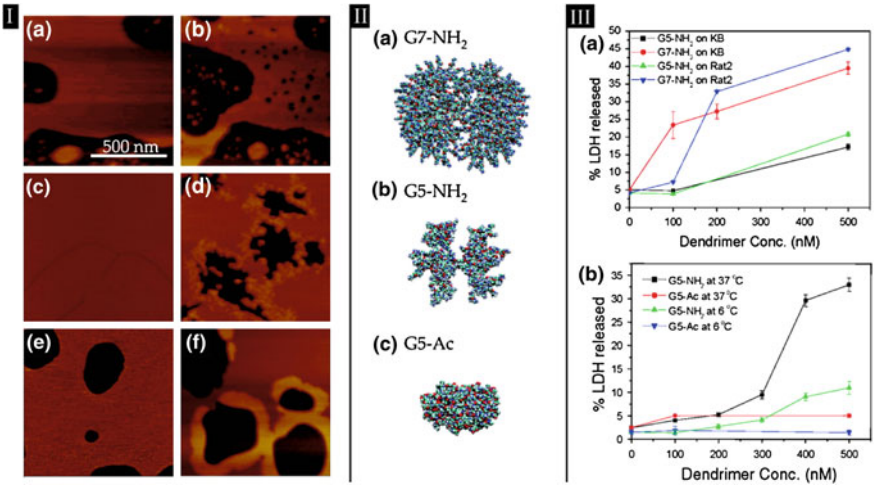

Fig. 6.1 In this figure the dendrimer interactions with biological membranes have been analyzed. In panel I, the atomic force microscopy (AFM) observation of dimyristoylphosphatidylcholine (DMPC)-supported lipid bilayers (a,c,e) before and after incubation with **b** G7-NH_2, **d** G5-NH_2, and **f** G5-Ac PAMAM dendrimers have been presented. Panel II: Space-filling models of chemical structures of **a** G7-NH_2, **b** G5-NH_2, and **c** G5-Ac PAMAM dendrimers have been presented. Panel III presents: lactate dehydrogenase (LDH) leakage as a result of cell exposure to PAMAM dendrimers, showing **a** size effect of G7-NH_2 and G5-NH_2 on the LDH leakage out of KB and Rat2 cells after incubation at 37 °C for 3 h and **b** surface group dependence on the LDH leakage at different temperatures. Note that larger (~8.2 nm) dendrimers (G7-NH_2) induce formation of new nanoscale holes in the bilayers as seen in the AFM images and cause a greater amount of LDH leakage out of live cells than relatively smaller G5-NH_2. G5-NH_2 dendrimers do not cause new hole formation in the lipid bilayers, but instead expand pre-existing defects. In contrast, G5-Ac dendrimers do not cause hole formation, expansion of pre-existing defects, or LDH leakage out of live cells. This figure with description has been taken with the publisher's permission from [11]

as the polymer size becomes smaller. No hole was found to be created by a very small dendrimer (e.g. G3-amine). Acetamide-terminated G5 dendrimers were also not found to be creating any holes.

The experimental observations mentioned above and elsewhere indicate the existence of clear size- and structure-specific effects of polycationic polymers in the nanoscale membrane disruption mechanism. In all instances, the edges of bilayer defects proved to be points of highest dendrimer activity. A proposed mechanism for the removal of lipids by dendrimers involves the formation of transient, nanoscale dendrimer-filled lipid vesicles, as shown in Fig. 6.3. By considering the thermodynamics, interaction free energy, and geometry of these self-assembled vesicles, a model that explains the influence of polymer particle size and surface chemistry on the interactions with lipid membranes was developed.

Considering interactions between lipid molecules in the vesicles and between lipid molecules and the specific dendrimer inside the vesicle, one can explain the energetics of the dendrimer-induced pore formation in the lipid bilayer.

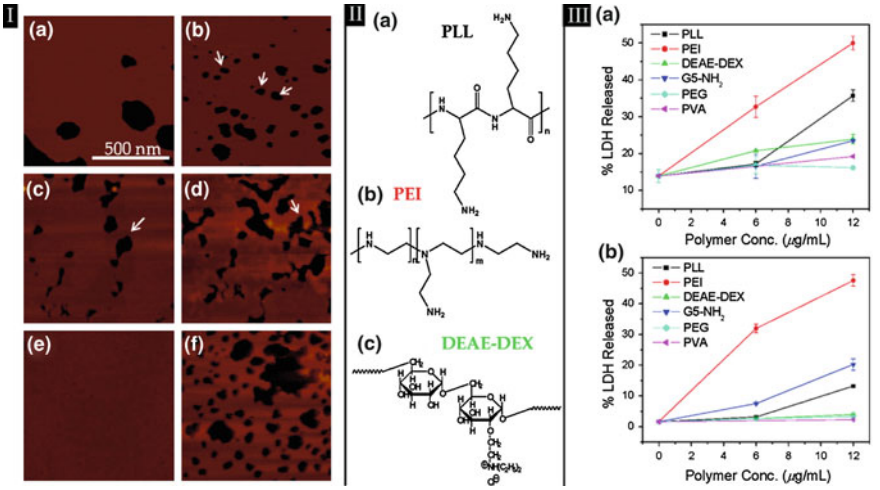

Fig. 6.2 Polymeric nanoparticle interactions with biological membranes are presented here. In panel I: AFM observation of DMPC-supported lipid bilayers (a,c,e) before and after incubation with **b** PLL, **d** PEI, and **f** DEAE-DEX, respectively, are presented. Panel II shows the chemical structures of **a** PLL, **b** PEI, and **c** DEAE-DEX. Panel III shows the LDH leakage out of **a** KB and **b** Rat2 cells as a result of exposure to the various polymeric nanoparticles at 37 °C for 3 h. Polycationic polymers are observed here to induce the enzyme leakage whereas charge neutral polymers such as PEG and PVA behave neutrally. This figure with description has been taken with the publisher's permission from [11]

The geometry of vesicles can be predicted by considering the free energy associated with the molecular interaction coupled with geometric constraints imparted by the choice of lipid. Although entropy favors structures with small aggregation numbers, packing constrains of the double-chained lipids energetically resist the formation of arbitrarily small structures below a critical radius RC [9, 10]. In these references, Israelachvili et al. proposed to combine thermodynamic and geometric principles to derive physical properties of self-assembled lipid vesicles such as their size distribution. They used the "opposing forces" model to describe the interaction between the lipid molecules, each occupying a surface area at the hydrocarbon–water interface of a lipid layer. In this theoretical approach, properties including vesicle size distributions and bilayer elasticity emerge from a unified theory that links thermodynamics, interaction free energy, and molecular geometry. Using an analogous but slightly modified protocol, Mecke's group [17] have proposed that the inclusion of a dendrimer into the vesicle (see Fig. 6.4) causes a change in the surface free energy of lipid molecules per unit area which is given by the following equation

$$\Delta\gamma = \frac{M\phi}{4\pi r^2} \tag{6.6}$$

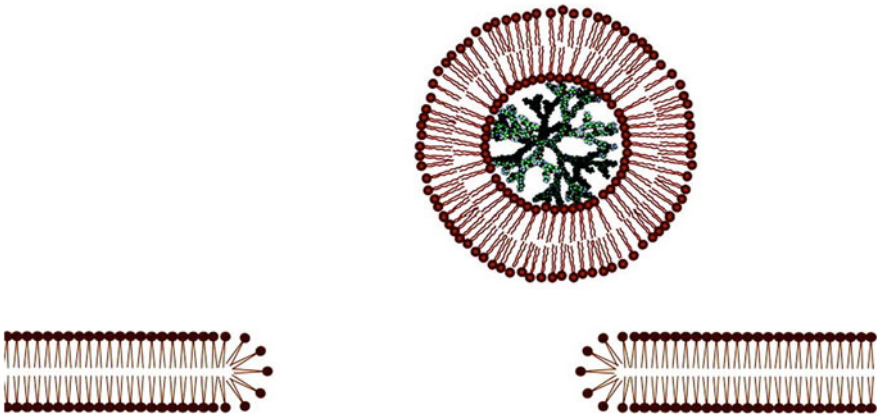

Fig. 6.3 Proposed dendrimer-lipid vesicles (*upper panel*). Breaking of the membrane is schematized in the bottom panel. This figure with its description has been taken with the publisher's permission from [17]

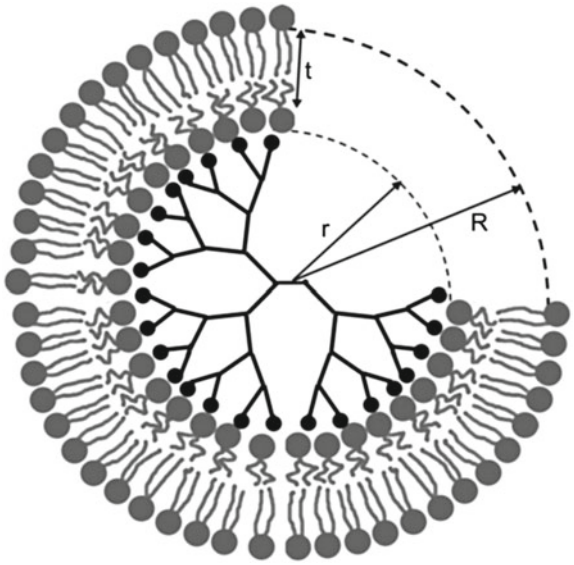

Fig. 6.4 Schematic cross-section of the proposed dendrimer-lipid vesicle. The number of dendrimer end-groups (*black circles*) $= M$. The number of lipid head groups in contact with the dendrimer surface (inner ring of *gray circles*) $= m$. This figure with its description has been taken with the publisher's permission from [17]

Here, ϕ is considered to be the energy per bond present in the interaction picture (see Fig. 6.4) which falls in the range of 12–30 kJ/mol for a typical hydrogen bond. r and R are dendrimer's inner and outer radius respectively. This free energy (Eq. 6.6) includes some key aspects of membrane energetics, but is seriously deficient in considering a few other important contributions, as explained in Chap. 5. Considering the identical interaction mechanisms in the membrane as discussed in Chap. 5, which consider the mechanical (membrane elastic and lipid cur-

vature) as well as electrostatic (screened Coulomb and van der Waal's interactions) between lipid–lipid and lipid-membrane agents (e.g. dendrimer, as is the case in Fig. 6.4), the value of $\Delta\gamma$ needs to be reassessed. The interested reader is encouraged to solve this rather simple problem as an advanced-level exercise, following the theoretical and computational protocols explained in Chap. 5 in the case of the lipid bilayer-ion channel interactions using screened Coulomb interactions.

Membrane Disruption Depends on Lipid Phase Properties

Chapter 3 has provided details regarding various lipid phases. These lipid phases, corresponding to various lipid organizations, vary greatly between inter- and intrastates in both the bilayer and nonbilayer lipid phases. Nanoparticles' membrane disruption mechanisms have been found not only to depend on nanoparticle properties such as size, charge, etc., but also on the lipid phase properties. In Fig. 6.5 it is shown that the liquid-crystalline phase of the bilayer favors nanoparticles to induce holes into the bilayer. The L-β phase appeared not be a favorable condition for the nanoparticles' membrane effects. This rather important result should be considered seriously in developing new nanotechnology where the membrane's physical properties need to be considered.

6.3.3 Certain Nanoparticles Avoid Membrane Interactions

The previous section (Sect. 6.3.2) introduced the phenomena of nanoparticle interactions with lipid bilayers. There we have found that certain nanoparticles integrate themselves with lipids under special conditions and, as a result, holes or pores are created in the membrane. In this section, we investigate a different type of interactions of a certain class of nanoparticles, which are silica nanoparticles ranging from 1 to 200 nm in diameter with supported lipid bilayer membranes prepared from DMPC. These nanoparticles, in fact, exhibit a general lack of interactions with membranes, but their specific properties strongly depend on the rank of the geometric mismatch between bilayer thickness and nanoparticle dimensions.

The model diagrams presented in Fig. 6.6 describe various possible effects of nanoparticles on the membrane integrity, depending on the size of the nanoparticles. In all cases, nanoparticles are assumed to avoid interactions with lipids but, as the nanoparticle dimension increases from very small to much larger than the bilayer thickness, both bilayer deformation and pore formation are found to occur. The nonspherical nature of nanoparticle dimensions can also induce pore formation. All these schematic diagrams are drawn based on specific experimental observations.

Figures 6.7, 6.8, and 6.9 provide AFM data which suggest that the model presented here in Fig. 6.6 showing membrane effects exerted by the nanoparticles with varied mismatch between the nanoparticle diameter and membrane thickness is valid. These results clearly indicate that the nanoparticles avoid binding with lipids and try

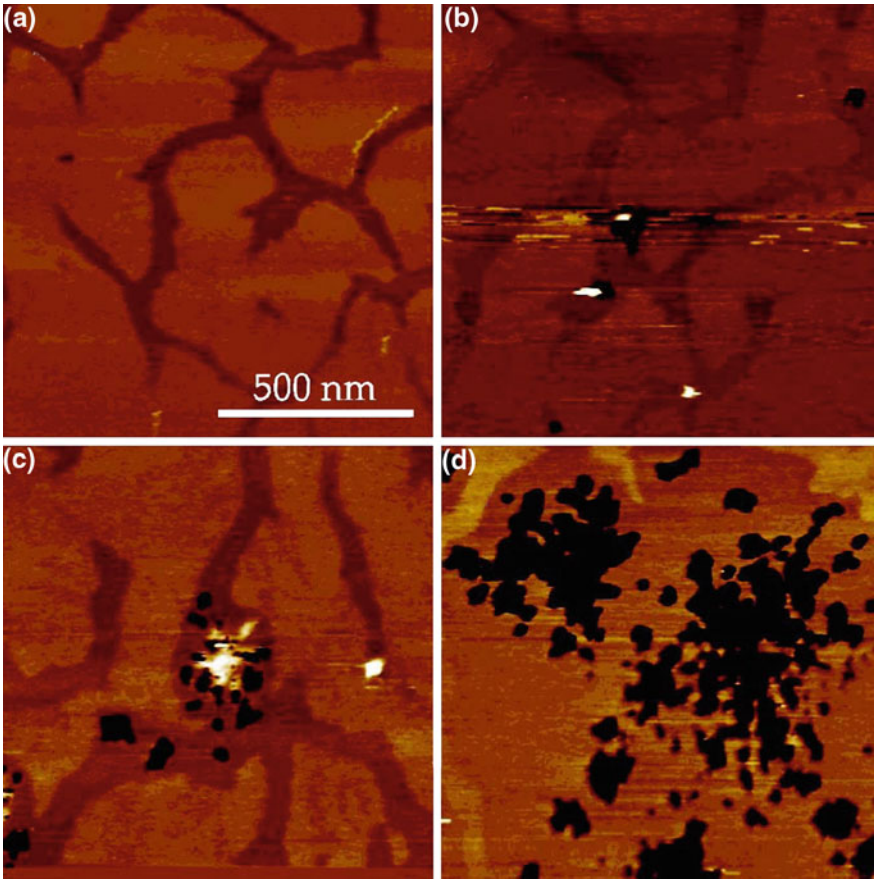

Fig. 6.5 Interaction of G7-NH_2 with a supported DMPC bilayer consisting of both gel (L-β phase, *lighter shade*) and liquid-crystalline phase (L-α phase, *darker shade*). The $G7$-NH_2 preferentially forms holes in the liquid-crystalline phase of the bilayer. This figure with its description has been taken with the publisher's permission from [11]

to remove lipids from the hydrophobic regions of their physical presence. As a result, heavy restrictions on the lipid curvature profile and bilayer geometry are observed near the nanoparticle bilayer contact regions. Unlike previously mentioned dendrimers or other polymer nanoparticles (Sect. 6.3.2) silica nanoparticles evidently do not bind with lipids but still induce holes or pores by repelling them. Under special conditions (see Fig. 6.8) drugs attached to the nanoparticles may be released through the induced pores. However, this process may result in huge cytotoxicity effects. In the next section, we demonstrate how the phenomenon of membrane repulsion/noninteraction of nanoparticles may help nanoparticle delivery of drugs into the cellular interior with apparently no nanoparticle-induced cytotoxicity.

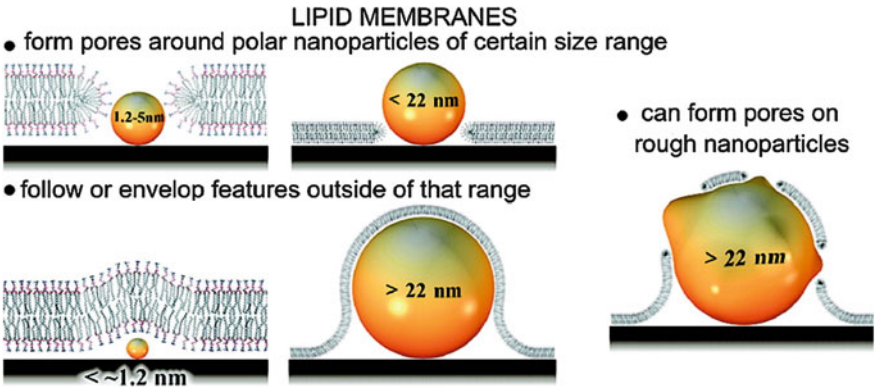

Fig. 6.6 An experimentally found nanoscale range of surface feature curvatures where lipid membranes lose integrity and form pores. For direct experimental results see other figures presented below. The pores were experimentally observed in the l-α-dimyristoyl phosphatidylcholine membrane around 1.2–22 nm polar nanoparticles deposited on mica surface. Lipid bilayer envelops or closely follows surface features with the curvatures outside that region. This finding provides essential information for the understanding of nanoparticle-lipid membrane interactions, cytotoxicity, preparation of bio molecular templates, and supported lipid membranes on rough and patterned surfaces. This figure with its description has been taken with the publisher's permission from [22]

6.4 Novel Nanotechnology: Membrane Transport of Nanoparticles Through Ion Pores/Channels

Nanoparticles which interact with a lipid membrane as well as forming nanoparticle-lipid complexes (as explained in an earlier section) may also find themselves to be trapped right inside the hydrophobic core of the membrane. This trapping of nanoparticles inside the membrane's hydrophobic core may lead to superior cytotoxic effects. We have also learned that larger dimensions in dendrimers and other polymer nanoparticles may help to induce holes or pores inside membranes. However, delivery of larger size nanoparticles near the cell environment is challenging, since the blood vessels which carry nanoparticles can have extremely narrow diameters reaching low nm dimension. This raises the risk of some nanoparticles being trapped inside the blood vessels even before experiencing release in the vicinity of the cell. Therefore, off-target cytotoxicity due to nanoparticles becomes inevitable. Also, the generation of large holes inside a membrane due to the use of sizeable nanoparticles may permanently destroy the barrier characteristics of membranes. As a result, cellular processes may suffer non-repairable damage. Consequently, the freedom of choice in using nanoparticles with various dimensions for drug delivery is therefore yet to be achieved. With the help of a combination therapy we wish to propose here a novel application of nanotechnology. This technology will involve the use of an external agent that modulates specific bilayer properties. Agents that induce ion-flowing pores inside membranes may appear as useful drug combinations. If a section of the hydrophobic membrane boundary can be removed for a short period of

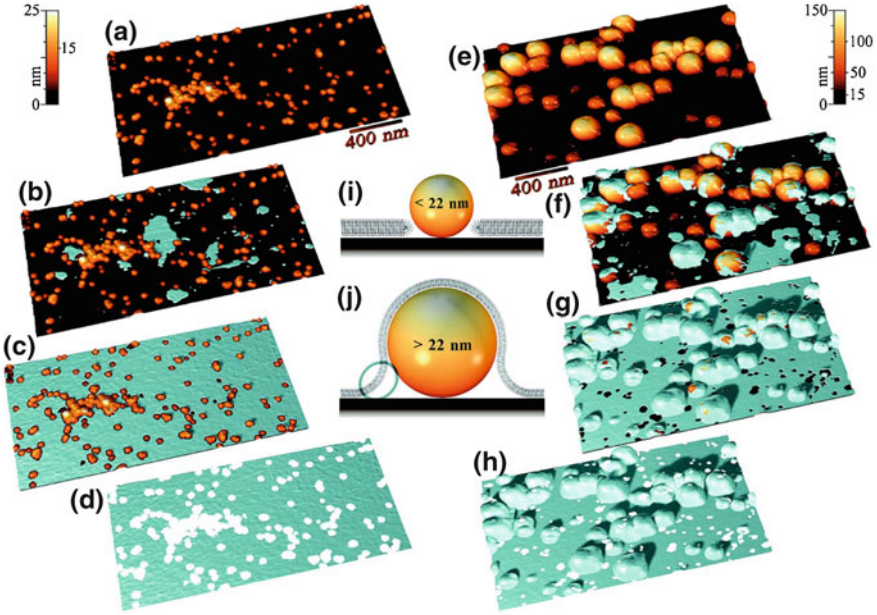

Fig. 6.7 Lipid bilayer formation in the presence of particles larger than the lipid bilayer thickness. AFM images (*left*) of lipid bilayer formation over a surface with 5–20 nm silica nanoparticles (a–d): **a** substrate with particles and no lipid, **b** a surface partially covered by lipid bilayer (shown in *silver color*), **c** a lipid bilayer formed on the substrate, **d** an image of the lipid bilayer after "subtraction" of the particles and the substrate. AFM images (*right*) of lipid bilayer formation over the surface with mixed 5–140 nm silica particles (e–h): **e** the substrate with particles and no lipid, **f** partial coverage of the surface by a lipid bilayer, **g** a lipid bilayer formed on the substrate, and **h** an image of the lipid bilayer after "subtraction" of the particles and the substrate. Schematics in the center illustrate how the lipid bilayer forms a pore around particles smaller than 22 nm (**i**) and how it may envelop the larger particles (**j**). The structure of the bilayer area encircled in **j** is speculative because it cannot be resolved or assumed from AFM experiments. This figure with its description has been taken with the publisher's permission from [22]

time, the nanoparticles may use that time-dependent opening to travel to the cellular interior. Based on this hypothesis we aim to develop a novel nanotechnology-based drug delivery method. A detailed explanation is presented below.

6.4.1 Membrane Transport of Nanoparticles Through Lipid-Lined Ion Pores

Chemotherapy drugs are found to induce lipid-lined toroidal pores in lipid membranes. A model diagram has been presented in Chap. 4. Many other antimicrobial peptides such as magainin, melittin, colicin, etc., also induce toroidal pores (see

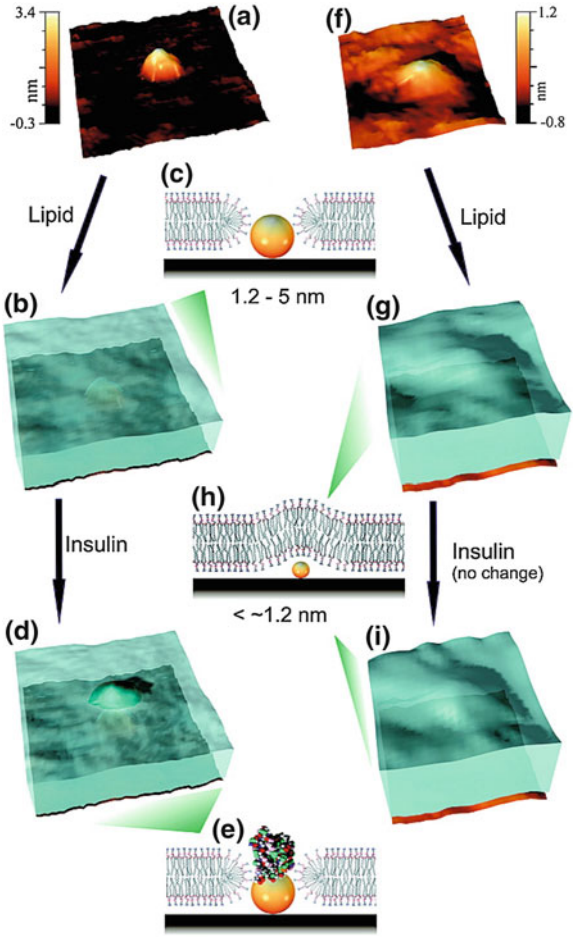

Fig. 6.8 Lipid bilayer formation in the presence of particles smaller than the lipid bilayer thickness. **a** An AFM image of the sample in the initial stage (no lipid) with a 3.4 nm diameter particle, **b** a lipid bilayer formed on the substrate with a 3.4 nm diameter particle with corresponding schematics in **c**, **d** AFM topography after adsorption of an insulin molecule onto the particle through the hole in SLB (schematic is in **e**), **f** an AFM image of the substrate with a 1.2 nm diameter particle (no lipid), **g** topography of the formed lipid bilayer over a 1.2 nm diameter particle (schematics is in **h**), and **i** image after the injection of insulin (no changes in topography). This figure with its description has been taken with the publisher's permission from [22]

the references quoted in Chap. 4). Chemotherapy drug-induced toroidal pores show some unique characteristics. The first ever observed triangular conductance events (explained in detail in Chaps. 4 and 5) are very important ingredients for the development of novel nanotechnology applications (see Fig. 6.10). The independent triangular conductance events suggest that the conductance in a single event is not constant, but increases/decreases spontaneously over the time interval comparable to the low millisecond (ms) order 'lifetime' of any specific conductance event. The amplitudes of these events are also different. We observed random spontaneous transitions between different current levels within a discrete conductance event during its lifetime. These discrete events were found to be approximately characterized by conductance values of ~0.01–0.1 pA/mV and lifetimes in the range ~5–30 ms. A spontaneous transition or a time-dependent current fluctuation between random

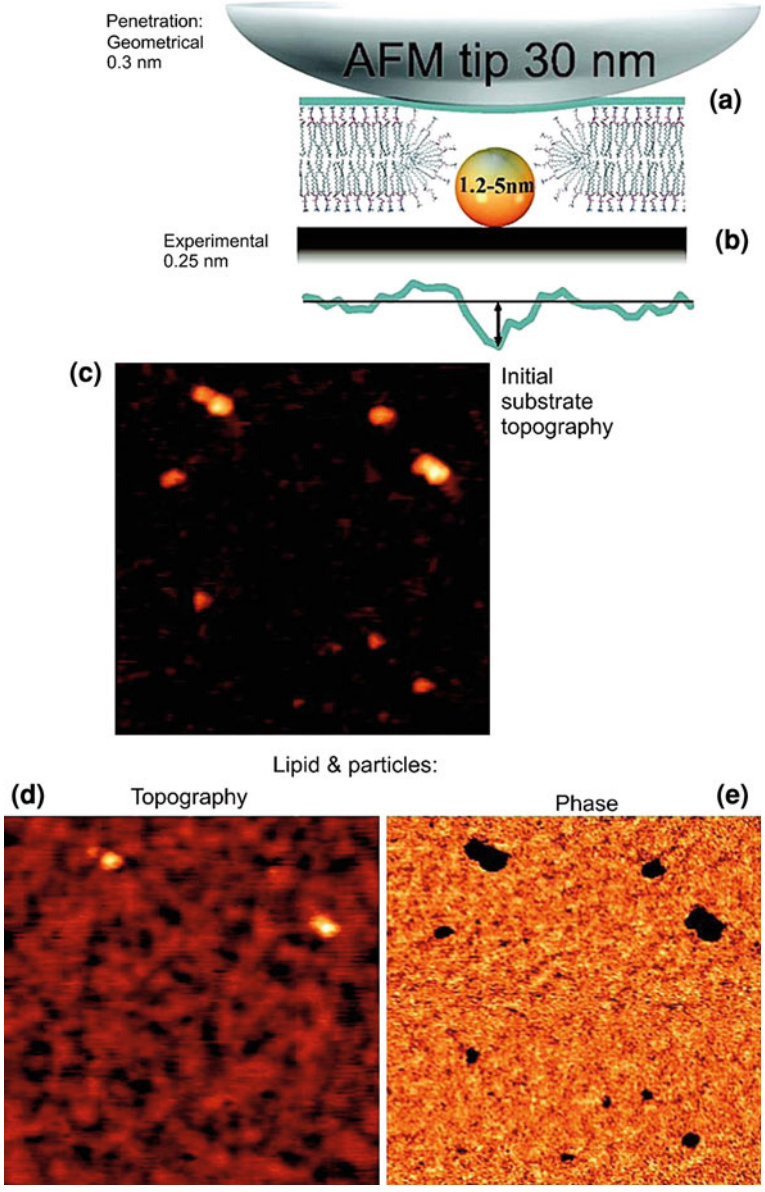

Fig. 6.9 AFM data confirming the formation of pores around 1.2–5 nm diameter nanoparticles: **a** theoretical and **b** experimental AFM topography of a pore in the membrane, **c** a topography image of the substrate with particles (no lipid), **d** topography, and **e** phase imaging of the lipid deposited on the sample with 1–8 nm diameter nanoparticles (scan size $475 \times 475\,\text{nm}^2$). This figure with its description has been taken with the publisher's permission from [22]

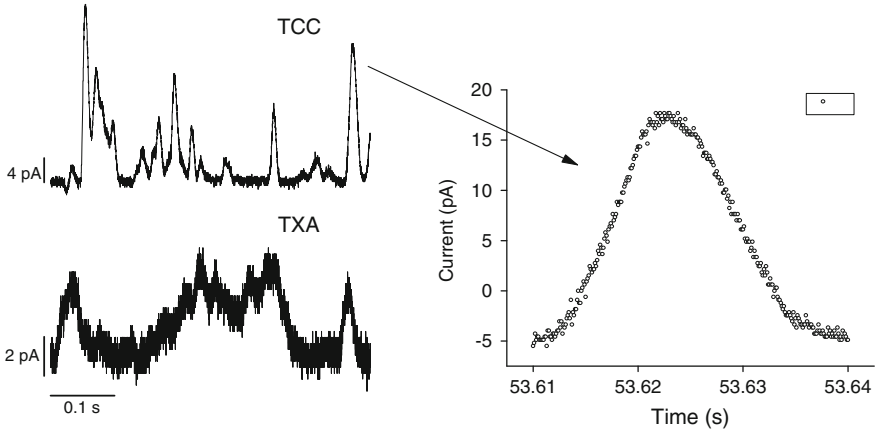

Fig. 6.10 Triangular-shaped conductance events induced by thiocolchicoside (TCC) and taxol (TXL)-A (TXA), both at 90 μM. $pH = 5.7$, $V = 100$ mV. Both traces were filtered at 20 kHz. The lower plot shows higher noise due to its presentation (current axis) at an amplified scale. In a high-resolution plot (shown on the right-hand side of the *arrow*) of a single event only with showing individual points (in Origin 8.5 plot) we observe all points (*open circles*) with increasing and decreasing values of conductance, respectively, at both left and right lateral sides of the chemotherapy drug-induced triangular conductance events

current levels in TCC or TXL-induced conductance events strongly indicates the existence of a pore whose cross-sectional area fluctuates with time.

The chemotherapy drug-induced broken regions of a membrane or the lipid-lined toroidal pores behave exactly like regions without the hydrophobic membrane core. Any material which avoids contact with the membrane environment (specifically the membrane inner hydrophobic core) may find these pores to be favorable regions for passage. It is predicted that the pore-inducing agents reside behind the lipids. Any material passing through the pore can therefore avoid direct interactions with the pore-inducing agents. A molecular dynamics simulation equivalent to the one explained in Chap. 5 may help to elucidate the quantitative nature of possible interactions (electrostatic, van der Waals, etc.) between nanoparticles and lipid or pore-inducing agents, e.g., chemotherapy drugs (see Fig. 6.10). From the discussion of the results presented in the previous section, it appears most likely that such interaction energies are strongly dependent on the electro-chemical properties of the nanoparticles willing to cross through specific membranes. It is also worth mentioning that certain nanoparticles, such as silica nanoparticles, are likely to experience weak interactions, while others, such as polycationic polymer nanoparticles, are likely to experience stronger interactions and show better binding with lipids. Nanoparticles with a neutral or non-binding propensity toward lipids can be easily driven through the chemotherapy drug-induced broken (toroidal pores) type regions. This is schematically diagrammed in Fig. 6.11. With the absence of considerable binding to membranes (due to a negligible value of $U_{\text{np-lip}}$, see Eq. 6.5) these nanoparticles

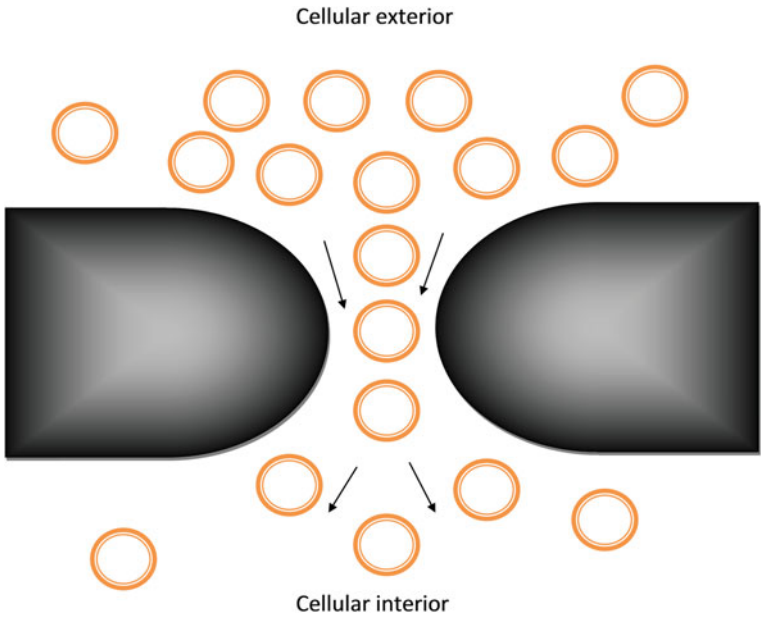

Fig. 6.11 Nanoparticles that are reluctant to interact with lipids naturally diffuse through the type of toroidal pores where the opening region inside the pore consists of no pore-inducing agents. The absence of pore-inducing agents in the opening regions helps nanoparticles to experience no considerable direct interactions with the agents. We have observed such a type of pore to be induced by chemotherapy drugs (e.g. TCC, TXL, etc.). In addition to chemotherapy drugs, a possible search for a better set of agents, e.g., any natural or synthetic antimicrobial peptides or biomolecules which might create the type of pore as mentioned here, should be worth pursuing. This is hoped to generate a combination therapy with low cytotoxicity

can easily diffuse to the cellular interior regions. From the comparable analysis on nanoparticle interactions with membranes presented in the last section, it is clear that silica nanoparticles and similar ones that show poor or no binding with lipids may emerge as good candidates for drug delivery through the lipid lined toroidal pores.

The proposed novel nanotechnology heavily depends on considerations involving charge and geometry of nanoparticles, as well as the dimension and stability of the nanoparticle-transporting pores. As the proposed pore is a 'lipid-lined' type, the lowest possible value of the cross-section of a pore is as small as 0. From there, the cross-section can increase to an arbitrary value. The triangular nature of the discrete conductance events (see Fig. 6.10) clearly suggests that the cross-sectional dimension either increases, decreases, or follows a back-and-forth oscillation pattern. This ensures the possibility of free transport of nanoparticles with any dimension, which can even be as low as the dimension of the order of a lipid head group ($\sim$0.6 nm diameter). This can provide the freedom of choice of nanoparticles of any size for drug delivery into the cellular interior. Smaller size drug-carrying nanoparticles will require induction of smaller pores, and the particle diffusion may also be faster

due to a lower value of nanoparticle inertia. This will thus require low stability (∼pore lifetime) for the pore. This novel nanotechnology should be able to deal with drug delivery targeting the cellular interior regions. Important applications of this technology could include the treatment of various types of cell-based diseases, such as cancer or Alzheimer's disease to name but a few. Besides, imaging of the cellular interior regions can also be performed using this type of novel nanotechnology. Consequently, this nanotechnology can find uses in both cell-based diagnosis and in therapeutic applications which will enhance our understanding of various life processes that originate inside cells.

6.4.2 Membrane Transport of Nanoparticles Through Non-Lipid-Lined Ion Pores

Chapters 4 and 5 showed that antimicrobial peptide alamethicin induces a 'barrel-stave'-type ion pore/channel inside lipid membranes. This structure is a long cylinder covering the whole bilayer thickness where the peptides align longitudinally on the cylindrical surface. The cross-sectional area of the channel changes back-and-forth depending on the number of participating peptides in the formation of a pore. Unlike the pores induced by chemotherapy drugs, presented in Fig. 6.11, the membrane thickness near the alamethicin pore never seems to vanish completely. If nanoparticles try to move through the alamethicin channles, they need to travel a length equivalent to the bilayer thickness right through the cylindrical axis. This raises the possibility for the nanoparticles to be interacting with peptides on the channels during their relatively long journey through the hydrophobic lipid bilayer core. When traveling through the type of pores that are induced by chemotherapy drugs, nanoparticles can avoid the hydrophobic membrane core and can also avoid direct interactions with pore-inducing agents. Any nanoparticles that are reluctant to interact with lipids may be dragged through the lipid-lined toroidal pores (see Fig. 6.11) much easier than those toroidal pores induced by magainin or many other peptides. Of course, a detailed investigation can be made whether the nanoparticle transport through ceramide channels (presented in Chaps. 4 and 5) appears to be an easier solution. Despite the necessity of traveling a long distance, equivalent to the thickness of the membrane, nanoparticles traveling through the ceramide channels meet lipids only. This may reduce cytoxicity, but there exists a significant risk of experiencing a much slower diffusion rate of nanoparticles into the cellular interior due to the long length of the channel's hydrophobic core that must be traversed by the nanoparticles. A detailed investigation aimed at finding better candidates (less toxic natural or synthetic peptides, any biomolecules, etc.) that induce channels similar to those induced by chemotherapy drugs may be worth undertaking in order to develop non-toxic nanotechnology enabling the delivery of drugs into cellular interior regions.

6.4.3 Theoretical Understanding of the Nanoparticle Diffusion Through Ion Pores/Channels in Membranes

We consider two simple cases in order to better understand the problem outlined above. We first assume that the solutes (nanoparticles) can cross through the porous membrane with cylindrical pores that are perpendicular to the membrane surface, due to the influence of a pressure gradient across the membrane. The other possibility is that the solutes diffuse through the porous membrane, due to a gradient of solute concentrations across the membrane.

In the case of nanoparticle diffusion due to the influence of a pressure gradient, a very simple formula, the so-called Poiseuille formula, can be applied, which states that

$$J_v = L_P \Delta P \tag{6.7}$$

Here J_v is defined as the total volume of fluid crossing the membrane per second and per unit membrane surface area. L_P is the hydraulic permeability of the membrane, and is expressed in the units of (cm/s)/atmosphere, which can be derived from the known values of fluid viscosity, pore density, cross-sectional area, and membrane thickness. ΔP is the pressure gradient across the membrane. The generalized form of J_v is as follows:

$$J_v = \frac{\text{flow per pore}}{\text{channel}} \times \text{pore number density on membrane surface}$$

Here, in the case of nanoparticle diffusion, we assume that the number of nanoparticles crossing the membrane per second and per unit membrane surface area $J_{\text{np},P}$ changes in proportion to the value of J_v.

In another case of nanoparticle diffusion due to the influence of nanoparticle concentration gradient across the membrane, a simple formula called Fick's law can help to analytically describe the diffusion mechanism. For a gradient of nanoparticle concentration Δc_{np}, the nanoparticle diffusion through the pores can be expressed by the following formula

$$J_{\text{np},c} = \eta_m \Delta c_{\text{np}} \tag{6.8}$$

Here, $J_{\text{np},c}$ is the number of nanoparticles crossing a unit membrane area per second, and η_m is the membrane permeability.

Equations 6.7 and 6.8 describe situations where the nanoparticles pass through cylindrical pores. However, in the proposed novel nanotechnology application for nanoparticle transport through a lipid-lined toroidal pore (see Fig. 6.11), the particle flow is expected to take place through a different class of pores. This accounts for mainly two important aspects which are: (i) that membrane thickness vanishes at the opening of the pore so that the time to cross the membrane by a nanoparticle is almost zero and (ii) that the pore cross-section changes back-and-forth with time. These dynamical aspects are very important and require a totally novel

analytical and computational treatment to theoretically describe the nanoparticle transport mechanism through an induced topological disorder or an ion pore inside the cell membrane. A brief outline of this situation is presented below.

We introduce a probability function that describes the trapping probability for a nanoparticle in a specific ion pore/channel in the membrane. Consider that the nanoparticles are randomly moving on the surface of the membrane. A nanoparticle with an average Hamiltonian H (Eq. 6.4) has a non-zero probability for being trapped inside the ith pore as long as the pore cross-sectional area ($A_{\mathrm{ch},i}(t)$) is larger than the nanoparticle diameter (A_{nc}). If the pore ensures that the membrane thickness vanishes at the core with a cross-section $A_{\mathrm{ch},i}(t)$ (see Fig. 6.11), the trapping rate will in fact be proportional to the rate of nanoparticle release into the cellular interior as long as $A_{\mathrm{ch},i}(t) \geq A_{\mathrm{nc}}$. The pore cross-section $A_{\mathrm{ch},i}(t)$ is considered here to be time dependent (t), due to the fact that the cross-sectional area of the pore is assumed to change back-and-forth with time within the lifetime (∼ms) of the pore/channel, following the characteristic behavior of the type of pores induced by chemotherapy drugs (see Fig. 6.10). However, the novelty found in chemotherapy drug-induced pores is that $A_{\mathrm{ch},i}(t)$ is usually found to be constant during a channel's lifetime, following specific energy states in most of the other known channels induced by antimicrobial peptides. $A_{\mathrm{ch},i}(t)$ is proportional to the electrical conductance of the pore. As the plot of a chemotherapy drug-induced pore conductance versus time is found to follow a triangular pattern (see Fig. 6.10), $A_{\mathrm{ch},i}(t)$ should consequently follow an identical pattern when it is plotted against time within the lifetime of a channel. Considering all these facts, we propose that the statistical probability ($p_i(t)$) for a nanoparticle to cross a cell membrane by traveling through a temporarily induced ith toroidal pore/channel (see Fig. 6.11) at zero external field (driving force) is as follows

$$p_i(t) \sim \frac{A_{\mathrm{ch},i}(t)}{A_{\mathrm{cell}}} e^{\frac{E_{\mathrm{np},i}}{k_B T}} \quad \text{for } A_{\mathrm{ch},i}(t) \geq A_{\mathrm{nc}} \text{ or } 0 \text{ for } A_{\mathrm{ch},i}(t) < A_{\mathrm{nc}} \tag{6.9}$$

Here, the probability is assumed to be proportional to the Boltzmann's function $\exp(E_{\mathrm{np},i}/k_B T)$ but it also changes with the changing cross-sectional area of the specific pore, normalized with the total surface area (A_{cell}) of the cell. This probability is therefore a time-dependent variable. Here, T is the absolute temperature and k_B is the Boltzmann's constant. $E_{\mathrm{np},i}$ stands for the total binding energy ($U_{\text{np-lip}}$, Eq. 6.5) of the nanoparticle inside the pore. Figure 6.12 illustrates this preferential nanoparticle migration through pores. In the specific case of nonbinding with lipids inside pores, a nanoparticle experiences a maximum energetic probability to be crossing through a pore, since for this condition $\exp(E_{\mathrm{np},i}/k_B T)$ approaches the absolute maximum (1). We suspect that silica nanoparticles and similar ones which exhibit non-interacting behavior with lipids (as explained in an earlier section) fall within this favorable nanoparticle category.

If at any time t there are N ion pores or channels induced across the membrane surrounding a biological cell, the total cell internalization probability for a nanoparticle $p_{\mathrm{tot}}(t)$ is given by

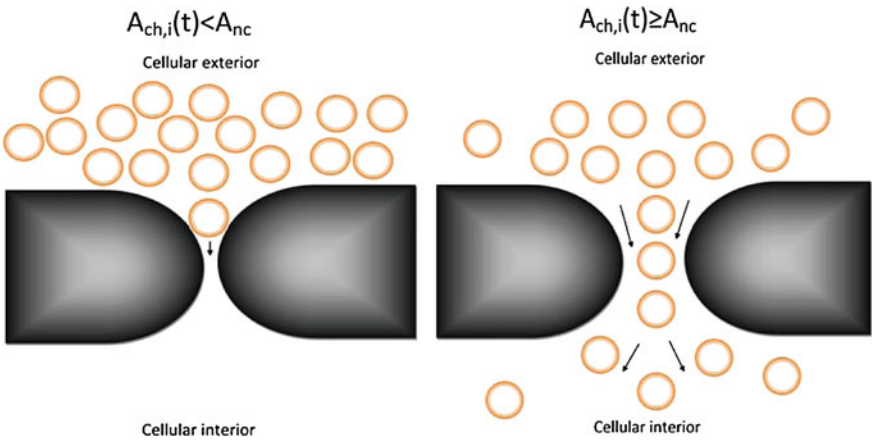

Fig. 6.12 Nanoparticles that avoid moving through the membrane's hydrophobic core cannot move through a pore/channel with a non-hydrophobic core under the condition $A_{\mathrm{ch},i}(t) < A_{\mathrm{nc}}$ (see the *left panel*). Under this condition, no matter how high the nanoparticle concentration in the cellular exterior region might be, there would be no presence of nanoparticles in the cellular interior region. Any nanoparticle shows a finite probability to move through the same pore/channel under the condition $A_{\mathrm{ch},i}(t) \geq A_{\mathrm{nc}}$. In this case, depending on a nanoparticle concentration in the cellular exterior region, there is a possibility to find a finite number of nanoparticles in the cellular interior region (see the *right panel*). The nanoparticle migration may also be influenced by many other physiological membrane properties like such as gradients of pressure or electrical potentials across the cell membrane

$$p_{\mathrm{tot}}(t) = \Sigma_{i=1}^{N} p_i(t) \tag{6.10}$$

As a first-order approximation, one can use the Gaussian form for $A_{\mathrm{ch},i}(t)$, $(\exp(-\alpha(t-t_0)^2))$, but to obtain a better fit with the triangular nature of the single conductance event (see Fig. 6.10) one needs to use the following form for $A_{\mathrm{ch},i}(t)$

$$A_{\mathrm{ch},i}(t) \sim \exp(\alpha|t-t_0|^{\beta}) \tag{6.11}$$

where $\alpha \sim 1/\tau$ and $\beta < 2$. The value of β should be calculated from a good fit to the experimental data (see Fig. 6.10). Here, τ is the lifetime of the conductance event and t_0 is the initial time. The form of $A_{\mathrm{ch},i}(t)$ is never unique, and must follow any function that fits with the pattern of a conductance event induced by an agent such as the chemotherapy drugs or other agents that are proven to be better candidates for a combination therapy to ensure improved transport of nanoparticles through the membrane. $E_{\mathrm{np},i}$ follows from a very complicated formulation using both analytical and computational considerations equivalent to that explained in Chap. 5. A molecular dynamics simulation (explained in Chap. 5) can also be applied to parameterize the energetics involved in nanoparticle-lipid interactions. Thus, an actual order of values for $p_{\mathrm{tot}}(t)$ regarding any specific nanoparticle can be derived.

References

1. Ashrafuzzaman, M., Lampson, M.A., Greathouse, D.V., Koeppe, R.E. II, Andersen, O.S.: Manipulating lipid bilayer material properties using biologically active amphipathic molecules. J. Phys.: Condens. Matter **18**, S1235–55 (2006)
2. Ashrafuzzaman, M., Andersen, O.S., McElhaney, R.N.: The antimicrobial peptide gramicidin S permeabilizes phospholipid bilayer membranes without forming discrete ion channels. Biochim. Biophys. Acta. **1778**, 2814–22 (2008)
3. Bruchez, M., Moronne, M., Gin, P., Weiss, S., Alivisatos, A.P.: Semiconductor nanocrystals as fluorescent biological labels. Science **281**, 2013–2016 (1998)
4. Chan, W.C.W., Nie, S.M.: Quantum dot bioconjugates for ultrasensitive nonisotopic detection. Science **281**, 2016–2018 (1998)
5. de la Isla, A., Brostow, W., Bujard, B., Estevez, M., Rodriguez, J.R., Vargas, S., Castano, V.M.: Nanohybrid scratch resistant coating for teeth and bone viscoelasticity manifested in tribology. Mat Resr Innovat **7**, 110–114 (2003)
6. Edelstein, R.L., Tamanaha, C.R., Sheehan, P.E., Miller, M.M., Baselt, D.R., Whitman, L.J., Colton, R.J.: The BARC biosensor applied to the detection of biological warfare agents. Biosensors Bioelectron **14**, 805–813 (2000)
7. Hamoudeh, M., Salim, H., Barbos, D., Paunoiu, C., and Fessi, H.: Preparation and characterization of radioactive dirhenium decacarbonyl-loaded PLLA nanoparticles for radionucleide intra-tumoral therapy. Eur. J. of Pharm. And Biopharm. **67**, 597–611 (2007)
8. Harper, P.E., Mannock, D.A., Lewis, R.N.A.H., McElhaney, R.N. and Gruner, S.M.: X-Ray Diffraction structures of Some Phosphatidylethanolamine Lamellar and Inverted Hexagonal Phases. Biophys. J. **81**, 2693–2706 (2001)
9. Israelachvili, J.N., Mitchell, D.J. and Ninham, B. W.: Theory of self-assembly of hydrocarbon amphiphiles into micelles and bilayers. J. Chem. Soc., Faraday Trans. 2 **72**, 1525–1568 (1976)
10. Israelachvili, J.N., Mitchell, D.J. and Ninham, B. W.: Theory of self-assembly of lipid bilayers and vesicles. Biochim. Biophys. Acta **470**, 185–201 (1977)
11. Leroueil, P. R., Hong, S., Mecke, A., Baker, J. R. Jr., Orr, B. G. and Holl, M. M. B.: nanoparticle interaction with biological membranes: does nanotechnology present a Janus Face? Acc. Chem. Res. **40**, 335–342 (2007)
12. Ma, J., Wong, H., Kong, L.B., Peng, K.W.: Biomimetic processing of nanocrystallite bioactive apatite coating on titanium. nanotechnology **14**,619–623 (2003)
13. Mah, C., Zolotukhin, I., Fraites, T.J., Dobson, J., Batich, C., Byrne, B.J.: Microsphere-mediated delivery of recombinant AAV vectors in vitro and in vivo. Mol Therapy **1**, S239 (2000)
14. Mahtab, R., Rogers, J.P., Murphy, C.J.: protein-sized quantum dot luminescence can distinguish between "straight", "bent", and "kinked" oligonucleotides. J Am Chem Soc **117**, 9099–9100 (1995)
15. Mecke, A., Uppuluri, S., Sassanella, T. J., Lee, D.-K., Ramamoorthy, A., Baker, J.R., Orr, B.G. and Holl, M.M.B.: Direct observation of lipid bilayer disruption by poly(amidoamine) dendrimers. Chem. Phys. Lipids **132**, 3–14 (2004)
16. Mecke, A., Lee, D.-K., Ramamoorthy, A., Orr, B.G. and Holl, M.M.B.: Synthetic and natural polycationic polymer nanoparticles interact selectively with fluid-phase domains of DMPC bilayers. Langmuir **21**, 8588–8590 (2005)
17. Mecke, A., Majoros, I. J., Patri, A. K., Baker, J.R. Jr., Holl, M.M.B. and Orr, B.G.: Lipid Bilayer Disruption by polycationic Polymers: The Roles of Size and chemical Functional Group. Langmuir **21**, 10348–10354 (2005)
18. Molday, R.S., MacKenzie, D.: Immunospecific ferromagnetic iron dextran reagents for the labeling and magnetic separation of cells. J Immunol Methods **52**,353–367 (1982)
19. Nam, J.M., Thaxton, C.C., Mirkin, C.A.: nanoparticles-based bio-bar codes for the ultrasensitive detection of proteins. Science 301, 1884–1886 (2003)
20. Panatarotto, D., Prtidos, C.D., Hoebeke, J., Brown, F., Kramer, E., Briand, J.P., Muller, S., Prato, M., Bianco, A.: Immunization with peptide-functionalized carbon nanotubes enhances virus-specific neutralizing antibody responses. Chemistry& Biology **10**, 961–966 (2003)

21. Parak, W.J., Boudreau, R., Gros, M.L., Gerion, D., Zanchet, D., Micheel, C.M., Williams, S.C., Alivisatos, A.P., Larabell, C.A.: Cell motility and metastatic potential studies based on quantum dot imaging of phagokinetic tracks. Adv. Mater. **14**, 882–885 (2002)
22. Roiter, Y., Ornatska, M., Rammohan, A.R., Balakrishnan, J., Heine, D.R. and Minko, S.: Interaction of Nanoparticles with Lipid Membrane. Nano Lett. **8(3)**, 941944 (2008)
23. Stein, W.D.: transport and diffusion across Cell Membranes. Academic Press: Orlando, FL, (1986)
24. Villars, F.M.H. and Benedek, G. B.: Physics with illustrative examples from Medicine and Biology, Vol 2.: Statistical Physics. Addison-Wesley Pub. Co., Inc. Reading, Massachusetts, California, USA (1974)
25. Wang, S., Mamedova, N., Kotov, N.A., Chen, W., Studer, J.: Antigen/antibody immunocomplex from CdTe nanoparticle bioconjugates. Nano Letters **2**,817–822 (2002)
26. Weissleder, R., Elizondo, G., Wittenburg, J., Rabito, C.A., Bengele, H.H., Josephson, L.: Ultrasmall superparamagnetic iron oxide: characterization of a new class of contrast agents for MR imaging. Radiology **175**:489–493 (1990)
27. Yoshida, J., Kobayashi, T.: Intracellular hyperthermia for cancer using magnetite cationic liposomes. J Magn Magn Mater **194**, 176–184 (1999)

Chapter 7
Membrane-Related Diseases

Life starts with a single cell, but the cell is also where the origin of most pathological changes and disorders can be traced. Disease states can, in most cases, be linked to the abnormal functioning of specific organs. A living cell is the fundamental unit where most of these abnormalities happen and where they are initiated. That is why a cell is also the ultimate target for the action of most drugs. Cancer, Alzheimer's disease, Parkinson's disease, various infectious diseases, etc. originate in individual cellular compartments, including the membrane. This chapter will be dedicated to a better understanding of the membrane's involvement in diseases, and disease treatment using drugs targeting cell membranes. Several examples will be used for illustration purposes. However, due to the book's subject matter, we will concentrate on the scientific aspects of a few of the membrane-based diseases, leaving the medical issues aside. Below, we list several diseases that are either directly or indirectly related to membrane properties and their abnormalities.

1. **Hyaline Membrane Disease** is commonly associated with preterm infants. Hyaline membrane disease affects the lungs at the time of birth, thus causing respiratory distress.
2. **Alzheimer's Disease**. The oxidative stress caused by Alzheimer's disease in the brain results in phospholipid alterations that compromise the cell membrane, disrupting the function of the brain cells. A host of other cellular abnormalities, including zinc deficiency and tauopathy, have been implicated in the origins of Alzheimer's disease.
3. **Cystic Fibrosis** is a disease that brings about an excessive production of fluid in the lungs due to a defective calcium-ion channel, which contains a protein that is crucially important to the membrane of lung cells. The calcium-ion channel controls the level of fluids and mucus in the lungs, hence, when it mutates in cystic fibrosis patients, it causes the mucus to build up in the lungs, making it hard to breathe.
4. **Duchenne Muscular Dystrophy (DMD)** affects the protein called dystrophin located in muscle cells. Dystrophin allows the muscle cell membrane to connect with the intracellular section. In the absence of dystrophin, the cell membrane

M. Ashrafuzzaman and J. Tuszynski, *Membrane Biophysics*,
Biological and Medical Physics, Biomedical Engineering,
DOI: 10.1007/978-3-642-16105-6_7, © Springer-Verlag Berlin Heidelberg 2012

would be incapable of repairing itself, thus destroying it and bringing about DMD.

The concept of a true or inherent membrane disorder, however, differs from other disease classes because many diseases involve the membrane to some degree but are not necessarily centrally affected by membrane abnormalities. Due to the significance of membranes in selectively shielding cells from the environment and interacting with it, it is not surprising that the disruption of membrane function leads to pathological changes. As discussed at length in this monograph, membranes play key roles in regulating transport into and out of cells, conferring selective receptivity via protein receptors, anchoring cytoskeletal filaments and structures forming the extracellular matrix, providing binding sites for enzymatic catalysis, and allowing cell motility. It is, therefore, easy to see why membrane defects lead to cellular pathologies. In fact, most, diseases involve the membrane as a major factor in disease etiology. Unfortunately, the existence of diverse multiple effects causing membrane disruption means that there is no coherent classification scheme of diseases affected by changes in cell membranes. Determining membrane-based pathologies, identifying the mechanisms that underlie them, and understanding how drugs used to treat them work is consequently complicated by distinct disruption types. For example, membrane transport can be affected by changes occurring in membrane proteins, in the lipid bilayer or in the cytoskeleton. There are also numerous diseases and disorders caused by alterations in the structure of proteins that reside in the membrane and function as receptors, transporters, enzymes or structural components. Drugs that target these defects in membrane-protein-based diseases typically interact with proteins, not membranes, and block, augment or mimic the actions of the protein involved.

Nonetheless, two categories of true membrane-based diseases can be singled out. The first are caused by defects in cytoskeletal components that impair membrane function, while the second occur when altered membrane lipid composition disrupts trans-membrane transport. The cytoskeleton contains structural proteins linked to the membrane that provide protection from the stresses generated by many cellular processes, for example, muscle contraction. Cytoskeletal structures also include signaling complexes close to cell adhesion molecules. Disruptions in the cytoskeleton can, therefore, lead to a range of diseases, such as sickle-cell anemia and DMD. Sickle-cell anemia is a genetic disease that results in the production of a defective form of hemoglobin, which distorts red blood cells into the characteristic sickle shape. Red blood cells maintain their shape using a network of the cytoskeletal proteins actin and spectrin. In sickle-cell anemia, the actin/spectrin network malfunctions, making red blood cells too rigid and causing obstructions in microcirculation [11]. The main drug used in the therapy for sickle-cell anemia, hydroxyurea, reduces the formation of sickle hemoglobin while also decreasing neutrophil numbers which promote adhesion of sickled cells to blood vessel walls. However, it has also been reported that hydroxyurea acts directly on the cell membrane. This drug is known to decrease expression of adhesion molecules on red blood cells including phosphatidylserine (PS), which is unusually expressed on the outer surface of red blood cells in sickle-cell

anemia. In DMD, a mutation in the dystrophin gene disrupts the ability of the protein product to anchor cytoskeletal elements to the surface membrane. Hence, structural support is lost, the cell membrane becomes permeable, intracellular pressure rises and the cell breaks apart.

Membrane transport has a wide-range of effects on the cell from the movement of macromolecules by vesicular transport between organelles during secretion and endocytosis, to mechanisms of organelle inheritance in mitosis. It is estimated that 10 % of cellular proteins play a role in membrane traffic and protein targeting [28]. Prominently figuring in regulating membrane traffic are those proteins whose disruption is implicated in several inherited human disorders, namely Rab proteins. More than 50 of these GTP-binding proteins have been identified as being associated with cellular membranes, via a lipid modification process called geranylation. The particular protein Rab27a plays a key role in trafficking disorders, such as choroideremia, Hermansky–Pudlak and Griscelli syndromes. Choroideremia is a late-onset retinal degeneration condition, characterized by progressive dystrophy of photoreceptors caused by a defect in Rab Escort protein 1. Hermansky–Pudlak and Griscelli syndromes are disorders of lysosome-related organelles such as melanosomes. These diseases are characterized by partial albinism, accompanied by hemorrhagic tendency in Hermansky–Pudlak syndrome, and poorly functioning cytotoxic T-lymphocytes in Griscelli syndrome. Griscelli syndrome is caused by mutations in Rab27a. Niemann–Pick disease type C (NPC) is a lysosomal storage disorder (LSD), one of more than 40 rare conditions in which the absence of an enzyme prevents lysosomes in cells from performing their natural recycling function. This leads to various materials being inappropriately stored in the cell, which results in a host of disorders in which there is progressive deterioration in physical and mental states. Most mutations in classic lysosomal LSDs result in the delivery of a defective enzyme that has a reduced catalytic activity to lysosomes [15]. LSDs are diseases of the membrane because they can be caused by defects in membrane lipids and proteins. For example, NPC is characterized by lysosomal accumulation of LDL-derived cholesterol.

Unfortunately, developing drugs for membrane-based disorders is severely hampered since the understanding of the mechanisms of membrane trafficking and lipid self-organization is still sorely lacking. Despite these complexities, membranes continue to generate more and more interest as additional knowledge is created about their roles in cellular processes.

Understanding the structure and functions of membrane compartments is a complex task, and often only indirect ways for diagnosis and therapy are available to fight the underlying diseases. The same applies to our understanding of the suitability of specific drugs targeting a disorder. Sometimes the cell membrane becomes a natural drug target because of its geometric location as it surrounds the cell. Moreover, any change in membrane function is easily detectable using various imaging techniques, electrophysiology recordings across membranes and observations of other membrane-related mechanisms.

More than one-third of all human genes code for proteins associated with cell membranes. The cell plasma membrane and the membranes separating cellular compartments play key roles in the entry and exit of ions and molecules, in separating

biochemical functions within distinct organelles, in localizing metabolic processes, and in communication between internal compartments and the extracellular environment. Dysfunction in membrane proteins and associated compartmentalization processes are common causes of human disease. The lipid bilayer of cell membranes presents a unique two-dimensional hydrophobic environment for membrane proteins. Specialized in both structure and function, the study of membrane proteins provides a unique array of technical challenges and research opportunities. Diseases related to membrane proteins result from changes in the function of the membrane protein caused by structural damage and mutations. Underlying genetic changes may cause either: (i) retention of the protein in an intracellular location, instead of reaching the plasma membrane, or (ii) change of function of the protein. The so-called MTC technique enables differentiation of these possibilities. Live-cell confocal microscopy, in combination with fluorescently tagged proteins and ion-sensitive dyes, allows high fidelity spatial and temporal measurements to reveal dysfunctional molecular trafficking, as well as to measure disturbances in the ionic milieu associated with alterations in the function of many membrane proteins. Many ion transport proteins operate by moving charged ions/molecules across the cell membrane, and this can be measured in "real time" on the scale of milliseconds using state-of-the-art patch-clamp technologies. Combining these electrophysiological recordings with confocal fluorescent measurements makes it possible to diagnose the nature of the membrane transport defect in a single step with unparalleled precision.

Gene Transduction Core (GTC) A common approach to understanding the basis for diseases caused by membrane proteins is to measure the function of recombinant mutant proteins. These studies are typically performed in immortalized tissue culture cells. However, these immortalized cells often do not behave as wild-type primary cells, and do not provide a normal background, so results obtained from measurements performed on these cells may be inaccurate. Recently developed viral transduction methodologies have begun to allow mutant genes to be introduced in vivo and in vitro into cells from many tissues. These primary tissue culture cells, very recently explanted from their host, behave in a more realistic manner, but these cells are resistant to the introduction of genes. The GTC enables new methodologies of viral gene transduction to induce expression of individual genes in primary tissue preparations and cell cultures.

Protein Modeling and Dynamics Core (PMDC) Membrane proteins are central to cellular function and also represent important targets for drug discovery. Indeed, G-protein coupled receptors (GPCR) are not only membrane proteins, but also constitute a major target of drug therapies in use today. Directed design of drugs requires information on the structure of the target (membrane protein). The PMDC provides a two-pronged approach to set the stage for targeted drug design involving: (i) computer modeling of protein membrane structures, and (ii) experimental determination of three-dimensional structures of membrane proteins. A cluster of computers with appropriate software packages enables: (a) modeling of the dynamics (movements) of membrane proteins, (b) virtual docking of molecules (potential drugs) onto the surfaces of membrane proteins to identify and rank potential

therapeutics, (c) complex kinetic analyses and mathematical simulations/modeling describing binding modes, off-target interactions and even binding dynamics, and (d) preparation of structural models by homology to known membrane protein structures, an increasingly important approach as more crystal structures of membrane proteins or their fragments are solved. Computational approaches facilitated by the PMDC require "real" structural data in order to be reliable. Component (ii) of the PMDC enables the preparation of membrane proteins to be used for X-ray, NMR and cryo-electron microscopic structure determination. In addition, it is also advantageous to construct a relational database for membrane protein properties and experimental data. This provides the basis of intensive data mining and meta-analyses of data developed by several research groups, and makes the results of research much more readily available to the larger community of researchers working in the field.

Target Investigation Core (TIC) The potential of membrane proteins as therapeutic targets has been realized only for GPCR so far. An enormous range of membrane proteins implicated in disease processes remains to be exploited. The TIC provides automated fluorescence-based and electrophysiological equipment to quickly acquire information on the behavior of multiple membrane protein variants, and to rapidly screen membrane proteins for inter-molecular (protein–protein, or protein–drug) interactions. Possible drug-like lead compounds can be identified by the TIC.

7.1 Lipids as Markers in Anti-Cancer Treatment: Lipid Membrane Binding of Aptamers

The induction of programmed cell death (apoptosis) is both a desired outcome of cancer therapy and a potential target allowing imaging and modulation of therapeutic effects. A novel information-driven approach has been recently discovered [47] which can be generalized for the development of theranostic (therapeutic and diagnostic) drugs targeting cellular changes related to apoptotic transformation. Apoptosis is a vital, highly regulated, natural process that contributes to the development and maintenance of human and animal cells [21, 50]. Apoptosis plays multiple roles in the normal development of organisms, extending from embryonic development to the maintenance of normal cell homeostasis [13, 34, 35]. Malfunctioning of the apoptotic process leads to the proliferation of many types of cancer, due to inadequate control of cell homeostasis. It is recognized that evasion of apoptosis is one of the hallmarks of cancer development and progression [17]. There are a number of related cellular processes observed during apoptosis including phosphatidylserine (PS) externalization, caspase activation, chromatin and nucleus condensation, reduction in cytoplasm volume and DNA degradation [13]. Drugs targeting and modulating apoptosis have a recognized potential in cancer diagnosis and therapy.

There are two main apoptotic pathways: the death receptor (extrinsic) pathway and the mitochondrial (intrinsic) pathway [39]. The death receptor pathway (MAPK) is activated by the binding of FAS or TRAIL ligands to their receptors (DR4/5), stimulating receptor aggregation. In the mitochondrial pathway, pro-survival sig-

naling through AKT activation stimulates phosphorylation of BAD, which allows B-cell lymphoma (BCL 2) protein (encoded by the BCL2 gene) to exert its anti-apoptotic effects by blocking pro-apoptotic proteins NOXA, BAX, etc. However, dephosphorylated BAD blocks BCL2 by hetero-dimerization (BAX/BCL2), which allows pro-apoptotic proteins to form pores in the mitochondria. This process then releases apoptogenic factors from the mitochondrial inter-membrane space, including cytochrome C (Cyt C), APAF1, and caspase 9. These factors form the so-called apoptosome, which stimulates apoptosis through caspase 3 cleavage. Conventional studies have shown the BCL 2 protein family is one group of gene products that governs the initial phase of apoptosis [42]. Both anti-apoptotic (BCL 2 protein) and pro-apoptotic (BAX) family members, whose crystal structures have been experimentally determined [32, 33, 43], are potential drug targets in cancer treatments [31]. The multiple sequence alignment for six BCL 2 family proteins presents common motifs among these proteins [33]. Two potent small-molecule inhibitors (ABT-737 and ANT-263) designed to inhibit BCL 2/BCL-xL proteins have been described recently [31, 46, 48]. This inhibition is likely to help overcome the BCL 2 protein-induced anti-apoptosis activity [46]. A strategic study can be suggested for apoptosis modulation in cancer treatment by considering an appropriate combination of "regulators". The regulators would act at different proteins which are responsible for triggering and/or inhibiting apoptosis. Here specifically we can consider a set of regulators consisting of inhibitors for BCL 2 protein (anti-apoptosis) and enhancers for BAX's pro-apoptosis effect. The modulation of cancer treatment, however, can be monitored looking at the lipid functions in membranes.

For diagnostic purposes, the redistribution of PS between inner and outer plasma membranes (Fig. 7.1) should be considered, as recently described in detail [27], (PS externalization), which has been shown as an early marker of apoptosis. PS externalization is specific to apoptotic cells with the exception of activated platelets and erythrocytes. PS externalization, therefore, is an attractive target to detect apoptosis [9, 10, 40] and to provide an early indication of the success or failure of therapy for cancer patients in a clinical setting. Lahorte et al. [23] provides a thorough overview in apoptosis-detecting radiotracers. Currently, annexin V is considered to be the most promising agent in clinical applications [49]. Several groups have prepared 18F labeled annexin V by different approaches to be used with positron emission tomography (PET) because of its higher resolution and more quantitative imaging [9, 25, 29, 45]. However, the value of these radiopharmaceuticals for human use remains to be determined. Detection of PS externalization can be a very good alternative method for apoptosis detection purposes. Work is underway to develop an accurate method to find correct PS aptamer sequences using nucleic acid oligos [47] which are less toxic, easy to synthesize and offer a cheap alternative to more hazardous other candidates. The interested reader is encouraged to read recently published articles [5, 47] for details regarding the generation of aptamer-based probes for detecting and for regulating apoptosis with potential relevance in cancer treatment. In this context the early detection of response to therapy and the possibility to augment treatment by the use of aptamers would have a huge clinical benefit. However, there are many other potential benefits to be derived from a molecular imaging probe for apoptosis in

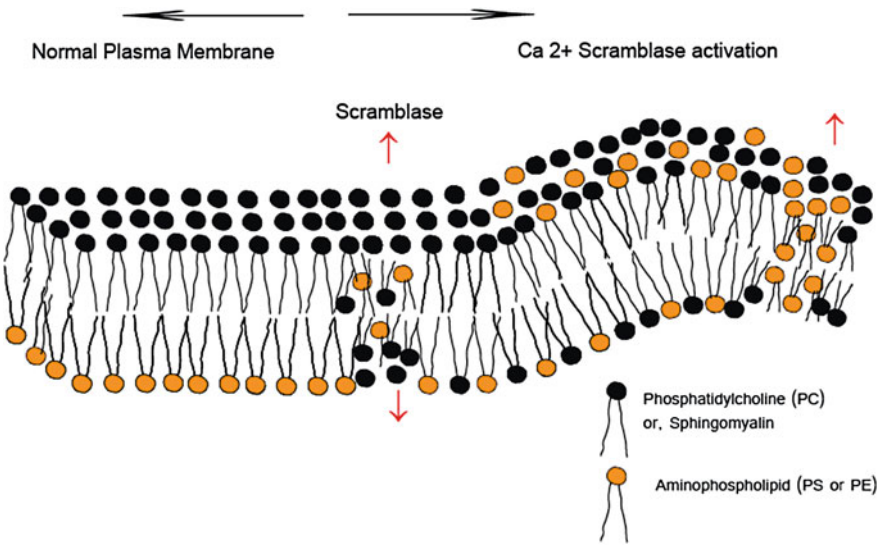

Fig. 7.1 PS externalization [9, 10] in the apoptotic cell membrane. Early in the apoptotic process there is a rapid redistribution and exposure of phosphatidylserine (PS) on the cell surface mediated by the enzyme scramblase. Due to specific lipid properties, especially intrinsic curvature, the PS concentration varies between inner and outer leaflets on lipid monolayers in a membrane. PS is normally restricted to the inner leaflet of the lipid bilayer by an ATP dependent enzyme called flippase (translocase). Flippase, in concert with a second ATP-dependent enzyme, floppase, that pumps cationic phospholipids such as phosphatidylcholine (PC) and sphingomyelin to the cell surface, maintains an asymmetric distribution of different phospholipids between the inner and outer leaflets of the plasma membrane. This figure is redrawn in light of the model diagram and description of the general apoptosis process presented in Refs. [9, 10]

other human health situations (e.g. transplantation) and human pathologies including neurological disorders and cardiovascular disease. In addition, we envision a role for an animal-based apoptosis imaging model in drug development of novel aptamer-based therapies. It is worth stressing that computational design of aptamers is not restricted to targets relevant to apoptosis, but can be employed in any situation where a well-characterized molecular target is known.

7.2 Lipid Membrane Binding of Prion Proteins

Creutzfeldt-Jakob disease (CJD) is a neurodegenerative disease that is incurable and invariably fatal. CJD is sometimes called a human form of the mad cow disease, given that bovine spongiform encephalopathy is believed to be the cause of variant CJD in humans. CJD is the most common among the types of transmissible spongiform encephalopathy found in humans. In CJD, the brain tissue develops holes and takes

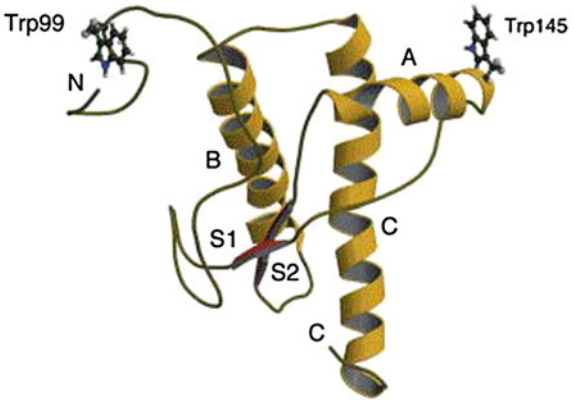

Fig. 7.2 Ribbon diagram of the structure of SHaPrP(90-231) based on the NMR structure in aqueous solution [19]. The two tryptophan residues (Trp99 and Trp145) are highlighted in ball-and-stick representation. The structure shows the three main helices (*A*, *B*, and *C*), and the two antiparallel β-strands (*S1* and *S2*). This figure has been adapted from the Ref. [38] with permission from the publisher

on a sponge-like texture. This is due to a type of infectious protein called a prion. The normal tissue structure is disrupted due to the formation of plaques (amyloid) by extracullular aggregation of prions within the central nervous system. Prions are misfolded proteins which replicate by converting their properly folded counterparts into the disease-associated, prion form [36]. Astrogliosis, inflammatory reaction loss, etc. are among the most important changes at the cellular level [6]. The healthy organism becomes affected through the penetration of prions into the healthy organisms. The newly misfolded prion forms induce further misfoldings and sometimes may trigger chain reactions which at the end may produce large amounts of misfolded or prion form states [4]. Although the incubation times of prion-related diseases are quite long due to the chain transmission of prion states, once the symptoms appear it is often too late to stop it as the diseases reaches an out-of-control status. At this stage, the rapid progression of disease may easily cause uncontrollable levels of damage in various parts of the brain. Death becomes inevitable due to the various unrepairable disordered protein states [3]. All prion diseases are considered to be fatal and untreatable using existing medical procedures.

Prions enter into the tissue structure, which is why their effects on lipids are very important. Various research groups are actively working to better understand the membrane effects of lipids. For example, the binding of the Syrian hamster prion protein SHaPrP(90-231) (see the structure in Fig. 7.2) to model lipid membranes was investigated by tryptophan fluorescence by Sanghera and Pinheiro [38], and this study provides important insights into prion-lipid interactions. This study suggests that an interaction of prion protein (PrP) with lipid membranes could play a role in PrP conversion. These investigators considered all of zwitterionic lipid membranes, raft-like membranes, cholesterol, etc and reported that the binding of

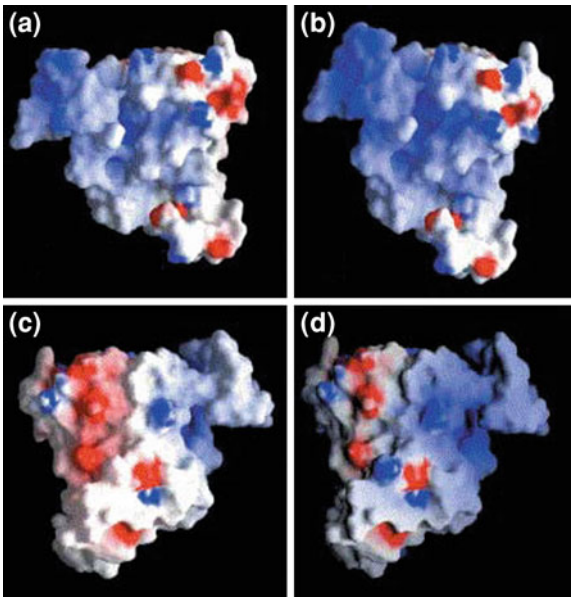

c

Fig. 7.3 Views of the surface of SHaPrP(90-231) colored according to the electrostatic potential [22], with *blue* for positive charges and *red* for negative charges, for the protein represented in (**a**) and (**c**) at pH 7 and (**b**) and (**d**) at pH 5. Views **a** and **b** are similar orientations of the molecule, and **c** and **d** are views following a 180° rotation about a vertical axis of (**a**) and (**b**), respectively. This figure has been adapted from the Ref. [38] with permission from the publisher

PrP to negatively charged lipid membranes involves both electrostatic and hydrophobic lipid-protein interactions. This results in partial insertion of PrP into the lipid bilayer. This membrane-inserted conformation of PrP is richer in β-sheet structures, and has a disruptive effect on the integrity of the lipid bilayer, leading to total release of vesicle contents. In contrast, this report also suggests that the binding of PrP to raft-like membranes is driven by hydrophobic lipid-protein interactions, and induces the formation of α-helical structures. This conformation of PrP with a high content of α-helix is formed only at pH 7 and does not destabilize the lipid bilayer. This pH-dependent effect of PrP structure (see Fig. 7.3) in the lipid environment does indicate the importance of the charge condition in the cellular environment in inducing the prion effects, that is, induction of prion-related disorder or protein misfolding. In cancerous cells, it is evident that the cellular exterior and interior across the lipid membrane experience different pH conditions. The pH dependence of PrP structures may, therefore, suggest that the prion effects in inducing protein disorders or misfoldings may depend on the localized charge environment as well.

Investigations have recently been made in order to understand how the morphology and mechanism of the growth of prion aggregates in membranes are influenced by lipid composition [37]. Here, the prion aggregation is observed in both zwitterionic and anionic membranes, and the morphology of the aggregates formed is dependent

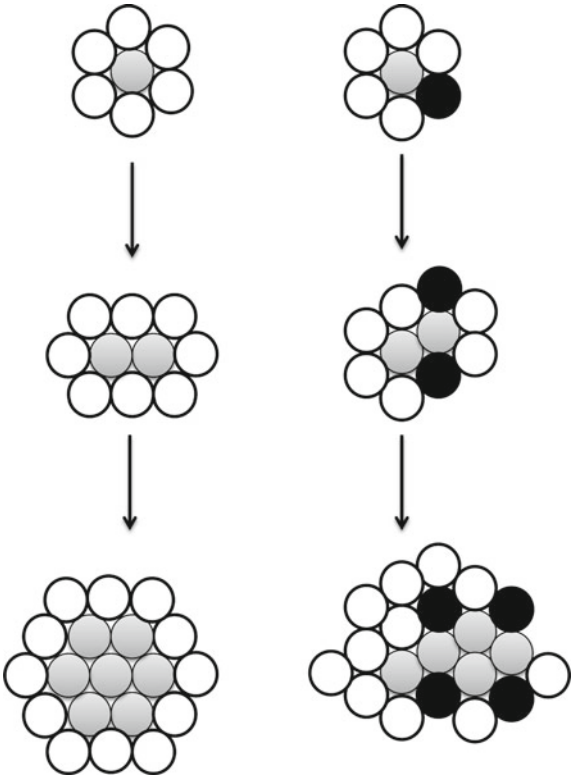

Fig. 7.4 A mechanism of growth of PrP aggregates on lipid membranes is schematized here. *Left panel* the Eden model of growth is presented. *Gray circles* represent bound PrP and *white circles* represent potential growth sites. In the *right panel*, the diagram following the epidemic model of growth, with *gray circles* representing bound PrP, *white circles* representing potential growth sites, and *black circles* representing sites of membrane disruption, where growth cannot occur. This schematic diagram is redrawn from Ref. [37]

on the anionic phospholipid content of the membrane. Based on this study, and other available knowledge, the aggregation mechanism of PrP on membranes has been explained by classic models of growth (see Fig. 7.4).

In conclusion, this section has briefly discussed the role of lipids (specifically) and membranes (generally) in the generation of prion transformations and related protein misfoldings responsible for various neurodegenerative diseases such as CJD. The effects due to lipid membranes require thorough studies to elucidate detailed mechanisms involved at a molecular level. Nonetheless, based on the existing information it is clear that membrane effects on PrP form an important area that should be investigated further to help find a cure for prion related diseases.

7.3 Membrane Topology and Alzheimer's Disease

The cause of familial Alzheimer's disease has been identified as being due to mutations in genes (for general understanding see the Refs. [8, 14, 51]). A large number of mutations spread throughout the structures of proteins presenilin 1 and 2 which are linked to Alzheimer's disease [7, 24]. The protein presenilin 1 is an integral membrane protein. Membrane topology of Alzheimer's disease-related presenilin 1 was explained in detail in the Ref. [30]. Presenilin 1 and 2, which are highly homologous to each other, were reported to be mainly localized in the membranes of intracellular compartments such as the endoplasmic reticulum. A convincing membrane topology model for both of these presenilins 1 and 2 was proposed. Due to the membrane association of the genes that are responsible for Alzheimer's disease, it can be predicted that membrane structure and mechanisms may also be affected in Alzheimer's disease patients. Conversely, membrane topology may also have a substantial role to play in both the onset and therapy for Alzheimer's disease. However, a rather insignificant number of investigations have so far been undertaken to understand this effect. Some progress has been made in developing theories that explain how Alzheimer's disease causes the death of brain cells [12], but a molecular mechanism is yet to be discovered. Similarly, the role of the membrane, an important cellular compartment, is yet to be discovered through membrane-based research by associating proteins like presenilins 1 and 2, amyloid precursor protein, etc.

7.4 Alcohol-Related Diseases, Their Effects on Lipid Membranes and Possible Treatments, Focusing on Membrane Effects

Alcohol is a social drink. Many people drink alcohol occasionally, many do it daily and for many drinking is an addiction. Numerous studies suggest that alcohol has different effects on the human body, depending on the amount and frequency of drinking, as well as the physiology of the individual. Heavy drinkers are found, in large proportion, to face serious liver disease. Liver injury may be caused by direct toxicity of metabolic byproducts of alcohol, as well as by inflammation induced by these byproducts [26]. In addition to liver problems, many other types of health issues may appear due to alcohol use beyond the tolerance limit, which is not yet precisely determined. Brain damage, cancers (especially of the mouth and throat), lung infections, high blood pressure, stomach ulcers, colon cancer, osteoporosis (by interfering with the body's ability to absorb calcium), body and skin dehydration, sexual and mental health issues, etc. may develop as a result of drinking alcohol in excess. Detailed analysis of all these alcohol-related diseases suggests that the cellular environment is somehow adversely affected by the effects of alcohol. We address some of the cell membrane effects of alcohol below.

Terama et al. [44] reported that the influence of ethanol on the lateral pressure profile of a lipid bilayer is prominent, reaching several hundred atmospheres. Ethanol

reduces the tension at the membrane–water interface, and reduces the lateral pressure profile close to the membrane–water interface. This supports the hypothesis that anesthetics may act by changing the lateral pressure profile exerted on proteins embedded in membranes. A later study [20] using the anesthetic drug (R)-(-)-ketamine also provides evidence for a lateral pressure-mediated mode of anesthesia. The effects of the membrane's lateral pressure profile on the integral membrane protein functions are well-addressed using some test model cases discussed in Chap. 5.

Another study [16] suggests that ethanol induces expansion of the membrane, accompanied by a drop in the membrane thickness, as well as disordering and enhanced inter-digitation of lipid acyl chains. These changes become more pronounced with increases in ethanol concentration, but the bilayer structure of the membrane is maintained as long as the ethanol concentration is not too high. However, due to the effects of extremely high ethanol concentration, even a non-bilayer phase can be achieved.

7.5 Cystic Fibrosis Transmembrane Conductance Regulator

Ion channels play an important role in human physiology. Different ions are used for various functions in various organs of the body. The human body employs different ion channels to secrete ions and maintain concentrations in fluids outside and inside the cells. For example, cystic fibrosis transmembrane conductance regulator (CFTR) is highly expressed in the pancreatic ductal epithelium. It plays an important role in ductal bicarbonate ion secretions. Furthermore, the thickness of mucus produced in the bronchi is controlled via the secretion or the absorption of ions by the alveoli cells. However, pathological changes to these ion channels lead to an imbalance. For example, the cell may become too tight, causing a shutdown of ion flow, as is the case in a disease referred to as cystic fibrosis. On the other hand, the cells may become too leaky, for example when a person falls sick due to flu or cold. This makes it very important to study the properties of various ion channels, and their interactions with each other in a cellular layer as well as the pathways taken by different ions.

Horisberger [26] developed the original quantitiative model of the epithelial sodium channels (ENaC) and the CFTR. ENaC–CFTR interactions were described including the role of electrical coupling of ion fluxes explored in an epithelial cell model involving ion transport across a layer of epithelial cells, aimed at explaining how effects in one channel would affect the other. The model employed different types of ion channels. The first type of channels employed by the model were passive transporters. These do not require energy input, i.e. adenosine triphosphate (ATP), since they transport ions along the concentration or charge gradient. Some of the prominent ion channels that fit this category are ENaC and CFTR. Figure 7.5 shows a general model of such a pathway.

The second type of ion transporter employed by the Horisberger model is an active pump. It uses ATP to pump three Na^+ ions outside the cell and two K^+ ions inside the cell against the concentration gradient. This is the only active transporter in the

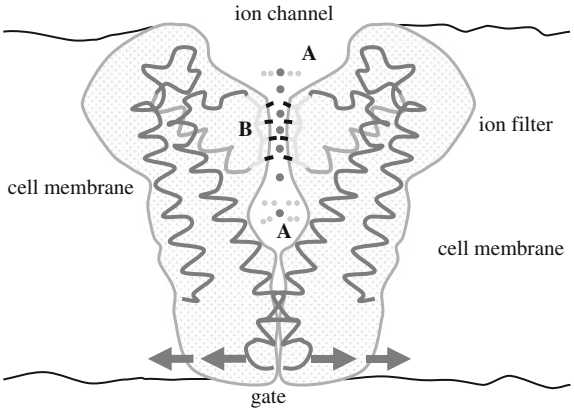

Fig. 7.5 General model of the CFTR pathway [2]

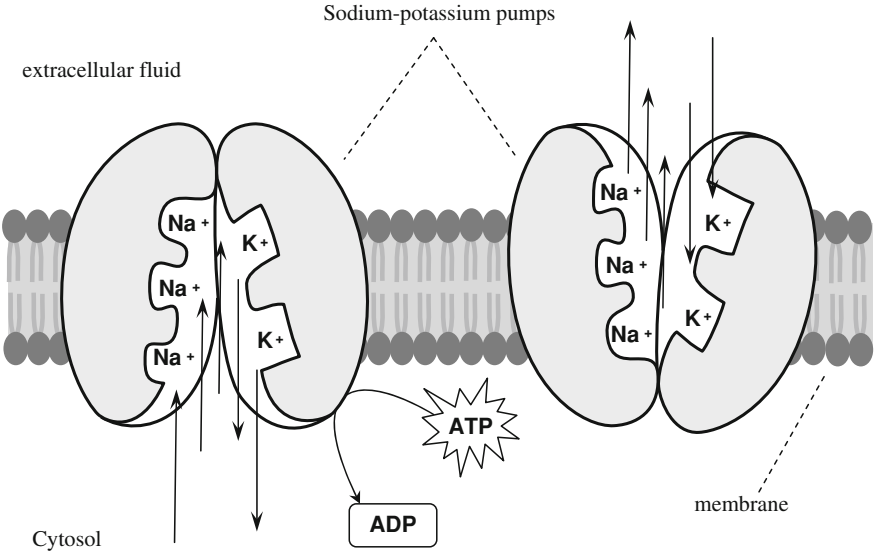

Fig. 7.6 Ion transport through ion pumps [1]

model. Figure 7.6 demonstrates the pathway of ion transport through this specific ion pump.

Figure 7.7 [18] gives a graphical representation of the key elements in the model. The right side of the epithelial layer represents the basolateral side and the basolateral membrane separates the basolateral compartment from the intracellular fluids. The left side of the cell is known as the apical side or the lumen, and the apical membrane separates the apical compartment from the intracellular fluids. The apical and the basolateral membranes have different ion channels embedded in them, which are

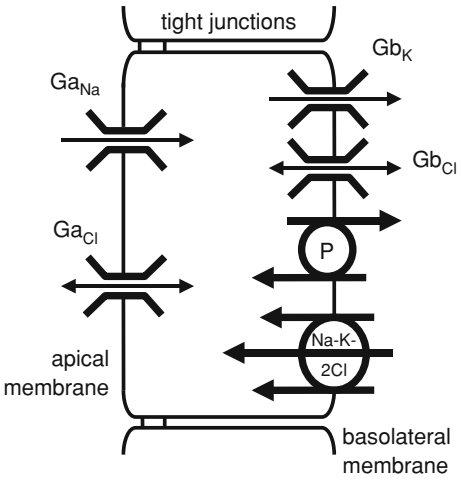

Fig. 7.7 Elements in Horisberger's model [18]

then defined by an equation giving the flux of ions or the current flowing through this transporter as a function of ion concentrations on both sides of the membrane, and the membrane potential.

Horisberger's model involved the following quantities:

In the apical membrane:

- Na^+ conductance (Ga_{Na}) provided by ENaC,
- Cl^- conductance (Ga_{Cl}) provided by CFTR,
- K^+ conductance (Ga_K).

In the basolateral Membrane:

- K^+ and Cl^- conductances (Gb_K and Gb_{Cl}),
- Na–K pump,
- Na/K/Cl cotransporter.

Furthermore, tight junctions between cells correspond to a paracellular "shunt" pathway.

The equation defining the pump is:

$$I_p = \frac{I_{p\max}}{1 + (k_{\mathrm{Na}_i}/c_{\mathrm{Na}_i})^{n\mathrm{Hill}}} \tag{7.1}$$

and it uses a predefined parameter, the $I_{p\max}$, $k\mathrm{N_a}$ and the steep Hill equation constant (n_{Hill}), which is determined experimentally. Horisberger found that the average value for this parameter is somewhere between 2 and 3, and judiciously chose 3 in the model.

The passive channels including the ENaC, CFTR, and the basolateral Cl^- channels were modeled by the Goldman–Hodgkin–Katz (GHK) equation.

$$I_i = \frac{pF^2v}{RT}\frac{c_2 - c_1 e^{-\frac{zvF}{RT}}}{1 - e^{-\frac{zvF}{RT}}} \tag{7.2}$$

In this equation, c_2 is the extracellular concentration, while c_1 symbolizes the intracellular concentrations. The paracellular shunt or the tight junctions are also described using the GHK equations. The basolateral potassium channels use an inward rectifying factor along with the GHK equation. The basolateral Na/K/2Cl cotransporter is defined by a single constant trCl, assuming no voltage dependence and no dependence with regards to the ion concentrations.

The model simulates ion transport under current- or voltage-clamp conditions and allows monitoring of individual ionic membrane currents, membrane potentials, and intracellular ion concentrations. Using a set of transport parameters, the model reproduces the effects of conductance inhibition on transepithelial transport.

$$I_a(V_a) = \sum_j iT_j(V_a) \tag{7.3}$$

$$I_b(V_b) = \sum_j iT_j(V_b) \tag{7.4}$$

These equations [18] represent the sum of currents flowing through different channels in the apical and the basolateral membranes, respectively. These equations are used to solve for V_a and V_b. Under the voltage-clamp condition, the model solves the following set of equations:

$$I_a(V_a) = I_b(V_b) \tag{7.5}$$

$$V_a + V_b = V_{te} \tag{7.6}$$

The following equations are solved under current-clamp conditions:

$$I_t = I_a(V_a) + I_s(V_{te}) \tag{7.7}$$

$$I_a(V_a) = I_b(V_b) \tag{7.8}$$

$$V_{te} = V_a + V_b \tag{7.9}$$

Horisberger's model produces steady-state results.

Y. Sohma, M.A. Gray, Y. Imai, and B.E. Argent [41] modeled ion transport in the pancreatic ductal epithelium cells using a model which was similar to that of Horisberger. As Fig. 7.8 shows, it includes many more ion channels and multiple co-transporters [41]. Furthermore, the model incorporates ions besides Na^+, K^+, and Cl^-. It also includes transportation of bicarbonate (HCO_3^-) and hydrogen (H^+) ions.

Sohma et al. proposed an equation for the turnover rate for the $Na^+ - nHCO_3^-$ cotransporter [41]:

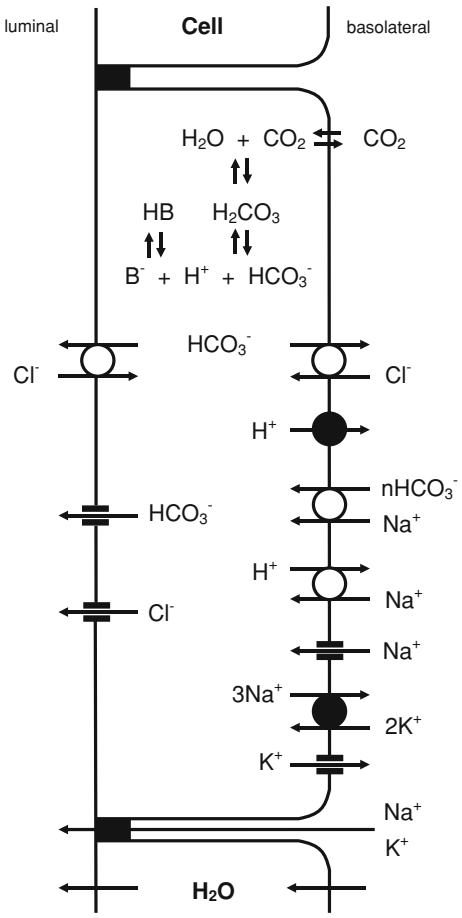

Fig. 7.8 Model of ion transport in the pancreatic ductal epithelium cells

$$J_{\mathrm{Na-HCO_3}} = \frac{G_{\mathrm{Na-HCO_3}} \left(\frac{[\mathrm{Na^+}]_{\mathrm{bl}} [\mathrm{HCO_3^-}]_{\mathrm{bl}}^n}{K_{c\mathrm{Na}} K_{c\mathrm{HCO_3}}^n} \times e^{-(1-n)\times F \times \frac{P D_{\mathrm{bl}}}{2RT}} - \frac{[\mathrm{Na^+}]_c [\mathrm{HCO_3^-}]_c^n}{K_{c\mathrm{Na}} K_{c\mathrm{HCO_3}}^n} \times e^{(1-n)\times F \times \frac{P D_{\mathrm{bl}}}{2RT}} \right)}{A + B} \tag{7.10}$$

where

$$A = \left(e^{(1-n)\times F \times \frac{P D_{\mathrm{bl}}}{2RT}} + R_{l/k} \times \frac{[\mathrm{Na^+}]_{\mathrm{bl}} [\mathrm{HCO_3^-}]_{\mathrm{bl}}^n}{K_{c\mathrm{Na}} K_{c\mathrm{HCO_3}}^n} \right) \times \left(1 + \frac{[\mathrm{Na^+}]_c}{K_{c\mathrm{Na}}} + \frac{[\mathrm{Na^+}]_c [\mathrm{HCO_3^-}]_c^n}{K_{c\mathrm{Ka}} K_{c\mathrm{HCO_3}}^n} \right)$$

and

Table 7.1 Average parameter values

Name	Value	Units
Apical sodium conductance (Pa_{Na})	2.2×10^{-6}	$\mathrm{cm} \cdot \mathrm{s}^{-1}$
Apical potassium conductance (Pa_{K})	4.0×10^{-7}	$\mathrm{cm} \cdot \mathrm{s}^{-1}$
Apical chloride conductance (Pa_{Cl})	1.6×10^{-6}	$\mathrm{cm} \cdot \mathrm{s}^{-1}$
Apical bicarbonate conductance ($Pa_{\mathrm{HCO_3}}$)	1.6×10^{-7}	$\mathrm{cm} \cdot \mathrm{s}^{-1}$
Basolateral potassium conductance (Pb_{K})	6.0×10^{-6}	$\mathrm{cm} \cdot \mathrm{s}^{-1}$
Basolateral chloride conductance (Pb_{Cl})	1.0×10^{-7}	$\mathrm{cm} \cdot \mathrm{s}^{-1}$
Na^+–$n\mathrm{HCO}_3^-$ cotransporter permeability ($G_{\mathrm{Na-HCO_3}}$)	1.5×10^{-6}	$\mathrm{mol/s/cm}^2$
Pump current ($I_{\max}$)	20	$\mu\mathrm{A} \cdot \mathrm{cm}^{-2}$
Sodium Affinity ($k\mathrm{Na}i$)	10	mM
nHill	3	
Na–K–2Cl cotransporter (trCl)	10	$P_{\mathrm{mol}} \cdot \mathrm{cm}^{-2} \cdot \mathrm{s}^{-1}$
Na shunt permeability ($P\mathrm{Na}s$)	1.0×10^{-8}	$\mathrm{cm} \cdot \mathrm{s}^{-1}$
K shunt permeability ($P\mathrm{K}s$)	1.0×10^{-8}	$\mathrm{cm} \cdot \mathrm{s}^{-1}$
Cl shunt permeability ($P\mathrm{Cl}s$)	1.0×10^{-8}	$\mathrm{cm} \cdot \mathrm{s}^{-1}$
$\mathrm{HCO_3}$ shunt permeability ($P\mathrm{HCO_3}s$)	2.0×10^{-9}	$\mathrm{cm} \cdot \mathrm{s}^{-1}$
Coupling ratio in Na–$n\mathrm{HCO_3}$ cotransporter (n_{Co})	2	
Effective charge of unloaded carrier (zL)	1	
Velocity constant ratio (R_{lk})	100	
Na^+ dissociation constant ($K_{c\mathrm{Na}}$)	500	mM
HCO_3^- dissociation constant ($K_{c\mathrm{HCO_3}}$)	30	mM

$$B = \left(e^{-(1-n)\times F\times \frac{PD_{\mathrm{bl}}}{2RT}} + R_{l/k} \times \frac{[\mathrm{Na}^+]_c[\mathrm{HCO}_3^-]_c^n}{K_{c\mathrm{Na}}K_{c\mathrm{HCO_3}}^n} \right) \times \left(1 + \frac{[\mathrm{Na}^+]_{\mathrm{bl}}}{K_{c\mathrm{Na}}} + \frac{[\mathrm{Na}^+]_{\mathrm{bl}}[\mathrm{HCO}_3^-]_{\mathrm{bl}}^n}{K_{c\mathrm{Na}}K_{c\mathrm{HCO_3}}^n} \right)$$

Table 7.1 lists the values of parameters used in the model, while Table 7.2 lists the average values used for different parameters and ionic concentrations as a starting point in the model.

The model computes the flow of ions across a layer of epithelial cells, the cellular currents, the amounts of different ions being secreted and other electrogenic properties of different ion transporters. By understanding the above, we can better understand the mechanisms that lead to ion imbalances, such as those during the flu, or more serious conditions such as cystic fibrosis. Another important use of the model is to test the effects of new drugs on the system. Besides testing, the model can help us hypothesize new mechanisms for future drug action. Affecting one channel has a direct effect on the way other ion channels behave. In case of cystic fibrosis, we may be able to compensate for low bicarbonate and chloride conductivity by affecting the permeability of other channels.

Table 7.2 Initial concentrations of the main ionic species

Ion	Initial concentration (mM)
Na^+ apical	130
K^+ apical	4
Cl^- apical	134
HCO_3^- apical	24
Na^+ basolateral	130
K^+ basolateral	4
Cl^- basolateral	134
HCO_3^- basolateral	24
Na^+ intracellular	20
K^+ intracellular	110
Cl^- intracellular	45
HCO_3^- intracellular	24

Models that quantify the functioning of the membrane and its components in health and disease are ultimately the area where biophysics can demonstrate its great value in medical research advances.

References

1. http://www.bioon.com/book/biology/whole/image/3/3-16.tif.jpg
2. http://fig.cox.miami.edu/cmallery/150/memb/ion_channel_lg1.jpg
3. "Prion Diseases". US Centers for Disease Control. 2006-01-26. Retrieved 2010-02-28.
4. Aguzzi, A.: Unraveling prion strains with cell biology and organic chemistry. Proc. Nat. Acad. Sci. USA **105**(1), 11–12 (2008) doi:10.1073/pnas.0710824105. PMC 2224168. PMID 18172195. Retrieved 2010-02-28
5. Ashrafuzzaman, M., Tseng, C.Y., Kapty, J., Mercer, J.R., and Tuszynski, J.A.: Computationally designed DNA aptamer specific for phosphatidylserine lipid (submitted). (2011)
6. Belay, E.D.: Transmissible spongiform encephalopathies in humans. Annual Review of Microbiology **53**, 283–314. (1999)
7. Berezovska, O., Lleo, A., Herl, L.D., Frosch, M.P., Stern, E.A., Bacskai, B.J., Hyman, B.T.: Familial Alzheimer's disease presenilin 1 mutations cause alterations in the conformation of presenilin and interactions with amyloid precursor protein. J Neurosci. **25**(11), 3009–17 (2005)
8. Bertram, L., Tanzi, R. E.: Thirty years of Alzheimer's disease genetics: the implications of systematic meta-analyses. Nature reviews. Neuroscience **9** (10): 768–778 (2008) doi:10.1038/nrn2494. PMID 18802446. edit
9. Blankenberg, F.G.: Imaging the molecular signatures of apoptosis and injury with radiolabeled annexin V. Proc Am Thorac Soc. **6**(5):469–76 (2009)
10. Blankenberg, F.G.: In vivo imaging of apoptosis. Cancer Biol Ther. **7**(10):1525–32 (2008)
11. Covas, D. T.: Effects of hydroxyurea on the membrane of erythrocytes and platelets in sickle cell anemia. Haematologica 89, 273–280 (2004)
12. Craddock, T.J.A., Tuszynski, J.A., Chopra, D., Casey, N., Goldstein, L.E., Hameroff, S.R., and Tanzi, R.: The Zinc Dyshomeostasis Hypothesis of Alzheimer's Disease. PLoS ONE **7**(3):e33552 (2012)
13. Elmore, S.: Apoptosis: a review of programmed cell death. Toxicol Pathol. 35:495–516 (2007)

14. Ertekin-taner, N.: Genetics of Alzheimer's disease: a centennial review. Neurologic clinics 25 (3): 611–667 (2007) doi:10.1016/j.ncl.2007.03.009. PMC 2735049. PMID 17659183
15. Futerman, A. H. & van Meer, G.: The cell biology of lysosomal storage disorders. Nature Rev. Mol. Cell Biol. 5, 554–565 (2004)
16. Gurtovenko, A.A., and Anwar, J. Interaction of Ethanol with Biological Membranes: The Formation of Non-bilayer structures within the Membrane Interior and their Significance. J. Phys. Chem. B **113** (7), 1983–1992 (2009)
17. Hanahan, D., Weinber, R.A.: The hallmarks of cancer. Cell **100**, 57–70 (2000)
18. Horisberger, J. D.: ENaC-CFTR interactions: the role of electrical coupling of ion fluxes explored in an epithelial cell model; Pflugers Arch. Jan **445**(4), 522–8 (2003)
19. James, T. L., Liu, H., Ulyanov, N. B., Farr-Jones, S., Zhang, H., Donne, D. G. et al.: Solution structure of a 142-residue recombinant prion protein corresponding to the infectious fragment of the scrapie isoform. Proc. Natl Acad. Sci. USA, **94**, 10086–10091 (1997)
20. Jerabek, H., Pabst, G., Rappolt, M., and Stockner, T.: Membrane-Mediated Effect on Ion Channels Induced by the Anesthetic drug Ketamine. J. Am. Chem. Soc. **132** (23), 7990–7997 (2010)
21. Kerr, J.F., Wyllie, A.H. and Currie, A.R.: Apoptosis – a basic biological phenomenon with wide-ranging implications in tissue kinetics. Br. J. Cancer. **4**, 239–257 (1972)
22. Kraulis, P. J.: MOLSCRIPT: a program to produce both detailed and schematic plots of protein structures. J. Appl. Crystallog. **24**, 946–950 (1991)
23. Lahorte, C. et al.: Apoptosis-detecting radio ligands: current state of the art and future perspectives. European J. of Nuclear Med and, Mol Imaging. **31**, 887–919 (2004)
24. Levy-Lahad, E., Wasco, W., Poorkaj, P., et al.: Candidate gene for the chromosome 1 familial Alzheimer's disease locus. Science **269** (5226), 973–7 (1995) Bibcode 1995Sci...269.973L. doi:10.1126/science.7638622. PMID 7638622
25. Li, X., Link, J.M., Stekhova, S., Yagle, K.J., Smith, C., Krohn, K.A. and Tait, J.F.: Site specific labeling of annexin V with F-18 for apoptosis imaging. Bioconjug Chem. **19**, 1684–1688 (2008)
26. Maher, J. J.: Exploring Alcohol's Effects on Liver Function. Alcohol Health & Research World Vol. **21** (1), 1–12 (1997)
27. Martin, S.J., Reutelingsperger, C.P., McGahon, A.J., Rader, J.A., van Schie, R.C., LaFace, D.M., Green, D.R.: Early Redistribution of Plasma Membrane phosphatidylserine Is a General Feature of Apoptosis Regardless of the Initiating Stimulus: Inhibition by Overexpression of BCl^{-}2 and Abl. J. Exp. Med. **182**, 1545–1556 (1995)
28. McNeil, P. L. & Steinhardt, R. A.: Plasma membrane disruption: repair, prevention, adaptation. Ann. Rev. Cell Dev. Biol. **19**, 697–731 (2003)
29. Murakami, Y., Takamatsu, H., Taki, J., Tatsumi, M., Noda, A., Ichise, R., Tait. J.F. and Nishimura, S.: 18F-labeled annexin V: a PET tracer for apoptosis imaging. Eur J Nucl Med Mol Imaging. **31**, 469–474 (2004)
30. Nakai, T., Yamasaki, A., Sakaguchi, M., Kosaka, K., Mihara, K., Amayai, Y., and Miura, S.: Membrane Topology of Alzheimer's Disease-related Presenilin 1. J. Biol. Chem. **274** (33), 23647–23658 (1999)
31. Oltersdorf, T. et al.: An inhibitor of BCl^{-}2 family proteins induces regression of solid tumours. Nature **435**, 677–681 (2005)
32. Petros, A.M., Nettesheim, D.G., Kim, D.H., Yoon, H.S., Swift, K., Matayoshi, E.D., Oltersdorf, T., Fesik, S.W.: Solution structure of the antiapoptotic protein bCl^{-}2 Proc. Natl. Acad. Sci. USA **98**, 3012–3017 (2001)
33. Petros, A.M., Oltersdorf, T., Fesik, S.W.: Structural biology of the BCl^{-}2family of proteins. Biochem. et Biophys. Acta **1644**, 83–94 (2004)
34. Rastogi, R.P., Richa, and Sinha, R.P.: Apoptosis: molecular mechanisms and pathogenicity. EXCLI Journal. **8**, 155–181 (2009) ISSN 1611–2156
35. Reed, J.C., Tomaselli, K.J.: drug discovery opportunities from apoptosis research. Curr Opin Biotechnol. **11**, 586–92 (2000)
36. Robbins, S.L., Cotran, R.S., Kumar, V., Collins, T., ed.: Robbins pathologic basis of disease. Philadelphia: Saunders. (1999) ISBN 0-7216-7335-X

37. Robinson, P.J. and Pinheiro, T.J.T.: phospholipid Composition of Membranes Directs Prions Down Alternative Aggregation Pathways. Biophys. J. **98** April 1520–1528 (2010)
38. Sanghera, N. and Pinheiro, T.J.T.: Binding of prion protein to lipid membranes and implications for prion conversion. J. Mol. Biol. **315**(5), 1241–1256 (2002)
39. Sekulic, A. et al.: Malignant Melanoma in the 21st Century: The Emerging Molecular Landscape. Mayo Clinic Proceedings **83**, 825–846 (2008)
40. Smrz, D., Lebduska, P., Dráberová, L., Korb, J. and Dráber, P.: Engagement of phospholipid scramblase 1 in activated cells: implication for phosphatidylserine externalization and exocytosis. J Biol Chem. **283**(16), 10904–18 (2008)
41. Sohma, Y., Gray, M.A., Imai, Y., Argent, B.E.: HCO_3^- transport in a mathematical model of the pancreatic ductal epithelium. J Member Biol. **176**(1), 77–100 (2000)
42. Stellar, H.: Mechanisms and Genes of Cellular Suicide. Science **267**, 1445–1449 (1995)
43. Suzuki, M., Youle, R.J., Tjandra, N.: structure of Bax: coregulation of dimer formation and intracellular localization. Cell **103**, 645–654 (2000)
44. Terama, E., Ollila, O. H.S., Salonen, E., Rowat, A.C., Trandum, C., Westh, P., Patra, M., Karttunen, M., and Vattulainen, I.: Influence of Ethanol on Lipid Membranes: From Lateral pressure Profiles to Dynamics and Partitioning. J. Phys. Chem. B **112**(13), 4131–4139 (2008)
45. Toretsky, J., Levenson, A., Weinberg, I.N., Tait, J.F., Uren, A. and Mease, R.C.: Preparation of F-18 labeled annexin V: a potential PET radiopharmaceutical for imaging cell death. Nucl Med Biol. **31**(6), 747–52 (2004)
46. Tse, C. et al.: ABT-263 A potent and orally bioavailable BCl^-2 family inhibitor. Cancer Res. **68**, 3421–3428 (2008)
47. Tseng, C.Y., Ashrafuzzaman, M., Mane, J., Kapty, J., Mercer, J. and Tuszynski, J.: Entropic Fragment-Based Approach to Aptamer. Chem Biol drug Des **78**, 1–13 (2011)
48. van Delft, M.F. et al.: The BH3 mimetic ABT-737 targets selective BCl^-2 proteins and efficiently induces apoptosis via Bak/Bax if MCl^-1 is neutralized. Cancer Cell **10**, 389–399 (2006)
49. van Engeland, M., Nieland, L.J.W., Ramaekers, F.C.S., Schutte, B., and Reutelingsperger, C.P.M.: Annexin V-Affinity Assay: A Review on an Apoptosis Detection System Based on phosphatidylserine Exposure Cytometry **31**, 1–9 (1998)
50. Weinberg, R.A.: The biology of Cancer. Garlan Science, NY USA (2007)
51. Williamson, J., Goldman, J., Marder, K.: Genetic aspects of Alzheimer disease. The Neurologist 15(2), 80–86 (2009) doi:10.1097/NRL.0b013e318187e76b. PMC 3052768. PMID 19276785. edit

Epilogue

In this book we have attempted to convey the message that cell membranes are essential to cell architecture and function. Membranes play key roles in the entry and exit of ions, metabolites, and foreign molecules, serve to localize biochemical and metabolic processes within distinct intracellular organelles, and participate in communication between internal compartments and the external environment. Reflecting this crucial and diverse role in cell function, more than one-third of all human genes specify proteins associated with cell membranes. Various types of dysfunction in membrane proteins are common causes of human diseases. Virtually, all diseases involve membrane proteins in their pathology. Not surprisingly, membrane proteins contribute significantly, or underlay, many disease states, including asthma, obesity, and diabetes. Cellular uptake of most therapeutic drugs, including those used to treat cancer and AIDS to name but two major applications, occurs through membrane transport proteins. Access to internal sites of action determines drug efficacy, and altered membrane transport by loss or downregulation of a required transport protein or induction of a drug efflux pump are common causes of the acquired drug resistance that occurs in many patients undergoing cancer therapy and other therapies. Deleterious cellular imbalances brought about by transporters and ion channels are critically involved in the causes and progression of cardiovascular and cerebrovascular diseases. Specific mutations within the genes of membrane proteins are the causes of common genetic disorders such as cystic fibrosis.

Having said that, we feel that the study of the biophysical properties of membranes and membrane proteins has lagged far behind both the basic science investigations and drug discovery targeting studies of soluble proteins. In particular, membrane proteins represent attractive but largely untapped targets for the development of new therapeutics to treat a broad range of human disorders. The reasons for this are the complexities of working with proteins that are embedded within or otherwise attached to the large and complex structure of a biological membrane. One of the motivations behind writing this monograph has been to

M. Ashrafuzzaman and J. Tuszynski, *Membrane Biophysics*,
Biological and Medical Physics, Biomedical Engineering,
DOI: 10.1007/978-3-642-16105-6,

catalyze a significant increase in our understanding of the biophysical properties of membranes and membrane proteins, and their roles in various diseases.

Only recently has the possibility of obtaining high-resolution structures of mammalian membrane proteins become reality. This, in turn, affords the molecular information needed for the development of atomistic models of membrane-bound proteins and eventually rational drug design for these proteins as targets. High sensitivity and high-resolution techniques to monitor membrane protein function (electrophysiology) and cellular location and dynamics (imaging) in live cells have also recently developed because of breakthroughs in electronics. Targeted high-throughput screening of membrane proteins for new pharmaceuticals is now also feasible. All these exciting developments herald a new era of membrane studies that offer high-level qualitative and quantitative understanding of membrane biophysics.

Membrane proteins are central to cellular function and also represent targets for drug discovery. In particular, G-protein coupled receptors (GPCR) are not only membrane proteins, but also the major target of drug therapies in use today. Directed design of drugs requires information on the structure of the target (membrane protein). The potential of membrane proteins as therapeutic targets has so far been realized only for GPCR. An enormous range of membrane proteins implicated in disease processes remain to be exploited.

Diseases of membrane proteins result from changes in the function of the membrane protein. Underlying genetic changes may cause either: (i) retention of the protein in intracellular location, instead of reaching the plasma membrane, or (ii) change of function of the protein. Live-cell real-time confocal microscopy, in combination with fluorescently tagged proteins and ion-sensitive dyes allows high fidelity spatial and temporal measurements to reveal dysfunctional molecular trafficking as well as to measure disturbances in the ionic milieu associated with alterations in the function of many membrane proteins. Many ion transport proteins operate by moving charged ions/molecules across the cell membrane and this can be measured in "real time" millisecond time scales using state-of-the-art patch-clamp technologies. Combining these elecrophysiological recordings with confocal fluorescent measurements enables to diagnose the nature of the membrane transport defect in a single step with unparalleled precision.

We hope that this monograph will be a catalyst for future studies of membranes and membrane proteins based on their biophysical properties. The authors would like this book to become a source of empirical information and conceptual inspiration to both students of biophysics and expert researchers.

Index

M. Ashrafuzzaman and J. Tuszynski, *Membrane Biophysics*,
Biological and Medical Physics, Biomedical Engineering,
DOI: 10.1007/978-3-642-16105-6, © Springer-Verlag Berlin Heidelberg 2012